High-Elevation Mountain Streamflow Generation: The Role of Deep Groundwater in the Rio Hondo Watershed, Northern New Mexico

by

Douglas Germond Tolley III

Submitted in Partial Fulfillment

of the Requirements for the Degree of

Master of Science in Hydrology

New Mexico Institute of Mining and Technology

Socorro, New Mexico

May, 2014

I dedicate this thesis to my family, who taught me the value of education and hard work, and who have never stopped supporting me throughout my academic pursuits.

I also dedicate this thesis to all of my friends who share a love for the mountains with me.

Douglas Germond Tolley III
New Mexico Institute of Mining and Technology
May, 2014

"Mountains are not stadiums where I satisfy my ambition to achieve, they are the cathedrals where I practice my religion."

Anatoli Bourkreev

-World renowned alpinist

ABSTRACT

With growing concerns about declining snowpack, warmer temperatures, and land use changes, it is becoming increasingly important to determine the sources that contribute to surface-water. Most hillslope hydrology models disregard deep groundwater contributions to surface-water (see Beven, 2006 for a review of seminal hillslope papers) due to limited bedrock permeability. Little correlation between stream geochemistry and basin drainage area has been observed in some mountain watersheds (Wolock et al., 1997), with mean residence times estimated to be less than one year (Vitvar et al., 2002). In contrast, Frisbee et al. (2011) observed a positive correlation between surface-water solute concentrations and basin drainage area in the Saguache Creek watershed, which the authors conclude is due to significant contributions of deep groundwater to streamflow. Are deep groundwater contributions to surface water in the Saguache Creek watershed anomalous due to hydrologic and geologic conditions unique to the area? Or is our assumption that the processes that generate streamflow at the hillslope scale the same as those that generate streamflow at the basin scale incorrect?

This thesis tests the transferability of the conceptual model developed for the Saguache Creek watershed (Frisbee et al., 2011) by applying it to the Rio Hondo watershed, which has different geology, topography, climate, scale, and human impacts. Tectonic activity near the Rio Hondo has resulted in highly fractured bedrock that may provide permeability similar to that of Saguache. Similar

methods used by Frisbee et al. (2011) were employed in the Rio Hondo to improve comparability between the two watersheds.

Stable isotopic data indicate that nearly all waters in the Rio Hondo are sourced from late winter and spring precipitation, despite only about one-third of total annual precipitation falling during this period. Solute concentrations in surface-water increase as a function of basin drainage area for nearly all solutes. Dating of waters in the Rio Hondo using ^{3}H, CFC's, and ^{14}C indicate that mean residence times in the watershed range from modern to thousands of years. Mean residence times in the Rio Hondo are similar to those reported by Rademacher et al. (2005) for the Sagehen basin and Frisbee et al. (2011) for the Saguache Creek watershed using CFC's and ^{14}C, respectively. Quantitative streamflow separations using EMMA indicate that most surface-waters have a large groundwater component. The proportion of groundwater tended to increase later into the year, with lower elevation sampling locations showing more evolved groundwater end-members. Contributions from groundwater were detected throughout the year, even during the peak of the snowmelt pulse.

These results indicate that deep groundwater is a significant source of streamflow in the Rio Hondo watershed throughout the year. This suggests the Saguache Creek watershed conceptual model is transferrable to another high-elevation mountain watershed. Furthermore, deep groundwater contributions to surface water in the Rio Hondo watershed appear to develop by about 10 km^2, a scale much smaller than previously published. This may be due to the steep topography of the Rio Hondo, which would allow for deeper, more localized flowpaths to develop (Tóth, 1963; Gleeson & Manning, 2008; Harding, 2012).

ACKNOWLEDGMENTS

I would like to thank my advisor, John Wilson, for his guidance during this project and my studies at New Mexico Tech. His expertise in navigating the waters of academia was invaluable, and his affable nature was greatly appreciated. I also thank Fred Phillips for his help with this project, and for pushing me to be a better scientist. While I will miss his humor and insight, I will not miss his tests and homework sets that made me feel like the dumbest person on the planet. I hope that both John and Fred are pleased with this thesis, and also enjoyed my impersonations of them at the faculty roasts.

Marty Frisbee deserves more thanks than I am able to give. His advice during this project really helped me focus my thesis, and he went above and beyond his duty by helping me with chapter revisions even when he had a heavy teaching load. I recently had someone ask me to think of someone that I admired and instantly I thought of Marty, which I hope conveys just how highly I think of him. I know that his students in the future will be incredibly lucky to have him as an advisor, and I am grateful to call him a friend and colleague.

Finally, I would like to thank all of the friends I made at New Mexico Tech for making what could have otherwise been a rather dull place a lot of fun. They say that the human body has no memory of pain, which must be true because I will look back on my gradute work at Tech with fondness. I wish that I could name every single person who helped me in some way during this project, but unfortunately I cannot. Thank you to everyone who has helped me along the way and contributed to this thesis in some way.

This thesis was typeset with LaTeX[1] by the author.

---

[1]The LaTeX document preparation system was developed by Leslie Lamport as a special version of Donald Knuth's TeX program for computer typesetting. TeX is a trademark of the American Mathematical Society. The LaTeX macro package for the New Mexico Institute of Mining and Technology thesis format was written for the Tech Computer Center by John W. Shipman.

CONTENTS

LIST OF TABLES

LIST OF FIGURES

xvi

This thesis is accepted on behalf of the faculty of the Institute by the following committee:

_____
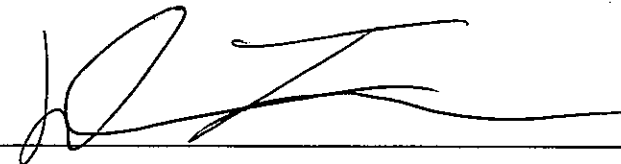
John Wilson, Advisor

_____

_____

_____

I release this document to the New Mexico Institute of Mining and Technology.

4/18/2014

Douglas Germond Tolley III   Date

CHAPTER 1

INTRODUCTION

1.1 Background

High-elevation mountain watersheds are one of the most salient features in the western US. Nearly all of the surface water in this region originates from as runoff from high-elevation mountain ranges like the Rocky Mountains and Sierra Nevada (Winograd et al., 1998; Mote et al., 2005; Bales et al., 2006;). These watersheds are able to store large quantities of water during the winter months as snowpack when demand (evapotranspiration, agricultural, recreational, etc.) is low and slowly release it during the summer months when demand is greatest (Mote et al., 2005). As this water is released, it is partitioned into different parts of the hydrologic budget including surface water runoff, groundwater recharge, soil moisture storage, evapotranspiration, and even sublimation directly off the snow surface. Although most of the snowpack is converted to surface runoff, there is evidence that groundwater is recharged within the mountains during the winter months and snowmelt season (Wilson & Guan, 2004; Earman et al., 2006; Sigstedt, 2010; Frisbee et al., 2009b). Eventually this mountain groundwater finds its way to mountain springs and streams where it provides baseflow, and all the way to the mountain front where it directly recharges adjacent basins. Human activities and ecological functioning are highly dependent on this slow release of water from the mountain block during the summer, as water is generally the

1

ultimate limiting resource in the western US (Newman et al., 2006; Phillips et al., 2011). Water managers and farmers rely on it to replenish resevoirs and water crops; fish and riparian species rely on it for habitat and spawning grounds; recreational industries rely on it for economic purposes. Unfortunately, mountain watersheds are particularly vulnerable to the effects of climate change due to the likelihood that warmer average global temperatures will result in greater potential evapotranspiration and more winter precipitation falling as rain instead of snow. These effects have already been observed in the western US, with earlier onset of spring snowmelt timing since the mid-1970s (Cayan et al., 2001) and widespread declines in spring-time snow-water equivalent (SWE) (Mote et al., 2005). These climatic changes will undoubtedly alter the partitioning and timing of water released from snowpack, including runoff and recharge to the mountain block. Therefore, it is critical that we have a better understanding of the role groundwater plays in how streamflow is generated (both processes and sources) in mountain watersheds so that we can better predict future hydrologic changes and how these systems will respond to climate perturbations (Rademacher 2005; Frisbee et al., 2011; Singleton & Moran, 2010; Manning et al., 2012).

It has been observed in the Saguache Creek watershed that runoff is increasingly generated from groundwater discharge as the scale of the upstream contributing area increases (Frisbee, 2010). One important factor likely contributing to this behavior is that the basin lithology is volcanic rock that is probably significantly permeable to great depth. I seek to answer the question: is similar runoff behavior observed in a nearby basin that is largely composed of crystalline bedrock, which has low primary permeability and porosity?

Most of the research on streamflow generation has been conducted at the hillslope or small catchment scale (see Beven, 2006 for reviews) at scales less than

100 km^2. Typical methods included hydrograph separation (Hewlett & Hibbert, 1967; Sklash & Farvolden, 1979), geochemical mass balance calculations (Pinder & Jones, 1969), hillslope trenching (Dunne & Black, 1970; McGlynn et al., 2002) and sprinkler experiments (Dunne & Black, 1970, Rodhe et al., 1996; Montgomery et al., 1997;). While this work has provided valuable insight into streamflow generation processes such as Hortonian overland flow, saturation excess flow, and variable source area to name a few, it is not certain that process information gained at smaller scales can be transferred to larger watershed scales where groundwater may become an increasingly important component of streamflow generation and where larger complexities in geology and terrain exist. Many study areas were also located in humid regions with potentially different process that result in streamflow generation compared with more arid, and larger spatial scale, western U.S. watersheds. Furthermore, most of these studies made a critical assumption that the mountain bedrock is impermeable (Beven, 2006); as a consequence, this implies that flow over or within the soil accounts for all or most of the water reaching a stream (Dunne & Black, 1970; Frisbee et al., 2013b). There have been a few studies that examined flow within the bedrock at the hillslope scale (Anderson et al., 1997b; Kosugi et al., 2006), but they focused on shallow flow within the upper portion of the fractured bedrock; deeper groundwater was almost always ignored.

By neglecting the presence of deep groundwater flowpaths, hillslope scale conceptual models confine the movement of water to surface and shallow subsurface flowpaths. The relatively short travel distances of these flowpaths result in short residence times, where residence time is defined as the weighted mean time it takes water to be routed out of the watershed. Short residence times imply that water reaches the stream quickly and does not remain in the watershed

for very long. The implications of short residence times are that changes in precipitation and/or land-surface will be quickly conveyed to the stream (Pearce et al., 1986; Hogan & Blum, 2003, McGuire & McDonnel, 2006). Residence times for these surface and shallow subsurface flowpaths are on the order of minutes to months (Horton, 1933; Hewlett & Hibbert, 1967; Dunne & Black, 1970; Anderson et al., 1997b; Brown et al., 1999; Vitvar et al., 2002; Tetzlaff et al., 2007). In comparison, residence times of outflows in some catchments have been estimated to be decades to tens of thousands of years, despite the relatively short transit times of runoff generated by mechanisms previously observed at the hillslope scale (Michel, 1992; Rademacher et al., 2005; Frisbee, 2010; Gardner et al., 2011 Manning et al., 2012; Smerdon et al., 2012). This suggests that there is a significantly older portion of streamflow that is not observed when looking only at hillslope-scale processes. This older portion is likely derived from deep groundwater flowing through the bedrock that eventually discharges to surface water.

Deep groundwater flow in mountain watersheds has largely been disregarded due to the belief that bedrock does not have significant storage compared with the soil zone (Hewlett, 1961; Anderson et al., 1993). While the primary permeability of bedrock can be very low, metamorphic and tectonic forces can create extensive fracture networks. This fracturing creates secondary permeability that is mainly responsible for deep circulation of groundwater within the mountain block. At the hillslope scale, groundwater contributions to surface water may not always be operative or the signals too weak and masked by more localized processes. At the watershed scale these deep groundwater contributions can become increasingly important as bedrock has the potential to comprise a significant reservoir within the catchment (Anderson et al., 1997a). Interactions between regional groundwater flow and surface water are more likely to occur

at the watershed scale, as the soil zone becomes a relatively thin veneer on the surface as scale increases.

Frisbee et al. (2011) have conceptualized mountain watersheds into a continuum comprised of 2-D and 3-D flow systems on each end (Figure 3.1). The 2-D conceptual model is characterized by streamflow contributions from surface and shallow subsurface flowpaths with no significant contributions from basin-scale groundwater. This type of system would have limited storage, suggesting rapid response of streamflow to precipitation events (Figure 3.1b) and short residence times (Figure 3.1c). Stream chemistry would look heterogeneous at sites near the headwaters, but would eventually reach some asymptotic value as lateral flow paths to the stream reached some characteristic length of the basin and become mixed within the stream and, possibly to a lesser degree, riparian areas (Figure 3.1d). The 3-D conceptual model has the same processes operating as the 2-D conceptual model, and also includes topography-driven (Tóthian) flow through fracture networks in the bedrock, producing basin-scale groundwater flow paths (Figure 3.1e). As the basin scale increases the importance of these deep groundwater flow paths also increases. In other words, more deep groundwater flow paths are intercepted as you move downstream. In comparison with the 2-D conceptual model, the 3-D conceptual model has greater storage and flowpath length variability, resulting in an attenuated discharge response (Figures 3.b and 3.1f). Due to this distribution of flowpath lengths, the 3-D model would also have a greater distribution of longer residence time waters (Figure 3.1g), with the longest flowpaths associated with basin-scale groundwater. Deeper groundwater flowpaths are expected to be more geochemically evolved as solute release from water/rock interactions is time-dependent (Lasaga, 1984; Bricker & Jones, 1995).
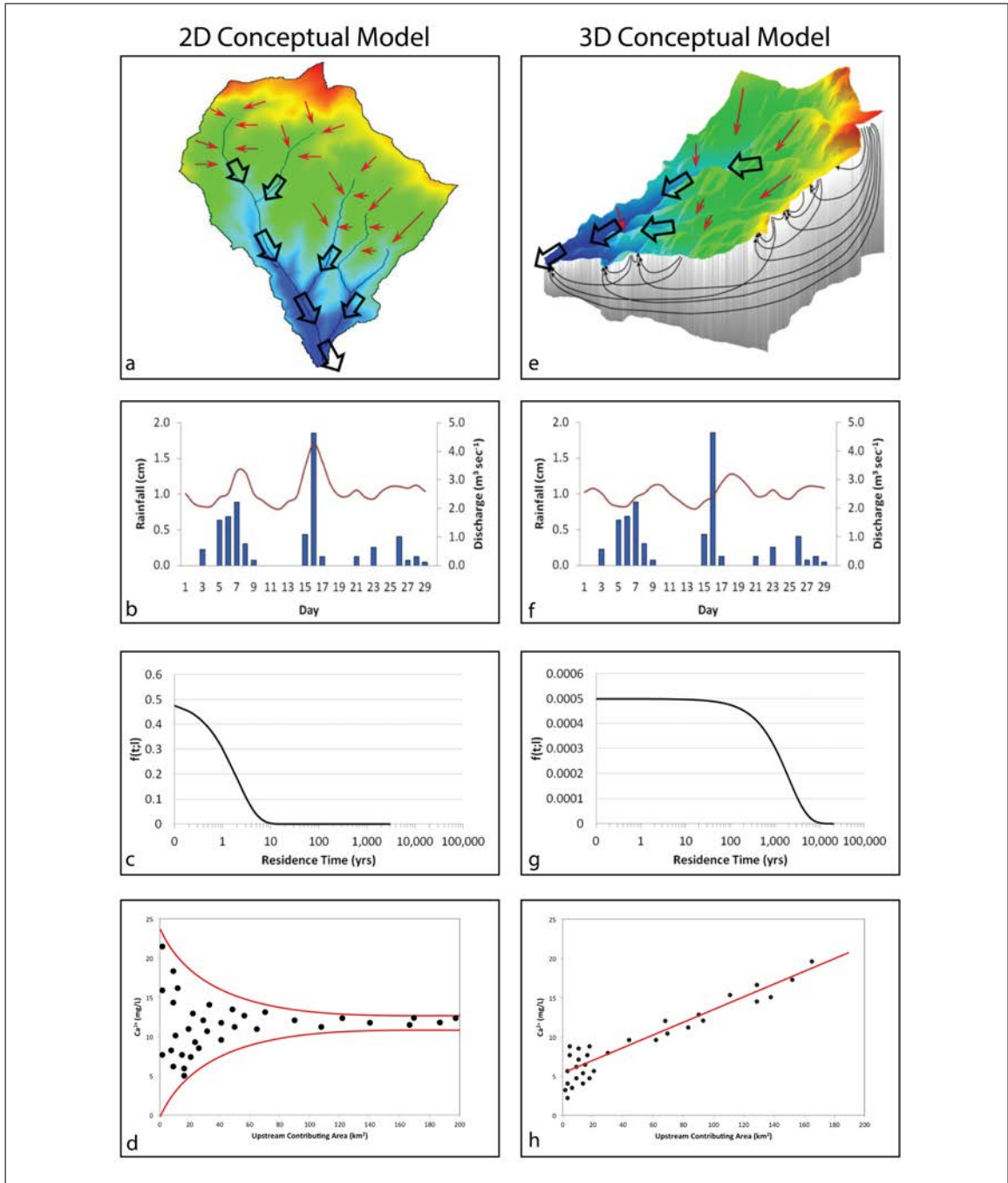
Figure 1.1: Conceptual models for endmembers of mountain block flow systems. The conceptual model for the 2-D flow system is on the left including a) schematic representation, b) runoff reponse to precipitation, c) residence time distribution, and d) streamflow chemistry as a function of upstream contributing area. The conceptual model for the 3-D flow system is on the right including e) schematic representation, f) runoff reponse to precipitation, g) residence time distribution, and h) streamflow chemistry as a function of upstream contributing area. Modified from Frisbee et al., (2011).

6

Therefore, solute concentrations in the stream are expected to increase with increasing basin area due to contributions from increasingly evolved groundwater (Figure 3.1h). This flux of old, evolved groundwater controls the geochemistry and age distributions of the stream from the headwaters to the outlet.

Streamflow in the Saguache Creek watershed has been shown to be increasingly generated from groundwater discharge as the scale of the upstream contributing area increases (Frisbee et al., 2011). One important factor likely contributing to this behavior is that the basin lithology is volcanic rock that is probably significantly permeable to great depth. I seek to answer the question: is similar runoff behavior observed in a nearby basin that is largely composed of crystalline bedrock, which has low primary permeability and porosity? The study presented in this Thesis was performed as part of a larger group effort looking at three different watersheds in northern New Mexico and southern Colorado, all tributaries to or headwaters of the Rio Grande but having different geology. The lithology of the Rio Hondo watershed represents crystalline rock, Saguache Creek lithology represents volcanics, and the lithology of a third northern New Mexico watershed, El Rito, represents sedimentary rock. The objective of this research is to explore streamflow generation and surface-water/groundwater interactions at the watershed scale in a crystalline-rock watershed. Due to the difficulty of directly observing groundwater contributions to surface water, I use patterns in geochemistry, stable isotopes, and radiometric dating to infer flow paths, timing of recharge, and relative contributions.

My hypotheses are 1) deep groundwater contributions are a significant source of streamflow generation in the Rio Hondo watershed, and 2) the relative contribution and/or geochemical evolution of this deep groundwater increases with watershed drainage-area. Here I define significant contributions as

being greater than or equal to 10% of the average annual flow. These hypotheses are based on the similarity of normalized hydrographs for the Rio Hondo and Saguache Creek watersheds, as well as geochemical and isotopic results from the Rio Hondo watershed presented by Harding (2012). If my hypotheses are correct, then I would expect to see longer residence times than those produced solely by fast runoff processes. Furthermore, mean residence times should increase from the headwaters to the outlet of the watershed as deeper, more regional groundwater flowpaths are intercepted by the stream. This increase in average residence time would result in more time for water-rock interactions. In such a case case, the concentration of chemical constituents in water will increase with increasing residence time (Lasaga, 1984; Bricker & Jones, 1995) as more geochemically evolved groundwater would control stream chemistry.

Unfortunately, there are only sparse data on the contribution of deep groundwater to surface water at small catchment scales. Kosugi et al. (2006) observed higher solute concentrations in a small (0.06 km^2), mountainous catchment in Japan that they concluded were the result of increased residence times. Rademacher et al. (2005) found mean residence times of groundwater feeding the 27km^2 Sagehen Creek watershed in California to be approximately 28 years using Chlorofluorocarbons. Frisbee (2010) collected water from a mini-piezometer installed in the streambed of a 89 km^2 subwatershed of Saguache Creek in southwestern Colorado that showed a radiocarbon age of over 3000 years. These studies were conducted in watersheds or subwatersheds with scales well within the range of those typically investigated in small catchment studies, and suggest that it is not always appropriate to ignore the effects of deep groundwater at scales less than 100 km^2.

The results from Saguache Creek suggest an emergent behavior of deep groundwater contributions to surface-water in mountain blocks. Emergent behavior are patterns that arise from a multiplicity of simple reactions in a complex system after a certain number of molecules are present. The volume required for this to happen is usually referred to as the representative elementary volume (REV), and is dependent on the type of system you are looking at. Behavior can be described differently depending in the scale at which you are looking. We use the idea of emergent behavior all the time in the field of hydrology. Instead of describing the behavior of each individual water molecule, emergent properties of the liquid, such as temperature, density, viscosity, etc. are used. Deep groundwater contributions to surace-water in mountain blocks may have been neglected by hillslope hydrologists because they were either looking in watersheds where they didn't exist, or were looking at headwater catchments that were below the REV and therefore not fully developed.

The main goal of this thesis is to test the transferability of the conceptual model developed for the Saguache Creek watershed in southwestern Colorado by Frisbee et al. (2011). Although the Rio Hondo and Saguache Creek are both high-elevation mountain watersheds, Saguache Creek drains a much larger area and is developed in a differing geologic terrain, . If similar geochemical patterns exist between the two watersheds it is likely that similar processes are active within both drainages. Frisbee et al. (2011) have shown that Saguache Creek receives significant contributions from groundwater that is thousands (possibly even tens of thousands) of years old. This suggests that the Rio Hondo, and possibly small mountainous watersheds in general, may also be receiving significant deep groundwater contributions that are much older than currently believed.

If this is indeed the case, it has important implications for the impact of climate-change, not only for the Rio Hondo but similar mountainous watersheds, as longer residence time water may provide an additional hydrologic buffering capacity against climate forcings. I define the hydrologic buffering capacity as the ability of a system to moderate climatic forcings such that the discharge statistics of the system stay relatively constant over a given period of time. Increasing global surface temperatures will likely result in less winter precipitation falling as snow and earlier onset of spring melting (Leung & Wigmosta, 1999; Cayan et al., 2001; Barnett et al., 2005). A reduction in snowpack and earlier onset of spring melting means that the snowmelt pulse in surface water will be routed through the system in a shorter period of time, and baseflow will dominate through the rest of the year. Baseflow that has a longer residence time is less likely to be influenced by shorter term climatic forcings.

Obviously this is dependent on the nature of the hydraulic system, as hydraulic response times are nearly instantaneous whereas chemical/tracer response times are much longer in comparison. Therefore, it is important to consider how the gradient driving groundwater from the subsurface to the surface is generated. If modern recharge is controlling hydraulic gradients in the system by creating groundwater mounds on ridges, then a reduction in recharge rates could reduce or completely eliminate hydraulic gradients that move groundwater from the subsurface to the surface. If this is the case, then groundwater discharges will be very sensitive to short term climatic changes even if the residence time of the groundwater is very old. However, if topography is the major control on subsurface hydarulic gradients, then even if modern recharge is completely shut off the groundwater system has the potential to maintain contributions to streamflow via gravity drainage. In this case groundwater discharges would not be sensitive

to short term climatic changes. It should be stated that this potential buffering capacity, if it does indeed exist, would not continue indefinitely but would only provide additional time for development of alternative management strategies.

In addition to surface-water flow, a significant component of the regional water balance is "mountain-front recharge" (MFR), in which groundwater is recharged along the contact of the alluvial basin and the mountain block (Wilson & Guan, 2004; Earman, 2004). While irrigation in the Rio Hondo Valley uses surface water almost exclusively, this is not the case in many other areas of the Southwest. Although this research does not attempt to specifically quantify MFR, it does provide some insight into the nature of groundwater flowpaths from the mountain block to the valley. Previous estimates of MFR have largely been based on mass-balance methods (Aishlin & McNamara, 2011) or calibration of a basin ground-water model (Wilson & Guan, 2004; Burck et al., 2004), but they ignore many of the complex processes operating within the mountain block itself. It is crucial to understand these complex, watershed-scale processes in order to improve existing water management policies and better inform future planning activites.

1.2 Scope

I tested my hypotheses of deep groundwater contributions to surface water and the geochemical evolutionary progression of groundwater by utilizing an approach that integrated multiple geochemical methods to quantify the age distribution and proportion of groundwater that contributes to surface-water . This is different from previous reseach in the area that has largely focused on groundwater flow in the basin aquifers and almost completely ignored ground-water flow within the mountain block. This research seeks to explicitly determine

the contribution of groundwater to surface water at both spatial and temporal scales. The methodology used to test my hypotheses was the following:

1. Characterize the isotopic and geochemical composition of waters within the Rio Hondo watershed to determine if there are any spatial or temporal patterns present.

2. Use several different age-dating techniques to constrain the residence time of the water in the system.

3. Use end-member mixing analysis (EMMA) with isotopic and geochemical data to quantify the porportion of groundwater contributions to the surface water system.

4. Integrate geochemical and age data to identify the sources of water that contribute to streamflow generation within the mountain block.

Chapter 2 discusses characteristics of the Rio Hondo watershed and previous hydrogeologic investigations that have been performed in the area. Chapter 3 addresses the first goal by analyzing isotopic and geochemical data collected from multiple field sampling campaigns. The isotopic and geochemical data collected are also used for EMMA in Chapter 4, where I attempt to quantify the contributing sources to surface water. Chapter 5 discusses the results from the different age dating techniques used in the watershed, and I seek to build a geochemical chronometer for the Rio Hondo watershed. Chapter 6 integrates the results from Chapters 3-5 and discusses how the data collected from the Rio Hondo supports the conceptual model developed by Frisbee et al. (2011), as well as the potential hydrologic buffering capacity of the watershed.

CHAPTER 2

SITE DESCRIPTION AND PREVIOUS INVESTIGATIONS OF RIO HONDO WATERSHED AND SURROUNDING AREA

2.1   Introduction

The Rio Hondo watershed is located in northern New Mexico on the western side of the Sangre de Cristo Mountains about 50 km south of the Colorado border (Figure 2.1), with Taos Ski Valley located at UTM 13S 460198 4050346. The watershed drainage area is approximately 190 km^2 and can be split into two distinct geologic landforms: the mountain block (comprising the Taos Range), which is made of mostly of crystalline basement rocks, and the Taos Valley, which is composed primarily of alluvial sediments and basalt flows and is part of the southern extent of the San Luis Valley. These two landforms are separated by the Sange de Cristo fault, part of the Rio Grande rift zone that extends from central Colorado to Mexico (Rawling, 2005). There is over 2 km of relief in the watershed, ranging from an elevation of 1971 m.a.s.l. at the outlet of the watershed (confluence with the Rio Grande) to 4013 m.a.s.l. at Wheeler Peak (the highest peak in New Mexico).
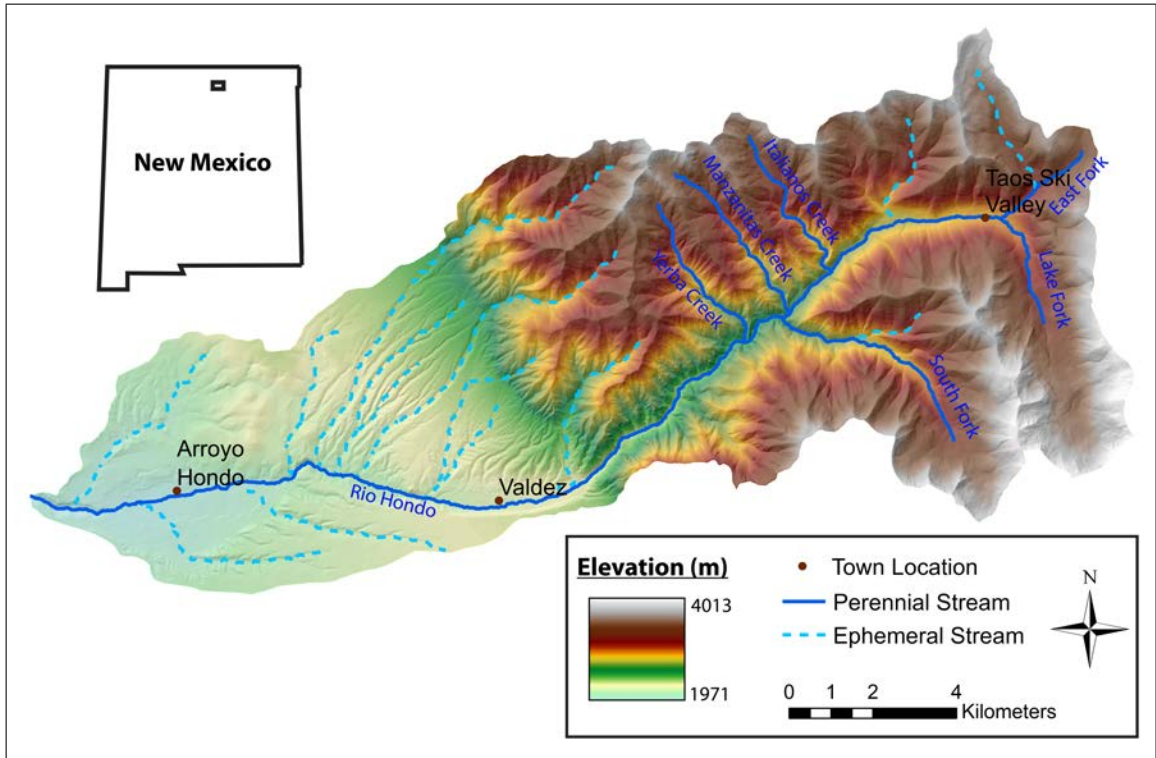
Figure 2.1: Basemap of the Rio Hondo Watershed showing perennial and ephemeral streams with population centers indicated.

2.2 Physical Setting

2.2.1 Geology and Structure

Several studies on the geology of the crystalline bedrock in the Sangre de Cristo mountains and the volcanics of the Taos Valley were completed throughout the 1900s (Gruner, 1920; Clark & Read, 1972; Condie, 1979; Lipman & Mehnert, 1979). Rocks within the mountain block are composed mostly of Precambrian gneisses, schists, and mafic metavolcanics (Gruner, 1920; Clark and Read, 1972; Condie, 1979) with Tertiary granodiorite to granitie intrusions (Clark and Read, 1972; Johnson et al.,1989) (Figure 2.2). Lithology of the mountain block is primarily quartz monzonite, felsic gneiss, amphibolite, quartzite, and minor quartz mica schist. The mountain block is characterized by high-relief topography, evi-

14
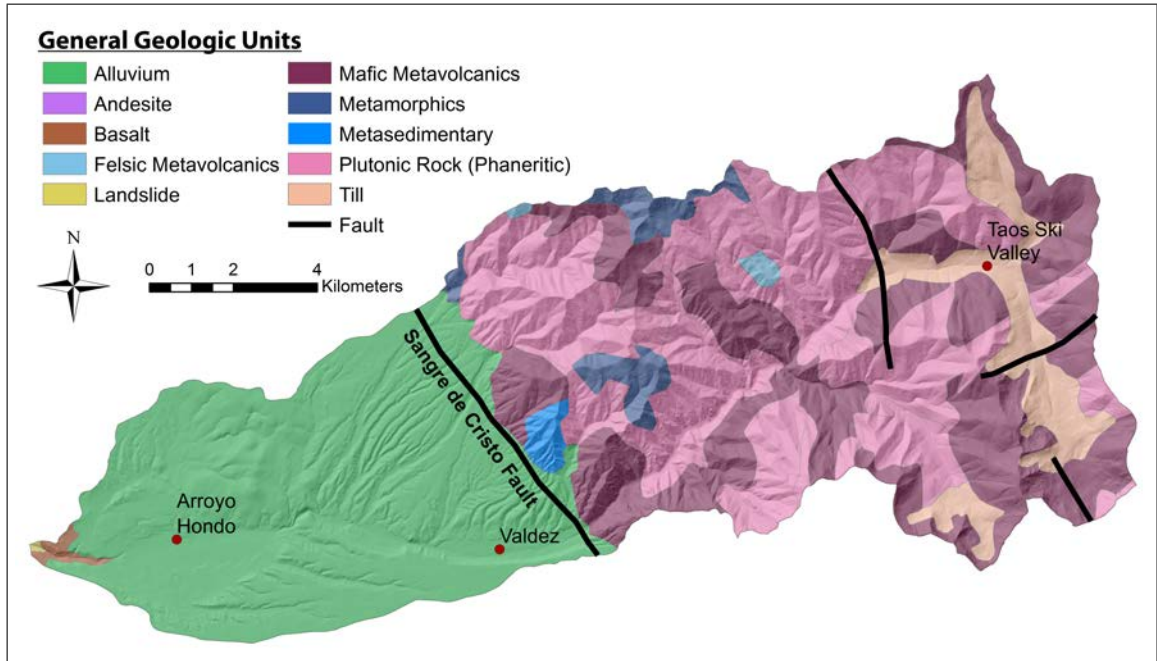
Figure 2.2: General geology of the Rio Hondo watershed with hillshade overlain and major faults shown.

denced by the local phrase, "Taos is a four letter word for steep" in reference to Taos Ski Valley (TSV). Slopes within the mountain block range from 0 to 72°, with an average slope of 26° and standard deviation of 9°. Coarse alluvium is present in the lowest portion of the valleys within the mountain block. Glaciation has been shown to exist in the Sangre de Cristo Mountains from the late Pleistocene to late Holocene (Armour et al, 2002), and glacial till deposits have been mapped near the headwaters of the Rio Hondo (Clark and Read, 1972). There is also evidence of a current rock glacier, discussed in the Hydrogeological Framework and Previous Investigations section below.

The mountain block is separated from the valley by the Sange de Cristo Fault, a steeply west-dipping normal fault that bisects the watershed generally from northeast to southwest. Estimates of displacement on the fault are up to 7 or 8 km (Lipman & Mehnert, 1979) although most of the fault is currently unex-
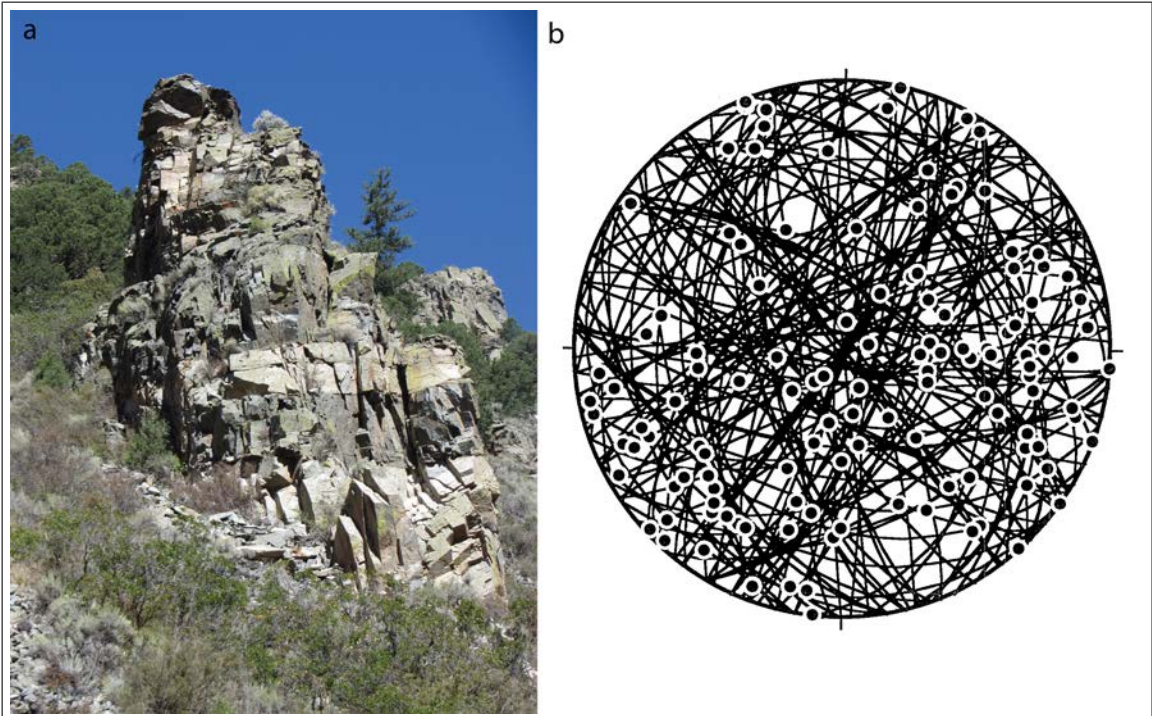
Figure 2.3: a) Photograph of a rock outcrop near the mouth of the Rio Hondo canyon. Note the high fracture density resulting in greatly enhanced secondary permeability. b) Stereonet projection of fracture planes in the southern portion of the Sangre de Cristo mountains (Paul Bauer, 2003, unpublished data) shows no preferential fracture orientation.

posed, being buried by young sediments. Fault geometry ranges from essentailly a single lineament in the north to several buried faults accomodating deformation in the south (Rawling, 2005). There are also several mapped faults with the mountain block itself (Figure 2.2), including normal and thrust faults. The stresses required to produce faults are generally not localized strictly to the fault itself but in a zone adjacent to the fault trace. When faults are located in relatively brittle rocks, like the crystalline basement rocks of the Rio Hondo, the stresses associated with movement of the fault tend to break the rocks instead of deforming them plastically. This area of brittle deformation adjacent to the fault is commonly referred to as a "damage zone." Damage zones are areas with increased fracture density, and therefore significantly enhanced secondary per-

meability (Caine et al., 1996; Gundmundsson, 2000; Caine & Tomusiak, 2003). The presence and relatively close spacing of both compressive and extensional faults in the area (Clark & Read, 1972) is evidence that the mountain block has experienced several tectonic stress periods, resulting in the pervasive nature of fractures within the mountain block that is observed today (Figure 2.3a). Stereonets (Lambert equal-area lower-hemisphere projection), a method of mapping 3D planes onto a 2D surface, display patterns in the orientation of these fractures, if indeed patterns do exist. Vertical fractures will plot as arcs near the center of the stereonet, while horizontal fractures will plot near the edge. The strike (the direction the fracture "points" relative to the earth's surface) determines the rotation of the arc around the stereonet. Therefore, fractures that have similar orientations will plot as similar arcs on the stereonet. Figure 2.3b shows a stereonet projection of multiple fracture orientations measured across the southern portion of the Sangre de Cristo mountains (Paul Bauer, 2003, unpublished). The lack of any pattern shows there is no preferential fracture orientation. Thus, it is highly likely that many of the fractures intersect with each other, creating a fracture network that acts as a resevoir in which water is able to be transmitted through and stored within the mountain block. The lack of preferential orietation of the fracture network would allow for the mountain block to be represented by an effective isotropic hydraulic conductivity for groundwater modeling purposes.

Sediments in the valley are composed of unlithified to poorly lithified Santa Fe Group sediments (Figure 2.4). These were eroded from the uplifted Sangre de Cristo Mountains in the east and deposited by streams flowing to the west (Rawling, 2005). Sediments were also formed by eolian and lacustrine processes (Burck et al., 2004). Interbedded within the Santa Fe Group is the Servilleta Formation, a series of basalt flows associated with rifting that tend to pinch out

to the east and south (Bauer et al., 1999). The best exposures of basalt are in the Rio Hondo Canyon near the confluence with the Rio Grande. The Cerro Negro dacite, an intermediate composition volcanic flow, is present near the middle of the Rio Hondo Valley just west of the town of Valdez (Figure 2.2) and shows onlapping basalt flows (Benson, 2004). Overlying the Santa Fe Group are Quaternary glacial outwash and alluvial fan sediments known as the Blueberry Hill deposits (Lipman & Mehnert, 1979; Johnson et al., 2009). The valley is characterized by deeply incised streams with relatively gentle slopes averaging 9° with a standard deviation of 7°.
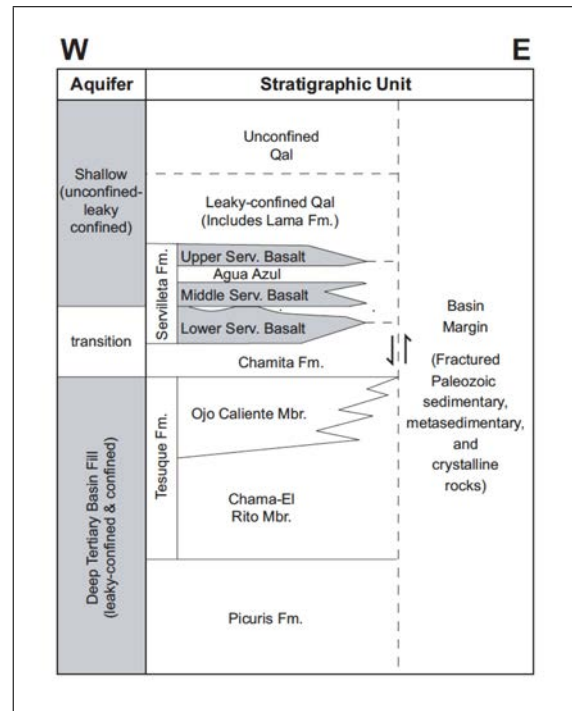
Figure 2.4: Stratigraphy of the Taos Valley (from Drakos et al., 2004a).

2.2.2 Climate

The Rio Hondo watershed is located in a semiarid climate with mild to moderate summers and cold winters. The topographic differences between the mountain block and the valley result in markedly different climates between the two. Average annual precipitation ranges from 48.2 to 99.0 cm (19 to 39 in) on the mountain range, while, in contrast, the average annual precipitation ranges from 28.0 to 45.7 cm (11 to 18 in) in the valley (OSU, 2012) (Figure 2.5). Approximately 33% of the precipitation on the mountain range falls as snow, while only 13 to 18%
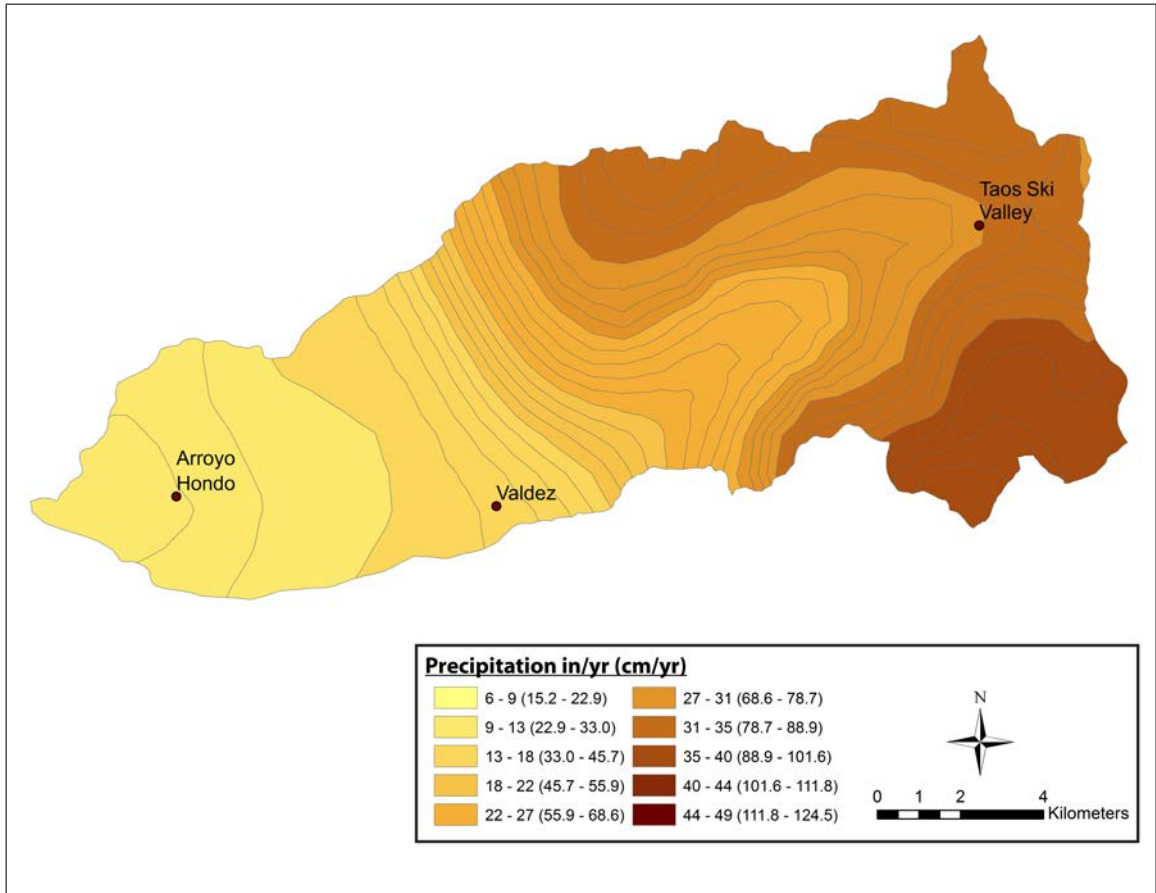
Figure 2.5: Average annual precipitation in the Rio Hondo Watershed from PRISM (OSU, 2012). Averages are from 1981-2010.

falls as snow in the valley (Garrabrant, 1993). The majority of the precipitation that falls

within the watershed comes from short, intense summer and fall convective thunderstorms that take place during the monsoon season. Average daily temperatures in the mountain block area range from -25 to 17 °C (NRCS, 2013), with average daily valley floor temperatures ranging from -1 to 31 °C (WRCC, 2013).

19
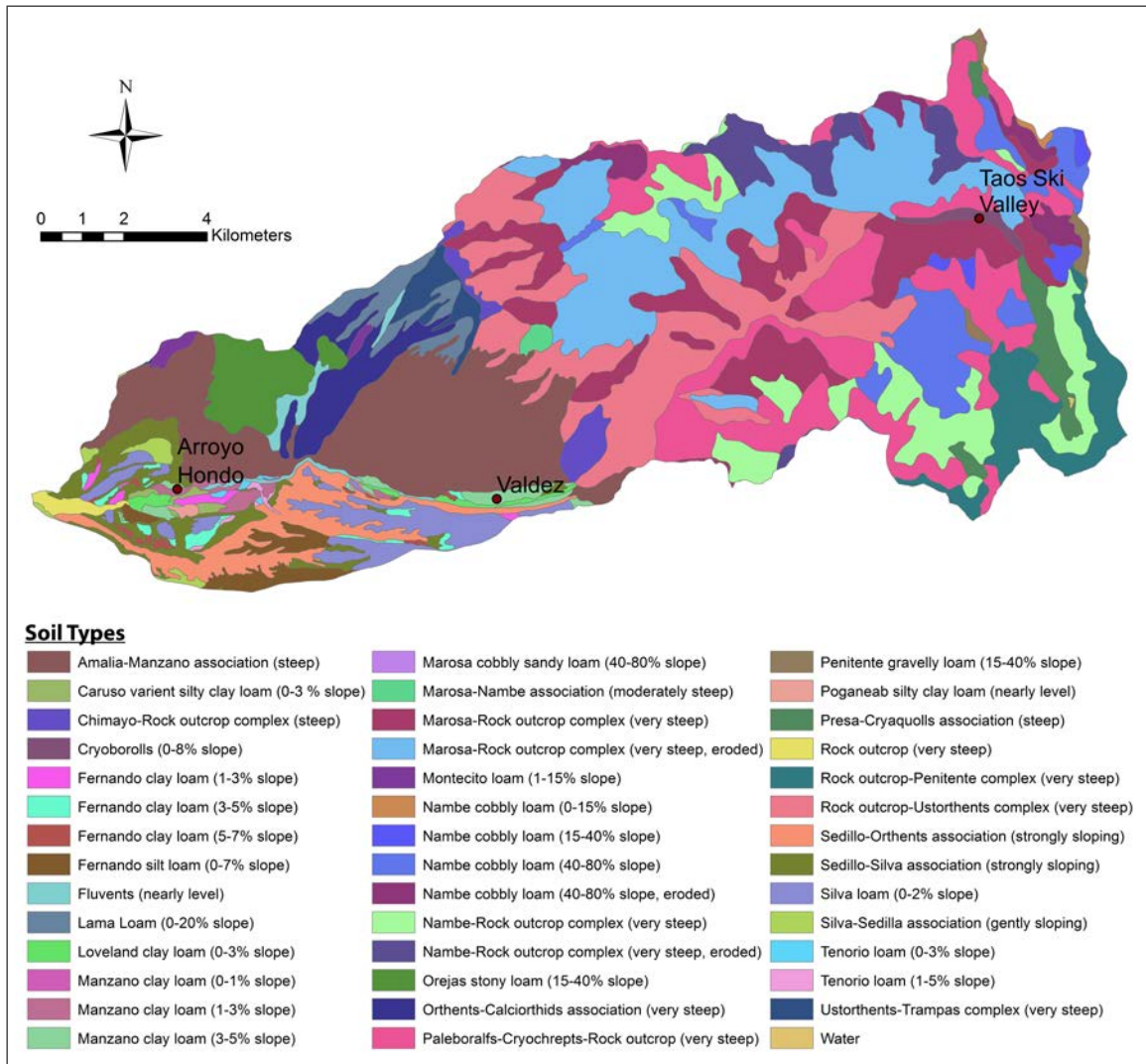
Figure 2.6: Soil map of the Rio Hondo watershed (data from NRCS, 2008).

2.2.3 Soils

Soil development within the watershed can be quite spatially variable. Outside of the mountain block the soils are mostly composed of loams and clay loams on generally shallow slopes. Within the mountain block, soil development is somewhat limited depending on location and slope. Most soils listed in the SSURGO database are listed as cobbly loams or steep rock outcrops (Figure 2.6), suggesting that a large portion of the watershed may have limited soil devel-

opment. One soil pit that was dug at approximately 3,566 m (11,700 ft) during the installation of a weather station showed that soils in the area were at least 1.4 m (4.6 ft) deep and bedrock was not encountered (Figure 2.7). However, the weather station was sited at the flattest spot in the area, which may have been due to a small rotational slide. This would result in artificially deep soils immediately under the weather station where the soil put was dug. Even if this is not the case, the soil map (Figure 2.5) shows a large number of steep rock outcrop associations that indicates significant soil development in the waterhsed, like that seen at the weather station site, is not likely widespread.

2.2.4   Vegetation

Due to the large elevation range, a number of different vegetation types are found within the watershed (Figure 2.8). The highest elevation portions of the watershed are above tree line and support subalpine grassland. Most of the mountain block is forested, consisting of pinyon, juniper, spruce, fir, bristlecone pine, and aspen woodland. The valley consists primarily of pinyon-juniper woodland and shrubland.

Figure 2.7: Soil pit dug into hillslope at about 3,577 m (11,735 ft) with tape measure for scale. Total depth was 1.4 m (4.6 ft) and bedrock was not encountered.

21
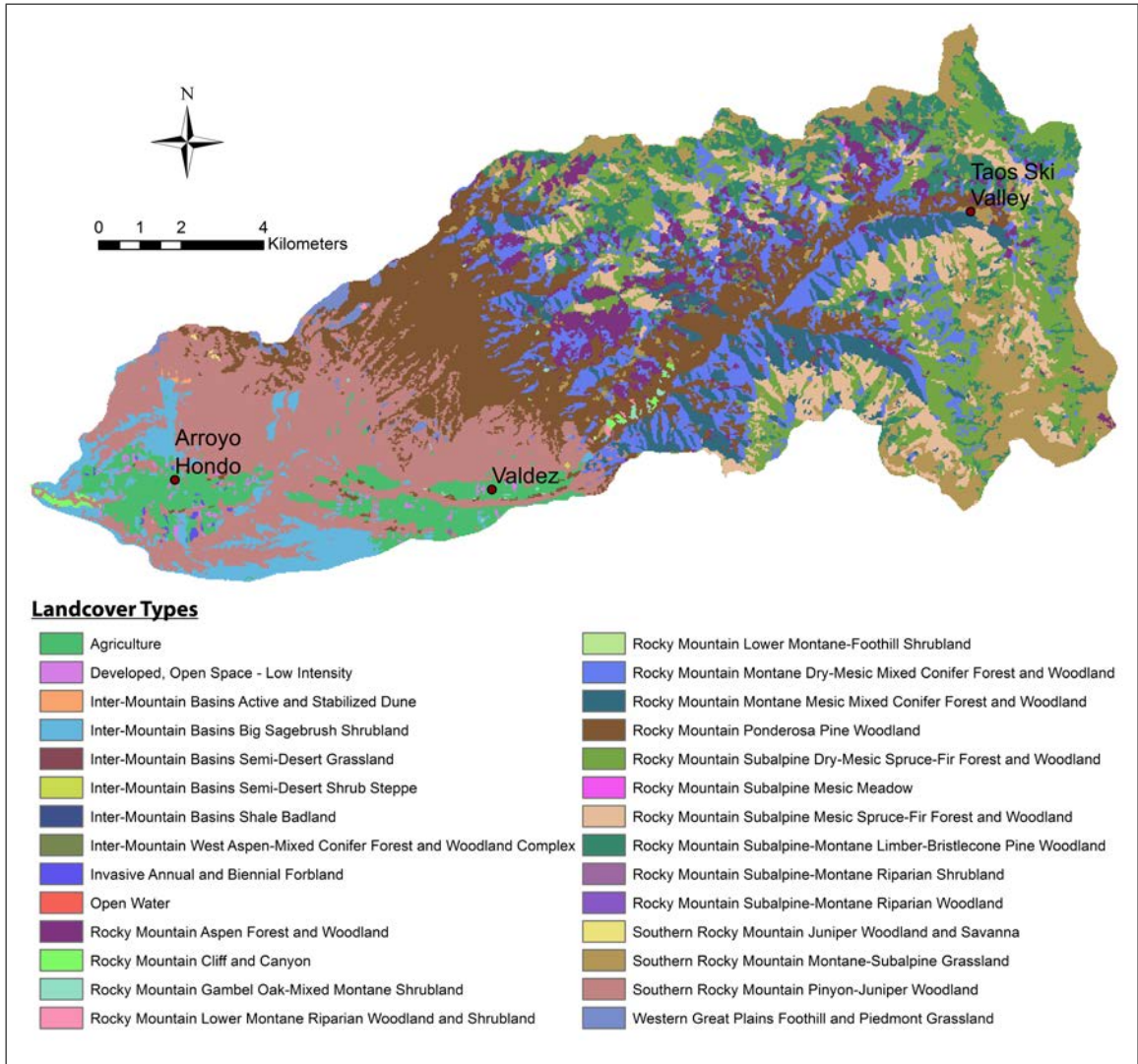
Figure 2.8: Landcover map of the Rio Hondo watershed (data from USGS, 2001).

2.2.5 Land Use

The majority of the watershed (65%) is managed as part of the Carson National Forest and Wheeler Peak Wilderness (Figure 2.9). Taos Ski Valley (TSV) and the Village of Toas Ski Valley (VTSV) comprise the largest development within the mountain block, with a few cabins and condominiums located about halfway up the mountain valley in a location known as "Taos East." One large tract of private land exists at the eastern edge of the watershed and is owned and administered

by the Pattison Family Trust. This land is used for mountain biking and guided horseback riding trips in the summer and snowmobiling in the winter. Due to the limited availability of private land and the steep slopes in the area, development within the mountain block has been limited. Outside of the mountain block the land is mostly privately owned, with some tribal and public lands as well. Private land in the watershed accounts for 34% of the total area, with Indian/Tribal lands making up just over 1%, and public Bureau of Land Management (BLM) lands being less than 1%. According to data from the USGS GAP Analysis Program (2004), agriculture occupies approximately 13% of the private land in the valley, or about 5% of the total watershed area.

The major impermeable areas of the watershed are the Toas Ski Valley parking lots and other development associated with Toas Ski Valley. These areas represent less than 1% of the total area, and therefore do not likely contribute significantly to runoff generation within the mountain block. Paved roads and houses are the largest contributors to impermeable areas outside of the mountian block, but the relatively low density of both precludes substantial generation of runoff from either source.

Agricultural lands are farmed almost exclusively using traditional acequia-style practices that have been present in New Mexico for hundreds of years (Rivera, 1998). Acequias are networks of hand-dug, generally unlined, gravity-fed watercourses. These systems are community-operated and divert water from the main channel to irrigate distant fields. For the Rio Hondo watershed, this diversion is just below the United States Geological Survey (USGS) stream gauging station (8267500). Most acequia-style farming is for subsistence purposes and uses flood irrigation with little-to-no application of fertilizers or pesticides. Acequias are
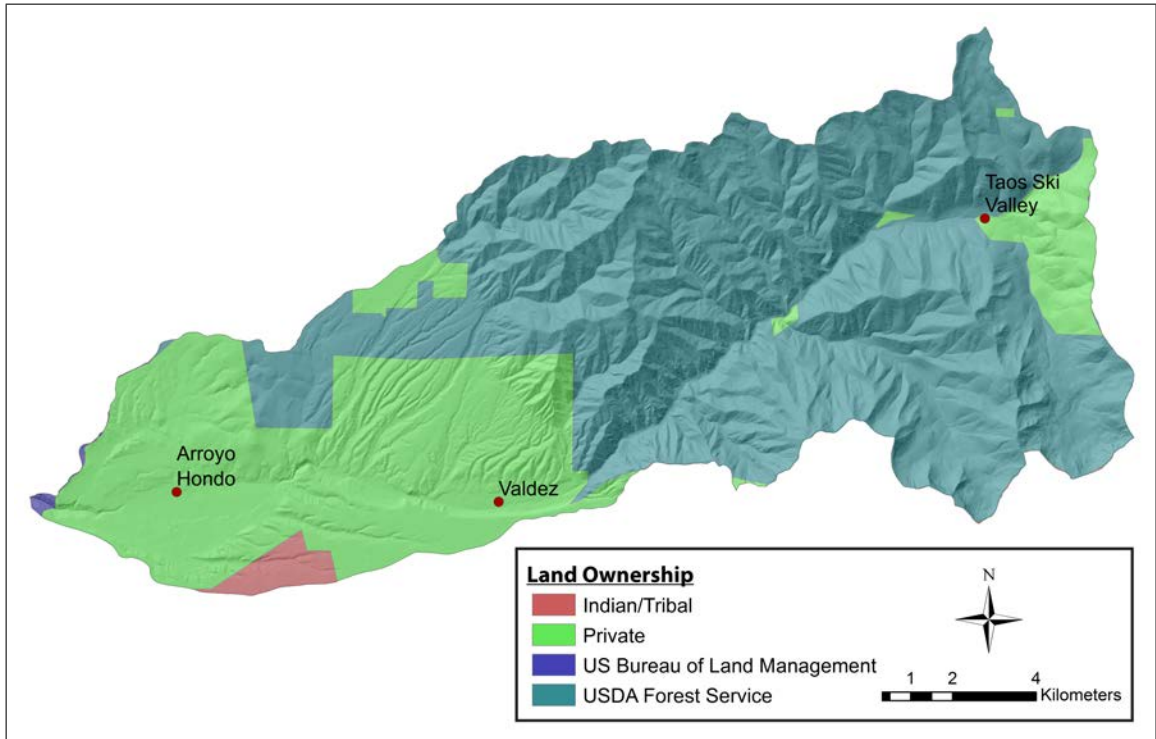
Figure 2.9: Land ownership in the Rio Hondo watershed by entity.

unique in New Mexico, as the water is shared equally among those in the community instead of allowing those with senior water rights to receive their full delivery before those with junior water rights during times of drought, a practice known as priority administration. A much more detailed account of acequia history and operation can be found in *Acequia Culture: Water, Land, and Community in the Southwest* (Rivera, 1998).

2.2.6   Water Use

According to the Taos Regional Water Plan (DBS&A, 2008), about 90% of water used in Taos County comes from surface water. However, nearly all municipal, domestic, and commercial water is derviced from groundwater. Although these numbers were not developed for the Rio Hondo watershed specifically, the

24

actual numbers are likely very close. The water supply for the Village of Taos Ski Valley is a developed spring near the Williams Lake trailhead, with an average flow of approximately 128,000 m^3/year (DBS&A, 2008). Residences that are not part of the village distribution system obtain their water from shallow wells drilled into the bedrock Unfortunately, no well information was readily available. The ski valley uses surface water in the winter for snow-making operations, and is the only known user of surface water in the mountain block (excluding the village sewage treatment plant which discharges to the Rio Hondo).

Water use outside of the mountain block is mostly confined to the areas serviced by the local acequia associations. Acequia communities have been built around the construction, maintenance, and management of Spanish-style hand-dug irrigation canals. There are three main acequia communities in the Rio Hondo watershed: Arroyo Hondo, Valdez, and Des Montes. Farmers in these communities typically employ flood irrigation. As in the mountain block, nearly all of the water for domestic use comes from private wells or small municipalities.

2.2.7 Water Quality

Surface-water quality within the Rio Hondo watershed is generally very good with low amounts of total dissolved solids (TDS) (38 to 240 mg/L, this study). The largest point source on the Rio Hondo is the Village of Taos Ski Valley sewage treatment plant that discharges just below Taos Ski Valley. The first treatment plant was built in 1967 and replaced in 1983 due to concerns that phosphorus and fecal coliform loading was too high. The new treatment plant greatly improved the water quality below the ski valley and has remained in complaince

with state regulations ever since. The current treatment plant services approximately 90% of the residents of the Village of Taos Ski Valley (Donald Schieber, VTSV, personal communication), and is scheduled to be replaced by 2020 (Joseph Apodaca, VTSV, personal communication). Other non-point sources include septic systems from the residences that are not serviced by the village treatment plant, although the number of these is fairly low and many of the residences are only occupied seasonally. Deicing activities in the watershed consist of spreading 3/8" pea gravel on the roads for traction and chemical deicers are not applied (Ray Keen, VTSV, personal communication). There is potential for chemical deicers to be transported into the watershed by vehicles that have traveled on roads where they have been applied. However, surface runoff samples (this study) do not indicate the presence of chemical deicers, and therefore they are not considered to be a source of contamination. One other potential non-point source is runoff from the parking lots but the area is relatively small and likely not a significant source of contamination.

Outside of the mountain block, agricultural runoff and discharge from septic systems are the primary non-point sources. Average nitrate concentration in the lower Rio Hondo (outside of the mountain block) is <1 mg/L (this study), suggesting that these sources have relatively little impact. Low nutrient loads are likely due to the low population density and limited application of fertilizers. High temperatures in the lower section of the river due to low flows from diversions, irrigation returns, and depletion of bank shade trees have caused the Rio Hondo to be listed by the New Mexico Surface Water Quality Bureau (NM-SWQB) as one of the tributaries to the Rio Grande regulated for total maximum daily load (TMDL) for temperature (NMSWQB, 2004). However, it appears that

there has been no consistent water quality sampling in the Rio Hondo by regulatory agencies since the NMSWQB effort in 2000 (NMSWQB, 2004b), with most water quality sampling currently completed by non-profit groups such as Amigos Bravos. Groundwater in the watershed is generally of very high quality, with elevated pH and arsenic concentrations in the deep valley aquifer (Drakos et al., 2004a). Water-quality data collected from wells in Valdez, Arroyo Hondo, and Arroyo Seco did not show any constituents exceeding Environmental Protection Agency primary drinking water maximum contaminant levels (MCLs) (DBS&A, 2008).

2.3 Hydrogeological Framework and Previous Investigations

2.3.1 Surface Water

The Rio Hondo flows approximately 32 km (28 mi) from the Sangre de Cristo Mountains in the east to the Rio Grande in the west. It is fed by numerous perennial tributaries, including South Fork, Manzanita Creek, Yerba Creek, and Italianos Creek, all located within the mountain block (Figure 2.1). Tributaries in the valley only appear to flow during large storm events. A USGS stream gauging station (USGS 08267500) measures the average daily discharge from the Rio Hondo just before it exits the mountain block and has been continuously monitored since 1934. Two other USGS gauging stations were located on the Rio Hondo just east of Valdez (USGS 08268200) and near Arroyo Hondo (USGS 08268500), but those have been discontinued. Yearly flow for the Rio Hondo as it exits the mountain block is approximately 28,853,608 to 31,889,206 m^3/yr (23,392 to 25,853 acre-ft/yr) using the median and mean of the streamflow dataset (Johnson, 1999). Numerous acequias divert water from the Rio Hondo (Figure
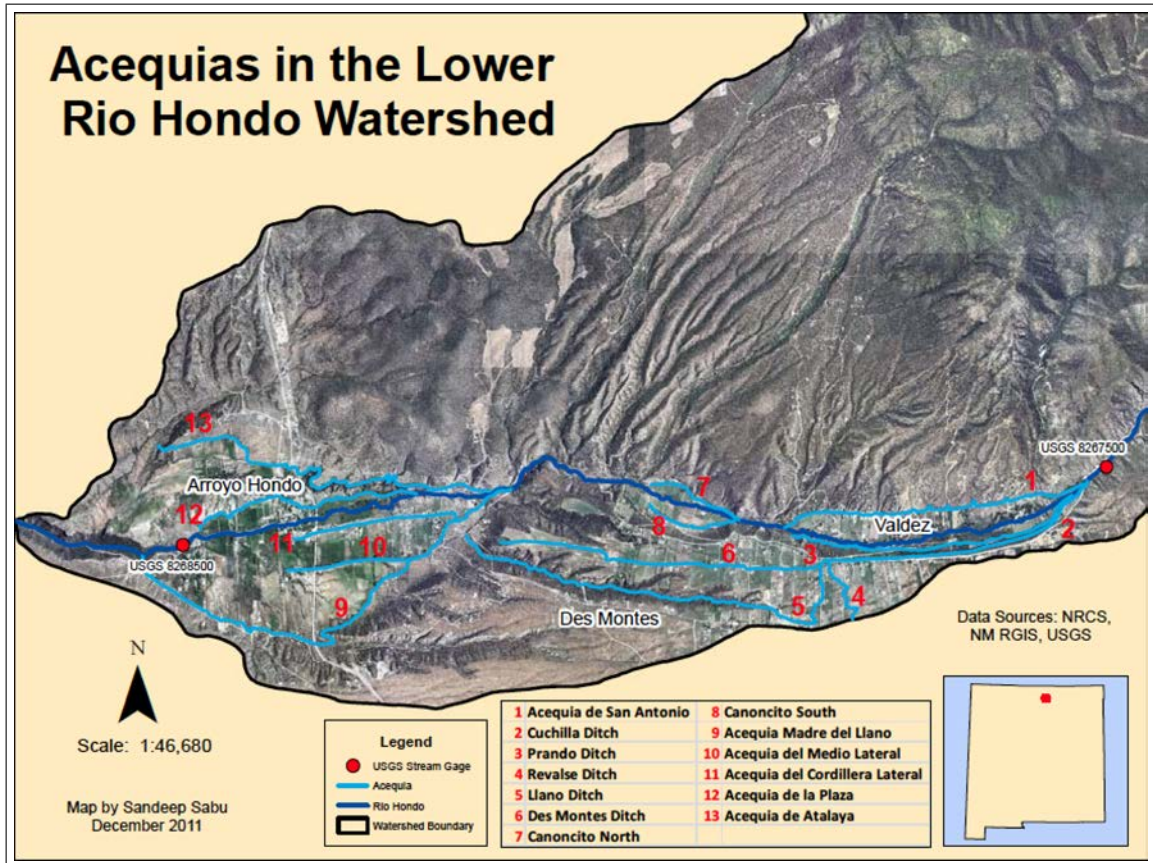
Figure 2.10: Map of acequias located within the Rio Hondo watershed. From Sabu et al. (2012)

2.10) below the current USGS stream gauge to irrigate approximately 11.6 km^2 (2,870 acres) (Johnson, 1998) in the valley. The largest surface water body in the watershed is Williams Lake, a tarn located at 3,365 m (11,040 ft) within a closed section of the basin. Williams Lake is fed by two streams and, likely, melt from a rock glacier (Clark & Read, 1972; Jerry Fairley, personal communication) on the western side of the cirque (Figure 2.11).

2.3.2 Groundwater

Groundwater studies in the area have primarily focused on the Taos Valley, sometimes including Rio Hondo Valley below the mountain front. The first
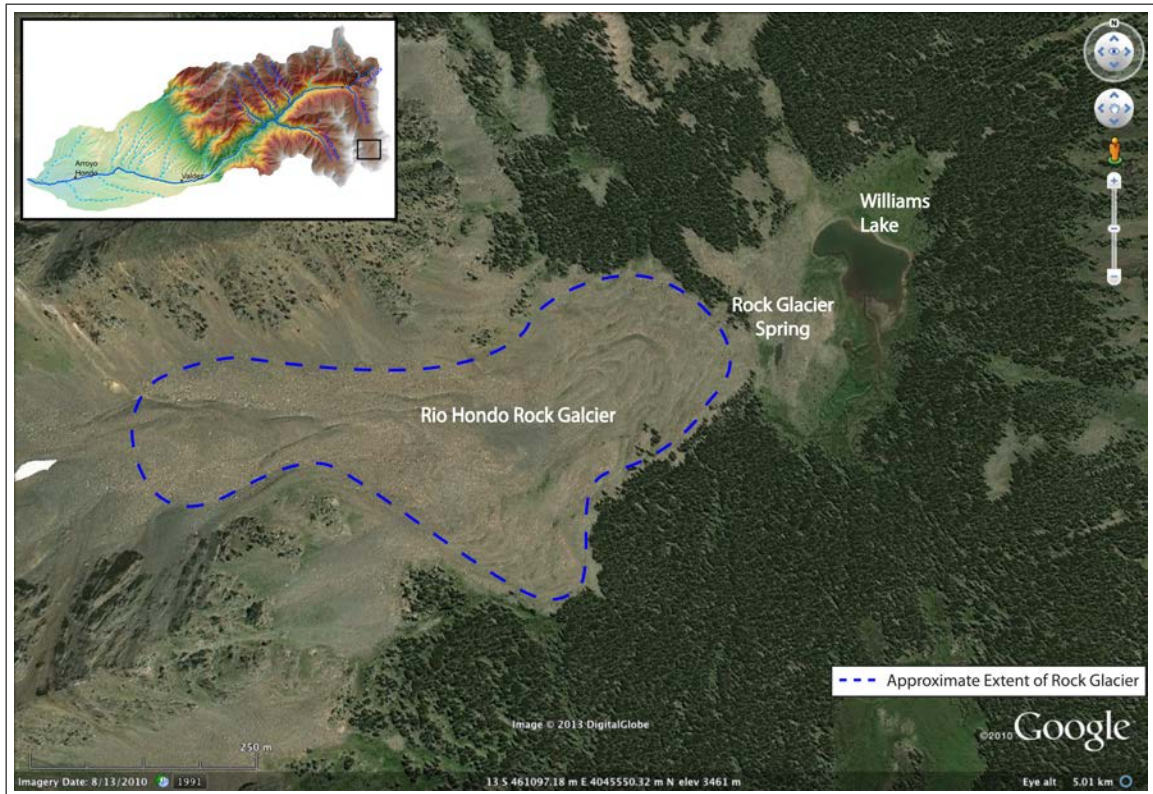
Figure 2.11: Aerial photograph of Williams Lake area showing approximate extent of Rio Hondo rock glacier. Notice lobes near the base of the rock glacier that are indicative of flow. A spring formed from rock glacier melt is located near the toe and has consistently colder temperatures and differing geochemistry than Williams Lake. Inset shows location within the Rio Hondo watershed. Image modified from Google Earth (2010).

hydrogeological study in the area was performed by Winograd (1959) and focused on the availability of groundwater for irrigation in the Sunshine Valley to the north of the Rio Hondo. It also examined the potential effects that heavy groundwater withdrawals would have on the Rio Grande and Red River. Coons & Kelly (1984) developed a conceptual model of the regional groundwater flow system consisting of a two-layer aquifer system: a shallow unconfined aquifer and a deeper semi-confined aquifer. They showed that the regional groundwater flow is to the south-southeast on the western side of the Rio Grande, and to the west-southwest on the eastern side. Bauer et al. (1999) conducted a study of the

hydrogeology in the southern portion of the Taos Valley and found evidence that supported the conceptual model developed by Coons & Kelly. They also noted the prevalence of fault-related fracture zones within bedrock aquifers, resulting in areas with high hydraulic conductivity and therefore low hydraulic gradients.

Burck et al. (2004) published a regional groundwater flow model for Taos which incorporated data from previous studies as well as from new Bureau of Reclamation wells. The authors stated that the model simulated observed heads and groundwater discharges reasonably well, however the value for mountain front recharge was chosen based off of calibration necessity and was quite similar to the rate of evapotranspiration in the valley. The same year Drakos et al. (2004a) published results from a basin-wide study identifying a shallow, unconfined aquifer consisting of the Servilleta Formation and overlying alluvium, and a deep, semi-confined aquifer consisting of Tertiary-age rift-fill sediments such as the Tesuque and Picuris Formations. The authors stated that the vertical hydraulic conductivity of the basalts can be very low, which was supported by Bauer et al. (1999). The vertical hydraulic conductivity of the basalt is dependent on factors such as fractures and cooling joints that can vary both spatially and from flow to flow.

A study of the Arroyo Seco area just to the south of the Rio Hondo was performed by Rawling (2005). He concluded that the general groundwater flow direction was from east to west in the northern part of the Taos Valley and to the southeast in the southern portion of the valley (Figure 2.12). However, structures such as the Sangre de Cristo fault, the Airport fault near Arroyo Hondo, and the Cerro Negro dacite appear to significantly affect groundwater flow patterns. This is manifested by aquifer compartmentalization (Drakos, 2004a), locally steep horizontal hydraulic gradients near the faults (Johnson et al., 2009), and regions with
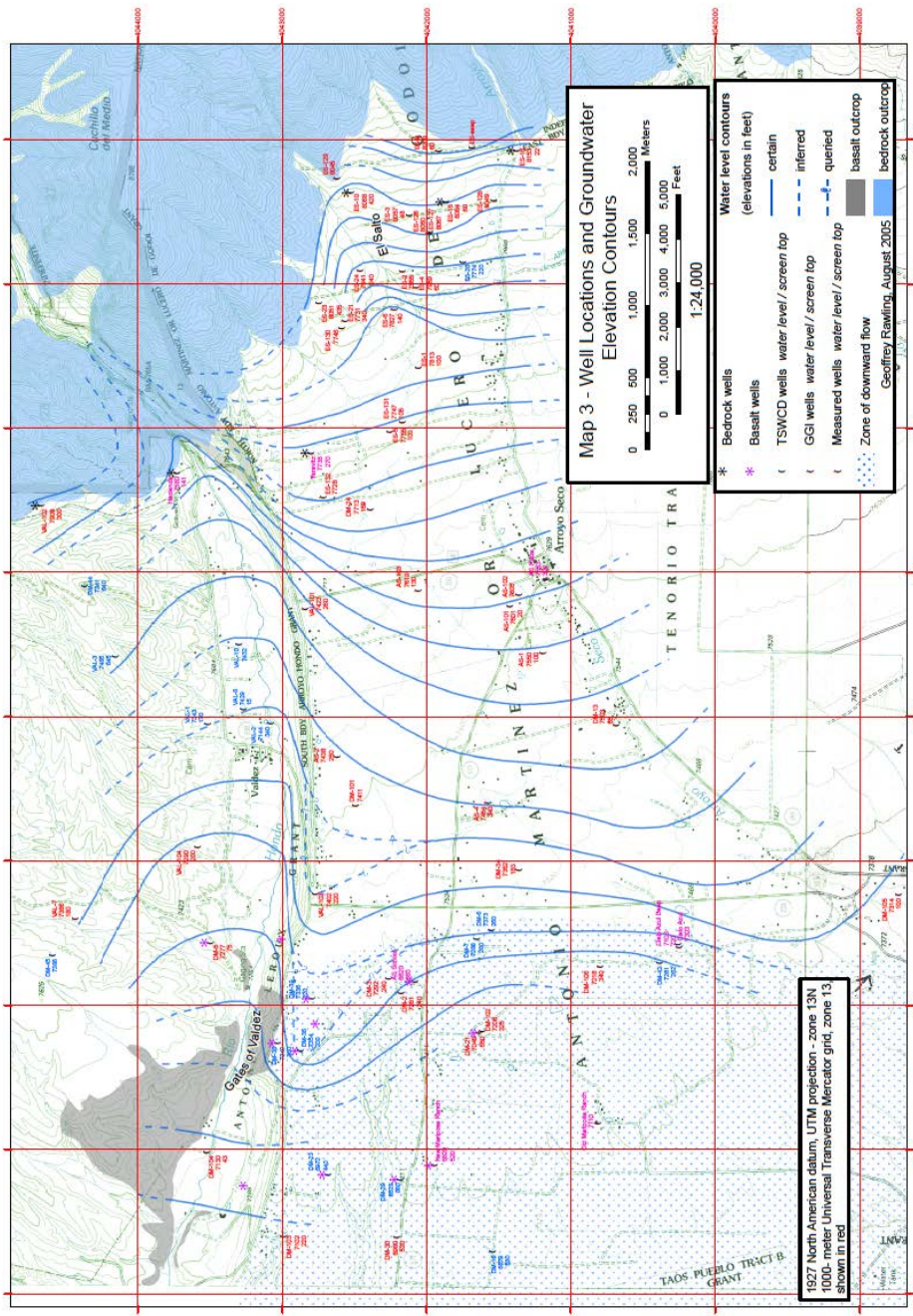
Figure 2.12: Potentiometric surface map created by Rawling (2005). Rio Hondo is strongly gaining within the mountain block (contours pointing upstream) and continues to gain water from the southern portion of the watershed to the Gates of Valdez.

31

strong vertical hydraulic gradients (Rawling, 2005). The Gates of Valdez, located just west of Valdez and formed by incision of the Rio Hondo into the Cerro Negro dacite complex, was identified as one such region, with predominantly downward flow due to the high transmissivity of the material. Pumping tests in the area indicated horizontal hydraulic conductivity values ranging from 0.1 to 2.8 m/day (0.4 to 9.2 ft/day), depending on depth. Estimated travel times from the mountain front to the town of Arroyo Seco using average hydraulic gradients and effective porosities were calculated between 300 to 10,000 years. These calculated travel times were discounted because recharge to the shallow and deep portions of the groundwater system was interpreted to be on a time scale of less than five to ten years based on tritium data collected by Drakos et al. (2004a). However, a tritium sample collected during the same study from the Rio Hondo had a value of 25.8 Tritium Units (TU) which can be interpreted to be mixture of modern and 1960s recharge (Clark & Fritz, 1997). Rawling's interpretation appears to ignore potential mixing of young and old water. The potentiometric surface map included in the report (Figure 2.12) indicates the Rio Hondo is a strongly gaining stream as it exits the mountain block (contours pointed upstream). The stream also appears to be gaining water from the southern portion of the valley, likely due to an increased gradient from the elevated stream terrace that is present in that area.

2.3.3 Surface-Water/Groundwater Interactions

Johnson (1999) performed an assesment of surface water in the Taos area. Using minimum stream-discharge values during the months of December through February, she suggested that baseflow can contribute from 9 to 20% of annual

32

discharge in the upper reaches of most basins in the Sangre de Cristo mountains where rocks with high permeability (high fracture density) and relatively low storage exist. Her work also indicated that the highest baseflow estimates range from 30 to 37% in places like the lower Rio Hondo where the streams cross Santa Fe Group basin fill. This is consistent with winter streamflow data that show the downstream Arroyo Hondo gauging station measured 1,356,838 m^3 (1,100 acre-ft) more than the upstream Valdez gauging station (Johnson, 1998). However, these conclusions are in conflict with Rawling's (2005) interpretations that the Rio Hondo is losing or approximately neutral west of the Gates of Valdez, and that the Precambrian basement rocks are essentially aquicludes despite their highly fratured nature (Winograd, 1959, DBS&A, 2008). This illustrates the complexity of the watershed and the need to take a new approach in examining the interactions between groundwater and surface water in the watershed.

2.3.4 Moving from a Valley-Centered to a Mountain-Centered View

While the previous studies have done a good job of improving our understanding of the hydrogeology of the area, they all have one thing in common: a valley-centered approach. This can be quite useful for determining groundwater resources within the valley, but it has been shown that the predominant source of water use in the area is surface water. Therefore, it seems that a better understanding of how streamflow is generated within the mountain block is needed, one that specifically incorporates the mountain block. Instead of working from the valley up, my approach was to work from the mountain block down. To accomplish this I collected samples along the Rio Hondo from the headwaters in the mountain block to the confluence with the Rio Grande in the valley. In

addition, I collected samples of precipitation, groundwater, springwater, runoff, and soil water throughout the watershed to determine if any spatial and/or temporal patterns in geochemisty, stable isotopes, or radiometric ages dates existed. The following chapters discuss the results from my geochemical sampling and indicate that, while only one third of the precipitation falls during the winter and spring months, nearly all of the water in the system is sourced from that period. Therefore, climatic perturbations to the winter and spring months can have profound impacts on streamflow generation in the system. However, the full effects on the surface water system may be delayed if a proportion of the water is dervived from long-residence-time groundwater flow paths discharging to the stream. This additional buffering capacity may affect predictions of water supply changes and how watersheds will respond to future climate perturbations.

CHAPTER 3

GEOCHEMICAL AND STABLE ISOTOPIC CHARACTERIZATION OF WATERS WITHIN THE RIO HONDO WATERSHED, NORTHERN NEW MEXICO

3.1   Introduction

This chapter uses geochemistry and stable isotopic data to test the transferability of the conceptual model developed by Frisbee at al. (2011) for the Saguache Creek watershed by applying it to the Rio Hondo watershed, and identifies spatial geochemical patterns between groundwater, surface water, and spring water. Hydrographs are also used as qualitative indicators of processes operating at the watershed scale. The Rio Hondo watershed is similar to the Saguache Creek watershed in that both are snow-covered, high-elevation mountain catchments, but the Rio Hondo watershed is much smaller, steeper, and geologically distinct from the Saguache Creek watershed. In addition, the Rio Hondo watershed also has a greater degree of anthropogenic impacts that must be taken into account.

Stable isotopes of water ^{18}O and ^{2}H were used as they provide information on the timing of recharge and physical processes such as evaporation. Geochemistry can provide insight to the residence time of different waters, as geochemical reaction kinetics control the rate at which solutes are released during weathering reactions (Lasaga, 1984; Bricker & Jones, 1995). It is unlikely that surface

water and groundwater would have similar geochemical signatures given their drastically different residence times, even if one assumes the very conservative residence time of days to months for all subsurface waters. Therefore, if surface-water and groundwater do not show similar geochemistry there are likely limited contributions of groundwater to surface-water. However, if there are significant contributions from deep groundwater, the geochemistry of the stream would likely be controlled or strongly influenced by this flux of old, evolved groundwater.

3.2 Methods

3.2.1 Surface water, groundwater, and spring samples

Samples of surface water, groundwater, and spring water, denoted with sample prefixes of RHR, RHW, and RHS, respectively, were collected throughout the watershed seasonally from July 2010 to March 2012, and monthly to sub-monthly from May 2012 to November 2012. Additional sampling rounds were completed in March 2013 for comparison with March 2012 data and in June 2013 to collect snowmelt recharge from passive capillary samplers (see Soil Moisture section below). Field parameters of temperature ($^{\circ}$C), pH (SU), specific conductivity (μS/cm @25°C), dissolved oxygen (DO) (%), and oxidation reduction potential (ORP) (mV) were collected using a YSI Professional Plus that was calibrated prior to each sampling trip. Samples were either field or lab filtered to 0.2 μm and analyzed for general chemistry at the University of New Mexico (prior to 2012) and the New Mexico Bureau of Geology and Mineral Resources Analytical Chemistry Lab (2012 and 2013) using approved methods (see Appendix C for full list of consistuents and analytical methods). Geochemical data collected in

the watersehd prior to 2012 has been presented by Harding (2012) and therefore will not be presented again here. In addition, samples with charge imbalances greater than 5% were excluded from additional analysis.

Stable isotopes ^{18}O and ^{2}H were measured using a Picarro L1102-*i* Isotopic Water Liquid Analyzer cavity ringdown spectrometer at the New Mexico Tech Stable Isotope Laboratory. Samples were run a total of six times with the first three runs excluded due to possible system memory effects, and the sample result being an average of the last three runs. Corrections were applied using internal standards and results are reported in per mil notation (‰) relative to Vienna Standard Mean Ocean Water (VSMOW).

3.2.2 Precipitation

Precipitation was collected seasonally (early winter, late winter, spring, summer/monsoon) from six bulk collectors (Earman et al., 2006) located from 3,643 m (ISO-01) to 2,057 m (ISO-06) with roughly equal elevation spacing. Collectors were 4 in diamater acrylonitrile butadiene styrene (ABS) or polyvinyl chloride (PVC) sealed on one end with a cemented cap. The PVC collectors were painted black to accelerate melting. Mineral oil was placed in the collectors with a sufficient thickness to prevent evaporation (Friedman, 1992). Sample volumes were measured to provide a weighted seasonal average, with general chemistry, ^{18}O and ^{2}H analyzed using the methods described above (see Appendix B for full list of consistuents).

3.2.3 Soil Moisture

Grab samples of soil were collected at the two highest precipitation collector sites (ISO-01 and ISO-02) and vacuum distilled to obtain the pore water according to the procedures described by Knowlton (1990). Modified passive capillary samplers (PCAPS) were installed at these two locations from October 20th, 2012 to June 29th, 2013 according to the methods described by Frisbee et al. (2009b) in order to obtain a time-integrated snowmelt signature in the soil. Each PCAPS installation contained four wick samplers with the wicks placed into two specific soil horizons at each site (Figure 3.1). Opposite walls of the soil pit had a wick placed in both the upper and lower soil horizon. PCAPS-1 had two upper wicks placed in a clay loam at 15 and 18 cm below ground surface (bgs), and two lower wicks placed in a silty clay at 49 and 51 cm bgs. PCAPS-2 had two upper wicks placed in a silty clay at 25 cm and 29 cm bgs, and two lower wicks placed in a clay loam at 41 cm and 42 cm bgs. Samples obtained from the PCAPS were measured for general chemistry, ^{18}O and ^{2}H using the methods described above, whereas only ^{18}O and ^{2}H were measured in soil grab samples.

3.2.4 Streamflow

A USGS stream gauge (08267500) has been continuously monitoring average daily discharge (cubic feet per second or cfs) from the Rio Hondo since 1934, at a location just upstream of the mountain front. Streamflow data were obtained from the station for the period of record. The mean of the average daily streamflow for each day of the year (excluding leap days) was calculated and then normalized to the maximum average daily mean for the same dataset. The same

38
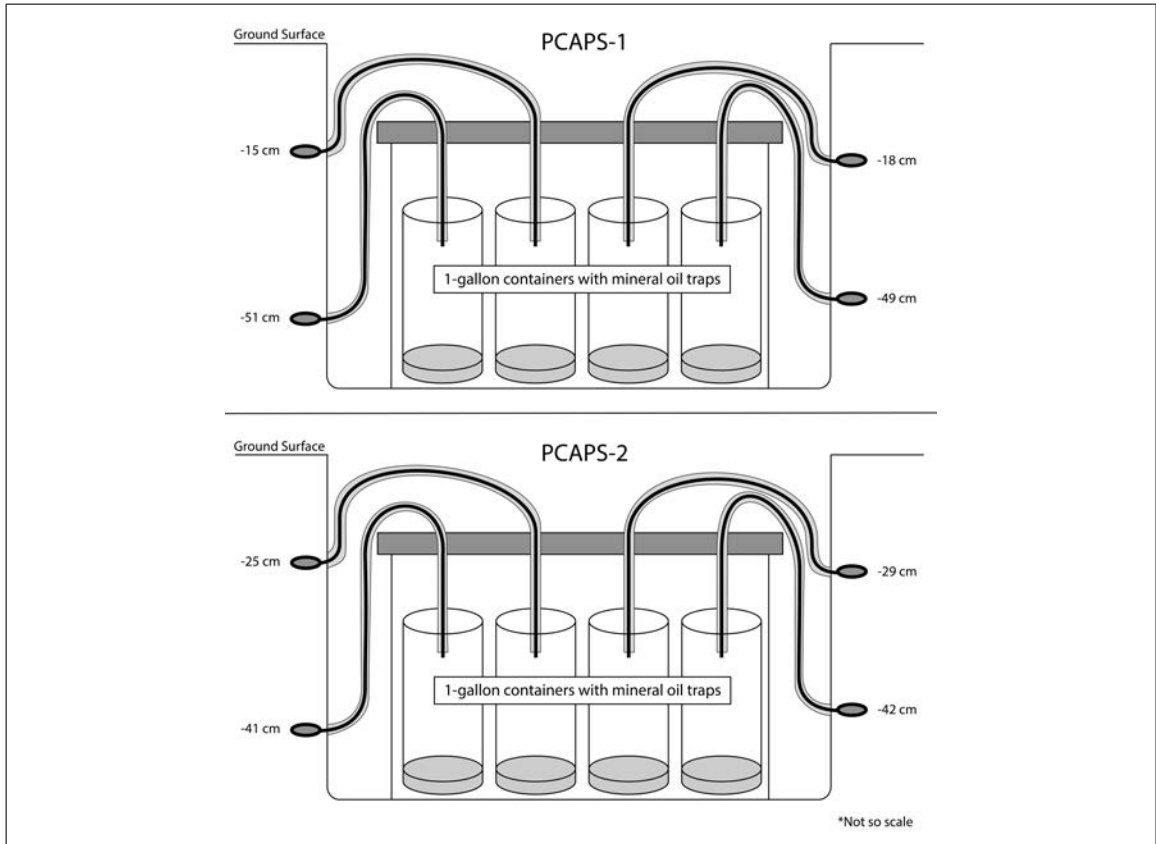
Figure 3.1: Schematic of passive capillary samplers (PCAPS) installed in the watershed. PCAPS-1 and PCAPS-2 were co-located with precipitation collectors ISO-01 and ISO-02, respectively.

was done for hydrographs from the mountain watersheds of El Rito (1931-1950) and Rio Ojo Caliente (1932-2005) located in northern New Mexico, and Saguache Creek (1910-2007) located in southern Colorado. This allowed comparison of the hydrographs, even though absolute flows between streams were not of the same magnitude. The maximum average daily streamflow used to normalize the average daily streamflow was 127.2 cfs, 198.5 cfs, 148.9 cfs, and 419.9 cfs for the Rio Hondo, Saguache Creek, El Rito, and Rio Ojo Caliente, respectively.
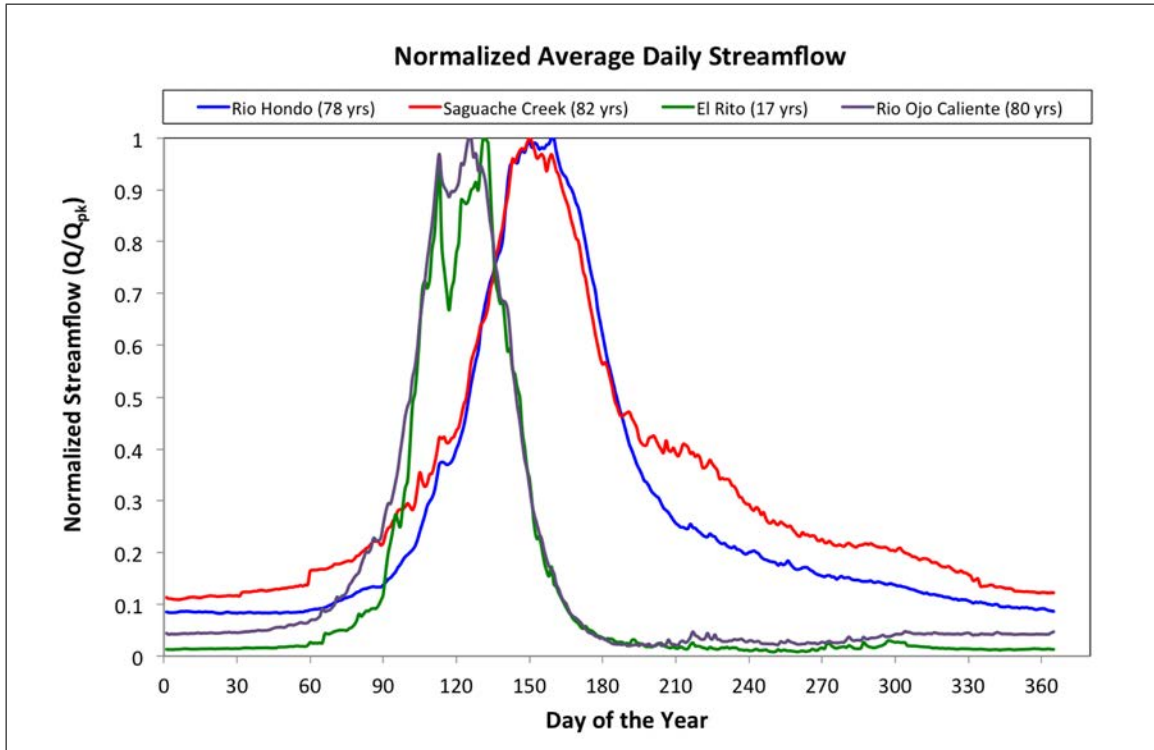
Figure 3.2: Normalized average daily streamflow for Rio Hondo, Saguache Creek, El Rito, and Rio Ojo Caliente. Previous research has shown Saguache Creek has significant groundwater contributions to surface water (Frisbee et al., 2011). The similar shape and timing of the Rio Hondo and Saguache creek watersheds suggest similar processes may be occuring in the two watersheds, despite differing geologic conditions. El Rito and Rio Ojo Caliente are located on the opposite side of the southern San Luis Valley from the Rio Hondo, in the Tusas Mountains. The sharp rise and fall of the hydrographs with little to no baseflow outside of the snowmelt season suggests limited groundwater connectivity with surface water in these watersheds.

3.3   Results and Discussion

3.3.1   Hydrographs

Normalized mean daily flow hydrographs from the Rio Hondo, Saguache Creek, El Rito, and Rio Ojo Caliente are shown in Figure 3.2. The shape and timing of the Rio Hondo and Saguache Creek curves are nearly identical, with steady rise and recession of flow during the snowmelt period. Baseflow is also present

for both streams, at approximately 9% of the peak flow or greater using straight-line analysis, suggesting there is significant storage and release from storage in the two systems. Hydrographs from El Rito and Rio Ojo Caliente do not indicate significant storage, as they have sharp rises and recessions of flow during the snowmelt season and there is little baseflow outside of the snowmelt season. The rise in baseflow for El Rito and Rio Ojo Caliente during the late summer is attributable to monsoonal storms.

The similar shape and timing of the Rio Hondo and Saguache Creek hydrographs suggest related processes are operating in both drainages. Previous work in the Saguache Creek watershed has shown significant groundwater contributions to surface water during the later parts of the year (Frisbee et al., 2010). The Saguache Creek watershed (1,670 km^2) is nearly ten times larger than the Rio Hondo and is dominated by felsic volcanic tuffs erupted from the San Juan Volcanic Field (Steven and Lipman, 1976; Lipman and McIntosh, 2008), a geologically distinct terrain from the Precambrian metamorphics and Tertiary igneous intrusions found in the Rio Hondo. However, heavily fractured units are found in both watersheds. While factors such as elevation, slope, aspect, vegetation, etc., can influence streamflow, the presense of fracture networks appear to be a significant control on streamflow generation in both mountain systems.

3.3.2 Stable Isotopes

Precipitation stable isotopes showed a strong seasonal signature of lighter isotopic compositions in the winter and spring and heavier isotopic compositions in the summer and fall. These results are consistent with trends in the published literature (Clark and Fritz, 1997). Volume-weighted averages of δ^{18}O for winter
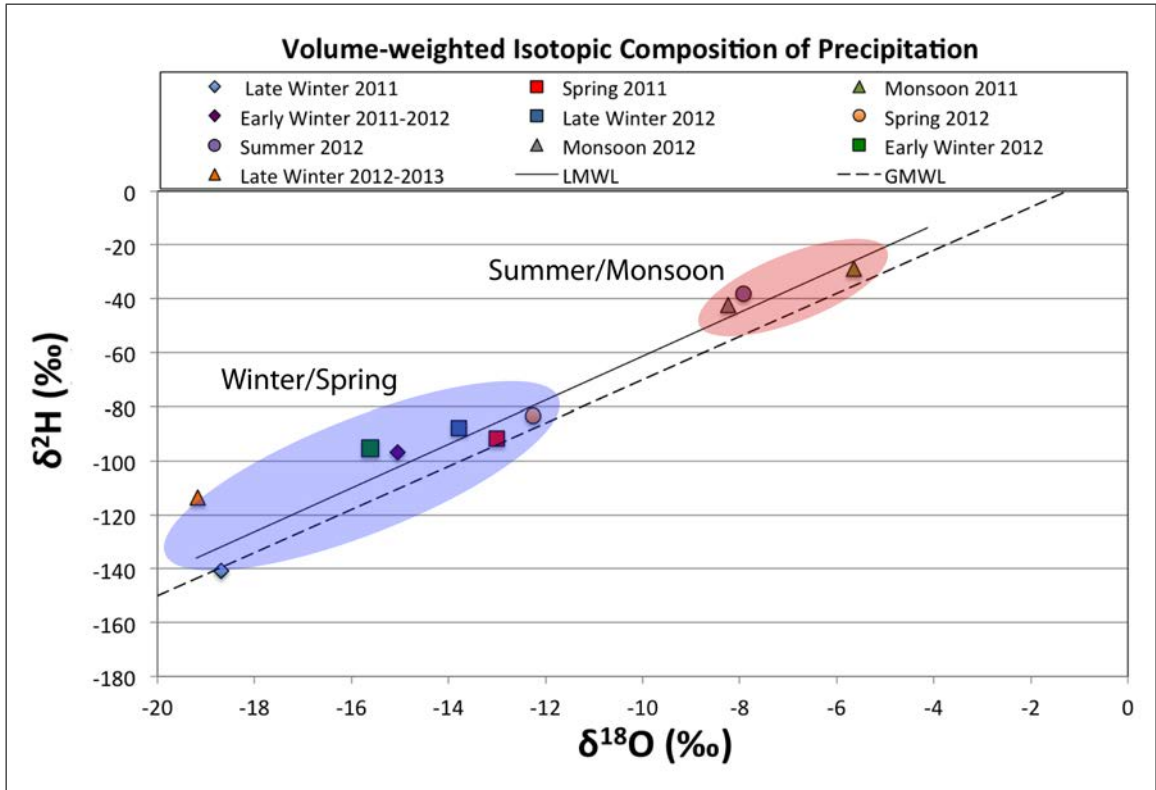
Figure 3.3: Volume-weighted isotopic composition of precipitation. Shaded areas show approximate seasonal precipitation range.

and spring precipitation fell between approximately -19‰ and -12‰, while summer and monsoonal precipitation values ranged from -8‰ to -5‰ (Figure 3.3). Winter and spring precipitation tends to originate from the Pacific Ocean, and by the time storms reach New Mexico they have already rained out and fractionated, resulting in a light isotopic composition. In comparison, summer/monsoonal storms start from the Gulf of California, Gulf of Mexico, and localized orographic lifting mechanisms. The shorter travel distance coupled with the greater amount of energy (higher temperature storms) explains why the summer/monsoonal storms are so much more enriched in heavy isotopes compared to the winter and spring precipitation fronts.

Despite the relatively large fluctuations in isotopic composition of sea-
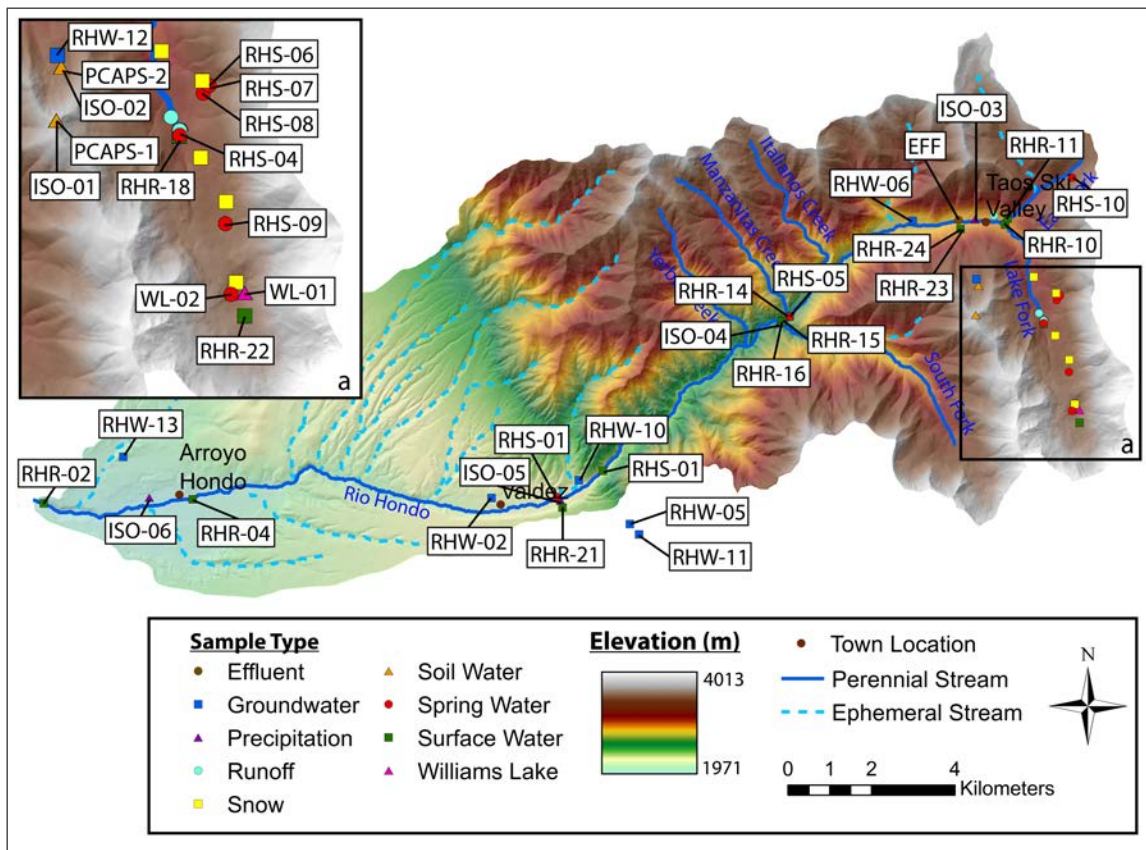
Figure 3.4: Major sampling locations in the Rio Hondo watershed with sample designation shown.

sonal precipitation, measured values of $\delta^{18}O$ and δ^2H are remarkably consistent for surface water, groundwater, and spring water samples (Table 3.1). Average $\delta^{18}O$ for surface water was -14.03‰ with a standard deviation of 0.73‰ (n=191). One surface water sampling location, RHR-20, was excluded from this and subsequent calculations, as it was collected from the Arroyo Seco watershed directly to the south and consistently showed significantly heavier isotopic ratios than were measured at any of the streams within the watershed. Groundwater samples had an average $\delta^{18}O$ of -13.87‰ with a standard deviation of 0.99‰ (n=79). $\delta^{18}O$ in springwater had an average value of -14.01‰ with a standard deviation of 0.75‰ (n=66). One spring water sample, RHS-03, was excluded from this and

Table 3.1: Mean isotopic compositions for surface water, spring water and groundwater at sampling locations. Values indicate that essentially all water is sourced from winter/spring precipitation. See Figure 3.4 for sampling locations.

Sample Type	Sample ID	$\delta^{18}O$ Mean	δ^2H Mean	n
Surface Water	RHR-01	-13.98 ($\pm$0.69)	-93.49 ($\pm$1.77)	18
	RHR-02	-13.67 ($\pm$ 0.67)	-93.09 ($\pm$1.98)	17
	RHR-04	-13.81 ($\pm$0.70)	-92.79 ($\pm$1.93)	17
	RHR-10	-14.06 ($\pm$0.71)	-93.39 ($\pm$2.20)	17
	RHR-11	-14.52 ($\pm$0.83)	-97.97 ($\pm$2.47)	17
	RHR-14	-14.36 ($\pm$0.79)	-95.30 ($\pm$2.58)	16
	RHR-15	-14.11 ($\pm$0.76)	-94.95 ($\pm$2.25)	16
	RHR-16	-13.77 ($\pm$0.76)	-91.50 ($\pm$2.56)	18
	RHR-18	-13.91 ($\pm$0.58)	-92.66 ($\pm$3.00)	13
	RHR-21	-14.41 ($\pm$0.73)	-92.92 ($\pm$1.23)	9
	RHR-22	-13.89 ($\pm$0.85)	-90.22($\pm$5.33)	8
	RHR-24	-14.40 ($\pm$0.67)	-93.69 ($\pm$1.64)	8
Spring Water	RHS-01	-14.07 ($\pm$0.71)	-93.97($\pm$2.22)	17
	RHS-05	-14.14 ($\pm$0.83)	-94.74 ($\pm$2.28)	12
	RHS-06	-14.29 ($\pm$0.58)	-93.50 ($\pm$1.04)	7
	RHS-07	-13.86 ($\pm$0.82)	-88.07 ($\pm$0.72)	4
	RHS-08	-13.99 ($\pm$0.58)	-88.07 ($\pm$0.77)	5
	RHS-09	-14.24 ($\pm$0.51)	-91.87 ($\pm$2.11)	4
	RHS-10	-15.52 (N/A)	-97.92 (N/A)	1
Groundwater	RHW-02	-14.31 ($\pm$0.52)	-96.31 ($\pm$1.17)	11
	RHW-05	-13.62 ($\pm$1.02)	-93.99 ($\pm$3.33)	12
	RHW-06	-14.19 ($\pm$0.65)	-96.48 ($\pm$2.31)	15
	RHW-10	-12.92 ($\pm$0.47)	-88.77 ($\pm$1.69)	10
	RHW-11	-13.43 ($\pm$0.55)	-91.31 ($\pm$0.98)	9
	RHW-12	-14.74 ($\pm$0.90)	-95.11 ($\pm$1.76)	7
	RHW-13	-14.82 ($\pm$0.75)	-96.54 ($\pm$1.36)	8

subsequent calculations as it was collected from a cave seep directly below RHR-20 in the Arroyo Seco watershed and had similar geochemistry and isotopic ratios as RHR-20. I could not rule out the possibility that this spring had emerged further upslope then recharged some distance downslope before discharging from the cave ceiling. Earman (2004) termed such groundwater discharge that later

infiltrated again "re-recharge".

Average isotopic values of $\delta^{18}O$ and $\delta^{2}H$ of surface water, groundwater, and spring water fall within the winter/spring precipitation range (Figure 3.5), despite only 1/3 of precipitation falling during that period on average. There are two possible explanations for this behavior: 1) mixing between winter and summer/monsoonal precipitation, or 2) evolved snow and spring precipitation is the primary source of surface and subsurface water. The mixing hypothesis is unlikely, as surface water samples did not show any isotopic evidence of monsoonal precipitation inputs. Monsoonal storms in the mountain block are generally intense and of short duration, usually occuring daily during the season. However, none of the surface water samples collected during the monsoon season showed isotopic ratios near monsoonal precipitation. This is possibly due to the runoff being routed through the system before sampling could be completed just after the storms, indicating short residence times on the order of minutes to hours for this type of runoff. The prevalence of rocky outcrops in the watershed would facilitate quickflow processes in portions of the watershed. Another explanantion is that most of the monsoonal precipitation is lost to canopy interception, bare soil evaporation, and uptake by vegetation. The potential evapotranspiration (ET) is greatest during the summer (Stewart et al., 1999) and it is likely that none of the precipitation that falls during monsoonal storms makes it past the root zone (Kurc & Small, 2004). Most likely a combination of fast runoff and ET processes is responsible for the lack of an observed monsoonal signature in surface-waters, although I suspect the latter is more dominant. A simple calculation of the average annual discharge of the Rio Hondo (1.10E9 ft^3; USGS, 2013) at the USGS stream gauge using the reported average daily streamflow values and the average annual precipitation in the mountain block (about 75 cm; OSU,
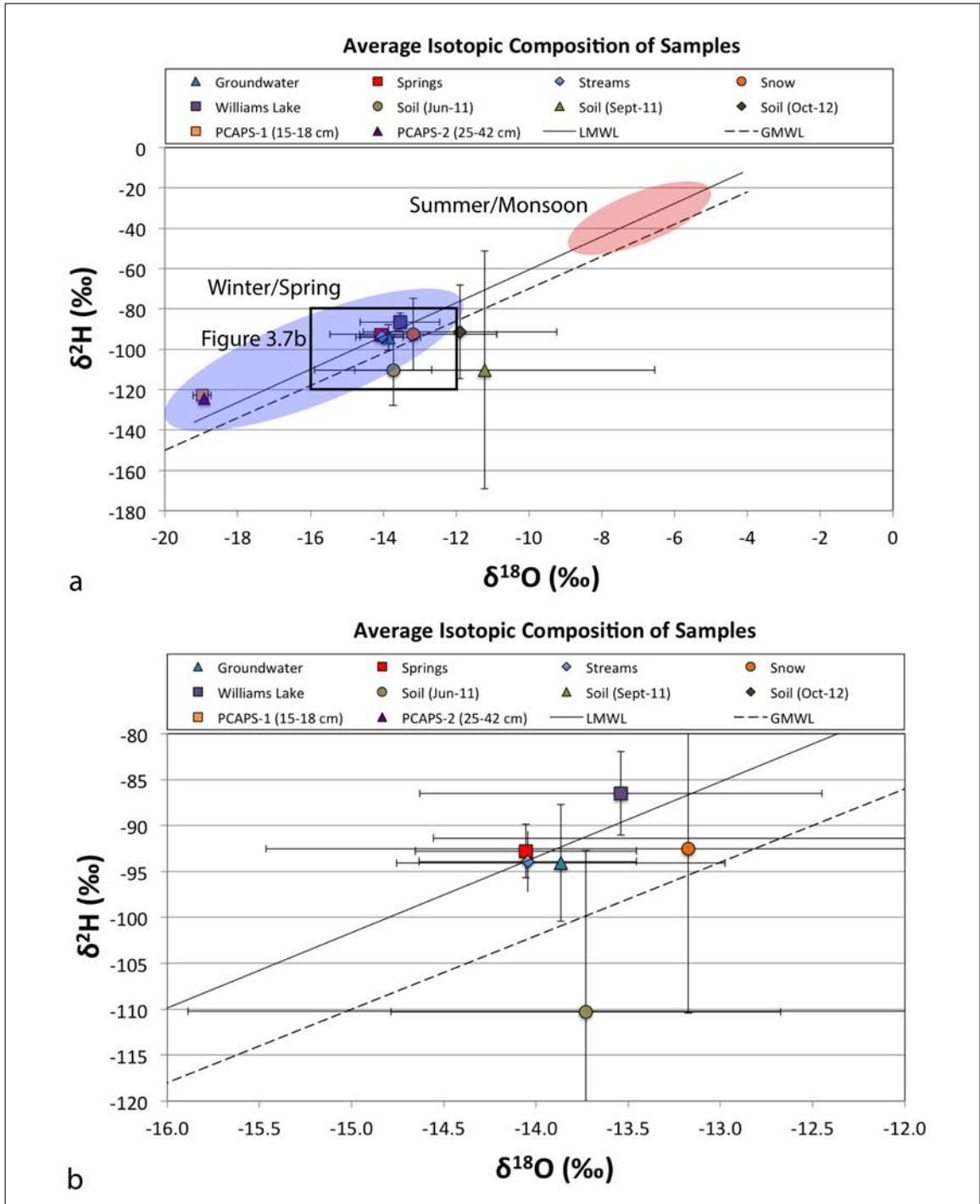
Figure 3.5: a) Average isotopic composition of different sample types with b) inset showing area indicated by box. Shaded areas indiate approximate precipitation range from Figure 3.3. Error bars show one standard deviation.

2012) shows that average annual streamflow volume is about 37% of average annual precipitation volume that falls on the mountain block. Although this is a rather crude estimation, it does provide some support for my assertion that the majority of water in the Rio Hondo is sourced from winter and spring precipitation despite only one-third of annual precipitation falling during that time. This importance of seasonality on groundwater recharge is similar to the conclusions reached by Earman et al. (2006) in their estimate of the snowmelt contribution to groundwater recharge in areas of Arizona and New Mexico.

3.3.3 Geochemistry

Piper diagrams show that waters range from calcium-bicarbonate to calcium-sulfate in composition (Figure 3.6). Precipitation chemistry shows a seasonal influence, with winter precipitation being more bicarbonate dominated, summer more chloride dominated, and spring precipitation having an intermediate composition of the two. Surface-water, groundwater, and spring-water samples do not appear to be controlled by precipitation, as they fall on a sulphate mixing line whereas precipitation falls on a chloride mixing line. When plotted on the main triangle, groundwater, surface-water, and spring-water samples are relatively indistinguishable from each other. Exceptions to this include groundwater samples from RHW-05, RHW-10, RHW-13, and effluent from the village wastewater treatment plant (WWTP). RHW-05 and RHW-10 are both wells located just outside of the mountain block in Arroyo Seco and at the mouth of the Rio Hondo, respectively. Although the screen interval of the wells is unknown, they are both near the Sangre de Cristo fault. RHW-05 shows distinct geochemistry from RHW-11, a well located only 330 m away and screened at approximately the same depth

47

(Neil Ogden, personal communication). This suggests that faults have a significant effect on well geochemistry in the area, and by extension groundwater flow paths. One possible explanation for the geochemical signature of RHW-13 may be that it is more geochemically evolved due to being located furthest down the valley. However, there may be some mixing with regional groundwater coming from the northern portion of the San Luis basin. The geochemical uniqueness of the WWTP effluent provides evidence that anthropogenic impacts to the system are limited as it is the largest point source of contamination in the watershed. The first sampling point downstream of the effluent (RHR-24) does not show significant chemistry change from the sampling point above (RHR-23). This indicates that while the effluent does have a distinct geochemical signature, the volume of effluent discharge is small in comparison to the volume of water in the stream discharge, at least while we conducted our sampling. There is a seasonal aspect to the discharge volume from the WWTP, as the highest volume of tourism is during the winter months when I was not sampling. While this seasonality should be taken into consideration if sampling is to be conducted year round, the impact of the effluent chemistry on the streamflow samples I collected appears to be minimal. However, this may change in the future as the ski valley expands its summer recreational offerings.

Although relative geochemistry of samples is mostly non-unique, absolute concentrations do show some interesting patterns. Surface-water samples show a positive correlation between solute concentration and basin drainage area for Ca^{2+}, K^+, Mg^{2+}, and Na^{2+} (see Appendix D). SiO_2 and Sr^{2+} (Figure 3.7), which are unlikely to be introduced antropogenically, show a similar trend. Trends like these were first reported by Frisbee et al. (2011) for the Saguache Creek watershed. They inferred that the trends were controlled by kinetically limited dissolution of aluminosilicates. While silica concentrations can be influenced by uptake
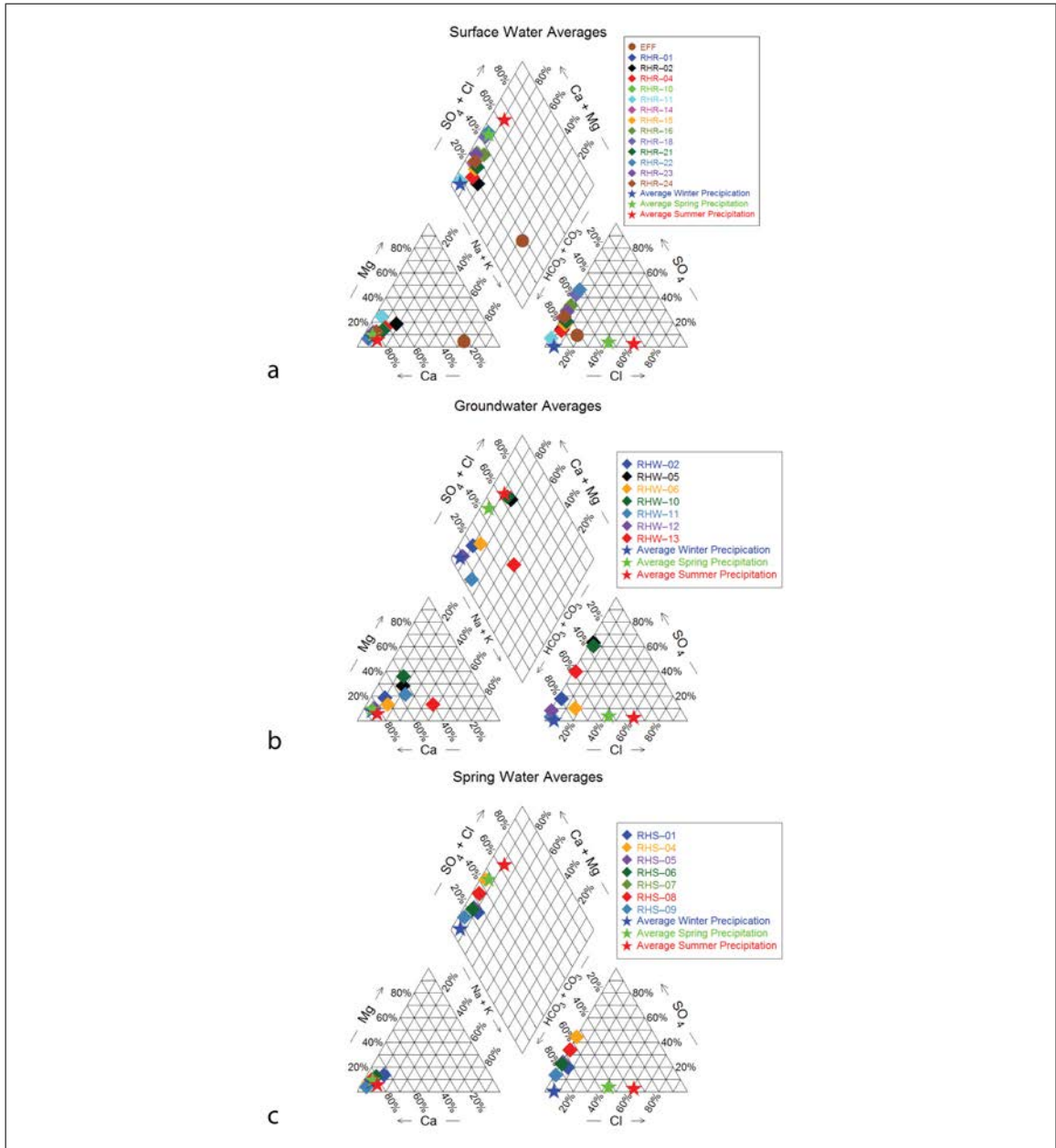
Figure 3.6: Piper diagrams of a) surface water, b) groundwater, and c) spring water. Waters are mostly calcium-bicarbonate to calcium-sulfate dominated and relatively indistinguishable from each other with the exception of groundwater samples from RHW-05, RHW-10, RHW-13, and effluent from the village wastewater treatment plant (WWTP). Samples collected just downstream of the treatment plant do not show mixing with the effluent, suggesting treatment plant discharges are not high enough to significantly affect stream chemistry below outlet. See Figure 3.4 for sampling locations.

49

or release by certain plant species (assuming the rate of growth and decomposition is not in equilibrium), strontium is not likely to be affected significantly (Rediske & Selders, 1953). Furthermore, evaporation alone cannot explain the increases in solute concentration, as there is no change in δ^2H values as basin area increases (Figure 3.8).

Plots of Mg^{2+} and Na^{2+} vs elevation for surface water, groundwater, and spring water samples (Figures 3.9, 3.10, and 3.11) show similar geochemical evolutionary pathways. High elevation samples tend to plot on the lower left portion of the Mg^{2+} and Na^{2+} graph and are tightly grouped. Lower elevation samples tend to plot to the upper right portion of the Mg^{2+} and Na^{2+} graph and have a greater range of concentrations. The greater variability in geochemistry for low elevation samples suggests that they are integrating a variety of flowpaths, and that these flowpaths or the contributions from them may change seasonally depending on hydrologic conditions. The low variability of the high-elevation samples suggests that they are integrating a limited number flowpaths that are relatively stable. When selected samples of surface water, groundwater, and spring water are plotted together (Figure 3.12) a geochemical evolution curve is apparent, showing the same general pattern of tightly grouped, high-elevation samples plotting to the lower left and lower elevation samples with greater variability plotting in the upper right. This strongly indicates that surface water, groundwater, and spring water have either evolved in a similar manner or surface water and groundwater have a high degree of connectivity. The much smaller proportion of water in contact with rock in the stream compared with groundwater leads me to infer that it is unlikely that surface waters would show the same degree of geochemcial evolution as groundwaters if the two were not in communication. Therefore, evolved groundwater contributions appear to be one, if not the major, control on surface water geochemistry.
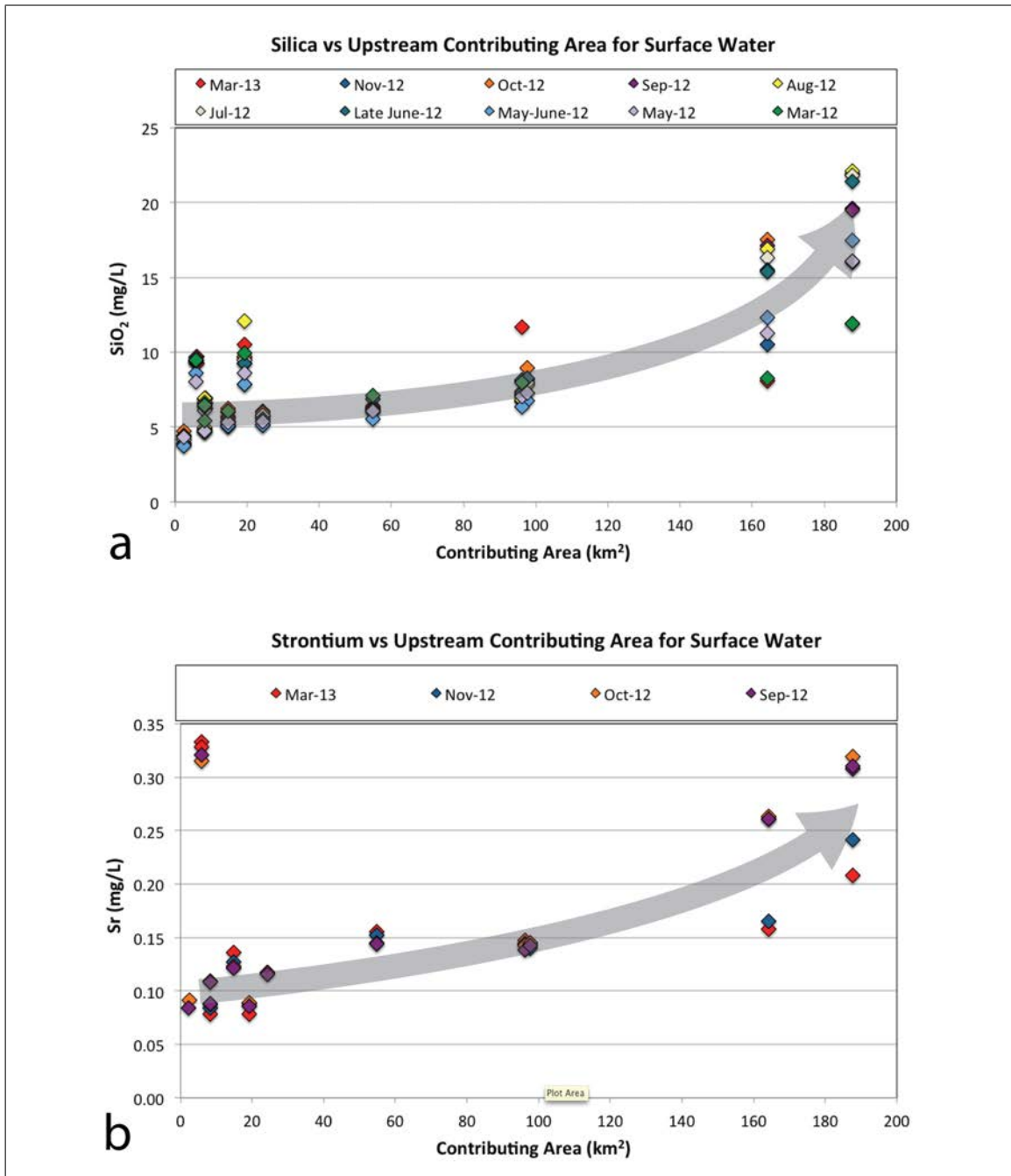
Figure 3.7: Plots of a) silica and b) strontium vs upstream contributing area for surface water samples. Both solutes show increasing concentration with increasing drainage area. Silica and strontium are unlikely to be introduced anthropogenically, and while silica can be taken up or released by certain plant species it is not expected for strontium.
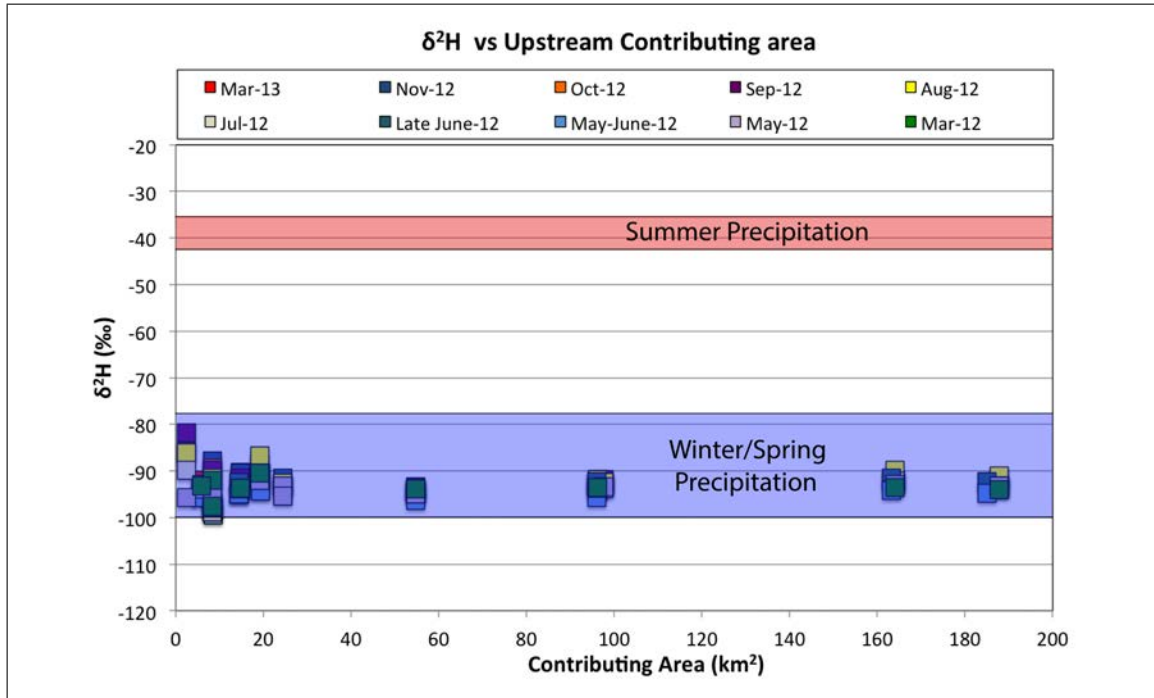
Figure 3.8: ^{2}H values vs upstream contributing area for surface water samples. Isotopic ratios do not change significantly downstream, indicating evaporation and/or mixing with another source are not likely mechanisms for increasing solute concentrations downstream. The red and blue shaded area indicate the weighted mean and one weighted standard deviation for summer and winter/spring precipitation, respectively.

3.4 Conclusions

Although the Rio Hondo and Saguache Creek watersheds have different geologic settings, climate, topography, drainage areas and impacts from human development, they both exhibit similar trends in normalized discharge and similar structuring of solute concentrations with increasing drainage area, indicating that the 3D conceptual model developed for the Saguache Creek watershed provides a good explanation of process behavior in the Rio Hondo as well. Normalized average daily streamflow for both watersheds are nearly identical in shape and timing, with slow rises and recessions indicative of significant storage within the basin despite relatively thin soil cover in the mountain block. Comparable

52
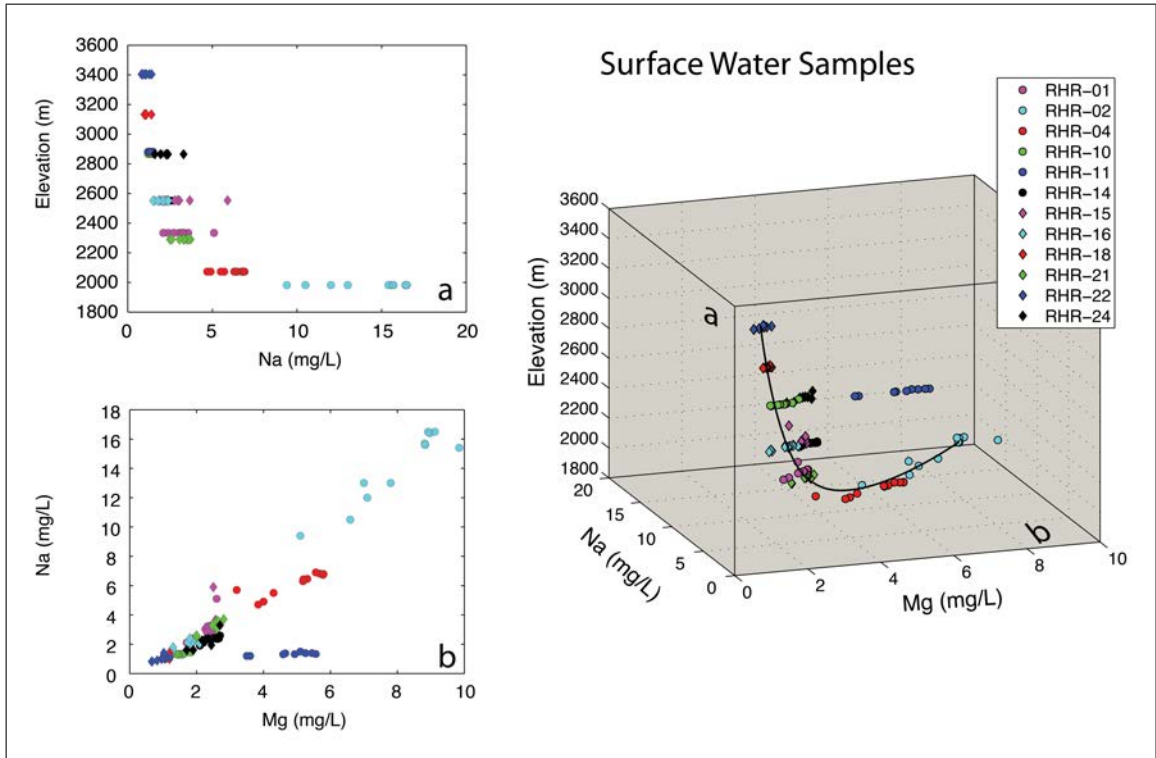
Figure 3.9: 3D scatter plot of magnesium, sodium, and sample elevation, along with 2D scatter plots of sodium vs elevation and magnesium vs sodium for surface water samples. The general trend is higher elevation samples showing lower solute concentrations compared to lower elevation samples. Higher elevation samples also tend to have lower variability in sampled solute concentrations. Letters correspond to the planes represented by the 2D plots. Estimated best fit line shown.

geochemical trends are also present in both watersheds, with surface-water solute concentrations increasing with basin drainage area. This is likely a result of the stream integrating more deep groundwater flowpaths as it travels from the headwaters to the basin outlet. These deep groundwater flowpaths should have long residence times, and therefore be much more geochemcially evolved. This is consistent with results presented by Frisbee et al. (2013), who showed that underestimation of residence times resulted in calculated weathering rates orders of magnitude higher than those observed. Therefore, some proportion of deep groundwater must be discharging to the surface water system, as short residence
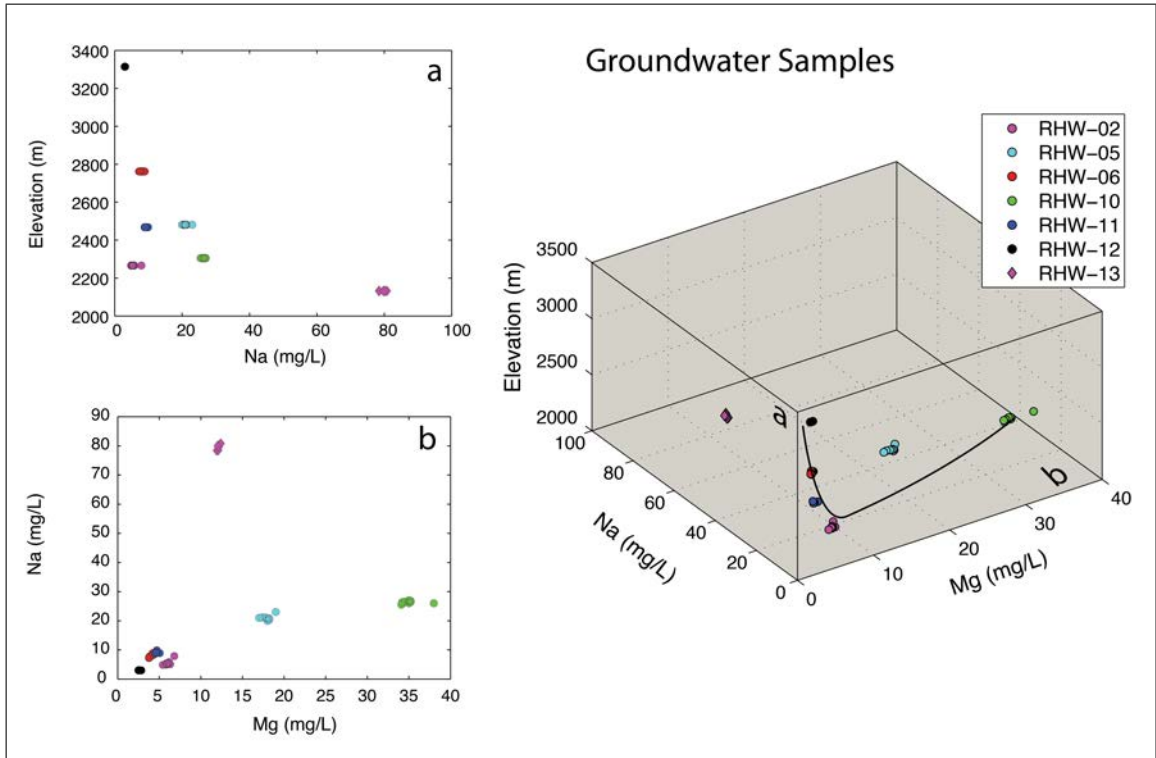
Figure 3.10: 3D scatter plot of magnesium, sodium, and sample elevation, along with 2D scatter plots of sodium vs elevation and magnesium vs sodium for groundwater samples. Samples show relatively little variability, indicating wells are not sampling from a large distribution of groundwater flowpaths. Letters correspond to the planes represented by the 2D plots. Estimated best fit line shown.

time waters (i.e., direct runoff and soil water) are unlikely to produce the elevated solute concentrations observed in surface water. In addition, it is unclear how shallow subsurface flow paths could reproduce the pattern of increasing solute concentration with increasing basin drainage area, as the maximum shallow subsurface flowpath length would quickly be reached, and geochemistry would likely stabilize beyond that point (2D Conceptual model).

Stable isotopic data is also evidence for a significant proportion of deep groundwater contributions to surface water in the Rio Hondo. Surface water, groundwater, and spring water samples all consistently showed isotopic signatures of late season evolved snow and spring precipitation. Isotopic values close
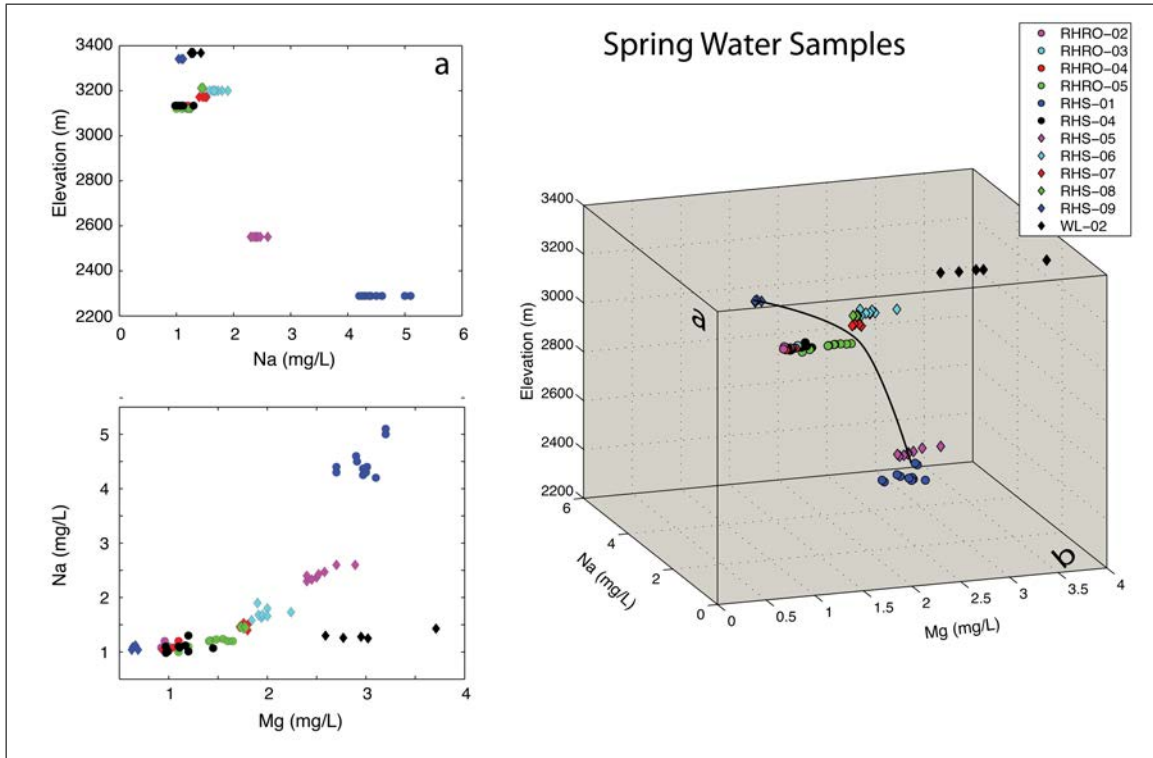
Figure 3.11: 3D scatter plot of magnesium, sodium, and sample elevation, along with 2D scatter plots of sodium vs elevation and magnesium vs sodium for spring water samples. The general trend is higher elevation samples showing lower solute concentrations compared to lower elevation samples. Higher elevation samples also tend to have lower variability in sampled solute concentrations. Letters correspond to the planes represented by the 2D plots. Estimated best fit line shown.

to that of monsoonal precipitation were not measured even when sampling was conducted soon after summer storms. This suggests either very short residence times for surface runoff, or that very little monsoonal precipitation makes it to the stream, although a combination of the two is the most likely. The most likely sources for streamflow in the basin would be waters that were not subject to the physical processes that result in isotopic fractionation; deep groundwater is one such source.

While Saguache and the Rio Hondo display similar geochemcial trends, they represent very different spatial scales. Frisbee et al. (2012) were unable
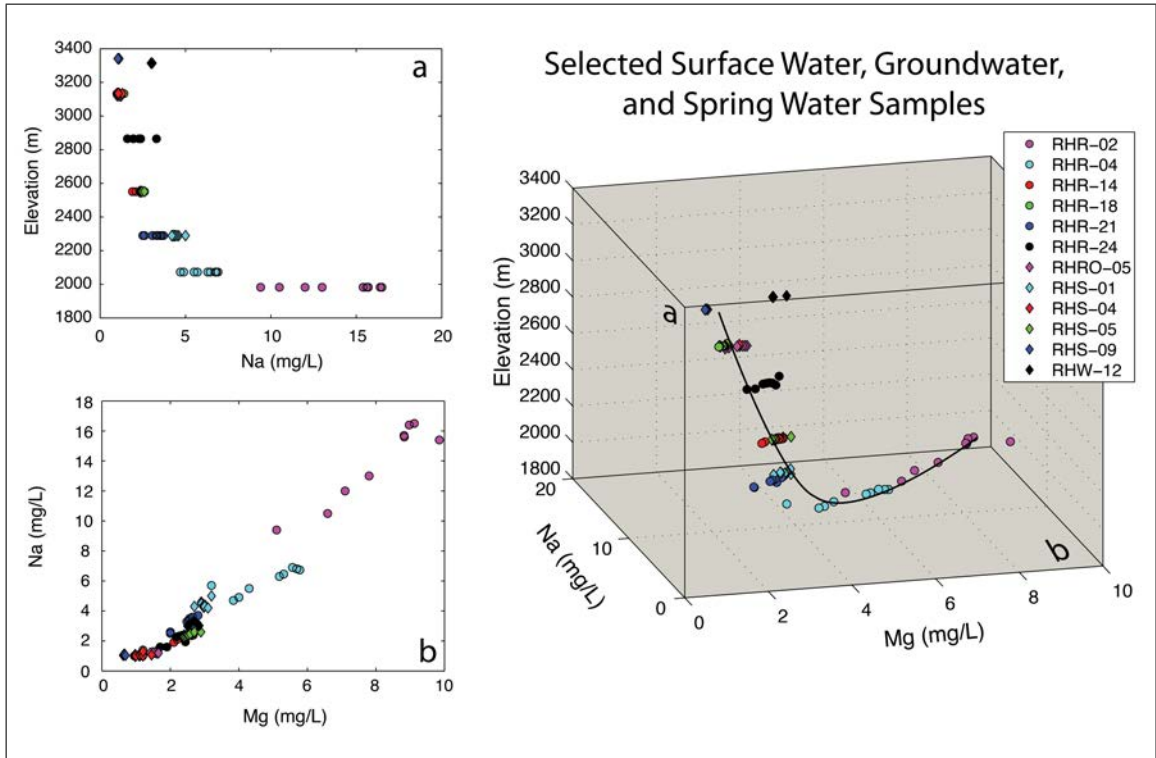
Figure 3.12: 3D scatter plot of magnesium, sodium, and sample elevation, along with 2D scatter plots of sodium vs elevation and magnesium vs sodium for selected surface water, groundwater, and spring water samples. Letters correspond to the planes represented by the 2D plots. Estimated best fit line shown.

to discern structured groundwater contributions below a critial drainage area of about 300 km^2, an area much larger than the entire Rio Hondo basin. My data indicates structured groundwater contributions begin to occur at around 5 to 10 km^2, as the pattern of increasing solute concentration with increasing basin drainage area develops at this scale. This is in contrast to the trend reported by Wolock et al. (1997), whereby stream chemistry became invariable above a critical threshold of 8 km^2. Topography may be an explanation for this, as elevation changes in the Saguache Creek watershed are much more subdued due to its large area compared to the Rio Hondo. It may take larger spatial scales for deeper flow paths to develop in the Saguache Creek watershed, whereas high relief in the Rio Hondo waterhsed allows them to form at smaller scales (Gleeson

& Manning, 2008). These results indicate that discharge from deep groundwater sources can be present at much smaller scales than previously thought.

The implications of significant deep groundwater discharge is dependent on a number of factors, including the residence time and the relative contribution to streamflow. If the residence time is relatively short, then short-term climatic perturbations will propogate through the system quickly and there will be little, if any, additional buffering capacity. The relative contribution of deep groundwater to surface water is also just as important, since water that is very old and evolved can control the geochemisty of the surface water but still be insignificant from a buffering standpoint as it does not contribute a large volume of water. The next two chapters of this thesis examine these two factors, first by attempting to quantify the residence time distribution of waters in the system and second by quantifying the contributions from deep groundwater using geochemical streamflow separation.

CHAPTER 4

RESIDENCE TIMES IN THE RIO HONDO WATERSHED USING CHLOROFLUOROCARBONS, TRITIUM, AND RADIOCARBON.

4.1 Introduction

Waters in mountain basins can take a variety of flowpaths (e.g., overland flow, interflow, deep percolation, etc.) to streams due to the heterogeneity and complexity of mountain systems. The time it takes water to be routed out of the basin either as surface water or groundwater after it has fallen as precipitation is commonly referred to as the "residence time" of the water. Like many aspects of earth science, residence times can span several orders of magnitude ranging from minutes to thousands of years (Dunne & Black, 1970; Weissmann et al., 2002; Frisbee et al., 2011). Due to convergence of groundwater flow paths, subsurface mixing, and hydrodynamic dispersion processes, water samples collected from a spring or well are not a single age but a distribution of ages. Estimation of mean residence times and residence time distributions (RTDs) has been important in hydrology as they have been used to determine process behavior such as stream-flow generation (Pearce et al., 1986; McGuire & McDonnell, 2006), weathering rates (Maher, 2010; Pacheco & Van der Weijden, 2012; Frisbee et al., 2013b) and more recently watershed response to climate change (Rademacher et al., 2005; Singleton & Moran, 2010; Manning et al., 2012).

58

Multiple environmental tracer techniques exist that are able to identify waters recharged at varying time scales. Quantitative age dating methods such as ^{3}H-^{3}He, chlorofluorocarbons (CFC's), and ^{14}C are able to estimate the amount of time waters have spent in the subsurface since being recharged, with ^{3}H-^{3}He and CFC's identifying young waters (<60 yrs) (Szabo et al., 1996, Plummer et al., 2006;) and ^{14}C identifying older waters (<45,000 yrs) (Plummer & Glynn, 2013). Tritium concentrations can also be used as a qualitative indicator to identify young, old, or mixed age waters (Clark & Fritz, 1997).

Recently, these water-dating techniques have been employed within high-elevation mountain catchments (Rademacher et al., 2005; Frisbee et al., 2011; Manning et al., 2012) in California and Colorado. Results from these basin-scale studies show that residence times can range from modern to thousands of years, significantly longer than the residence times found for hillslope and small headwater catchment studies (Horton, 1933; Hewlett & Hibbert, 1967; Dunne & Black, 1970; Anderson et al., 1997b; Brown et al., 1999; Vitvar et al., 2002; Tetzlaff et al., 2007). This suggests that streamflow generation processes have drastically different residence time distributions for different scales, and illustrates the need to use multiple age-dating techniques for the same sample. Limited age dating using CFC's and tritium has been performed outside of the Rio Hondo mountain block to help characterize the groundwater flow system of the southern San Luis valley basin sediments (Drakos et al., 2004; Rawling, 2005; Johnson et al., 2009), but have not been used to identify groundwater and surface-water residence times within the mountain block of the Rio Hondo watershed.

The importance of determining mean residence times for surface water is matched only by the difficulty in sampling for them. Since surface water is in

constant communication with the atmosphere, many water-dating techniques are useless as radioisotopic clocks (^{3}H-^{3}He, ^{4}He, ^{14}C) and known-concentration atmospheric tracers (CFC's) are reset when waters re-equilibrate with atmospheric water vapor and gases. In-stream piezometers can be used to sample groundwater that is upwelling into the stream, however without specialized equipment they were impossible to install in the rocky streambed of the Rio Hondo. Tritium can be used as a qualitative tracer in surface water as atmospheric exchange does not significantly affect ^{3}H concentrations, but it is unable to provide quantitative measures of apparent residence times. Therefore, it is necessary to determine the sources of streamflow and apply water-dating techniques to streamflow end-members in situ where re-equilibration with the atmosphere is unlikely to have occurred. This chapter focuses specifically on age dating of different waters in the Rio Hondo, while Chapter 5 examines the sources contributing to streamflow using End-Member Mixing Analysis (EMMA).

The goal of this chapter is to identify the range of residence times for groundwater, spring water, and surface water in the Rio Hondo watershed. Three different age dating techniques were employed for this purpose. CFC's and ^{14}C were used to quantify young and old waters, respectively, while ^{3}H concentrations were used as a qualitative age indicator of recharge timing. The use of these three different methods allowed for estimation of the range in residence times within the watershed.

4.2 Methods

4.2.1 Tritium

Tritium samples were collected at groundwater, spring water, and surface water sampling locations. A total of 1,000 mL was collected from each site and

stored in two 500 mL high density polyethylene (HDPE) bottles with polypropylene (PP) lids. Samples were enriched by electrolysis prior to analysis by liquid-scintillation counting at either Isotope Tracer Technologies, Inc. in Waterloo, Canada or the Tritium Laboratory at the Rosenstiel School of Marine and Atmospheric Science at the University of Miami in Miami, FL. Results are reported in Tritium Units (TU), where 1 TU = 1 tritium atom per 10^{18} hydrogen atoms. Standard deviations from Isotope Tracer Technologies and the University of Miami were reported at 0.8 TU and about 0.2 TU, respectively.

4.2.2 Chlorofluorocarbons

CFC samples were collected from selected groundwater and spring water sites. Only springs believed to be the first emergence of the water were chosen. Samples were collected in three 500 mL narrow-mouth, clear, Boston Round borosilicate glass containers with foil-lined caps. Viton® tubing was used to minimize contact between the sample and the atmosphere during collection. A peristaltic pump was used for collection from springs and a metal adaptor with the o-rings removed was used to attach the Viton® tubing to well spigots. Sample collection was done according to USGS CFC sampling procedure (http://water.usgs.gov/lab/chlorofluoro- carbons/sampling/bottles/). Bottles were filled from the bottom up, allowed to overflow with at least two liters of water, and then capped underwater. Bottles were checked to make sure there were no bubbles present and then taped. Samples were then sent to the USGS Reston Chlorofluorocarbon Laboratory in Reston, VA for analysis.

Apparent ages for CFC samples were determined using the data-reduction sheet provided with the results. Recharge temperature was assumed to be 0° C

as stable isotopic results from Chapter 3 indicate nearly all recharge in the watershed is sourced from snowmelt. Recharge elevations were assumed to be 4,000 m, 3,200 m, or 2,900 m depending on the elevation of the sampling site.

4.2.3 Radiocarbon

Radiocarbon samples were collected from selected groundwater and spring-water sampling locations. A total of 1,000 mL was collected from each site and stored in two 500 mL HDPE bottles with PP lids and taped shut. Only springs believed to be the first emergence of the water were chosen. Samples were then sent to Beta Analytic at their headquarters in Miami, FL where they were analyzed for ^{14}C activity and $\delta^{13}C$ using the Accelerator Mass Spectrometry (AMS) technique. ^{14}C activities are reported as percent modern carbon (pmc) with measurement error about 0.37%. $\delta^{13}C$ values are reported in per mil (‰) notation relative to Vienna Pee Dee Belemnite (VPDB).

Apparent ages were determined using the equation

$$t = \frac{5730}{ln2} ln\left(\frac{A_0}{A}\right) \tag{4.1}$$

where t is the time elapsed since recharge, 5730 is the modern half-life of ^{14}C, A_0 is the initial ^{14}C activity (pmc value), and A is the measured ^{14}C activity (pmc value) of the sample. The Vogel correction method (Vogel, 1967; Plummer & Glynn, 2013) was used and assumes a value of 85.0 ($\pm$5.0) pmc for A_0.

4.3 Results and Discussion

4.3.1 Chlorofluorocarbons

Apparent piston flow ages for CFC-11, CFC-12, and CFC-113 (Table 4.1; Figure 4.1) range from about 24 to 57 years. There is moderate agreement between

Table 4.1: Apparent piston-flow ages for groundwater (RHW) and spring water (RHS) samples for CFC-11, CFC-12, and CFC-113. Apparent age using all CFC analysis is shown in the last column with one standard deviation. Dashed entries indicate the sample was contaminated and was not used. See Figure 4.1 for sample locations.

Sample ID	CFC-11 Age (yrs)	CFC-12 Age (yrs)	CFC-113 Age (yrs)	All CFC's (yrs)
RHS-01	35.0	29.5	27.0	30.0 (±3.7)
RHS-08	28.3	24.3	25.5	25.6 (±1.8)
RHW-05	56.8	61.2	50.0	55.5 (±4.9)
RHW-06	31.5	27.7	27.5	28.4 (±2.0)
RHW-10	50.0	44.0	39.5	44.0 (±4.7)
RHW-12	32.0	–	26.0	28.5 (±3.5)

the different tracers, with CFC-11 giving the oldest age dates and CFC-113 giving the youngest, in general. According to the USGS Guidelines for Assignment of Apparent CFC Age (http://water.usgs.gov/lab/chlorofluorocarbons/lab/assigning_age/), young CFC-113 age relative to CFC-11 and CFC-12 age indicates mixing of young and old groundwater has occurred. Nearly all samples show the youngest age for CFC-113, suggesting some degree of mixing between young and old waters is present. This mixing would bias waters young, so the apparent CFC ages presented here are likely minimum ages. Even with the potential mixing of young and old water, samples near the mountain front show ages approaching the useful limit (∼60 yrs) of the CFC dating technique.

Although only a limited number of CFC samples were collected, apparent ages within the moutain block show some degree of correlation with elevation (Figure 4.2). High elevation samples have younger CFC apparent ages while low elevation samples show older apparent ages. RHS-01 is not consistent with this
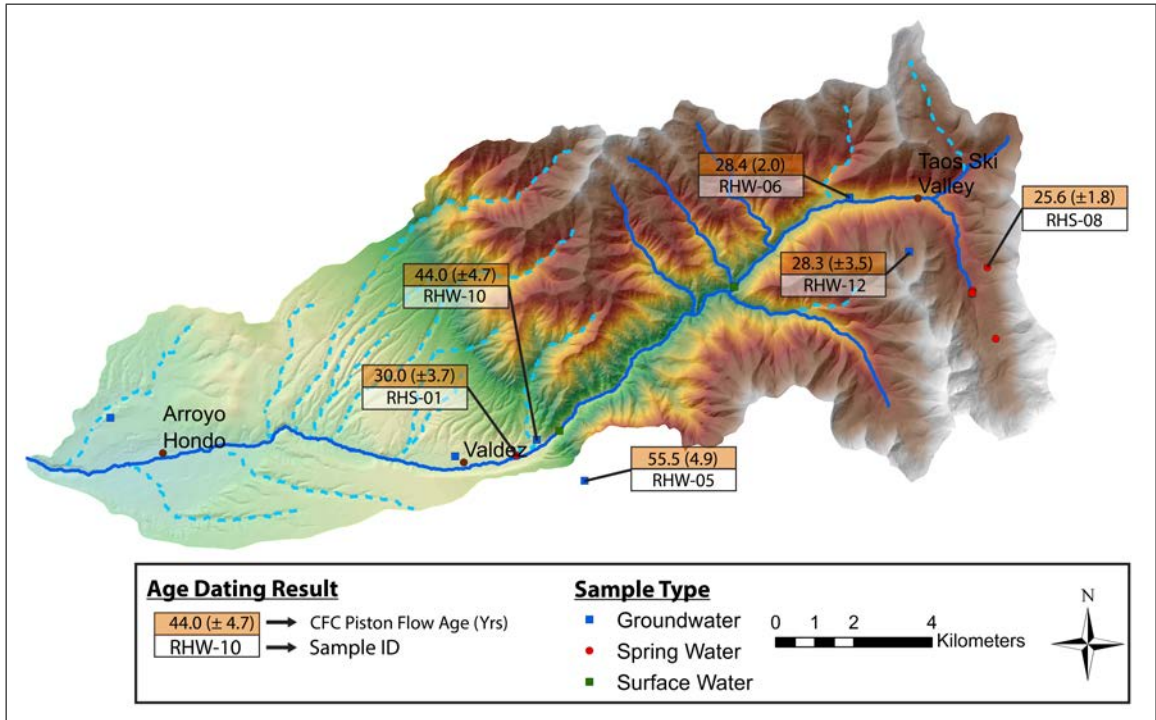
Figure 4.1: Apparent piston flow ages using average of CFC-11, CFC-12, and CFC-113 results. High-elevation samples show younger ages with lower elevation samples showing older ages approaching the useful age limit ($\sim$60 yrs) of the technique. RHS-01 is located in an area that receives irrigation waters and is potentially biased young due to mixing with infiltrating recharge waters that have equilibrated with contemporary atmospheric concentrations of CFC's.

trend, possibly due to the fact that it is located in an area that receives irrigation waters and therefore is likely to have a greater degree of mixing between young and old waters. While it is difficult to make accurate inferences from only five data points, the apparent correlation of age with elevation shown in Figure 4.2 is consistent with my hypothesis of increasing contributions to streamflow from deep groundwater with increasing basin scale.
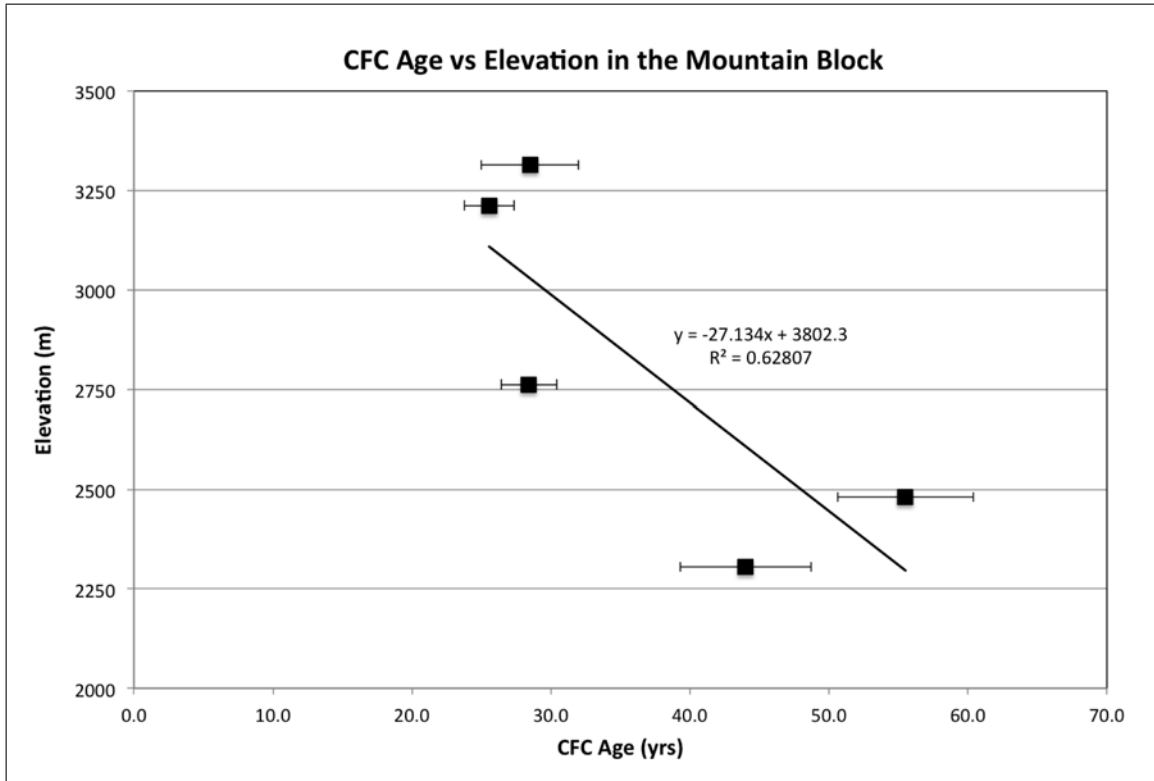
Figure 4.2: Apparent CFC age vs elevation for mountain block springs and wells and mountain front wells. Age appears to be moderately correlated with elevation, with high-elevation samples showing younger ages and lower elevation samples showing older ages. RHS-01 was exluded due to possible contamination from infiltrating irrigation waters. If RHS-01 is included the R^2 value is reduced to 0.33. Error bars indicate one standard deviation.

4.3.2 Tritium

Tritium concentrations in precipitation were not measured in the Rio Hondo watershed during this study, but have recently been reported to range from about 3 to 10 TU in the Sacramento Mountains to the south (Newton et al., 2012). The highest concentrations were sampled during the spring, consistent with typical seasonal trends (Michel, 2005; Newton et al., 2012). The warming of land masses in the spring causes an instability in the tropopause between 30° and 60°N. This instability mixes air from the stratosphere, the main repository for

65

Table 4.2: Tritium concentrations for groundwater (RHW), spring water (RHS), and surface water (RHR) sampling locations. See Figure 4.3 for sampling locations.

Sample ID	Tritium Concentration (TU)
Ditch	7.9 ($\pm$0.8)
RHR-01	6.59 ($\pm$0.22)
RHR-14	6.67 ($\pm$0.22)
RHR-18	7.41 ($\pm$0.24)
RHS-01	6.2 ($\pm$0.8)
RHS-04	7.2 ($\pm$0.8)
RHS-08	7.0 ($\pm$0.8)
RHS-09	8.5 ($\pm$0.8)
RHW-10	1.5 ($\pm$0.8)
RHW-12	4.8 ($\pm$0.8)
RHW-13	13.2 ($\pm$0.8)

atmospheric tritium, into the troposphere. Tritium concentrations in the stratosphere are greater than those in the troposphere because the stratosphere is unable to exchange with ocean water vapor that has relatively low tritium concentrations. This annual increase in tritium concentrations in the troposphere of the northern hemisphere resulting from this mixing is commonly referred to as the "Spring Leak" (Michel, 2005). Stable isotopic evidence presented in Chapter 3 suggests that most water in the Rio Hondo is sourced from a mixture of winter and spring precipitation, so a contemporary tritium concentration of 10 TU was chosen for the Rio Hondo watershed. Pre-1953 tritium concentrations in precipitation for Albuquerque, New Mexico have been estimated to be at least 6 TU, with 1963 bomb-pulse maximum concentrations of about 1900 TU (Shevenell & Goff, 1995).

Given the half-life of tritium is 12.33 years (Lucas & Unterweger, 2000), pre-1953 recharge has underwent approximately five half-lives and would have a concentration of 0.21 TU today. Waters recharged during the 1963 bomb-pluse

would have tritium concentrations of about 114 TU today as they have underwent approximately four half-lives. It should be noted that hydrodynamic dispersion would likely result in dilution of the maximum peak of the bomb-pulse. Contemporary tritium concentrations in the atmosphere, though seasonally variable, appear to have been reached by about the mid 1990's (Clark & Fritz, 1997). Therefore, It is likely safe to assume that all precipitation falling after the year 2000 would have an intital concentration of about 10 TU. Using this value, waters recharged 5 and 10 years ago would have tritium concentrations of 7.5 and 5.7 TU, respectively. Since tritium mixes conservatively we can also calculate an estimate of tritium concentrations for mixtures of modern and submodern water. An equal mixture of pre-1953 water (0.21 TU) and modern recharge (10 TU) would be yield a tritium concentration of 5.1 (TU).

Tritium concentrations (Table 4.2; Figure 4.3) range from 1.5 to 13.2, with the lowest tritium concentration measured in a mountain-front well and the highest measured in a valley well near the Rio Grande. Concentrations were used as a qualitative indicator of the age and degree of mixing between young and old waters that the sample underwent. Table 4.3 shows the qualitative age estimates used based on the concentration of precipitation during recharge and the number of half-lives the water has likely experienced. Most of the samples fell on the lower (older) end of the "Young (<5 to 10 yr)" age estimation, with two samples, RHW-10 and RHW-12, having concentrations less than 5 TU and one sample, RHW-13 having a tritium concentration greater than 10 TU. This suggests age distributions in the watershed range from modern to submodern and are likely mixtures of young and old water.

Tritium concentrations for mountain block springs and wells show the same general correlation as CFC ages with elevation (Figure 4.4). Higher ele-
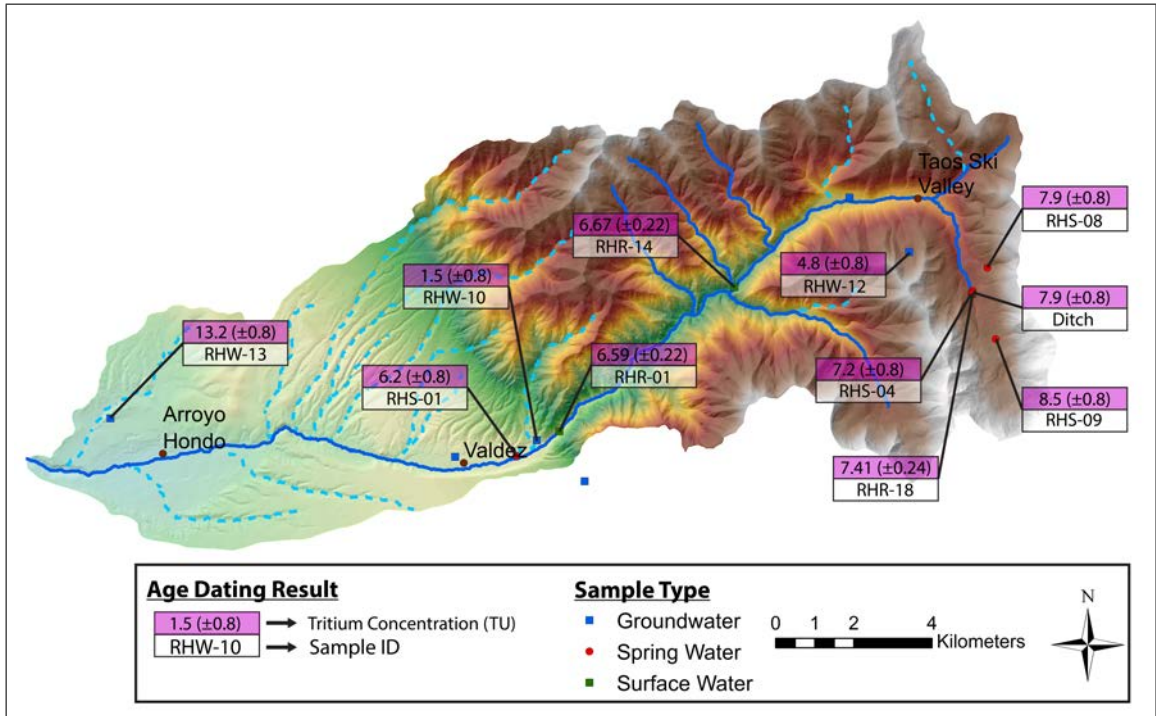
Figure 4.3: Map of sampling locations showing measured tritium concentrations.

vation springs and wells tend to have greater (younger) tritium concentrations compared with lower elevation samples. Shallow wells and springs located in the valley do not show this trend, likely due to mixing with infiltrating irrigation waters. The highest tritium concentration (13.2 TU) came from a deep well located near the Rio Grande. This suggests the well is likely receiving a significant amount of modern recharge such that tritium concentrations are reset to modern values. The lowest tritium concentration (1.5 TU) came from a well located on the hillslopes of the mountain front, suggesting predominantly pre-1952 recharge mixed with a small proportion of modern recharge.

Three measurements of tritium collected at surface water sampling locations (RHR-01, RHR-14, and RHR-18) show a similar, though less pronounced, correlation of tritium concentrations with elevation. However, with only three samples it is impossible to definitively state a correlation exists. If the correlation

Table 4.3: Qualitative age estimates for tritium concentrations. See Clark and Fritz (1997) for comparison.

Tritium Concentration (TU)	Qualitative Age Estimate
<0.2	Submodern recharged prior to 1952
0.2 to ~5	Mixture between submodern and recent recharge
5 to 8	Young (<5 to 10 yr)
8 to 10	Modern
10 to 30	Some "bomb" ^{3}H present
>30	Considerable component of recharge from 1960's or 1970's
>60	Dominantly the 1960's recharge

is accurate, it would be consistent with my hypothesis of increased deep groundwater contributions to surface water with increasing scale.

A similar, though less pronounced, trend can be seen in surface water tritium concentrations (Figure 4.4). Higher elevation samples show greater tritium concentrations compared to lower elevation samples within the mountain block. Mixing of young and old waters within the stream may explain why the correlation with elevation is not as pronounced as for groundwater and surface water samples.

4.3.3 Radiocarbon

Radiocarbon activities, δ^{13}C values, and calculated ages using Equation 4.1 are presented in Table 4.4 and Figure 4.5. Geochemical analyses of the major cations and anions associated with each sample are shown in Table 4.5. Measured
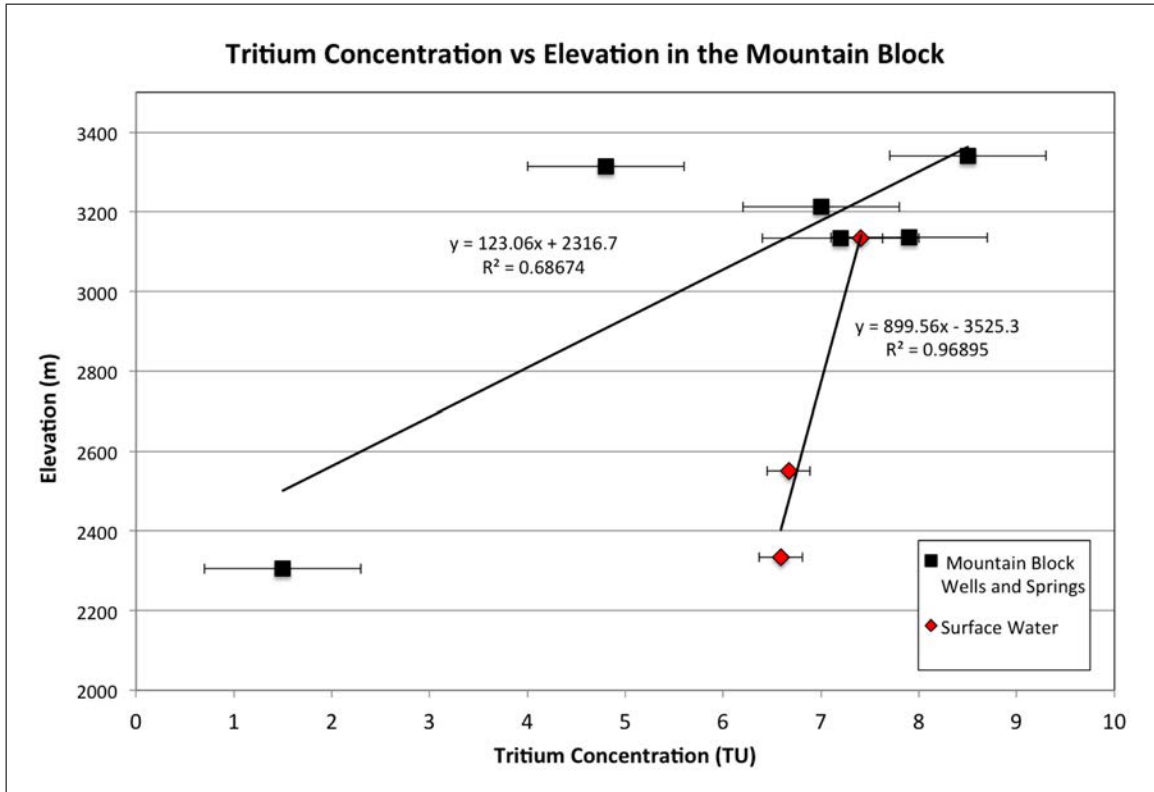
Figure 4.4: Tritium vs elevation for mountain block springs and wells. There appears to be a correlation between tritium concentration and elevation, with higher elevation samples showing greater (younger) tritium concentrations relative to lower elevation samples. Surface water samples show a similar, though less pronounced trend. Trend lines with equations and correlation coefficients shown.

radiocarbon activities range from about 65 to 99 pmc, with associated ages ranging from modern to 2,300 yrs. Radiocarbon activity does not show any significant correlation with $\delta^{13}C$ values or bicarbonate concentrations (Firgure 4.6). Mountain block waters also do not show a strong correlation between ^{14}C activity and elevation (Figure 4.7), unlike CFC ages and tritium concentrations. However, the limited number of data points makes it difficult to definitively state that no correlation exists. CFC and tritium data indicate a mixture between old and young waters, so the lack of correlation may be due to the highly non-linear mixing relationship of ^{14}C compared with CFC's and tritium. This is also a possible ex-

Table 4.4: ^{14}C activities, δ^{13}C values, and calculated ages using the Vogel correction method. See Figure 4.5 for sampling locations.

Sample ID	^{14}C Activity (pmc)	δ^{13}C (‰)	Calculated Age (yrs)
RHS-01	91.77 ($\pm$0.34)	-17.7	Modern
RHS-08	64.68 ($\pm$0.24)	-16.8	2300 ($\pm$500)
RHW-02	95.02 ($\pm$0.35)	-18.9	Modern
RHW-06	89.62 ($\pm$0.33)	-18.3	<100
RHW-10	71.28 ($\pm$0.26)	-22.4	1500 ($\pm$500)
RHW-12	69.01 ($\pm$0.25)	-18.2	1700 ($\pm$500)
RHW-13	98.76 ($\pm$0.36)	-16.2	Modern

planation for the modern ages observed in the all of the valley wells. Mixing of older waters with infiltration from irrigation waters that have equilibrated with modern ^{14}C would reset the radiocarbon clock, making the waters appear modern.

Although the Vogel correction method is useful, it does not account for more complex geochemcial reactions that can add or remove dissolved inorganic carbon (DIC) from waters, such as equilibration of waters with soil-gas during recharge and dissolution of radiocarbon-dead calcite. δ^{13}C values can be an indicator of these types of reactions, with soil-gas CO_2 values for C3 plants ranging from -23 to -35‰, and commonly assumed to be -25‰ (Clark & Fritz, 1997). δ^{13}C values in my samples range from -16.2 to -22.4‰, indicating dissolution of some enriched carbon source relative to soil-gas. Potential carbon sources include calcite derived from magmatic degassing of CO_2 during the late stages of plutonism, and potentially calcite precipitated along fracture walls. Two samples that yield old ages have δ^{13}C values that are close to those of soil-gas CO_2, suggesting only slight interactions with minerals that alter the carbon composition of the water. Therefore, it is likely that some of the old ages I am seeing are accurate, and that significantly old water (>100 yrs) does indeed exist in the system. Future refinement of radiocarbon ages using the geochemical modeling software NETPATH
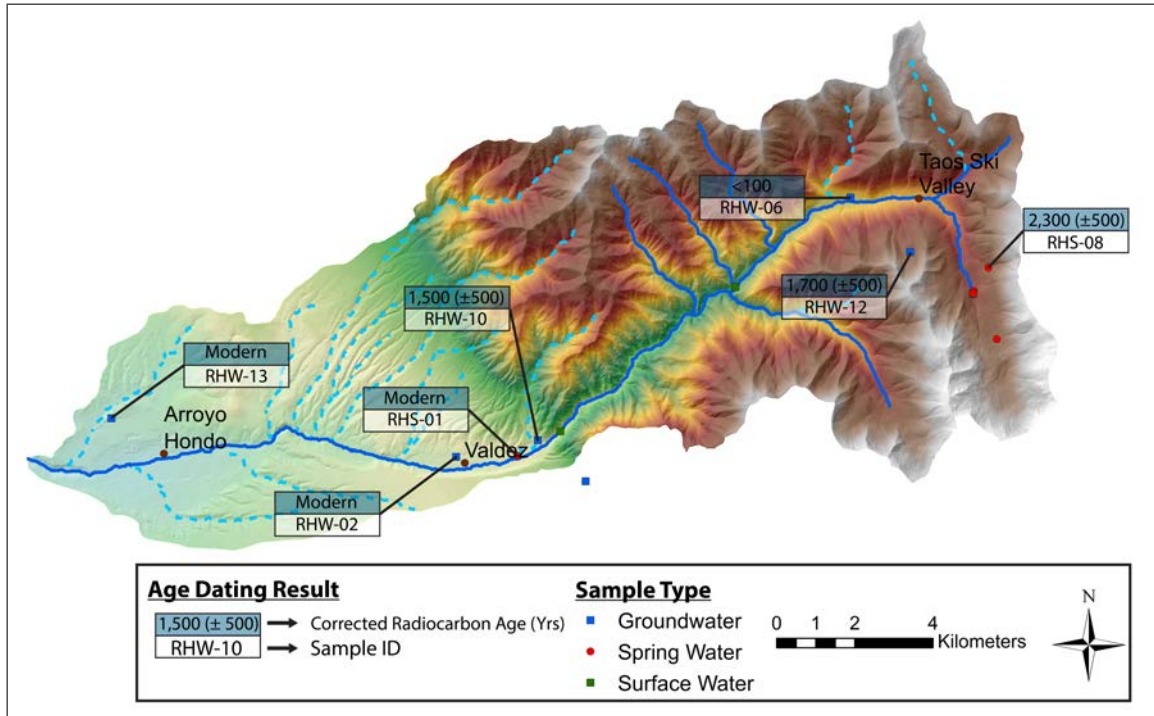
Figure 4.5: Map of sampling locations showing ^{14}C age dates calculated using Vogel correction method.

(Plummer et al., 1994) may be helpful, however the apparent mixing of waters in the Rio Hondo watershed might prove to be outside the capabilities of the model.

One of the big questions that remains is are the multiple age-tracers revealing different portions of the age distribution, or are they simply sampling different flow paths that are converging at the same sampling point. For springs, this is difficult to separate as deep groundwaters must pass throuth the shallow soil zone before emerging at the surface. While passing through the shallow soil zone mixing of deep groundwater and short residence-time soil water is likely. However, this is less likely to occur in groundwater samples, where well screens are located at some location along a flowpath and therefore not a likely location of flowpath convergence. I saw the same age-tracer patterns in groundwater samples as spring-water samples, which leads me to believe that my age-tracer

results are sampling different portions of the age distribution and not different flow paths that happen to converge at the same sampling location. In our case, the different dating techniques are similar to frequency filters. Since we appear to have a large age distribution, whichever filter we use will select only the frequency, or age in our case, that it is designed for. For example, we see ages up to 60 years using CFC's because that is the age range it is best suited to detect. One way to test this would be to create synthetic age distributions for different distribution types (normal, logarithmic, etc.) and compare them to the age distributions we have. Whichever synthetic age distribution matched our observed age distribution would be the best explanation. However, this does assume that the age distribution of the watershed can be represented with a single, relatively simple age distribution, which may not be the case.

4.4 Conclusions

The results from multiple age-dating tracers in the Rio Hondo watershed (Figure 4.8) indicate residence times range from modern to possibly thousands of years old. Average CFC ages are similar to those reported by Rademacher et al. (2005) for the Sagehen basin in California and ^{14}C ages are the same order of magnitude reported by Frisbee et al. (2011) for the Saguache Creek watershed in southern Colorado. This suggests that similar basin scale processes resulting in streamflow generation are operative in all three basins, although because multiple tracer techniques were not used in Sagehen basin or Sagurache creek this remains speculative. This illustrates the need to utilize multiple age dating techniques in mountain watersheds because there appears to be a wide distribution of ages, with mean residence times likely on the order of decades to thousands

Table 4.5: Geochemcial data associated with radiocarbon samples.

Sample ID	Alkalinity (mg/L as CaCO$_3$)	Ca (mg/L)	Cl (mg/L)	K (mg/L)	Mg (mg/L)	Na (mg/L)	NO$_3$ (mg/L)	SO$_4$ (mg/L)	pH (SU)
RHS-01	88	28.0	2.78	0.900	3.1	4.2	0.50	20.0	7.4
RHS-08	61	25.1	0.50	0.627	1.8	1.45	2.84	24.8	8.0
RHW-02	132	38.2	2.37	1.310	6.3	5.25	0.61	23.8	7.5
RHW-06	114	36.4	13.5	0.844	4.0	7.41	2.22	12.2	7.7
RHW-10	203	84.8	12.4	0.995	37	25	-0.10	229	7.8
RHW-12	120	35.0	0.58	0.663	2.5	3.11	1.80	8.58	7.9
RHW-13	274	62.0	5.34	2.660	12.2	80	5.80	146	7.8
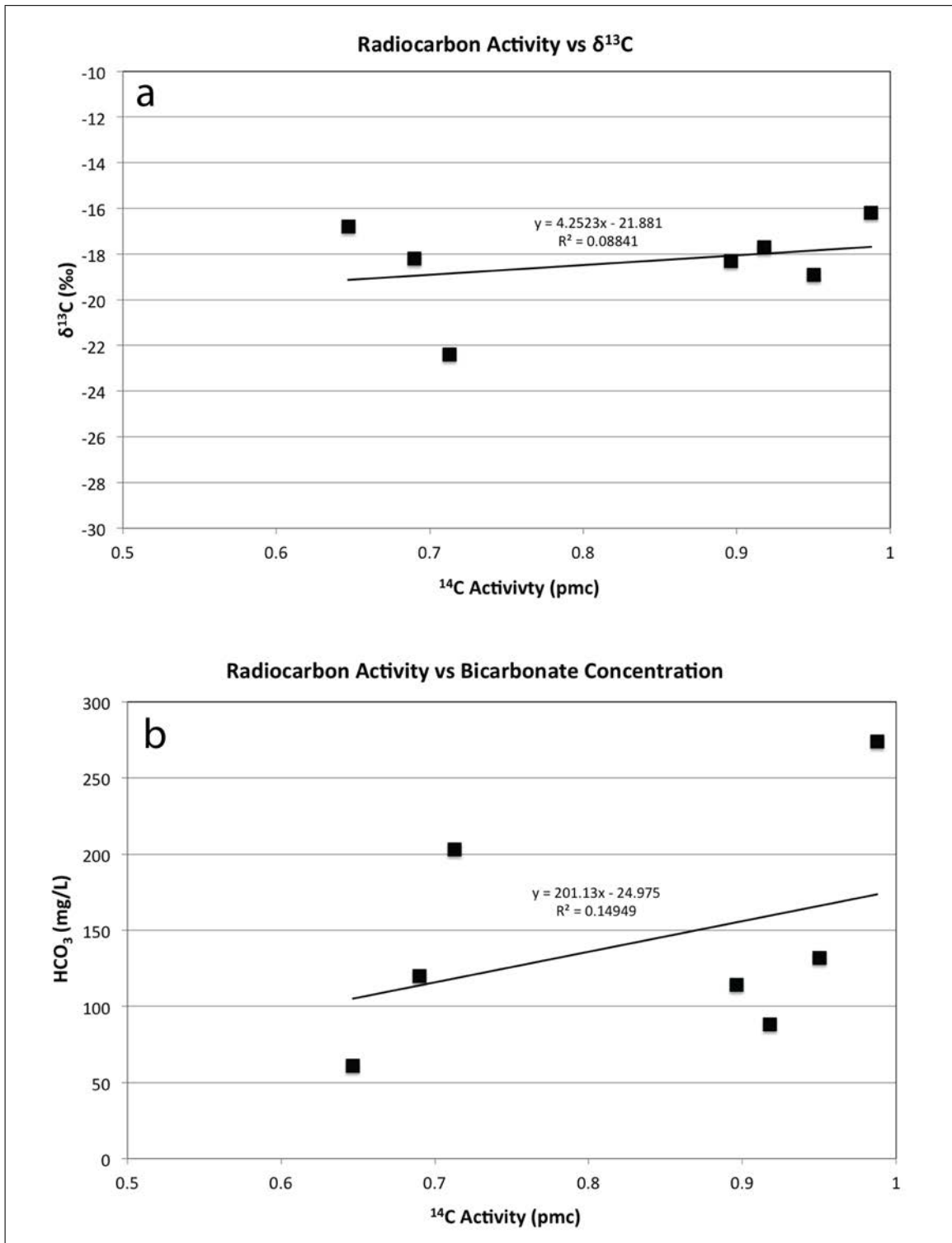
Figure 4.6: Plots of ^{14}C activity vs a) $\delta^{13}C$ values and b) bicarbonate concentrations. Trend lines with equation and correlation coefficient shown.
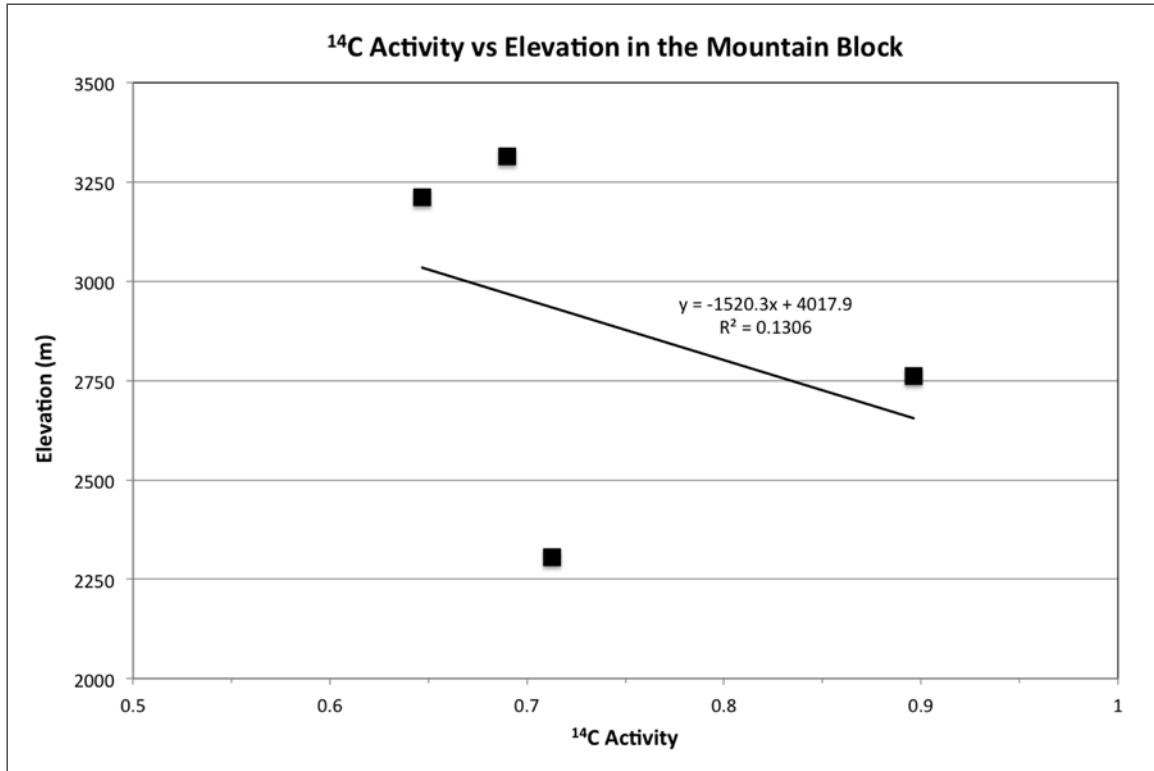
Figure 4.7: ^{14}C activity vs elevation for mountain-block springs and wells. Unlike CFC ages and tritium concentrations, ^{14}C activities do not appear to be correlated with elevation. This may be the result of the highly non-linear mixing relationship between young and old waters for radiocarbon.

of years. Frisbee et al. (2013) used solute concentrations and geochemical weathering rates to demonstrate that long residence times are necessary to produce observed solute concentrations in springflow. These long residence times are several orders of magnitude greater than the months-to-years that is the current belief (Horton, 1933; Hewlett & Hibbert, 1967; Dunne & Black, 1970; Anderson et al., 1997b; Brown et al., 1999; Vitvar et al., 2002; Tetzlaff et al., 2007).

The correlation of CFC ages and tritium concentrations with elevation also supports my hypothesis of increasing deep groundwater contributions with increasing basin scale. Although ^{14}C ages do not show this correlation, mixing between young and old waters may be one possible explanation why they do
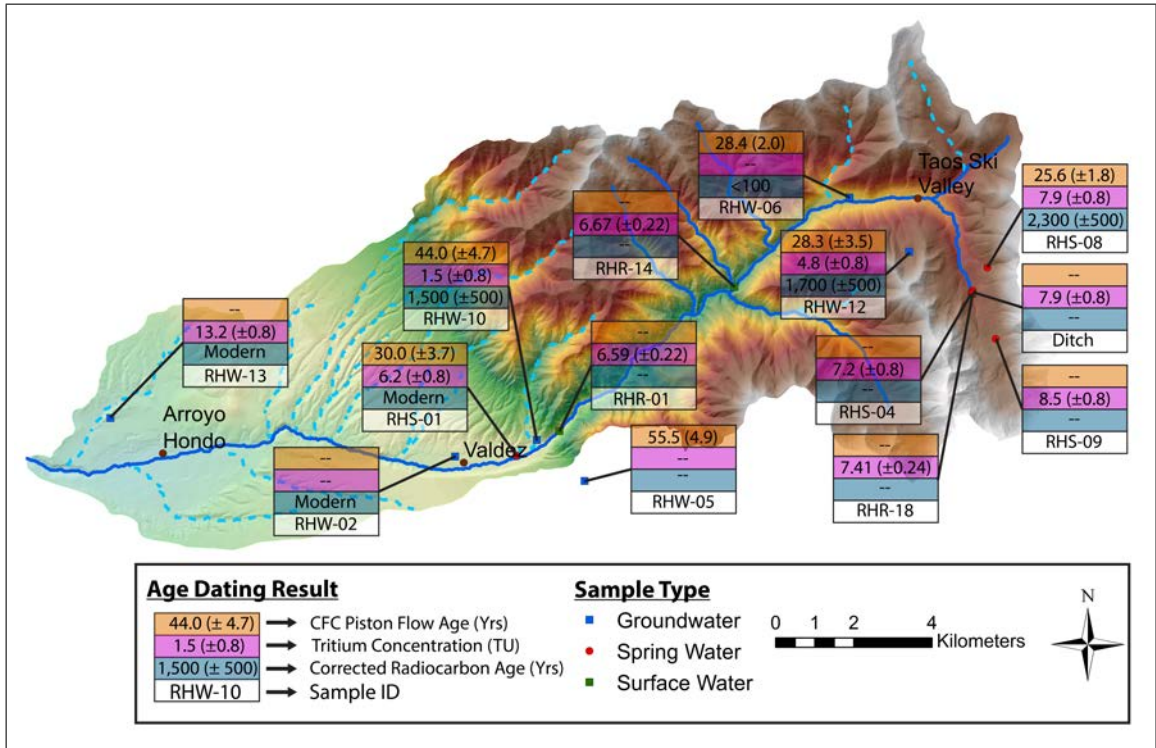
Figure 4.8: Age dating summary for all samples collected in the Rio Hondo Watershed.

not show this trend. Chapter 3 provided evidence for similar geochemical evolutionary pathways for groundwater, surface water, and spring water, suggesting contributions from deep groundwater are controlling stream geochemistry. Ages for CFC's and tritium concentrations show older waters near the mountain front and younger waters near the headwaters, a trend predicted by the 3D conceptual model with deep groundwater contributions to surface water. The wide range in age distributions is also predicted by the conceptual model, and is evidence for the existence of deep flowpaths within the watershed. The next chapter will use geochemical and isotopic separations of streamflow using end-member mixing analysis to determine the end-members contributing to streamflow, as well as quantify the realtive contributions from each end-member at each surface water sampling location.

77

CHAPTER 5

GEOCHEMICAL STREAMFLOW SEPARATION USING END-MEMBER MIXING ANALYSIS

5.1   Introduction

Hydrologists have investigated streamflow generation for 150 years or more, particularly low-flow characteristics as they provide threshold values for resource management and water quality. Understanding the sources that contribute to streamflow is essential for proper water resource management and future sustainability and adaptive management strategies. The sources of water, or end-members, that mix and ultimately contribute to streamflow represent water that has reached the stream via different flow paths within the watershed. These flowpaths have different residence times, and as a result different geochemical signatures. While conceptually it may seem relatively easy to identify these end-members, in practice in can be quite difficult. Despite this difficulty numerous methods have been developed to determine the recession behavior of hydrographs and the sources that contribute to streamflow.

One of the earliest methods of identifying the sources that contribute to streamflow was graphical separation of the discharge hydrograph into "groundwater" and "direct runoff" during storm events, where groundwater was defined as any "pre-event" (pre-storm) water and direct runoff was event (storm) water. This was accomplished by extrapolating the groundwater recession curve

beneath the flood peak (Pinder & Jones, 1969), with extrapolations ranging from the very simple (Linsley & Franzini, 1964; Hewlett & Hibbet, 1967; McNamara et al., 1997) such as a line with an arbitrary slope drawn from the rising to the falling limb of the stormflow hydrograph, to more complex (Frolich et al., 1994; Szilagyi & Parlange, 1998; Mendoza et al., 2003) procedures such as transformation of the hydrograph into a dimensionless recession curve. Graphical techniques for hydrograph separation have received considerable criticism due to the arbitrary classification of rates and sources of flow (Hewlett & Hibbert, 1967), and have been referred to as "convenient fiction" (Freeze, 1972; Dingman, 1994) since there is no physical basis to their assumptions. As a result, new methods for stream-flow separation using chemical and isotopic tracers were established.

The first chemical separation methods were developed to estimate surface water quality by determining the quality and quantity of groundwater and direct runoff that was discharging to the stream (Archer et al., 1968; LaSala, 1967; Pinder & Jones, 1969). This was accomplished using a simple two-component mass balance mixing model given by

$$C_{tr} = (Q_{dr}C_{dr} + Q_{gw}C_{gw})/Q_{tr} \qquad (5.1)$$

$$Q_{tr} = Q_{dr} + Q_{gw} \qquad (5.2)$$

where C is the tracer solute concentration (mg/L), Q is the discharge (m^3/s), and the subscripts tr, dr, and gw refer to the total runoff (streamflow), direct runoff (stormflow), and groundwater discharge, respectively. This method was eventually expanded to include more than two end-members, using measurements of isotopic tracers (^{2}H, ^{3}H, ^{18}O) and geochemical composition (Martinec, 1975; Sklash & Farvolden, 1979). One of the currently used methods of geochemical

and isotopic separation of streamflow is referred to as end-member mixing analysis (EMMA) (Christopherson & Hooper, 1990), where streamflow chemistry is mathematically transformed using least-squares multivariate analysis. EMMA is more statistically robust than previous methods and offers advantages in that many different sources of water can be screened simultaneously. Chemical constituents and end-members that account for the greatest amount of variability are identified, and the transformation reduces the dimensionality of the mixing subspace to n-1 dimensions, where n is the number of endmembers. For example, a three end-member mixing mixing model can be plotted in a 2D mixing subspace. This method is well established and has been used in several studies of streamflow generation at hillslope, small catchment, and basin scales in a variety of catchments (Christopherson & Hooper, 1992; Hooper, 2003; Liu et al., 2004, 2008; Frisbee et al., 2011, 2013).

One of the major outcomes of previous hydrograph separation investigations was the discovery that pre-event water makes up a large portion of storm runoff even during peak flow (Pinder & Jones, 1969; Martinec, 1975; Sklash & Farvolden, 1979; Laudon & Slaymaker, 1997; Brown et al., 1999). Unfortunately, most of the conceptual models developed for hillslope hydrology assume impermeable bedrock or only consider relatively shallow groundwater flow, and as a result it has become commonplace to use the terms "pre-event water" and "groundwater" interchangeably. If the conceptual model developed by Frisbee et al. (2011) is correct then this practice is misleading because soil water and groundwater would be expected to have different geochemical compositions due to their respective residence times in the system (i.e., groundwater being more geochemically evolved than soil water). Therefore I specifically differentiate between shallow soil water and deeper groundwater contributions to streamflow.

Table 5.1: Surface water sampling locations used for streamflow separation.

Sample ID	Sample Location (UTM 13S)	Elevation (m)	Drainage Area (km^2)
RHR-01	450184E 4044192N	2334	96.1
RHR-02	436785E 4043411N	1982	187.7
RHR-04	440357E 4043510N	2073	164.1
RHR-10	459817E 4050082N	2867	14.8
RHR-11	459878E 4050231N	2881	8.3
RHR-14	454658E 4047878N	2551	5.9
RHR-15	454485E 4047765N	2553	54.8
RHR-16	454458E 4047756N	2555	19.2
RHR-18	460742E 4047705N	3133	8.3
RHR-21	449213E 4043314N	2290	97.7
RHR-22	461603E 4045329N	3404	2.4
RHR-24	458751E 4049977N	2865	24.4

One might comment that the conclusions reached by Frisbee et al. (2011), that old groundwater is contributing to streamflow in the Saguache watershed, are a result of unique conditions that may only exist within that watershed. In order for the Saguache conceptual model to be robust, it must apply to a range of climates, topographies, geologies, etc.. Therefore, I used similar techniques and applied them to the Rio Hondo watershed in northern New Mexico (See Chapter 2 for complete site description). The Rio Hondo varies from Saguache geologically (crystalline vs volcanic bedrock), climatically (one-third of annual precipitation as snowfall vs two-thrids), and in size (187 km^2 vs 1,600 km^2). The Rio Hondo watershed also has a much larger degree of human development and impacts that must be accounted for in comparison to the Sagauche Creek watershed. Therefore any similarities between the two watersheds are likely the result of similar processes operating within both basins. By identifying the sources contributing to streamflow in the Rio Hondo, I can simultaneously investigate the processes generating streamflow within the basin and test the transferability of the Saguache conceptual model to a very different watershed.
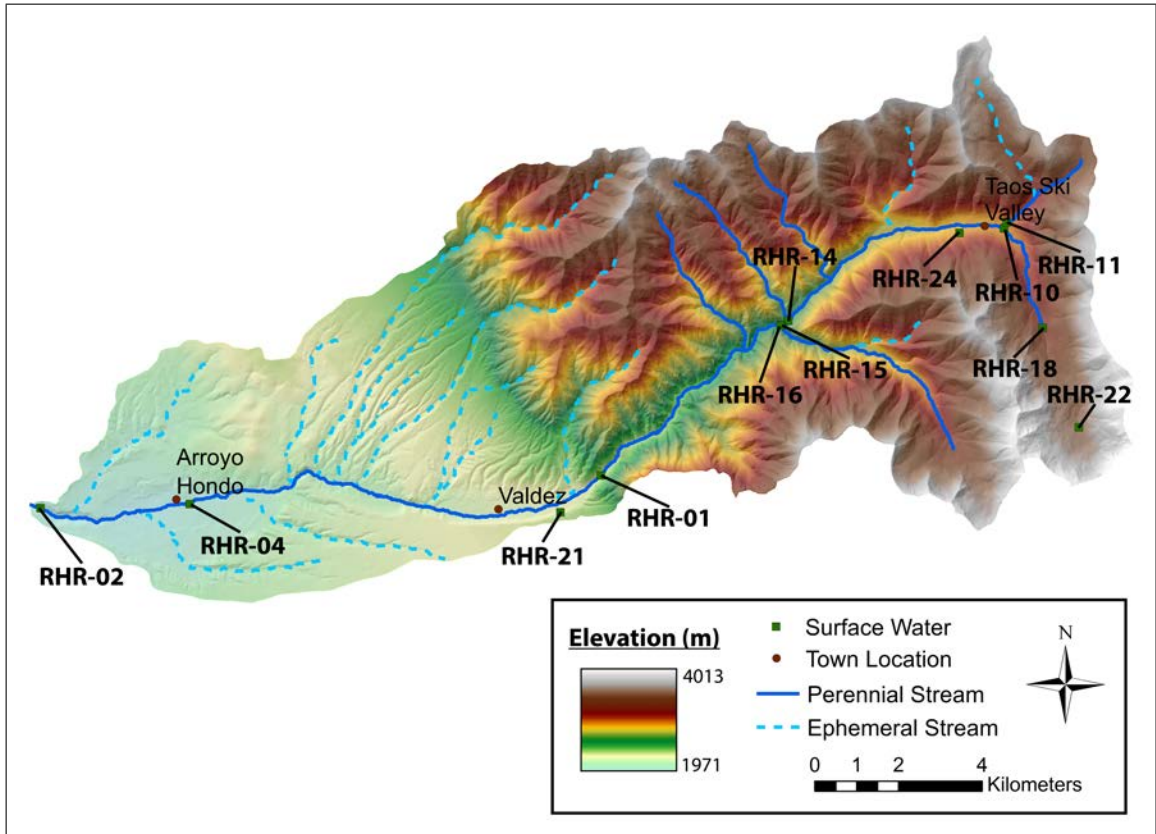
Figure 5.1: Surface water sampling locations used for streamflow separation by EMMA.

The goal of this chapter is to investigate the processes controlling stream-flow generation primarily within the mountain block of the Rio Hondo water-shed and assess the transferability of the Saguache conceptual model developed by Frisbee et al. (2011). I do this by identifying the major sources of water contributing to the 12 surface water sampling locations (listed in Table 5.1 and shown on Figure 5.1) using measurements of stream chemistry and EMMA to identify the groundwater fraction in streamflow. I will then compare my results to those from the Neversink River and Saguache Creek watersheds, which appear to represent the 2D and 3D conceptual models, respectively.

Wolock et al. (1997) have shown that stream geochemistry in the Neversink River watershed in New York stabilizes above a threshold basin size of

approximately 3 km^2. The authors state that this trend is attributable to stabilization of subsurface contact times, as the topographic gradients assumed to control subsurface contact time significantly decrease above this scale. Vitvar et al. (2002) have also estimated mean baseflow residence times on the order of nine months in a 2 km^2 headwater basin in the Neversink River watershed using the convolution integral approach. The asymptotic trend in surface-water geochemistry with basin drainage area and the relatively short residence times in the watershed imply a limited distribution of shallow subsurface flowpaths consistent with the 2D conceptual model.

In contrast, Frisbee et al. (2011) have demonstrated increasing surface-water solute concentrations with increasing scale in the Saguache Creek watershed. Radiometic dating and EMMA results indicate that the weighted mean residence time of surface-water can range from modern during the snowmelt pulse to hundreds of years during the later part of the year (Frisbee et al., 2013). The consistent increase in surface-water solute concentration with increasing basin drainage area and the significantly long residence times found in groundwater suggest deep groundwater flowpaths are present in the watershed and have significant control on surface-water geochemistry, consistent with the 3D conceptual model.

My hypothesis is that the Rio Hondo watershed will behave more like the 3D conceptual model due to the presence of highly fractured bedrock, and therefore surface-water geochemistry will be controlled by contributions from deep groundwater. If this hypothesis of increasing deep groundwater contributions is correct, then I should see 1) a significant proportion of groundwater end-members chosen and 2) an increasing proportion of groundwater moving from

the headwaters to the outlet, sites with larger basin drainage areas showing more evolved groundwater contributions, or both. Because there is a distribution of groundwater flow paths, and waters are assumed to be evolving as they travel along a given flowpath, we cannot assume a single composition of groundwater (the same applies to soil water). Instead, non-stream water samples are assumed to represent different potential flow paths in the system, each with a different degree of geochemical evolution and residence time. Table 5.2 shows the end-members critiqued in this study and the types of waters or flowpaths they likely represent based off of geochemistry and field observations.

5.2   Methods

Geochemical and isotopic sampling and analysis is explained in detail in Chapter 3, but a brief summary is provided here. A total of 11 sampling rounds were conducted between March 2012 and March 2013 using standard sampling procedures, with monthly to sub-monthly sampling between May 2012 and November 2012. Samples were either lab or field filtered to 0.45 μm before being sent to the New Mexico Bureau of Geology Analytical Chemistry Lab to be analyzed for general chemistry using accepted procedures and the New Mexico Stable Isotope Lab to be analyzed for δ^{18}O and δ^2H using a Picarro L1102-i Isotopic Water Liquid Analyzer cavity ringdown spectrometer. Samples with pre-fixes RHRO, RHS, and RHW are ephemeral springs, perennial springs, and wells, respectively. The PCAPS (Passive Capillary Sampler) sample is an integrated soil signature collected during the snowmelt season (see Chapter 3 for more details). The Ditch sample was an opportunistic sample collected from a spring emerging from a construction ditch dug near the Williams Lake trailhead. EFF is effluent

Table 5.2: Non-surface-water samples used as end-members. Subjective classification of the type of water that each sample represents is listed in the second column. Classification is based on geochemistry and field observations. All samples were put into EMMA as specific end-members and then grouped into their respective categories during post-processing for easier identification of spatial and temporal patterns.

Sample ID	Classification	EC (μS/cm)	Ca²⁺ (mg/L)	Mg²⁺ (mg/L)	Na⁺ (mg/L)	K⁺ (mg/L)	SiO₂ (mg/L)	δ^{18}O (‰)	δ^2H (‰)	n
PCAPS	Very	28.3 (±5.0)	2.39 (±0.11)	0.55 (±0.22)	2.45 (±1.63)	0.68 (±0.40)	2.78 (±1.10)	-18.96 (±0.18)	-123.43 (±1.07)	3
Winter Precip	Immature	35.1 (±5.7)	6.02 (±2.83)	0.32 (±0.17)	0.24 (±0.43)	0.07 (±0.06)	0.19 (±0.14)	-14.64 (±1.36)	-94.47 (±9.65)	4
Spring Precip	Water	58.2 (±4.9)	9.14 (±11.37)	0.70 (±0.51)	0.44 (±0.26)	0.68 (±0.52)	0.19 (±0.14)	-12.29 (±1.08)	-83.44 (±7.32)	5
RHS-10		72.0 (N/A)	10.10 (N/A)	1.98 (N/A)	0.94 (N/A)	0.80 (N/A)	5.95 (N/A)	-15.52 (N/A)	-97.92 (N/A)	1
Summer Precip		127.2 (±7.2)	17.20 (±5.66)	0.77 (±0.05)	1.58 (±1.17)	3.07 (±1.18)	1.55 (±1.43)	-7.80 (±0.45)	-38.92 (±4.06)	5
RHRO-02		131.8 (±6.9)	22.30 (±0.98)	0.97 (±0.04)	1.10 (±0.05)	0.47 (±0.03)	4.99 (±0.12)	-14.56 (±0.45)	-94.05 (±1.49)	5
RHS-09	Soil	134.0 (±2.9)	24.08 (±0.69)	0.65 (±0.03)	1.07 (±0.04)	0.49 (±0.05)	5.06 (±0.07)	-14.25 (±0.51)	-91.87 (±2.11)	4
RHRO-04	Water	134.2 (±9.2)	22.50 (±1.39)	1.01 (±0.07)	1.09 (±0.04)	0.45 (±0.03)	5.02 (±0.16)	-14.12 (±0.55)	-94.03 (±2.13)	5
RHRO-03		135.0 (±8.7)	22.67 (±1.30)	1.02 (±0.07)	1.12 (±0.04)	0.46 (±0.02)	4.98 (±0.17)	-14.01 (±0.36)	-94.47 (±1.70)	3
RHS-06		137.6 (±4.0)	21.99 (±0.80)	1.97 (±0.12)	1.70 (±0.09)	0.80 (±0.07)	7.05 (±0.21)	-14.29 (±0.58)	-93.50 (±1.04)	8
RHS-04		142.5 (±12.5)	23.95 (±1.95)	1.14 (±0.15)	1.10 (±0.09)	0.46 (±0.03)	4.79 (±0.17)	-14.18 (±0.73)	-91.26 (±3.49)	10
Ditch		144.0 (N/A)	24.0 (N/A)	1.09 (N/A)	1.12 (N/A)	0.48 (N/A)	5.07 (N/A)	-13.11 (N/A)	-91.09 (N/A)	1
WL-01	Williams Lake	154.3 (±49.6)	25.64 (±8.43)	1.23 (±0.39)	1.18 (±0.30)	0.39 (±0.08)	3.34 (±0.31)	-13.23 (±0.94)	-85.72 (±6.51)	7
RHS-08		154.8 (±1.6)	25.14 (±0.09)	1.75 (±0.02)	1.46 (0.02)	0.62 (±0.01)	6.86 (±1.92)	-13.99 (±0.58)	-88.07 (±0.77)	5
RHS-07		155.5 (±0.60)	25.20 (±0.24)	1.75 (±0.02)	1.49 (±0.05)	0.63 (±0.04)	5.96 (±0.12)	-13.86 (±0.82)	-88.07 (±0.72)	4
WL-02	Moderately	170.2 (±22.0)	23.84 (±3.25)	3.01 (±0.43)	1.30 (±0.07)	0.73 (±0.02)	5.88 (±.034)	-13.97 (±1.09)	-87.57 (±4.54)	5
RHS-05	Evolved	170.8 (±9.1)	27.74 (±1.40)	2.57 (±0.17)	2.47 (±0.13)	0.69 (±0.06)	9.44 (±0.35)	-14.41 (±0.75)	-94.45 (±1.12)	9
RHW-11	Groundwater	173.9 (±3.1)	20.17 (±0.34)	4.69 (±0.18)	9.14 (±0.35)	0.74 (±0.10)	21.53 (±0.41)	-13.55 (±0.56)	-90.98 (±0.75)	7
RHS-01		183.2 (±7.4)	27.23 (±0.98)	2.97 (±0.12)	4.46 (±0.25)	0.84 (±0.04)	8.79 (±0.53)	-14.40 (±0.70)	-93.11 (±1.17)	10
RHW-12		203.8 (±4.7)	34.85 (±0.47)	2.56 (±0.14)	3.03 (±0.05)	0.66 (±0.01)	7.82 (±0.47)	-14.83 (±0.94)	-95.00 (±1.90)	6
RHW-06	Evolved	249.5 (±8.3)	35.96 (±1.51)	4.03 (±0.23)	7.93 (±0.57)	0.89 (±0.10)	7.89 (±0.15)	-14.42 (±0.57)	-96.21 (±1.15)	9
RHW-02	Groundwater	259.8 (±17.5)	38.80 (±2.07)	6.09 (±0.39)	5.57 (±0.92)	1.38 (±0.33)	17.15 (±0.37)	-14.40 (±0.54)	-95.98 (±0.95)	9
RHW-05		507.6 (±8.2)	56.56 (±1.29)	17.99 (±0.51)	20.98 (±0.71)	1.48 (±0.12)	24.32 (±0.47)	-14.00 (±0.75)	-94.42 (±1.34)	9
EFF	Effluent	621.9 (±214.4)	27.79 (±2.79)	3.07 (±0.67)	101.80 (±42.33)	8.18 (±4.63)	4.03 (±0.68)	-14.31 (±0.77)	-91.67 (±2.62)	8
RHW-13	Very Evolved	704.7 (±12.5)	61.88 (±0.99)	12.14 (±0.13)	79.55 (±0.89)	2.67 (±0.03)	25.83 (±0.31)	-14.67 (±0.76)	-96.81 (±1.33)	6
RHW-10	Groundwater	733.0 (±18.3)	80.23 (±3.43)	35.39 (±1.29)	26.22 (±0.70)	0.93 (±0.09)	22.11 (±1.12)	-12.99 (±0.74)	-88.47 (±1.50)	9

from the Village of Taos Ski Valley sewage treatment plant, and WL-01 and WL-02 are samples collected from Williams Lake and a spring near Williams Lake, respectively.

EMMA was used to determine end-members and their proportional contribution to surface water sampling locations, following the procedures by Christopherson et al. (1990) and Christopherson & Hooper (1992). Only samples with a cation-anion charge balance within 5% were used. The geochemical tracers Electrical Conductivity (EC), Ca^{2+}, Mg^{2+}, Na^+, K^+, SiO_2 were chosen as they were measured on a consistent basis in every sample and are believed to represent the major weathering release products; δ^2H, and $\delta^{18}O$ were also chosen as isotopic tracers due to their known conservative mixing bahavior. A principal-component analysis (PCA) was applied first as a diagnostic tool to determine conservative tracers of the end-member matrix. Eigenvectors extracted from the conservative tracer correlation matrix were used to reproject both surface-water samples and end-members into a mixing subspace (Liu et al., 2008). Appropriateness of a tracer was determined by examining the residuals calculated from the original and reprojected chemistry data. According to Hooper (2003), "A well-posed model is indicated by random pattern of residuals; any structure in this plot suggests a lack of fit in the model, which can arise from the violation of any of the assumptions inherent in the mixing model." Therefore, only tracers with residuals from the PCA having $p > 0.05$ and $R^2 < 0.4$ were chosen. The accumulated percent variance of the eigenvalues was analyzed to determine model fit with a well-posed model accounting for the greatest amount of variance in the lowest dimension mixing subspace. After the conservative tracers were selected for each sample location, new eigenvectors were calculated and the orthogonal
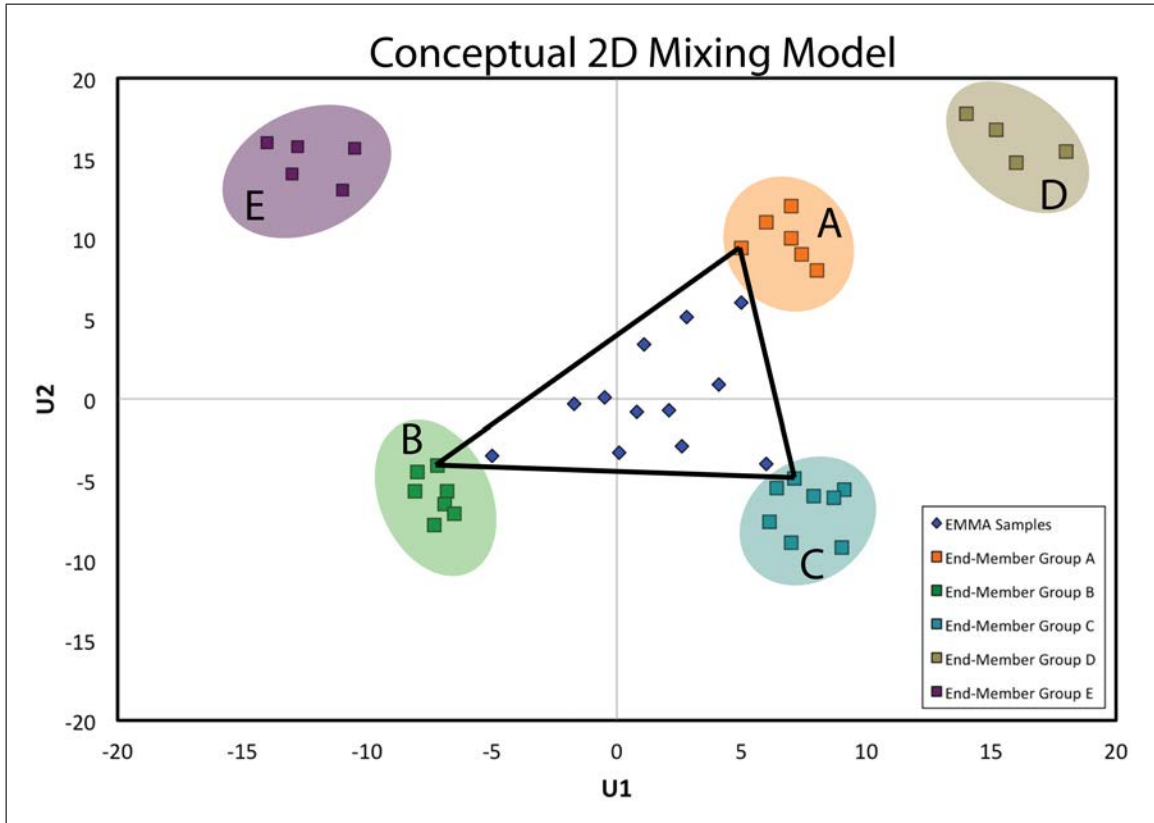
Figure 5.2: Conceptual representation of how end-members are plotted in U-Space. Blue diamonds represent streamflow samples while colored squares are different end-members, with each color representing a different end-member classification (i.e., soil water, evolved groundwater, etc.). In this idealized case, the end-member groups A, B, and C provide the best mixing subspace as they constrain all of the samples and result in the smallest mixing area (i.e., lowest dimensional mixing subspace).

projections of the surface-water samples and end-members were plotted together in the mixing subspace.

In order to prevent conceptual model bias, all non-stream water samples were used as potential end-members. This was done to identify regions in the mixing subspaces that represent distinct geochemical pathways and processes. Thus, it provides an assessment of whether or not end-members share similar geochemical histories. A stream sample will therefore be a mixture of waters representing these geochemical pathways (Figures 5.2 and 5.3). If my hypothe-
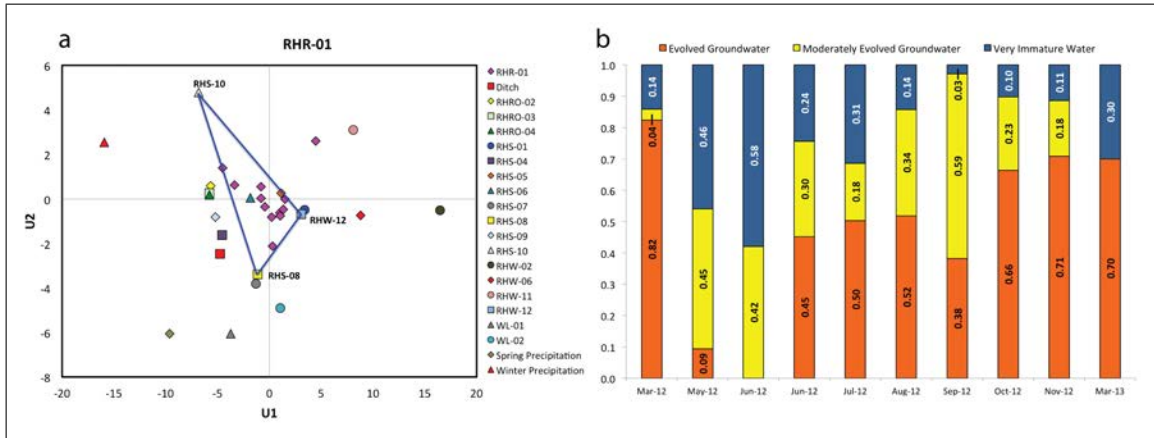
Figure 5.3: A) U-space plot of end-members and streamflow samples collected from RHR-01 (USGS gauging station 08267500). The blue triangle indicates the area bounded by the end-members that produced the smallest mixing subspace. B) Time series of relative contributions from selected end-members (end-members displayed as subjective category, see Table 5.2) calculated from geometric position within the mixing subspace.

sis was correct then streamflow contributions from evolved groundwater with increasing scale requires geochemical evolution, and therefore I could not assume a single composition of groundwater. In other words, a single groundwater sample represents a specific point along a given flow path, but is not descriptive of all groundwater in the system. However, if my hypothesis was incorrect then EMMA would simply point to precipitation and/or geochemically immature source waters (and by default, shorter residence time waters); more evolved groundwater projections would plot far away from streamflow projections. Given the large pool of end-members and the spectrum of flowpaths they represent, the likelihood that two or more end-members plotted near each other in the mixing subspace, and therefore could both be chosen as end-members, was a very real possibility. Again, this is because samples that plot near each other in the mixing subspace represent similar flowpaths and geochemical pathways in the watershed. When this occurred, it was necessary to select from the potential end-members according to the following criteria: 1) Surface-water samples were

mostly, if not completely, within the area bounded by the end-members, and 2) the mixing area of the three end-members was minimized as much as possible. For most samples this was easily achieved; specific samples that appeared to have missing end-members are discussed below. After end-members were chosen, the geometric mixing proportion of each contributor was calculated for each sample date. Reconstructed stream chemistry was calculated according to the equation

$$C_R = F_1 C_1 + F_2 C_2 + F_3 C_3 \tag{5.3}$$

where C is the solute concentration, F is the geometric mixing proportion, the subscript R refers to the reconstruction, and the subscripts 1, 2, and 3 represent the selected end-members. Model fit was ascertained by plotting reconstructed streamflow chemistry against observed stream chemistry. A well-posed model produces $p <$0.05 and $R^2 >$0.70 (Frisbee et al., 2010).

Although input into EMMA individually, potential end-members were also grouped into seven categories according to geochemistry and field observations (Table 5.2) to aid in the interpretation of the EMMA results. These subjective categories represent the type of geochemical pathway the sample is assumed to have traveled, with more evolved geochemistry suggesting a longer flowpath. While it is impossible to determine if each potential end-member is classified correctly, given the unknown flowpath of each sample, the inclusion of some samples in a certain category can be deduced. For example, precipitation and snowmelt recharge would be expected to be relatively dilute, and indeed they fall within the "Very Immature Water" category. All of the ephemeral spring potential end-members fall within the "Soil Water" classification, suggesting they are fed by a limited subsurface reservoir (i.e., the soil zone) and have a relatively short residence time. Finally, only groundwater samples collected from wells are

included in the "Evolved Groundwater" and "Very Evolved Groundwater" category, as they would be expected to have the longest residence time and therefore the most evolved geochemistry. Radiocarbon results presented in Chapter 4 corroborate the long residence times of some of the groundwater wells sampled. This is not to say that springs in the watershed do not receive waters from very evolved groundwater flowpaths, but the signal is likely damped by mixing with shallower subsurface flowpaths the spring is integrating. Since well screens are usually far below the surface, groundwater wells are more likely to exclude these shallow, shorter residence time flowpaths and be more representative of a point along a given flowpath.

5.3 Results and Discussion

Surface water samples were collected longtitudinally down the Rio Hondo as well as from the East Fork (RHR-11), Manzanita Canyon (RHR-14), and South Fork (RHR-16) subwatersheds. A surface water sample was also collected from a perennial stream that discharges into the closed portion of the headwaters that forms Williams Lake (RHR-22). The results from plotting original stream chemistry against its orthoganol reprojection are shown in Table 5.3. Of the 12 streamflow sampling locations, PCA indicated that eight locations showed conservative behavior for all tracers (EC, Ca^{2+}, Mg^{2+}, Na^+, K^+, SiO_2, δ^2H, and $\delta^{18}O$), while two locations selected seven tracers and another two six tracers. All but one sample location (RHR-11) showed cumulative percent variances greater than 80% for the second eigenvalue (Table 5.4), indicating a three end-member (2D subspace) mixing model was most appropriate. The high cumulative percent variance of

Table 5.3: Correlations between residuals of reprojected and original stream chemistry from PCA for a 2D, three end-member mixing model. Only tracers that showed random distributions in the plots ($p > 0.05$) were selected to be used for EMMA. R^2 is the coefficient of determination (goodness of fit) and p describes the statistical significance of the correlation. Bolded and shaded cells show correlations with $p < 0.05$.

Sample ID	EC (μS/cm)		Ca^{2+}		Mg^{2+}		Na$^+$	
	R^2	p	R^2	p	R^2	p	R^2	p
RHR-01	0.03	0.62	0.05	0.52	0.09	0.39	0.13	0.30
RHR-02	0.01	0.74	0.13	0.30	0.05	0.52	0.05	0.52
RHR-04	0.02	0.73	0.03	0.62	0.03	0.60	0.22	0.16
RHR-10	0.09	0.40	0.03	0.62	0.02	0.67	0.07	0.44
RHR-11	0.06	0.51	0.18	0.21	0.09	0.39	**0.65**	**0.003**
RHR-14	0.04	0.56	0.01	0.76	0.005	0.85	0.03	0.65
RHR-15	0.03	0.61	0.22	0.16	0.04	0.57	0.11	0.35
RHR-16	0.03	0.61	0.05	0.54	0.11	0.34	0.22	0.16
RHR-18	0.02	0.67	0.09	0.40	**0.56**	**0.01**	0.03	0.63
RHR-21	0.02	0.70	0.06	0.49	0.02	0.73	0.05	0.54
RHR-22	0.04	0.58	0.05	0.52	0.06	0.50	0.19	0.20
RHR-24	0.04	0.60	0.02	0.68	0.08	0.42	0.16	0.25

Sample ID	K$^+$		SiO$_2$		δ^{18}O		δ^2H	
	R^2	p	R^2	p	R^2	p	R^2	p
RHR-01	0.15	0.26	0.06	0.48	0.39	0.05	0.21	0.17
RHR-02	**0.57**	**0.01**	0.01	0.78	0.12	0.32	**0.45**	**0.03**
RHR-04	0.39	0.05	0.04	0.57	0.09	0.40	0.33	0.08
RHR-10	0.04	0.58	0.03	0.64	0.33	0.08	0.10	0.36
RHR-11	0.24	0.14	0.32	0.08	0.33	0.07	0.37	0.06
RHR-14	0.13	0.30	0.09	0.39	0.22	0.16	0.10	0.37
RHR-15	0.11	0.35	**0.48**	**0.02**	0.17	0.24	0.09	0.40
RHR-16	0.21	0.18	0.26	0.12	0.13	0.30	0.27	0.11
RHR-18	0.05	0.51	0.07	0.45	**0.55**	**0.01**	0.14	0.28
RHR-21	0.10	0.38	0.13	0.30	0.26	0.13	0.30	0.09
RHR-22	0.10	0.38	0.26	0.12	0.26	0.12	0.05	0.54
RHR-24	0.16	0.25	0.02	0.72	0.02	0.71	0.16	0.25

Table 5.4: Cumulative variance explained by eigenvalues.

Sample ID	Cumulative variance explained by eigenvalues					
	1st Eigenvalue	2nd Eigenvalue	3rd Eigenvalue	4th Eigenvalue	5th Eigenvalue	6th Eigenvalue
RHR-01	67.9	85.9	94.8	97.3	99.0	99.7
RHR-02	62.4	82.7	94.4	98.1	99.3	99.8
RHR-04	69.1	86.0	93.6	97.5	99.9	100
RHR-10	80.9	91.1	98.2	99.1	99.4	99.7
RHR-11	54.9	73.3	88.7	96.9	98.4	99.5
RHR-14	76.2	91.9	97.8	99.3	99.7	99.9
RHR-15	72.2	84.4	93.3	97.9	99.6	99.9
RHR-16	68.2	84.2	92.4	97.0	98.9	99.7
RHR-18	67.2	81.4	91.5	99.1	99.9	100
RHR-21	66.6	88.1	94.1	98.3	99.7	100
RHR-22	67.8	87.4	96.3	99.8	100	–
RHR-24	78.8	91.6	95.4	98.0	99.4	99.8

the eigenvalues for each sampling location provides confidence that I have correctly identified the required number of end-members and dimensionality of the mixing subspace.

Table 5.5 shows the correlation coefficients and p-values of the relationship between the original and reconstructed stream chemistry for each sampling location. Overall, stream chemistry is predicted very well using the selected end-members with 76% of reconstructions showing significant correlation ($p < 0.05$) with original stream chemistry. EC, Ca^{2+}, Mg^{2+}, and Na^+ showed the best reconstructions, with 91% of reconstructions using only these four tracers showing significant correlation ($p < 0.05$) with original stream chemistry. This suggests that Ca^{2+}, Mg^{2+}, and Na^+ are useful descriptors of the dominant bedrock weathering minerals, consistent with the mineralogy of the mountain block described in Chapter 2.

Figure 5.4 shows the spatial and temporal EMMA results for each sampling location, with end-members converted to the subjective classification given in Table 5.2. Groundwater and soil water end-members were chosen consistently

Table 5.5: Correlations between reconstructed and orignal stream chemistry for a 2D, three end-member mixing model. Statistically significant correlations of p <0.05 are indicated by bold entries. R^2 >0.70 shows a well-posed model and are indicated by shaded entries. Dashed entries indicate the tracer was not selected from the PCA. R^2 is the coefficient of determintation (goodness of fit) and p describes the statistical significance of the correlation.

Sample ID	EC (μS/cm)		Ca^{2+}		Mg^{2+}		Na$^+$	
	R^2	p	R^2	p	R^2	p	R^2	p
RHR-01	0.88	0.0004	0.85	4.91E-05	0.77	0.0004	0.44	0.03
RHR-02	0.99	1.15E-10	0.91	4.91E-06	0.90	8.35E-06	0.76	0.0005
RHR-04	0.87	2.54E-10	0.74	0.0007	0.77	0.0004	0.68	0.002
RHR-10	0.79	0.0003	0.74	0.0008	0.27	0.12	0.78	0.0003
RHR-11	0.89	1.06E-05	0.88	1.57E-05	0.04	0.57	–	–
RHR-14	0.81	0.0001	0.72	0.001	0.98	2.09E-09	0.57	0.009
RHR-15	0.94	4.24E-07	0.87	2.11E-05	0.79	0.0002	0.78	0.0003
RHR-16	0.96	5.65E-08	0.94	4.43E-07	0.49	0.02	0.67	0.002
RHR-18	0.69	0.002	0.64	0.004	–	–	0.74	0.001
RHR-21	0.91	4.72E-06	0.81	0.0002	0.98	8.62E-10	0.40	0.045
RHR-22	0.41	0.04	0.40	0.04	0.20	0.19	0.42	0.04
RHR-24	0.39	0.046	0.10	0.37	0.87	2.63E-05	0.81	0.0002

Sample ID	K$^+$		SiO$_2$		δ^{18}O		δ^2H	
	R^2	p	R^2	p	R^2	p	R^2	p
RHR-01	0.19	0.20	0.16	0.25	0.29	0.10	0.15	0.27
RHR-02	–	–	0.04	0.58	0.81	0.0002	–	–
RHR-04	0.59	0.007	0.48	0.02	0.01	0.82	0.13	0.29
RHR-10	0.01	0.79	0.47	0.02	0.44	0.03	0.73	0.0009
RHR-11	0.001	0.92	0.85	4.62E-05	0.66	0.003	0.31	0.09
RHR-14	0.29	0.10	0.32	0.08	0.78	0.0004	0.89	1.21E-05
RHR-15	0.80	0.0002	–	–	0.67	0.002	0.18	0.21
RHR-16	0.84	6.82E-05	0.49	0.02	0.53	0.01	0.03	0.64
RHR-18	0.39	0.046	0.42	0.04	–	–	0.91	4.30E-06
RHR-21	0.68	0.002	0.75	0.0006	0.02	0.67	0.003	0.87
RHR-22	0.87	2.38E-05	0.45	0.03	0.47	0.02	0.27	0.12
RHR-24	0.36	0.06	0.70	0.001	0.79	0.0002	0.51	0.02
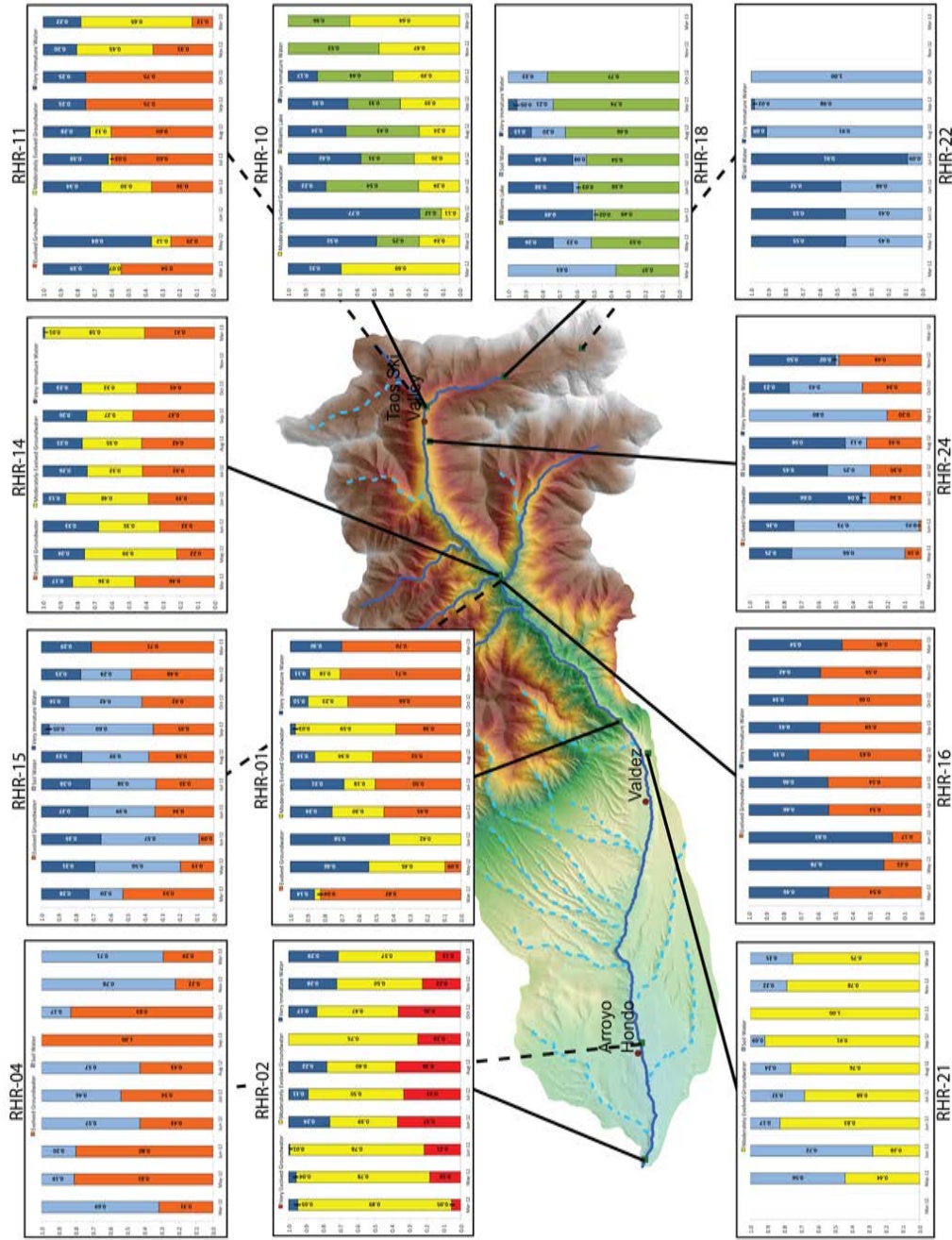
Figure 5.4: EMMA results for each surface water sampling location showing relative contributions from end-members. Cooler colors indicate less evolved waters where warmer colors indicate more evolved waters. Structed contributions begin to appear at RHR-18 (8.3 km²), with increasing groundwater contributions through the year after the snowmelt pulse as well as more evolved end-members at lower elevations.

94

for each sampling location, with precipitation (winter and spring) and direct snowmelt recharge (PCAPS) making up only 11% of the selected end-members. Summer precipitation was not a viable choice for any of the sites, consistent with stable isotopic data presented in Chapter 3. In addition, U-Space projections of effluent from the Taos Ski Valley sewage treatment plant did not plot near any of the stream sites, providing evidence that anthropogenic contamination is not likely to be responsible for geochemical changes in the surface water system. Moderately-evolved, evolved, and very-evolved groundwater end-members were selected for all but the two highest elevation surface water sites, with more evolved groundwater end-members being selected for lower elevation sites. The other two end-members identified for each site were usually soil water and very immature water (e.g., RHS-10 and PCAPS).

The most common end-member chosen for the very immature water classification was RHS-10, a diffuse spring that was only sampled once in late June 2013 due to poor accessability. Although it was classified as immature water due to its overall geochemistry, RHS-10 does have elevated silica concentrations compared with the rest of the end-members in that group; however, its isotopic composition is very similar to snowmelt. It would appear that this spring may not have a long mean residence time based on its geochemical composition; however, the landowner has stated that the spring is perennial and discharge from the spring is consistent throughout the year (Roger Pattison, personal communication). This observation is corroborated by the existence of a V-notch weir located just below the spring outlet that was installed by the Village of Taos Ski Valley. Other springs in the watershed do not exhibit much temporal geochemical variability (typically <10% variation from the mean for a given solute). If RHS-10 behaves similarly to the other springs it could indicate that its flowpath

residence time is being underpredicted by its relatively dilute geochemistry. This would not significantly alter any of the patterns present in the EMMA results, but would indicate that very rapid overland or subsurface flow is not a significant contributor to streamflow.

One pattern that is apparent from Figure 5.4 is the increase in the proportion of the most evolved end-member for most locations after the snowmelt pulse (late May-Early June 2012). During the snowmelt pulse, groundwater contributions are small relative to other sources of water, most likely being masked by the relatively dilute geochemisty of the snowmelt. As the snowmelt pulse subsides, realtive groundwater contributions continue to increase until the next snowmelt season. For most sample locations, the least geochemically evolved end-member (typically very immature water) is the first to decrease its contribution to streamflow, followed by the second most geochemically evolved (typically soil water or moderately evolved groundwater). This suggests there are three main flowpath categories contributing to streamflow, each having very different residence times. Conceptually these are likely represented (in order of increasing residence time) by flow through 1) soil macropores or coarse talus slopes that are prevalent in the watershed, 2) soil horizons or the soil-bedrock interface, and 3) bedrock fractures that make up the deeper groundwater flow system. During and immediately after the snowmelt pulse, flow through soil macropores or coarse talus slopes is the dominant source of water to streamflow. After the snowmelt pulse subsides, this source is depleted and most of the streamflow generation results from soil and deep groundwater sources. As the year progresses, the soil zone becomes increasingly depleted and deep groundwater from bedrock fractures becomes the dominant source of streamflow. This process is consistent with the 3D conceptual model proposed by Frisbee et al. (2011) since fluid fluxes from groundwater sources are not changing their relative contributions to streamflow. In other

words, during the transitions from snowmelt season to summer monsoon, and from summer monsoon to autumn baseflow, the relative contribution from deep groundwater becomes a larger proportion of streamflow.

The other trend consistent with the 3D conceptual model is the increasing contributions from more evolved groundwater with increasing scale. Figure 5.5 shows the relative contributions from the most evolved end-members for three locations along the main stem of the Rio Hondo ranging from 2234 to 2867 m. The highest elevation site (RHR-10) shows moderately evolved groundwater as the most evolved end-member, with contributions averaging 32% for all samples. Groundwater contributions to RHR-15 are slightly higher, averaging 38%, but there is a change to a more evolved groundwater component. The lowest elevation site (RHR-01) also shows evolved groundwater as the most mature end-member, with average groundwater contributions increasing to 50%. Not only is the groundwater evolving as it moves through the mountain block, but the stream integrates more of these deep flowpaths as it travels from the headwaters to the basin outlet. This deep groundwater signal is masked during the snowmelt season, as the smallest relative contribution of deep groundwater was observed during the peak of snowmelt (Figure 5.5), as expected. Structured subsurface contributions to the stream appear to be well developed at location RHR-18, where the catchment has grown to 8.3 km^2 (see Figure 5.4). This is on the same order of basin size that Wolock et al. (1997) observed that stream chemistry did not change significantly with increasing scale. Here in the Rio Hondo watershed, however, my data suggests that structured trends in groundwater contributions begin to appear at that small scale.
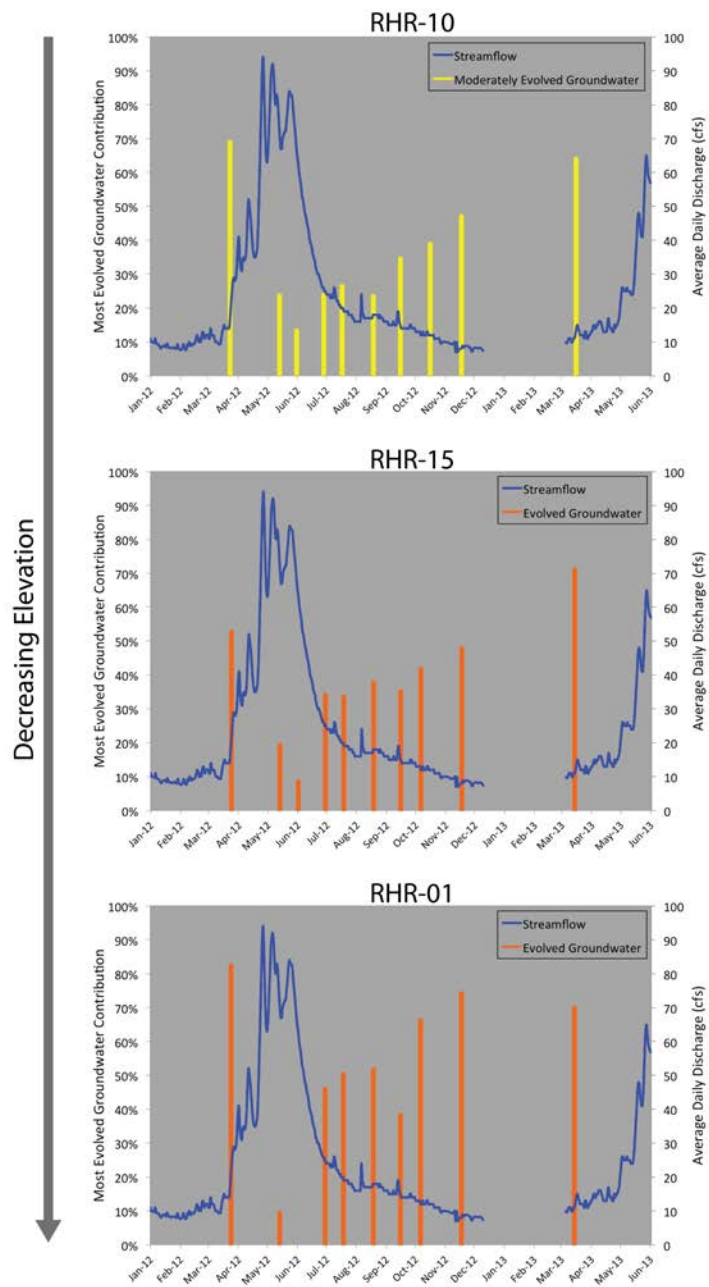
Figure 5.5: Relative contribution of most evolved groundwater end-member and average daily streamflow measured at USGS gauging station (08267500). Lower elevation sites show more evolved groundwater contributions as well as a greater proportion of more mature waters.

5.4 Conclusions

Geochemical and isotopic separations of streamflow using EMMA show that a large proportion surface water in the Rio Hondo is derived from subsurface flow paths, and these contributions remain important even during the peak of the snowmelt season. The positive correlation between upstream contributing area and stream solute concentrations presented in Chapter 3 can be explained by increasingly more evolved deep groundwater discharing to surface water and an increase in the relative contribution from these deep groundwater sources as basin drainage area increases. The geochemical patterns observed in the Rio Hondo are similar to those reported by Frisbee et al. (2011) for the Saguache Creek watershed and suggest that flowpaths in the watershed are best explained by the 3D conceptual model. This also indicates that the 3D conceptual model is transferrable to at least one other high-elevation watershed with different geology, climate, drainage area, and human impacts.

One substantial difference between the patterns observed in the Rio Hondo and Saguache Creek watersheds is the development of ordered deep groundwater contributions at the scale of square kilometers in the Rio Hondo instead of hundreds of square kilometers as in Saguache. This is likely due to the steep topography of the Rio Hondo which would allow for deeper, more localized flowpaths to develop (Tóth, 1963; Gleeson & Manning, 2008; Harding, 2012). Topography is likely a first-order control on the hydrologic system while geology, climate, and human development are not. Although not explored in the study, the bedrock effective hydraulic conductivity is likely another first order control on the scale and quantity of deep groundwater discharged to streamflow.

Increasing average surface temperatures are expected to reduce snowpack as well as cause earlier and more intense snowmelt, resulting in decreased infiltration of spring precipitation and evolved snowmelt that has been shown to be a large contributor to waters within the basin (Chapter 3). Shorter residence time waters are more likely to respond rapidly to changes in climate, while this same signal may not propogate to long residence time flowpaths for some time. This would result in a greater relative contribution from longer residence time flowpaths (i.e., deep groundwater) as short residence time reserviors (i.e., surface runoff and the soil zone) become depleted due to decreased recharge (and potentially increased ET). Baseflow may be sustained at or near current levels throughout the summer when it is needed most, as deep groundwater appears to be the major contributor to streamflow later in the year. This is important for the Rio Hondo watershed since about 90% of the water used in the area is surface water (DBS&A, 2008). Flows would not be sustained indefinitely, but may provide enough time for adaptive management strategies to be implemented. This deep groundwater component of streamflow has now been identified in two high-elevation mountain watersheds having very different drainage areas, geology, and topography, and indicates observed geochemical patterns are process based and not unique to a single system.

CHAPTER 6

SYNTHESIS AND CONCLUSIONS

This thesis has sought to provide a greater understanding of how stream-flow is generated in a fractured crystalline bedrock watershed at the basin scale. Multiple methods, including isotopic, geochemical, age dating, and streamflow separation techniques were used to test the transferability of a conceptual model developed by Frisbee et al. (2011) for a watershed having different geology, scale, topography, climate, and human impact. This chapter seeks to synthesize results from the previous chapters to provide a holistic view of basin scale watershed processes. In addition, lessons learned from this project and recommendations for future work are also provided.

Stable isotopic results for ^{18}O and ^{2}H indicate that nealy all waters in the Rio Hondo are sourced from winter and spring precipitation, despite only about one-third of annual precipitation falling during that period. This is consistent with results from other stable isotopic studies conducted in the southwestern U.S. that show importance of seasonality on groundwater recharge (Cunningham et al., 1998; Winograd et al., 1998; Blasch & Bryson, 2007). Streamflow separations using End-Member Mixing Analysis (EMMA) also indicate that summer precipitation is not a significant direct contributor to surface water, as it was only selected as an end-member for one sampling location (RHR-16) and even then it was not a very good fit. Since isotopic values are stable for nearly all sampling

locations, waters must be stored in the subsurface below the rooting depth where they are not subject to evapotranspiration processes or mixing with summer precipitation before they are discharged to the stream. This suggests a minimum residence time of six months for waters in the Rio Hondo during the later part of the year, as the snowpack in the watershed has largely melted out by mid-June.

The importance of snowpack to streamflow generation has important climate change implications since increasing global surface temperatures will likely result in less winter precipitation falling as snow and earlier onset of spring melting (Leung & Wigmosta, 1999; Cayan et al., 2001; Barnett et al., 2005). A reduction in snowpack and earlier onset of spring melting means that the snowmelt pulse in surface water will be routed through the system in a shorter period of time, and baseflow will dominate through the year. While total annual flows may not change, available water throughout summer may be reduced in the near future if residence times in the mountain block are short. Since approximately 90% of the water used in the area is surface water (DBS&A, 2008), this will likely have negative impacts to agricultural communities in the area as well as Taos Ski Valley, which uses winter surface flows for snow-making operations.

Although the peak and timing of runoff is likely to be affected by climate change, and has potential implications for damage associated with flooding, agriculture in the area primarily relies on streamflow during peak flow recessions and baseflow. Data presented in Chapter 3 indicate groundwater, surface water, and spring water all evolve along similar geochemical pathways, and that solute concentrations increase with basin drainage area. Evaporative concentration of surface waters was discounted due to no evidence of isotopic fractionation of streamflow. Nearly all of the selected end-members from the EMMA analysis

were subsurface sources (i.e., direct contributions of precipitation to streamflow are minimal), and usually a mixture of geochemically immature and mature waters. Furthermore, streamflow separations showed increasingly evolved groundwater end-members and/or increased relative contributions of the most evolved end-member with increasing basin drainage area. All of these observations are predicted by the 3D conceptual model developed by Frisbee et al. (2011) and by my hypothesis of increasing deep groundwater contributions with increasing basin drainage area.

While the trends in solute concentration and basin drainage area are similar for Saguache Creek and the Rio Hondo, they do occur at drastically different scales. Structured groundwater contributions to Saguache Creek began at around 350 km^2 (Frisbee et al., 2011), whereas they appear to develop in the Rio Hondo at approximately 5 to 8 km^2. Curiously, this nearly the same scale that Wolock et al. (1997) found stream chemistry to stabilze in the Neversink River watershed, which is described as a narrow valley with steep slopes, similar to the Rio Hondo watershed. This may represent some critical basin area required to generate groundwater flow paths, or may just be coincidental.

Since groundwater appears to be the dominant source of streamflow in the watershed after the snowmelt pulse, there should be some additional buffering capacity against climate change if the residence time of these waters is sufficiently long. The age dating results presented in Chapter 4 indicate that residence times in the mountain block range from modern to possibly thousands of years old. There also appears to be correlation of chlorofluorocarbon (CFC) age and tritium concentration with elevation, with younger waters near the headwaters and older waters near the mountain front. This trend is predicted by the 3D conceptual

model and is also consistent with my hypothesis of increasing deep groundwater contributions with increasing basin drainage area.

Mixing between young and old waters is suggested from chlorofluorocarbon dating results and tritium concentrations. This is supported by EMMA results that consistently show an immature subsurface end-member along with more mature groundwater end-members. While groundwater end-members may be assumed to have little mixing with modern waters if a well is sufficiently deep and properly completed, the same is not true for springs which may intercept a portion of modern soil water at the discharge point. This complicates ^{14}C dating of springs due to the highly non-linear mixing relationship between young and old waters that biases the mixture young. Therefore, ^{14}C ages collected from springs may be a minimum age. This may also be an explanation for why nearly all of the ages collected from the valley floor wells and springs are modern. Infiltration of irrigation waters may have mixed with older waters to such a degree that the radiogenic and tracer clocks were effectively reset. More detailed age-dating and numerical modeling is required to determine the degree of buffering potential the Rio Hondo watershed has against climate change, but these preliminary results indicate there is potential for it.

The EMMA results are strong support for my hypotheses that 1) deep groundwater contributions are a significant source of streamflow generation in the Rio Hondo watershed, and 2) the relative contribution and/or geochemical evolution of this deep groundwater increases with watershed drainage-area, with significant contributions defined as being greater than or equal to 10% of the average annual flow. Deep groundwater contributions averaged about 30 to 50% in all surface-water samples after deep groundwater was selected as an end-member,

a much greater proportion than the arbitrary 10% selected for hypothesis testing. In addition, lower elevation samples showed greater average contributions from deep groundwater, as well as more evolved groundwater end-members, supporting my second hypothesis.

Overall, the predictions made by the 3D conceptual model are observed in the isotopic, geochemical, age-dating, and streamflow separation results. Surface-water solute concentrations continue to increase with increasing basin drainage area and cannot be explained by evaporative concentration or wastewater treatment plant effluent discharge. Groundwater, surface-water, and spring-water appear to follow a similar geochemical evolutionary pathway, and waters appear to become progressively older moving towards to the mountain front. Finally, numerical streamflow separations using EMMA specifically select groundwater end-members for nearly all sampling locations. Therefore, the conceptual model developed by Frisbee et al. (2011) appears to be transferrable to at least one other high-elevation mountain watershed with different geology, climate, scale, topography, and human impacts. This indicates that groundwater flow within mountain blocks may be much more important than previously thought, as it is the dominant contributor to streamflow and may have residence times orders of magnitude longer than currently believed.

Longer mean residence time of waters in high-elevation mountain basins may provide an additional buffering capacity against climate change. Although annual total precipitation may not change for a given geographic area, predicted increases in temperature are likely to reduce the fraction of precipitation that falls as snow. Data presented in Chapter 3 has shown that nearly all waters in the Rio Hondo watershed are sourced from late season snow and spring precipitation,

so a reduction in snowpack will likely have a large impact on recharge rates into the mountain block. However, with mean residence times possibly on the order of hundreds of years, this climate change signal may not propogate through the system for some time, potentially buffering the Rio Hondo against climate change temporarily. Discharge of groundwater to surface water is also dependent on sufficient hydraulic gradients which are able to travel much more quickly through the system than solutes or tracers. The steep topography of the Rio Hondo and highly fractured allow for gravity drainage of the fractured mountain block. Computer models would be helpful in determining if sufficiently long residence times give mountain watersheds an additional buffering capacity against climate change.

Future work that could improve on the quality of interpretations from this study would be installation of in-stream piezometers in the Rio Hondo, detailed stream gauging of the Rio Hondo and its tributaries, and greater sampling density along the Rio Hondo. Instream piezometers would allow for the measurement of vertical hydraulic gradients as well as provide another geochemical sampling point in much greater spatial proximity to the stream than the wells and springs currently sampled. Installation of stainless steel piezometers using a pneumatic hammer is recommended, as manual installion of CPVC piezometers using a sheath and rod type assembly failed due to the extremely rocky nature of the streambed. Stream gauging would also be helpful, as we would expect streamflows to increase from the headwaters to the mountain front as a result of the increasing groundwater contributions. Greater sampling density may also provide evidence of diffuse or concentrated groundwater inputs along the stream.

Numerical modeling of the watershed would also be useful in exploring the controls deep groundwater flow has on streamflow generation within the mountain block. Reproduction of groundwater flowpaths though the mountain block using realistic values of permeability and recharge rates would support our conceptual model. The apparent importance of deep groundwater has implications for modeling mountain watersheds. Harding (2012) has demonstrated that topographic divides and groundwater divides are rarely coincident, and therefore extension of model boundaries beyond the basin in question is desireable. However, this results in increased computational costs, as well as increased data requirements.

Understanding how high-elevation watersheds operate at larger scales is important for better predicting how they will respond to future climate change. Using a mountain-centered approach, rather than a valley-centered or hillslope-centered approach will likely provide more information about the hydrologic flow systems of high-elevation mountain watersheds operative at the watershed scale. In some watersheds, significant contributions from old, deep groundwater may provide some additional buffering capacity against future climate change, at least for a limited time.

REFERENCES

Aishlin, P. and McNamara, J. P. (2011). Bedrock infiltration and mountain block recharge accounting using chloride mass balance. *Hydrological Processes*, 25(12):1934–1948. doi: 10.1002/hyp.7950.

Anderson, S. P., Dietrich, W. E., Montgomery, D. R., Torres, R., Conrad, M. E., and Loague, K. (1997b). Subsurface flow paths in a steep, unchanneled catchment. *Water Resources Research*, 33(12):2637–2653.

Anderson, S. P., Dietrich, W. E., Torres, R., Montgomery, D. R., and Loague, K. (1993). A case for geochemical control of concentration-discharge relationships. *Chemical Geology*, 107(3-4):369–371.

Anderson, S. P., Dietrich, W. E., Torres, R., Montgomery, D. R., and Loague, K. (1997a). Concentration-discharge relationships in runoff from a steep, unchanneled catchment. *Water Resources Research*, 33(1):211–225.

Archer, R. J., LaSala Jr., A. M., and Kammerer, J. C. (1968). Chemical Quality of Streams in the Erie-Niagara Basin. Technical report, New York State Conservation Department Basin Planning Report ENB-4, New York. 104 pages.

Armour, J., Fawcett, P. J., and Geissman, J. W. (2002). 15 k.y. paleoclimatic and glacial record from northern New Mexico. *Geology*, 30(8):723–726. doi:10.1130/0091–7613(2002)030<0723:KYPAGR>2.0.CO;2.

Bales, R. C., Molotch, N. P., Painter, T. H., Dettinger, M. D., Rice, R., and Dozier, J. (2006). Mountain hydrology of the western United States. *Water Resources Research*, 42(8):W08432. doi: 10.1029/2005WR004387.

Barnett, T. P., Adam, J. C., and Lettenmaier, D. P. (2005). Potential impacts of a warming climate on water availability in snow-dominated regions. *Nature*, 438(17):303–309. doi: 10.1038/nature04141.

Bauer, P., Johnson, P., and Kelson, K. (1999). Geology and Hydrogeology of the Southern Taos Valley, Taos County, New Mexico. Technical report, New Mexico Bureau of Geology and Mineral Resources Open-file Report 501. 55 pages.

Benson, A. L. (2004). Groundwater Geology of Taos County. *New Mexico Geological Society Guidebook, 55th Field Conference, Geology of the Taos Region*, pages 420–432.

Beven, K. (2006). *Streamflow Generation Processes*. IAHS Press. 431 pages.

Blasch, K. W. and Bryson, J. R. (2007). Distinguishing sources of ground water recharge by using δ^2H and δ^{18}O. *Ground Water*, 45(3):294–308. doi: 10.1111/j.1745–6584.2006.00289.x.

Bricker, O. P. and Jones, B. F. (1995). Main Factors Affecting the Composition of Natural Waters. In Salbu, B. and Steinnes, E., editors, *Trace Elements in Natural Waters*, chapter 1, pages 1–20. CRC Press, Inc.

Brown, V. A., McDonnell, J. J., Burns, D. a., and Kendall, C. (1999). The role of event water, a rapid shallow flow component, and catchment size in summer stormflow. *Journal of Hydrology*, 217(3-4):171–190.

Burck, P., Barroll, P., Core, A., and Rappuhn, D. (2004). Taos Regional Groundwater Flow Model. In Brister, B., Bauer, P. W., Read, A. S., and Lueth, V. W., editors, *New Mexico Geological Society Guidebook, 55th Field Conference, Geology of the Taos Region*, pages 433–439.

Caine, J., Evans, J., and Forster, C. (1996). Fault zone architecture and permeability structure. *Geology*, 24(11):1025–1028.

Caine, J. and Tomusiak, S. (2003). Brittle structures and their role in controlling porosity and permeability in a complex Precambrian crystalline-rock aquifer system in the Colorado Rocky Mountain Front. *Geological Society of America Bulletin*, 115(11):1410–1424.

Cayan, D., Kammerdiener, S., Dettinger, M., Caprio, J., and Peterson, D. (2001). Changes in the onset of spring in the western United States. *Bulletin of the American Meteorological Society*, 82(3):399–415.

Christopherson, N. and Hooper, R. P. (1992). Multivariate Analysis of Stream Flow Chemistry Data: The Use of Principal Components for the End-Member Mixing Problem. *Water Resources Research*, 28(1):99–107.

Christopherson, N., Neal, C., Hooper, R. P., Vogt, R. D., and Andersen, S. (1990). Modeling Streamwater Chemistry as a Mixture of Soilwater End-Members - A Step Towards Second-Generation Acidification Models. *Journal of Hydrology*, 116:307–320.

Clark, I. D. and Fritz, P. (1997). *Environmental Isotopes in Hydrogeology*. CRC Press. 352 pages.

Clark, K. and Read, C. (1972). Geology and ore deposits of Eagle Nest area, New Mexico. Technical report, New Mexico Bureau of Mines and Mineral Resources Bulletin 94. 166 pages.

Condie, K. (1979). Precambrian rocks of the Taos Range and vicinity, northern New Mexico. In Ingersoll, R. V., Woodward, L. A., and James, H. L., editors, *New Mexico Geological Society Guidebook, 30th Field Conference*, pages 107–111.

Coons, L. M. and Kelly, T. E. (1984). Regional Hydrology and the Effect of Structural Control on the Flow of Groundwater in the Rio Grande Trough, Northern New Mexico. In Badlridge, W. S., Dickerson, P. W., and Riecker, R. E., editors, *New Mexico Geological Society Guidebook, 35th Field Conference, Rio Grande Rift: Northen New Mexico*, pages 241–244.

Daniel B. Stephens & Associates, I. (2008). Toas Regional Water Plan. Technical Report. 346 pages.

Dingman, S. L. (1994). *Physical Hydrology*. Macmillan, Indianapolis, IN. 646 pages.

Drakos, P., Lazarus, J., and White, B. (2004). Hydrologic Characteristics of Basin-Fill Aquifers in the Southern San Luis Basin, New Mexico. *New Mexico Geological Society Guidebook, 55th Field Conference, Geology of the Taos Region*, 7.

Dunne, T. and Black, R. (1970). Partial Area Contributions to Storm Runoff in a Small New England Watershed. *Water Resources Research*, 6(5):1296–1311.

Earman, S. (2004). *Groundwater recharge and movement through mountain-basin systems of the Southwest: a case study in the Chiricahua Mountains-San Bernardino Valley system, Arizona and Sonora*. PhD thesis, New Mexico Institute of Mining and Technology.

Earman, S., Campbell, A. R., Phillips, F. M., and Newman, B. D. (2006). Isotopic exchange between snow and atmospheric water vapor: Estimation of the snowmelt component of groundwater recharge in the southwestern United States. *Journal of Geophysical Research*, 111(D9):D09302. doi:10.1029/2005JD006470.

Fernald, A. G., Baker, T. T., and Guldan, S. J. (2007). Hydrologic, Riparian, and Agroecosystem Functions of Traditional Acequia Irrigation Systems. *Journal of Sustainable Agriculture*, 30(2):147–171. doi: 10.1300/J064v30n02.

Freeze, R. A. (1972). The Role of Subsurface Water in Generating Surface Runoff: 1. Base Flow Contributions to Channel Flow. *Water Resources Research*, 8(3):609–623.

Friedman, I., Smith, G. I., Gleason, J. D., Warden, A., and Harris, J. M. (1992). Stable isotope composition of waters in southeastern California 1. Modern precipitation. *Journal of Geophysical Research*, 97(D5):5795–5812.

Frisbee, M., Phillips, F., Campbell, A. R., Hendrickx, J., and Engle, E. (2009). Passive capillary samplers for collecting samples of snowmelt infiltration for stable isotope analysis in remote, seasonally inaccessible watersheds 2: field evaluation. *Hydrological Processes*, 24(7):834–849. doi: 10.1002/hyp.7524.

Frisbee, M. D. (2010). *Streamflow Generation Processes and Residence Times in a Large, Mountainous Watershed in the Southern Rocky Mountains of Colorado, USA*. PhD thesis, New Mexico Institute of Mining and Technology. 229 pages.

Frisbee, M. D., Phillips, F. M., White, A. F., Campbell, A. R., and Liu, F. (2013a). Effect of source integration on the geochemical fluxes from springs. *Applied Geochemistry*, 28:32–54. doi: 10.1016/j.apgeochem.2012.08.028.

Frisbee, M. D., Wilson, J. L., Gomez, J. D., Phillips, F. M., and Campbell, A. R. (2013b). Are we missing the tail (and the tale) of residence-time distributions in watersheds? *Geophysical Research Letters*, 40(17):4633–4637. doi: 10.1002/grl.50895.

Frohlich, K., Frohlich, W., and Wittenberg, H. In Seuna, P., Gustard, A., Arnell, N. W., and Cole, G. A., editors, *FRIEND: Flow Regimes from International Experimental and Network Data*, pages 69–75.

Gardner, W. P., Harrington, G. A., Solomon, D. K., and Cook, P. G. (2011). Using terrigenic ^{4}He to identify and quantify regional groundwater discharge to streams. *Water Resources Research*, 47(6):W06523. doi:10.1029/2010WR010276.

Garrabrant, L. A. (1993). Water Resources of Taos County, New Mexico. Water-Resources Investigations Report 93-4107. 93 pages. Technical report, USGS.

Gleeson, T. and Manning, A. H. (2008). Regional groundwater flow in mountainous terrain: Three-dimensional simulations of topographic and hydrogeologic controls. *Water Resources Research*, 44(10):W10403. doi: 10.1029/2008WR006848.

Gruner, J. (1920). Geologic Reconaissance of the Southern Part of the Taos Range, New Mexico. *The Journal of Geology*, 28(8):731–742.

Gudmundsson, A. (2000). Active fault zones and groundwater flow. *Geophysical Research Letters*, 27(18):2993–2996.

Harding, J. J. (2012). *Building the Foundation for a Hydrogeology Model of the Rio Hondo Watershed , NM*. Master's thesis, New Mexico Institute of Mining and Technology. 208 pages.

Hewlett, J. (1961). Soil moisture as a source of base flow from steep mountain watersheds. U.S. Department of Agriculture, U.S. Forest Service Station Paper no. 132. 12 pages.

Hogan, J. F. and Blum, J. (2003). Tracing hydrologic flow paths in a small forested watershed using variations in ^{87}Sr/^{86}Sr, [Ca]/[Sr], [Ba]/[Sr] and δ^{18}O. *Water Resources Research*, 39(10):1282.

Horton, R. (1933). The Role of infiltration on the hydrologic cycle. *Transactions, American Geophysical Union*, 14:446–460.

Johnson, C., Czamanske, G., and Lipman, P. (1989). Geochemistry of the intrusive rocks associated with the Latir volcanic field, New Mexico, and contrasts between evolution of plutonic and volcanic rocks. *Contributions to Mineralogy and Petrology*, 103:90–109.

Johnson, P. (1998). Surface Water Assessment, Taos County, New Mexico. NM-BGMR Open File Report 440. Technical report, New Mexico Bureau of Geology and Mineral Resources. 332 pages.

Johnson, P. (1999). Availability and variability of surface-water resources in Taos County , New Mexico an assessment for regional planning. *New Mexico Geology*, 21(1):1–9.

Johnson, P. S., Bauer, P. W., and Felix, B. (2009). Hydrogeologic investigation of the Arroyo Hondo area , Taos county, New Mexico. Open-File Report 505. Technical report, New Mexico Bureau of Geology and Mineral Resources. 52 pages.

Knowlton, R. G. J. (1990). *A Stable Isotopic Study of Water and Chloride Movement in Natural Desert Soils*. PhD thesis, New Mexico Institute of Mining and Technology. 254 pages.

Kosugi, K., Katsura, S., Katsuyama, M., and Mizuyama, T. (2006). Water flow processes in weathered granitic bedrock and their effects on runoff generation in a small headwater catchment. *Water Resources Research*, 42(2):W02414. doi: 10.1029/2005WR004275.

Kurc, S. A. and Small, E. E. (2004). Dynamics of evapotranspiration in semi-arid grassland and shrubland ecosystems during the summer monsoon season, central New Mexico. *Water Resources Research*, 40(9):W09305. doi: 10.1029/2004WR003068.

Lasaga, A. C. (1984). Chemical kinetics of water-rock interactions. *Journal of Geophysical Research*, 89(4):4009–4025.

Laudon, H. and Slaymaker, O. (1997). Hydrograph separation using stable isotopes, silica and electrical conductivity : an alpine example. *Journal of Hydrology*, 201:82–101.

Leung, L. and Wigmosta, M. (1999). Potential Climate Change Impacts on Mountain Watersheds in the Pacific Northwest. *Journal of the American Water Resources Association*, 35(6):1463–1471.

Linsley, R. K. and Franzini, J. B. (1964). *Water-resources Engineering*. McGraw-Hill, New York. 690 pages.

Lipman, P. W. and McIntosh, W. C. (2008). Eruptive and Noneruptive Calderas, Northeastern Colorado: Where did the Ignimbrites come from? *Geological Society of America Bulletin*, 120(7-8).

Lipman, P. W. and Mehnert, H. H. (1979). The Taos Plateau volcanic field, northern Rio Grande rift, New Mexico. Technical report, USGS. 24 pages.

Liu, F., Bales, R. C., Conklin, M. H., and Conrad, M. E. (2008). Streamflow generation from snowmelt in semi-arid, seasonally snow-covered, forested catchments, Valles Caldera, New Mexico. *Water Resources Research*, 44(12):W12443. doi: 10.1029/2007WR006728.

Liu, F., Williams, M. W., and Caine, N. (2004). Source waters and flow paths in an alpine catchment, Colorado Front Range, United States. *Water Resources Research*, 40(9):W09401. doi: 10.1029/2004WR003076.

Lucas, L. and Unterweger, M. (2000). Comprehensive review and critical evaluation of the half-life of tritium. *Journal of Research of the National Institute of Standards and Technology*, 105(4):541–549.

Maher, K. (2010). The dependence of chemical weathering rates on fluid residence time. *Earth and Planetary Science Letters*, 294(1-2):101–110. doi: 10.1016/j.epsl.2010.03.010.

Manning, A. H., Clark, J. F., Diaz, S. H., Rademacher, L. K., Earman, S., and Niel Plummer, L. (2012). Evolution of groundwater age in a mountain watershed over a period of thirteen years. *Journal of Hydrology*, 460-461:13–28. doi: 10.1016/j.jhydrol.2012.06.030.

Martinec, J. (1975). Subsurface Flow From Snowmelt Traced by Tritium. *Water Resources Research*, 11(3):1964–1966.

McDonnell, J. J. (2003). Where does water go when it rains? Moving beyond the variable source area concept of rainfall-runoff response. *Hydrological Processes*, 17(9):1869–1875.

McGuire, K. J. and McDonnell, J. J. (2006). A review and evaluation of catchment transit time modeling. *Journal of Hydrology*, 330(3-4):543–563. doi: 10.1016/j.jhydrol.2006.04.020.

McNamara, J. (1997). Hydrograph separations in an Arctic watershed using mixing model and graphical techniques. *Water Resources Research*, 33(7):1707–1719.

Mendoza, G. F., Steenhuis, T. S., Walter, M., and Parlange, J.-Y. (2003). Estimating basin-wide hydraulic parameters of a semi-arid mountainous watershed by recession-flow analysis. *Journal of Hydrology*, 279(1-4):57–69.

Michel, R. (2005). Tritium in the Hydrologic Cycle. In Aggarwal, P. K., Gat, J. R., and Froehlich, K. F. O., editors, *Isotopes in the Water Cycle: Past Present, and Future of a Developing Science*, chapter 5, pages 53–66. IEA.

Michel, R. L. (1992). Residence times in river basins as determined by analysis of long-term tritium records. *Journal of Hydrology*, 130(1-4):367–378.

Montgomery, D. R., Dietrich, W. E., Torres, R., Anderson, S. P., Heffner, J. T., and Loague, K. (1997). Hydrologic response of a steep, unchanneled valley to natural and applied rainfall. *Water Resources Research*, 33(1):91–109.

Mote, P. W., Hamlet, A. F., Clark, M. P., and Lettenmaier, D. P. (2005). Declining Mountain Snowpack in Western North America. *Bulletin of the American Meteorological Society*, 86(1):39–49.

Newman, B. D., Wilcox, B. P., Archer, S. R., Breshears, D. D., Dahm, C. N., Duffy, C. J., McDowell, N. G., Phillips, F. M., Scanlon, B. R., and Vivoni, E. R. (2006). Ecohydrology of water-limited environments: A scientific vision. *Water Resources Research*, 42(6):W06302. doi: 10.1029/2005WR004141.

Newton, B. T., Rawling, G. C., Timmons, S. S., Land, L., Johnson, P. S., Kludt, T. J., and Timmons, J. M. (2012). Sacramento Mountains Hydrogeology Study. Open-file Report 543. Technical Report June, New Mexico Bureau of Geology and Mineral Resources. 84 pages.

NMED (2004). Total Maximum Daily Load (TMDL) for the Upper Rio Grande Watershed (Part 1): Pilar, NM, to Colorado Border. Technical report, New Mexico Environment Department. 128 pages.

OSU (2012). New Mexico average monthly and average annual precipitation (1981-2010). Available at http://datagateway.nrcs.usda.gov/GDGOrder.aspx by the Oregon Climate Service at Oregon State University.

Pacheco, F. A. L. and Van der Weijden, C. H. (2012). Integrating topography, hydrology and rock structure in weathering rate models of spring watersheds. *Journal of Hydrology*, 428-429:32–50. doi: 10.1016/j.jhydrol.2012.01.019.

Pearce, A. J., Stewart, M. K., and Sklash, M. G. (1986). Storm runoff generation in humid headwater catchments: 1. Where does the water come from? *Water Resources Research*, 22(8):1263–1272.

Phillips, F. M., Hall, G. E., and Black, M. E. (2011). *Reigning in the Rio Grande: People, Land, and Water*. University of New Mexico Press. 262 pages.

Pinder, G. and Jones, J. (1969). Determination of the Ground-Water Component of Peak Discharge from the Chemistry of Total Runoff. *Water Resources Research*, 5(2):438–445.

Plummer, L., Busenberg, E., and Cook, P. (2006). *Use of Chlorofluorocarbons in Hydrology*. IAEA. 291 pages.

Plummer, L. N. and Glynn, P. (2013). Radiocarbon Dating in Groundwater Systems. In *Isotope Methods for Dating Old Groundwater*, chapter 4, pages 33–89. IAEA.

Plummer, L. N., Prestemon, E. C., and Parkhurst, D. L. (1994). An Interactive Code (NETPATH) for Modeling Net Geochemical Reactions Along a Flow Path. USGS Water-Resources Investigations Report 94-4169. Technical report, Reston, VA. 231 pages.

Rademacher, L. K., Clark, J. F., Clow, D. W., and Hudson, G. B. (2005). Old groundwater influence on stream hydrochemistry and catchment response times in a small Sierra Nevada catchment: Sagehen Creek, California. *Water Resources Research*, 41(2):W02004. doi: 10.1029/2003WR002805.

Rawling, G. C. (2005). Geology and hydrogeology of the Arroyo Seco Area , Taos County , New Mexico. Open-File Report 492. Technical report, New Mexico Bureau of Geology and Mineral Resources. 53 pages.

Rediske, J. H. and Selders, A. A. (1953). The Absorption and Translocation of Strontium by Plants. *Plant physiology*, 28(4):594–605.

Rivera, J. A. (1998). *Acequia Culture: Water, Land, and Community in the Southwest*. University of New Mexico Press. 269 pages.

Rodhe, A., Nyberg, L., Bishop, K., and Abstract, A. (1996). Transit times for water in a small till catchment from a step shift in the oxygen 18 content of the water input. *Water Resources Research*, 32(12):3497–3511.

Sabu, S., Fleming, W., Rivera, J., Thompson, B., and Tidwell, V. (2012). Modeling Acequia Water Use in the Rio Hondo Watershed. *New Mexico Journal of Science*, pages 1–26.

Shevenell, L. and Goff, F. (1995). The use of tritium in groundwater to determine fluid mean residence times of Valles caldera hydrothermal fluids, New Mexico, USA. *Journal of volcanology and geothermal research*, 67:187–205.

Sigstedt, S. C. (2010). *Environmental Tracers in Groundwater of the Salt Basin, New Mexico and Implications for Water Resources*. PhD thesis, New Mexico Institute of Mining and Technology. 202 pages.

Singleton, M. J. and Moran, J. E. (2010). Dissolved noble gas and isotopic tracers reveal vulnerability of groundwater in a small, high-elevation catchment to predicted climate changes. *Water Resources Research*, 46(10):W00F06. doi: 10.1029/2009WR008718.

Sklash, M. G. and Farvolden, R. N. (1979). The role of groundwater in storm runoff. *Journal of Hydrology*, 43(1-4):45–65.

Smerdon, B. D., Payton Gardner, W., Harrington, G. a., and Tickell, S. J. (2012). Identifying the contribution of regional groundwater to the baseflow of a tropical river (Daly River, Australia). *Journal of Hydrology*, 464-465:107–115. doi: 10.1016/j.jhydrol.2012.06.058.

Soil Survey Staff. Natural Resources Conservation Service. United States Department of Agriculture. Soil Survey Geographic (SSURGO) Database for [Taos County and Parts of Rio Arriba and Mora Counties, New Mexico]. Available online at http://soildatamart.nrcs.usda.gov. Accessed [12/15/2011].

Steven, T. A. and Lipman, P. W. (1976). Calderas of the San Juan Volcanic Field, Southwestern Colorado. USGS Professional Paper 958. Technical report, USGS. 35 pages.

Stewart, J., Watts, C., Rodriguez, J., De Bruin, H., van den Berg, A., and Garatuza-Payán, J. (1999). Use of satellite data to estimate radiation and evaporation for northwest Mexico. *Agricultural Water Management*, 38(3):181–193. doi:10.1175/BAMS–86–1–39.

Szabo, Z., Rice, D. E., Plummer, L. N., Busenberg, E., and Drenkard, S. (1996). Age dating of shallow groundwater with chlorofluorocarbons, tritium/helium 3, and flow path analysis, southern New Jersey coastal plain. *Water Resources Research*, 32(4):1023–1038. doi: 10.1029/96WR00068.

Szilagyi, J. and Parlange, M. (1998). Baseflow Separation Based on Analytical Solution of the Boussinesq equation. *Journal of Hydrology*, 204:251–260.

Tetzlaff, D., Soulsby, C., Waldron, S., Malcolm, I. A., Bacon, P. J., Dunn, S. M., Lilly, A., and Youngson, A. F. (2007). Conceptualization of runoff processes using a geographical information system and tracers in a nested mesoscale catchment. *Hydrological Processes*, 21(October 2006):1289–1307. doi: 10.1002/hyp.

Tóth, J. (1963). A theoretical analysis of groundwater flow in small drainage basins. *Journal of Geophysical Research*, 68(16):4795–4812.

USGS (2005). Open-File Report 2005-1351. Preliminary integrated geologic map databases for the United States: Central states: Montana, Wyoming, Colorado, New Mexico, North Dakota, South Dakota, Nebraska, Kansas, Oklahoma, Texas, Iowa, Missouri, Arkansas, and Louisiana. Available at [http://pubs.usgs.gov/of/2005/1351/].

USGS (2011). Gap Analysis Program (GAP). National Land Cover, Version 2. Available at http://gapanalysis.usgs.gov/gaplandcover/viewer/.

Vitvar, T., Burns, D. a., Lawrence, G. B., McDonnell, J. J., and Wolock, D. M. (2002). Estimation of baseflow residence times in watersheds from the runoff hydrograph recession: method and application in the Neversink watershed, Catskill Mountains, New York. *Hydrological Processes*, 16(9):1871–1877.

Vogel, J. (1968). Investigation of groundwater flow with radiocarbon. *Isotopes in Hydrology. Vienna, International Atomic Energy Agency*, pages 355–369.

Weissmann, G. S., Zhang, Y., LaBolle, E. M., and Fogg, G. E. (2002). Dispersion of groundwater age in an alluvial aquifer system. *Water Resources Research*, 38(10):1198–1210. doi: 10.1029/2001WR000907.

Wilson, J. and Guan, H. (2004). Mountain-Block Hydrology and Mountain-Front Recharge. In *Groundwater Recharge in a Desert Environment: The Southwestern United States*, volume 9, pages 113–137.

Winograd, I. J. (1959). Ground-water Conditions and Geology of Sunshine County and Western Taos County, New Mexico. Technical Report 12, New Mexico Office of the State Engineer. 70 pages.

Winograd, I. J., Riggs, A. C., and Coplen, T. B. (1998). The relative contributions of summer and cool-season precipitation to groundwater recharge, Spring Mountains, Nevada, USA. *Hydrogeology Journal*, 6(1):77–93.

Wolock, D., Fan, J., and Lawrence, G. (1997). Effects of basin size on low-flow stream chemistry and subsurface contact time in the Neversink River watershed, New York. *Hydrological Processes*, 11:1273–1286.

WRCC (2013). Taos, New Mexico. Retrieved from http://www.raws.dri.edu/cgi-bin/rawMAIN.pl?nmXTAO [4/1/2013].

Appendices

APPENDIX A

SUMMARY OF SAMPLING LOCATIONS AND DATES

Sample ID	Site Description	Sample Date	Sample Round	UTM- E	UTM- N	Elevation (m)	Drainage Area (km²)
Ditch	Ditch cut near WL Trailhead	9/14/12	8	458702	4050187	3135	
EFF	TSV Sewage Treatment Plant Effluent	3/15/13	11	458702	4050187	2805	
EFF	TSV Sewage Treatment Plant Effluent	10/5/12	9	458702	4050187	2805	
EFF	TSV Sewage Treatment Plant Effluent	9/14/12	8	458702	4050187	2805	
EFF	TSV Sewage Treatment Plant Effluent	8/17/12	7	458702	4050187	2805	
EFF	TSV Sewage Treatment Plant Effluent	7/17/12	6	458702	4050187	2805	
EFF	TSV Sewage Treatment Plant Effluent	6/28/12	5	458702	4050187	2805	
EFF	TSV Sewage Treatment Plant Effluent	6/1/12	4	458702	4050187	2805	
EFF	TSV Sewage Treatment Plant Effluent	5/15/12	3	458702	4050187	2805	
EFF	TSV Sewage Treatment Plant Effluent	5/15/12	3	458702	4050187	2805	
ISO1	TSV ridge isotope collector	3/16/13		459116	4047916	3643	
ISO1	TSV ridge isotope collector	12/18/12		459116	4047916	3643	
ISO1	TSV ridge isotope collector	10/5/12		459116	4047916	3643	
ISO1	TSV ridge isotope collector	7/17/12		459116	4047916	3643	
ISO1	TSV ridge isotope collector	5/31/12		459116	4047916	3643	
ISO1	TSV ridge isotope collector	3/23/12		459116	4047916	3643	
ISO1	TSV ridge isotope collector	1/8/12		459116	4047916	3643	
ISO2	SNOTEL Isotope Collector	3/16/13		459180	4048618	3358	
ISO2	SNOTEL Isotope Collector	12/18/12		459180	4048618	3358	
ISO2	SNOTEL Isotope Collector	10/5/12		459180	4048618	3358	
ISO2	SNOTEL Isotope Collector	7/17/12		459180	4048618	3358	
ISO2	SNOTEL Isotope Collector	5/31/12		459180	4048618	3358	
ISO2	SNOTEL Isotope Collector	1/9/12		459180	4048618	3358	
ISO3	TSV parking lot isotope collector	3/15/13		459099	4050206	2835	
ISO3	TSV parking lot isotope collector	12/18/12		459099	4050206	2835	
ISO3	TSV parking lot isotope collector	10/6/12		459099	4050206	2835	
ISO3	TSV parking lot isotope collector	7/17/12		459099	4050206	2835	
ISO3	TSV parking lot isotope collector	6/1/12		459099	4050206	2835	
ISO3	TSV parking lot isotope collector	3/24/12		459099	4050206	2835	
ISO4	Max Couton isotope collector	3/15/13		454402	4047712	2547	
ISO4	Max Couton isotope collector	12/18/12		454402	4047712	2547	
ISO4	Max Couton isotope collector	10/6/12		454402	4047712	2547	
ISO4	Max Couton isotope collector	7/17/12		454402	4047712	2547	
ISO4	Max Couton isotope collector	6/1/12		454402	4047712	2547	
ISO4	Max Couton isotope collector	6/1/12		454402	4047712	2547	
ISO4	Max Couton isotope collector	3/24/12		454402	4047712	2547	
ISO4	Max Couton isotope collector	1/9/12		454402	4047712	2547	
ISO5	Palemon Martinez isotope collector	3/15/13		449173	4043476	2294	
ISO5	Palemon Martinez isotope collector	12/19/12		449173	4043476	2294	
ISO5	Palemon Martinez isotope collector	10/6/12		449173	4043476	2294	
ISO5	Palemon Martinez isotope collector	7/17/12		449173	4043476	2294	
ISO5	Palemon Martinez isotope collector	6/2/12		449173	4043476	2294	

Sample ID	Site Description	Sample Date	Sample Round	UTM-E	UTM-N	Elevation (m)	Drainage Area (km^2)
ISO5	Palemon Martinez isotope collector	3/24/12		449173	4043476	2294	
ISO5	Palemon Martinez isotope collector	3/24/12		449173	4043476	2294	
ISO5	Palemon Martinez isotope collector	1/9/12		449173	4043476	2294	
ISO6	Peter Merscher isotope collector	3/14/13		439315	4043549	2057	
ISO6	Peter Merscher isotope collector	12/19/12		439315	4043549	2057	
ISO6	Peter Merscher isotope collector	10/5/12		439315	4043549	2057	
ISO6	Peter Merscher isotope collector	7/16/12		439315	4043549	2057	
ISO6	Peter Merscher isotope collector	6/2/12		439315	4043549	2057	
ISO6	Peter Merscher isotope collector	3/24/12		439315	4043549	2057	
ISO6	Peter Merscher isotope collector	1/9/12		439315	4043549	2057	
PCAPS-1	Snowmelt Recharge (15cm)	6/29/13		459116	4047916	3643	
PCAPS-1	Snowmelt Recharge (18cm)	6/29/13		459116	4047916	3643	
PCAPS-1 Upper	Soil Water (15-18 cm)	10/20/12		459116	4047916	3643	
PCAPS-1 Lower	Soil Water (49-51 cm)	10/20/12		459116	4047916	3643	
PCAPS-2	Snowmelt Recharge (25-42cm)	6/29/13		459180	4048618	3358	
PCAPS-2 Upper	Soil Water (25-29 cm)	10/20/12		459180	4048618	3358	
PCAPS-2 Lower	Soil Water (41-42 cm)	10/20/12		459180	4048618	3358	
RHA01	Acequia in front of Hacienda del Valdez	7/18/12	6	449565	4043615	2289	
RHA01	Acequia in front of Hacienda del Valdez	6/29/12	5	449565	4043615	2289	
RHA01	Acequia in front of Hacienda del Valdez	6/2/12	4	449565	4043615	2289	
RHA01	Acequia in front of Hacienda del Valdez	6/2/12	4	449565	4043615	2289	
RHA01	Acequia in front of Hacienda del Valdez	5/13/12	3	449565	4043615	2289	
RHR01	USGS gauge (08267500)	3/14/13	11	450184	4044192	2334	96.1
RHR01	USGS gauge (08267500)	11/17/12	10	450184	4044192	2334	96.1
RHR01	USGS gauge (08267500)	11/17/12	10	450184	4044192	2334	96.1
RHR01	USGS gauge (08267500)	10/6/12	9	450184	4044192	2334	96.1
RHR01	USGS gauge (08267500)	9/15/12	8	450184	4044192	2334	96.1
RHR01	USGS gauge (08267500)	8/18/12	7	450184	4044192	2334	96.1
RHR01	USGS gauge (08267500)	7/18/12	6	450184	4044192	2334	96.1
RHR01	USGS gauge (08267500)	6/29/12	5	450184	4044192	2334	96.1
RHR01	USGS gauge (08267500)	6/29/12	5	450184	4044192	2334	96.1
RHR01	USGS gauge (08267500)	6/1/12	4	450184	4044192	2334	96.1
RHR01	USGS gauge (08267500)	5/13/12	3	450184	4044192	2334	96.1
RHR01	USGS gauge (08267500)	3/24/12	2	450184	4044192	2334	96.1
RHR02	Arroyo Hondo Gorge near Jon Dunn Bridge	3/14/13	11	436785	4043411	1982	187.7
RHR02	Arroyo Hondo Gorge near Jon Dunn Bridge	11/16/12	10	436785	4043411	1982	187.7
RHR02	Arroyo Hondo Gorge near Jon Dunn Bridge	10/5/12	9	436785	4043411	1982	187.7
RHR02	Arroyo Hondo Gorge near Jon Dunn Bridge	9/15/12	8	436785	4043411	1982	187.7
RHR02	Arroyo Hondo Gorge near Jon Dunn Bridge	9/15/12	8	436785	4043411	1982	187.7
RHR02	Arroyo Hondo Gorge near Jon Dunn Bridge	8/18/12	7	436785	4043411	1982	187.7
RHR02	Arroyo Hondo Gorge near Jon Dunn Bridge	7/16/12	6	436785	4043411	1982	187.7
RHR02	Arroyo Hondo Gorge near Jon Dunn Bridge	6/29/12	5	436785	4043411	1982	187.7

Sample ID	Site Description	Sample Date	Sample Round	UTM-E	UTM-N	Elevation (m)	Drainage Area (km²)
RHR02	Arroyo Hondo Gorge near Jon Dunn Bridge	6/2/12	4	436785	4043411	1982	187.7
RHR02	Arroyo Hondo Gorge near Jon Dunn Bridge	5/13/12	3	436785	4043411	1982	187.7
RHR02	Arroyo Hondo Gorge near Jon Dunn Bridge	5/13/12	3	436785	4043411	1982	187.7
RHR02	Arroyo Hondo Gorge near Jon Dunn Bridge	3/24/12	2	436785	4043411	1982	187.7
RHR04	Arroyo Hondo Bridge	3/14/13	11	440357	4043510	2073	164.1
RHR04	Arroyo Hondo Bridge	11/16/12	10	440357	4043510	2073	164.1
RHR04	Arroyo Hondo Bridge	10/5/12	9	440357	4043510	2073	164.1
RHR04	Arroyo Hondo Bridge	10/5/12	9	440357	4043510	2073	164.1
RHR04	Arroyo Hondo Bridge	9/15/12	8	440357	4043510	2073	164.1
RHR04	Arroyo Hondo Bridge	8/18/12	7	440357	4043510	2073	164.1
RHR04	Arroyo Hondo Bridge	7/16/12	6	440357	4043510	2073	164.1
RHR04	Arroyo Hondo Bridge	6/29/12	5	440357	4043510	2073	164.1
RHR04	Arroyo Hondo Bridge	6/29/12	5	440357	4043510	2073	164.1
RHR04	Arroyo Hondo Bridge	6/2/12	4	440357	4043510	2073	164.1
RHR04	Arroyo Hondo Bridge	5/13/12	3	440357	4043510	2073	164.1
RHR04	Arroyo Hondo Bridge	3/24/12	2	440357	4043510	2073	164.1
RHR10	Rio Hondo at TSV near foot bridge	3/16/13	11	459817	4050082	2867	14.8
RHR10	Rio Hondo at TSV near foot bridge	11/17/12	10	459817	4050082	2867	14.8
RHR10	Rio Hondo at TSV near foot bridge	10/6/12	9	459817	4050082	2867	14.8
RHR10	Rio Hondo at TSV near foot bridge	9/15/12	8	459817	4050082	2867	14.8
RHR10	Rio Hondo at TSV near foot bridge	8/18/12	7	459817	4050082	2867	14.8
RHR10	Rio Hondo at TSV near foot bridge	7/17/12	6	459817	4050082	2867	14.8
RHR10	Rio Hondo at TSV near foot bridge	6/28/12	5	459817	4050082	2867	14.8
RHR10	Rio Hondo at TSV near foot bridge	5/31/12	4	459817	4050082	2867	14.8
RHR10	Rio Hondo at TSV near foot bridge	5/31/12	4	459817	4050082	2867	14.8
RHR10	Rio Hondo at TSV near foot bridge	5/31/12	3	459817	4050082	2867	14.8
RHR10	Rio Hondo at TSV near foot bridge	3/23/12	2	459817	4050082	2867	14.8
RHR11	East Fork	3/14/13	11	459878	4050231	2881	8.3
RHR11	East Fork	11/17/12	10	459878	4050231	2881	8.3
RHR11	East Fork	10/6/12	9	459878	4050231	2881	8.3
RHR11	East Fork	9/15/12	8	459878	4050231	2881	8.3
RHR11	East Fork	8/18/12	7	459878	4050231	2881	8.3
RHR11	East Fork	7/17/12	6	459878	4050231	2881	8.3
RHR11	East Fork	6/28/12	5	459878	4050231	2881	8.3
RHR11	East Fork	5/31/12	4	459878	4050231	2881	8.3
RHR11	East Fork	5/13/12	3	459878	4050231	2881	8.3
RHR11	East Fork	3/23/12	2	459878	4050231	2881	8.3
RHR11	East Fork	3/23/12	2	459878	4050231	2881	8.3
RHR14	Manzanitas Canyon	3/14/13	11	454658	4047878	2551	5.9
RHR14	Manzanitas Canyon	3/14/13	11	454658	4047878	2551	5.9
RHR14	Manzanitas Canyon	11/17/12	10	454658	4047878	2551	5.9

Sample ID	Site Description	Sample Date	Sample Round	UTM- E	UTM- N	Elevation (m)	Drainage Area (km^2)
RHR14	Manzanitas Canyon	10/6/12	9	454658	4047878	2551	5.9
RHR14	Manzanitas Canyon	9/15/12	8	454658	4047878	2551	5.9
RHR14	Manzanitas Canyon	8/18/12	7	454658	4047878	2551	5.9
RHR14	Manzanitas Canyon	7/18/12	6	454658	4047878	2551	5.9
RHR14	Manzanitas Canyon	6/29/12	5	454658	4047878	2551	5.9
RHR14	Manzanitas Canyon	5/31/12	4	454658	4047878	2551	5.9
RHR14	Manzanitas Canyon	5/13/12	3	454658	4047878	2551	5.9
RHR14	Manzanitas Canyon	3/24/12	2	454658	4047878	2551	5.9
RHR14	Manzanitas Canyon	3/24/12	2	454658	4047878	2551	5.9
RHR15	Rio Hondo upstream of Taos East Condos	3/14/13	11	454485	4047765	2553	54.8
RHR15	Rio Hondo upstream of Taos East Condos	11/17/12	10	454485	4047765	2553	54.8
RHR15	Rio Hondo upstream of Taos East Condos	10/6/12	9	454485	4047765	2553	54.8
RHR15	Rio Hondo upstream of Taos East Condos	9/15/12	8	454485	4047765	2553	54.8
RHR15	Rio Hondo upstream of Taos East Condos	8/18/12	7	454485	4047765	2553	54.8
RHR15	Rio Hondo upstream of Taos East Condos	7/18/12	6	454485	4047765	2553	54.8
RHR15	Rio Hondo upstream of Taos East Condos	6/29/12	5	454485	4047765	2553	54.8
RHR15	Rio Hondo upstream of Taos East Condos	6/1/12	4	454485	4047765	2553	54.8
RHR15	Rio Hondo upstream of Taos East Condos	5/13/12	3	454485	4047765	2553	54.8
RHR15	Rio Hondo upstream of Taos East Condos	3/24/12	2	454485	4047765	2553	54.8
RHR16	South Fork	3/14/13	11	454477	4047756	2555	19.2
RHR16	South Fork	11/17/12	10	454477	4047756	2555	19.2
RHR16	South Fork	10/6/12	9	454477	4047756	2555	19.2
RHR16	South Fork	9/15/12	8	454477	4047756	2555	19.2
RHR16	South Fork	8/18/12	7	454458	4047756	2555	19.2
RHR16	South Fork	7/18/12	6	454458	4047756	2555	19.2
RHR16	South Fork	6/29/12	5	454458	4047756	2555	19.2
RHR16	South Fork	6/1/12	4	454458	4047756	2555	19.2
RHR16	South Fork	6/1/12	4	454458	4047756	2555	19.2
RHR16	South Fork	5/13/12	3	454458	4047756	2555	19.2
RHR16	South Fork	5/13/12	3	454458	4047756	2555	19.2
RHR16	South Fork	3/24/12	2	454458	4047756	2555	19.2
RHR18	Rio Hondo above TSV spring	11/16/12	10	460742	4047705	3133	8.3
RHR18	Rio Hondo above TSV spring	10/6/12	9	460742	4047705	3133	8.3
RHR18	Rio Hondo above TSV spring	9/14/12	8	460742	4047705	3133	8.3
RHR18	Rio Hondo above TSV spring	8/17/12	7	460742	4047705	3133	8.3
RHR18	Rio Hondo above TSV spring	7/17/12	6	460742	4047705	3133	8.3
RHR18	Rio Hondo above TSV spring	6/28/12	5	460742	4047705	3133	8.3
RHR18	Rio Hondo above TSV spring	5/31/12	4	460742	4047705	3133	8.3
RHR18	Rio Hondo above TSV spring	5/13/12	3	460742	4047705	3133	8.3
RHR18	Rio Hondo above TSV spring	3/23/12	2	460742	4047705	3133	8.3
RHR20	AS waterfall	7/18/12	6	451873	4043147	2547	1.5
RHR20	AS waterfall	6/29/12	5	451873	4043147	2547	1.5

Sample ID	Site Description	Sample Date	Sample Round	UTM-E	UTM-N	Elevation (m)	Drainage Area (km^2)
RHR20	AS waterfall	6/1/12	4	451873	4043147	2547	1.5
RHR20	AS waterfall	5/12/12	3	451873	4043147	2547	1.5
RHR20	AS waterfall	3/25/12	2	451873	4043147	2547	1.5
RHR21	Rio Hondo Near Eric Patterson Spring	3/15/13	11	449213	4043314	2290	97.7
RHR21	Rio Hondo Near Eric Patterson Spring	11/17/12	10	449213	4043314	2290	97.7
RHR21	Rio Hondo Near Eric Patterson Spring	10/6/12	9	449213	4043314	2290	97.7
RHR21	Rio Hondo Near Eric Patterson Spring	9/15/12	8	449213	4043314	2290	97.7
RHR21	Rio Hondo Near Eric Patterson Spring	8/18/12	7	449213	4043314	2290	97.7
RHR21	Rio Hondo Near Eric Patterson Spring	7/18/12	6	449213	4043314	2290	97.7
RHR21	Rio Hondo Near Eric Patterson Spring	6/29/12	5	449213	4043314	2290	97.7
RHR21	Rio Hondo Near Eric Patterson Spring	6/2/12	4	449213	4043314	2290	97.7
RHR21	Rio Hondo Near Eric Patterson Spring	5/13/12	3	449213	4043314	2290	97.7
RHR22	Stream flowing into Williams Lake	10/5/12	9	461603	4045329	3404	2.4
RHR22	Stream flowing into Williams Lake	9/14/12	8	461603	4045329	3404	2.4
RHR22	Stream flowing into Williams Lake	8/17/12	7	461603	4045329	3404	2.4
RHR22	Stream flowing into Williams Lake	7/18/12	6	461603	4045329	3404	2.4
RHR22	Stream flowing into Williams Lake	6/28/12	5	461603	4045329	3404	2.4
RHR22	Stream flowing into Williams Lake	6/1/12	4	461603	4045329	3404	2.4
RHR22	Stream flowing into Williams Lake	6/1/12	4	461603	4045329	3404	2.4
RHR22	Stream flowing into Williams Lake	5/14/12	3	461603	4045329	3404	2.4
RHR23	Upstream of Effluent Discharge	6/1/12	4	458792	4049969	2876	24.4
RHR23	Upstream of Effluent Discharge	5/15/12	3	458792	4049969	2876	24.4
RHR24	Downstream of Effluent Discharge	11/17/12	10	458751	4049977	2865	24.4
RHR24	Downstream of Effluent Discharge	10/5/12	9	458751	4049977	2865	24.4
RHR24	Downstream of Effluent Discharge	9/14/12	8	458751	4049977	2865	24.4
RHR24	Downstream of Effluent Discharge	8/18/12	7	458751	4049977	2865	24.4
RHR24	Downstream of Effluent Discharge	7/17/12	6	458751	4049977	2865	24.4
RHR24	Downstream of Effluent Discharge	6/28/12	5	458751	4049977	2865	24.4
RHR24	Downstream of Effluent Discharge	6/1/12	4	458751	4049977	2865	24.4
RHR24	Downstream of Effluent Discharge	5/15/12	3	458751	4049977	2865	24.4
RHRO01	Runoff Along Twinning Road next to Snow08	3/23/12	2	460502	4048828	3020	
RHRO02	Runoff along road near RHR-18 (WL Trailhead)	8/17/12	7	460755	4047746	3134	
RHRO02	Runoff along road near RHR-18 (WL Trailhead)	7/17/12	6	460755	4047746	3134	
RHRO02	Runoff along road near RHR-18 (WL Trailhead)	6/28/12	5	460755	4047746	3134	
RHRO02	Runoff along road near RHR-18 (WL Trailhead)	6/1/12	4	460755	4047746	3134	
RHRO02	Runoff along road near RHR-18 (WL Trailhead)	5/14/12	3	460755	4047746	3134	
RHRO03	Northernmost runoff near WL trailhead	6/28/12	5	460740	4047791	3133	
RHRO03	Northernmost runoff near WL trailhead	6/1/12	4	460740	4047791	3133	
RHRO03	Northernmost runoff near WL trailhead	6/1/12	4	460740	4047791	3133	
RHRO03	Northernmost runoff near WL trailhead	5/14/12	3	460740	4047791	3133	
RHRO04	Runoff just to the south of RHRO03	9/14/12	8	460744	4047781	3133	
RHRO04	Runoff just to the south of RHRO03	7/17/12	6	460744	4047781	3133	

Sample ID	Site Description	Sample Date	Sample Round	UTM- E	UTM- N	Elevation (m)	Drainage Area (km^2)
RHRO04	Runoff just to the south of RHRO03	6/28/12	5	460744	4047781	3133	
RHRO04	Runoff just to the south of RHRO03	6/1/12	4	460744	4047781	3133	
RHRO04	Runoff just to the south of RHRO03	5/14/12	3	460744	4047781	3133	
RHRO05	Runoff from stream west of the Bavarian	10/6/12	9	460629	4047957	3120	
RHRO05	Runoff from stream west of the Bavarian	10/6/12	9	460629	4047957	3120	
RHRO05	Runoff from stream west of the Bavarian	9/15/12	8	460629	4047957	3120	
RHRO05	Runoff from stream west of the Bavarian	8/17/12	7	460629	4047957	3120	
RHRO05	Runoff from stream west of the Bavarian	7/17/12	6	460629	4047957	3120	
RHRO05	Runoff from stream west of the Bavarian	7/17/12	6	460629	4047957	3120	
RHRO05	Runoff from stream west of the Bavarian	6/28/12	5	460629	4047957	3120	
RHRO05	Runoff from stream west of the Bavarian	6/1/12	4	460629	4047957	3120	
RHRO05	Runoff from stream west of the Bavarian	5/14/12	3	460629	4047957	3120	
RHRO05	Runoff from stream west of the Bavarian	5/14/12	3	460629	4047957	3120	
RHRO06	Runoff behind the Condos near the Bavarian	6/1/12	4	461041	4048439	3166	
RHRO06	Runoff behind the Condos near the Bavarian	5/15/12	3	461041	4048439	3166	
RHRO07	Runoff next to upper TSV Parking Lot	3/15/13	11	459553	4050301	2874	
RHS01	Patterson spring	3/15/13	11	449084	4043566	2289	
RHS01	Patterson spring	11/17/12	10	449084	4043566	2289	
RHS01	Patterson spring	10/6/12	9	449084	4043566	2289	
RHS01	Patterson spring	9/15/12	8	449084	4043566	2289	
RHS01	Patterson spring	8/18/12	7	449084	4043566	2289	
RHS01	Patterson spring	7/18/12	6	449084	4043566	2289	
RHS01	Patterson spring	6/29/12	5	449084	4043566	2289	
RHS01	Patterson spring	6/2/12	4	449084	4043566	2289	
RHS01	Patterson spring	6/2/12	4	449084	4043566	2289	
RHS01	Patterson spring	5/13/12	3	449084	4043566	2289	
RHS01	Patterson spring	3/24/12	2	449084	4043566	2289	
RHS01	Patterson spring	3/24/12	2	449084	4043566	2289	
RHS03	AS waterfall ceiling	7/18/12	6	451873	4043147	2547	
RHS03	AS waterfall ceiling	6/29/12	5	451873	4043147	2547	
RHS03	AS waterfall ceiling	6/1/12	4	451873	4043147	2547	
RHS03	AS waterfall ceiling	5/12/12	3	451873	4043147	2547	
RHS03	AS waterfall ceiling	3/25/12	2	451873	4043147	2547	
RHS04	TSV water supply spring outlet	3/16/13	11	460743	4047716	3134	
RHS04	TSV water supply spring outlet	11/16/12	10	460743	4047716	3134	
RHS04	TSV water supply spring outlet	10/6/12	9	460743	4047716	3134	
RHS04	TSV water supply spring outlet	9/14/12	8	460743	4047716	3134	
RHS04	TSV water supply spring outlet	8/17/12	7	460743	4047716	3134	
RHS04	TSV water supply spring outlet	7/17/12	6	460743	4047716	3134	
RHS04	TSV water supply spring outlet	6/28/12	5	460743	4047716	3134	
RHS04	TSV water supply spring outlet	5/31/12	4	460743	4047716	3134	
RHS04	TSV water supply spring outlet	5/13/12	3	460743	4047716	3134	

Sample ID	Site Description	Sample Date	Sample Round	UTM- E	UTM- N	Elevation (m)	Drainage Area (km^2)
RHS04	TSV water supply spring outlet	3/23/12	2	460743	4047716	3134	
RHS05	Soil seep at Manzanitas Canyon	3/14/13	11	454659	4047878	2551	
RHS05	Soil seep at Manzanitas Canyon	10/6/12	9	454659	4047878	2551	
RHS05	Soil seep at Manzanitas Canyon	9/15/12	8	454659	4047878	2551	
RHS05	Soil seep at Manzanitas Canyon	8/18/12	7	454659	4047878	2551	
RHS05	Soil seep at Manzanitas Canyon	7/18/12	6	454659	4047878	2551	
RHS05	Soil seep at Manzanitas Canyon	6/29/12	5	454659	4047878	2551	
RHS05	Soil seep at Manzanitas Canyon	5/31/12	4	454659	4047878	2551	
RHS05	Soil seep at Manzanitas Canyon	5/13/12	3	454659	4047878	2551	
RHS05	Soil seep at Manzanitas Canyon	3/24/12	2	454659	4047878	2551	
RHS06	Spring Behind Condos near WL TH prking	11/16/12	10	461056	4048273	3200	
RHS06	Spring Behind Condos near WL TH prking	10/6/12	9	461056	4048273	3200	
RHS06	Spring Behind Condos near WL TH prking	9/15/12	8	461056	4048273	3200	
RHS06	Spring Behind Condos near WL TH prking	8/17/12	7	461056	4048273	3200	
RHS06	Spring Behind Condos near WL TH prking	7/17/12	6	461056	4048273	3200	
RHS06	Spring Behind Condos near WL TH prking	6/28/12	5	461056	4048273	3200	
RHS06	Spring Behind Condos near WL TH prking	6/1/12	4	461056	4048273	3200	
RHS06	Spring Behind Condos near WL TH prking	5/15/12	3	461056	4048273	3200	
RHS07	Southern Spring Above Condo Loop Trail	10/6/12	9	461060	4048421	3172	
RHS07	Southern Spring Above Condo Loop Trail	9/15/12	8	461060	4048421	3172	
RHS07	Southern Spring Above Condo Loop Trail	8/17/12	7	461060	4048421	3172	
RHS07	Southern Spring Above Condo Loop Trail	7/17/12	6	461060	4048421	3172	
RHS08	Northern Spring Above Condo Loop Trail	11/16/12	10	461134	4048376	3212	
RHS08	Northern Spring Above Condo Loop Trail	10/6/12	9	461134	4048376	3212	
RHS08	Northern Spring Above Condo Loop Trail	9/15/12	8	461134	4048376	3212	
RHS08	Northern Spring Above Condo Loop Trail	8/17/12	7	461134	4048376	3212	
RHS08	Northern Spring Above Condo Loop Trail	7/17/12	6	461134	4048376	3212	
RHS09	Spring Along Williams Lake Trail	11/16/12	10	461347	4046548	3341	
RHS09	Spring Along Williams Lake Trail	10/5/12	9	461347	4046548	3341	
RHS09	Spring Along Williams Lake Trail	9/14/12	8	461347	4046548	3341	
RHS09	Spring Along Williams Lake Trail	8/17/12	7	461347	4046548	3341	
RHS10	Pattison Weir Spring	6/28/13	12	461423	4051208	3270	
RHS10	Pattison Weir Spring	6/28/13	12	461423	4051208	3270	
RHSNO01	Snowbank along Twinning Road next to RHRO1	3/23/12	2	460502	4048828	3019	
RHSNO01	Snowbank along Twinning Road next to RHRO1	3/23/12	2	460502	4048828	3019	
RHSNO02	Old Snow near Williams Lake	5/14/12	3	461489	4045773	3367	
RHSNO03	Old Snow halfway up to Wiliams Lake	5/14/12	3	461357	4046839	3295	
RHSNO04	Old Snow Near WL Trailhead	5/14/12	3	461020	4047421	3187	
RHSNO05	Old Snow behind Condos near WL Trailhead	5/15/12	3	461042	4048437	3169	
RHSNO05	Old Snow behind Condos near WL Trailhead	5/15/12	3	461042	4048437	3169	
RHW02	Eric Patterson well	3/14/13	11	447514	4043544	2266	
RHW02	Eric Patterson well	10/6/12	9	447514	4043544	2266	

Sample ID	Site Description	Sample Date	Sample Round	UTM- E	UTM- N	Elevation (m)	Drainage Area (km^2)
RHW02	Eric Patterson well	9/15/12	8	447514	4043544	2266	
RHW02	Eric Patterson well	8/18/12	7	447514	4043544	2266	
RHW02	Eric Patterson well	7/18/12	6	447514	4043544	2266	
RHW02	Eric Patterson well	6/28/12	5	447514	4043544	2266	
RHW02	Eric Patterson well	6/2/12	4	447514	4043544	2266	
RHW02	Eric Patterson well	6/2/12	4	447514	4043544	2266	
RHW02	Eric Patterson well	5/14/12	3	447514	4043544	2266	
RHW02	Eric Patterson well	3/24/12	2	447514	4043544	2266	
RHW05	Neal Ogden well (Arroyo Seco)	3/14/13	11	450828	4042917	2481	
RHW05	Neal Ogden well (Arroyo Seco)	10/5/12	9	450828	4042917	2481	
RHW05	Neal Ogden well (Arroyo Seco)	9/14/12	8	450828	4042917	2481	
RHW05	Neal Ogden well (Arroyo Seco)	8/17/12	7	450828	4042917	2481	
RHW05	Neal Ogden well (Arroyo Seco)	7/17/12	6	450828	4042917	2481	
RHW05	Neal Ogden well (Arroyo Seco)	6/29/12	5	450828	4042917	2481	
RHW05	Neal Ogden well (Arroyo Seco)	6/1/12	4	450828	4042917	2481	
RHW05	Neal Ogden well (Arroyo Seco)	5/15/12	3	450828	4042917	2481	
RHW05	Neal Ogden well (Arroyo Seco)	3/25/12	2	450828	4042917	2481	
RHW06	Taos Mtn Lodge Well	3/14/13	11	457604	4050170	2762	
RHW06	Taos Mtn Lodge Well	10/6/12	9	457604	4050170	2762	
RHW06	Taos Mtn Lodge Well	10/6/12	9	457604	4050170	2762	
RHW06	Taos Mtn Lodge Well	9/15/12	8	457604	4050170	2762	
RHW06	Taos Mtn Lodge Well	8/18/12	7	457604	4050170	2762	
RHW06	Taos Mtn Lodge Well	7/17/12	6	457604	4050170	2762	
RHW06	Taos Mtn Lodge Well	6/28/12	5	457604	4050170	2762	
RHW06	Taos Mtn Lodge Well	5/31/12	4	457604	4050170	2762	
RHW06	Taos Mtn Lodge Well	5/31/12	4	457604	4050170	2762	
RHW06	Taos Mtn Lodge Well	5/13/12	3	457604	4050170	2762	
RHW06	Taos Mtn Lodge Well	3/24/12	2	457604	4050170	2762	
RHW10	Hacienda de Valdez well (likely same as RHW09)	3/15/13	11	449603	4043968	2305	
RHW10	Hacienda de Valdez well (likely same as RHW09)	10/6/12	9	449603	4043968	2305	
RHW10	Hacienda de Valdez well (likely same as RHW09)	9/15/12	8	449603	4043968	2305	
RHW10	Hacienda de Valdez well (likely same as RHW09)	8/18/12	7	449603	4043968	2305	
RHW10	Hacienda de Valdez well (likely same as RHW09)	7/18/12	6	449603	4043968	2305	
RHW10	Hacienda de Valdez well (likely same as RHW09)	6/29/12	5	449603	4043968	2305	
RHW10	Hacienda de Valdez well (likely same as RHW09)	6/2/12	4	449603	4043968	2305	
RHW10	Hacienda de Valdez well (likely same as RHW09)	5/13/12	3	449603	4043968	2305	
RHW10	Hacienda de Valdez well (likely same as RHW09)	3/24/12	2	449603	4043968	2305	
RHW11	Michael Howard Well	10/5/12	9	451048	4042669	2468	
RHW11	Michael Howard Well	9/14/12	8	451048	4042669	2468	
RHW11	Michael Howard Well	8/17/12	7	451048	4042669	2468	
RHW11	Michael Howard Well	7/17/12	6	451048	4042669	2468	
RHW11	Michael Howard Well	6/29/12	5	451048	4042669	2468	

Sample ID	Site Description	Sample Date	Sample Round	UTM- E	UTM- N	Elevation (m)	Drainage Area (km^2)
RHW11	Michael Howard Well	5/15/12	3	451048	4042669	2468	
RHW11	Michael Howard Well	5/15/12	3	451048	4042669	2468	
RHW11	Michael Howard Well	3/25/12	2	451048	4042669	2468	
RHW12	Whistlestop Well	3/16/13	11	459129	4048774	3314	
RHW12	Whistlestop Well	9/14/12	8	459129	4048774	3314	
RHW12	Whistlestop Well	8/17/12	7	459129	4048774	3314	
RHW12	Whistlestop Well	7/17/12	6	459129	4048774	3314	
RHW12	Whistlestop Well	6/28/12	5	459129	4048774	3314	
RHW12	Whistlestop Well	6/28/12	5	459129	4048774	3314	
RHW12	Whistlestop Well	5/31/12	4	459129	4048774	3314	
RHW13	Frank Oatman Well	3/14/13	11	438691	4044528	2132	
RHW13	Frank Oatman Well	3/14/13	11	438691	4044528	2132	
RHW13	Frank Oatman Well	9/15/12	8	438691	4044528	2132	
RHW13	Frank Oatman Well	8/18/12	7	438691	4044528	2132	
RHW13	Frank Oatman Well	7/16/12	6	438691	4044528	2132	
RHW13	Frank Oatman Well	6/28/12	5	438691	4044528	2132	
RHW13	Frank Oatman Well	6/28/12	5	438691	4044528	2132	
RHW13	Frank Oatman Well	6/2/12	4	438691	4044528	2132	
WL01	Williams Lake	10/5/12	9	461603	4045637	3367	
WL01	Williams Lake	9/14/12	8	461603	4045637	3367	
WL01	Williams Lake	8/17/12	7	461603	4045637	3367	
WL01	Williams Lake	7/18/12	6	461603	4045637	3367	
WL01	Williams Lake	6/28/12	5	461603	4045637	3367	
WL01	Williams Lake	6/1/12	4	461603	4045637	3367	
WL01	Williams Lake	5/14/12	3	461603	4045637	3367	
WL02	Williams Lake (possibly spring fed)	10/5/12	9	461420	4045617	3368	
WL02	Williams Lake (possibly spring fed)	9/14/12	8	461420	4045617	3368	
WL02	Williams Lake (possibly spring fed)	8/17/12	7	461420	4045617	3368	
WL02	Williams Lake (possibly spring fed)	7/18/12	6	461420	4045617	3368	
WL02	Williams Lake (possibly spring fed)	6/28/12	5	461420	4045617	3368	

APPENDIX B

GEOCHEMISTRY RESULTS

Sample ID	Sample Date	Alkalinity ppm as $CaCO_3^-$	Total Anions meq/L	Alkalinity ppm as HCO_3^-	Br^- ppm	Ca^{2+} ppm	Alkalinity ppm as CO_3^{2-}	Total Cations meq/L	Cl^- ppm
Ditch	9/14/12	40	1.43	48	-0.1	24	-5	1.35	0.43
EFF	3/15/13	428	11.62	522	-0.1	32.6	-5	10.76	71.10
EFF	10/5/12	212	6.96	259	0.13	27.5	-5	6.72	43.40
EFF	9/14/12	251	7.04	306	-0.10	25.7	-5	6.78	43.3
EFF	8/17/12	238	6.79	291	-0.10	24.2	-5	6.71	47.8
EFF	7/17/12	178	5.23	217	-0.01	25.8	-5	4.94	38.1
EFF	6/28/12	180	5.18	219	0.02	27	-5	5.1	25.8
EFF	6/1/12		4.78	195	0.15	29		4.68	22
EFF	5/15/12		4.48	200	0.029	31		4.56	29
EFF	5/15/12		4.56	205	-0.1	31		4.55	29
ISO1	3/16/13								
ISO1	12/18/12								
ISO1	10/5/12	49	1.30	60	-0.1	3	-5	0.40	2
ISO1	7/17/12	41	1.12	50	-0.10	7.23	-5	0.54	1.3
ISO1	5/31/12		0.28	15	-0.10	4.7		0.29	0.63
ISO1	3/23/12		0.43	26	0.013	7.7		0.44	0.26
ISO1	1/8/12		0.36	22	-0.01	6.6		0.36	0.16
ISO2	3/16/13								
ISO2	12/18/12								
ISO2	10/5/12	19	0.54	23	-0.10	1.59	-5	0.29	1.35
ISO2	7/17/12	54	1.59	66	-0.10	4.02	-5	0.7	1.71
ISO2	5/31/12		0.24	13	-0.10	3.0		0.23	0.80
ISO2	1/9/12								
ISO3	3/15/13								
ISO3	12/18/12								
ISO3	10/6/12	25	1.01	31	-0.10	12.3	-5	0.93	16.4
ISO3	7/17/12	12	1.05	15	-0.10	19.7	-5	1.14	23.7
ISO3	6/1/12		0.58	18	-0.10	9.5		0.56	9.3
ISO3	3/24/12		0.29	14	-0.01	5.4		0.30	2.0
ISO4	3/15/13								
ISO4	12/18/12								
ISO4	10/6/12	24	0.97	29	-0.10	14.3	-5	0.92	16
ISO4	7/17/12	23	1.35	28	-0.10	22.4	-5	1.27	29.7
ISO4	6/1/12		0.82	31	-0.10	13		0.80	10
ISO4	6/1/12		0.82	31	-0.10	13		0.79	10
ISO4	3/24/12		0.25	13	-0.01	3.3		0.21	1.2
ISO4	1/9/12		0.11	7.0	-0.01	1.2		0.12	0.43
ISO5	3/15/13								
ISO5	12/19/12								
ISO5	10/6/12	-5	2.82	-5	-0.10	38	-5	4.73	39.3
ISO5	7/17/12	141	4.94	172	-0.10	43.3	-5	3.19	63.3
ISO5	6/2/12		3.55	155	-0.10	24		1.57	34

Sample ID	Sample Date	Alkalinity ppm as CaCO$_3^-$	Total Anions meq/L	Alkalinity ppm as HCO$_3^-$	Br$^-$ ppm	Ca^{2+} ppm	Alkalinity ppm as CO$_3^{2-}$	Total Cations meq/L	Cl$^-$ ppm
ISO5	3/24/12		1.94	84	-0.10	10		1.02	7.8
ISO5	3/24/12		1.92	83	-0.01	10		1.02	7.8
ISO5	1/9/12		2.74	125	-0.01	19		1.19	10
ISO6	3/14/13								
ISO6	12/19/12								
ISO6	10/5/12	62	2.62	75	-0.10	18.6	-5	1.61	23.8
ISO6	7/16/12	19	1.48	23	-0.10	26	-5	1.43	38.6
ISO6	6/2/12		1.71	38	-0.10	31		1.76	38
ISO6	3/24/12		2.74	130	-0.01	24		1.57	19
ISO6	1/9/12		0.39	17	-0.01	2.4		0.21	4.1
PCAPS-1 (15cm)	6/29/13	15	0.35	19	-0.10	2.51	-5	0.36	0.47
PCAPS-1 (18cm)	6/29/13	12	0.27	14	-0.10	2.36	-5	0.32	0.55
PCAPS-1 Upper	10/20/12								
PCAPS-1 Lower	10/20/12								
PCAPS-2 (25-42cm)	6/29/13	5	0.21	6	-0.10	2.3	-5	0.18	0.76
PCAPS-2 Upper	10/20/12								
PCAPS-2 Lower	10/20/12								
RHA01	7/18/12	56	1.52	69	-0.10	22.9	-5	1.48	1.94
RHA01	6/29/12	55	1.49	68	-0.10	21.5	-5	1.39	1.99
RHA01	6/2/12		1.29	57	-0.010	20		1.24	1.3
RHA01	6/2/12		1.27	56	-0.10	20		1.23	1.3
RHA01	5/13/12		1.25	56	-0.010	19		1.21	1.7
RHR01	3/14/13	63	1.83	76.0	-0.10	24.9	-5.0	1.76	7.98
RHR01	11/17/12	62	1.67	75.0	-0.10	24	-5	1.59	2.26
RHR01	11/17/12	62	1.67	75.0	-0.10	24	-5	1.59	2.27
RHR01	10/6/12	63	1.68	76.0	-0.10	24.8	-5	1.60	1.89
RHR01	9/15/12	60	1.62	73	-0.10	24.4	-5	1.58	1.91
RHR01	8/18/12	60	1.59	73	-0.10	23	-5	1.5	1.71
RHR01	7/18/12	57	1.52	70	-0.10	22.2	-5	1.45	1.79
RHR01	6/29/12	56	1.52	69	-0.10	22.4	-5	1.45	2.03
RHR01	6/29/12	56	1.52	69	ND	22.5	-5	1.46	2.04
RHR01	6/1/12		1.29	57	-0.010	20		1.23	1.4
RHR01	5/13/12		1.22	54	-0.010	19		1.25	1.7
RHR01	3/24/12		1.61	70	-0.010	24		1.65	5.4
RHR02	3/14/13	104	2.71	126.00	-0.10	34.5	-5	2.62	6.93
RHR02	11/16/12	126	3.18	154.00	-0.10	39.2	-5	2.99	4.71
RHR02	10/5/12	168	4.12	191	-0.10	49.1	7	3.96	5.81
RHR02	9/15/12	157	3.87	168	-0.10	44.8	11	3.73	6.28
RHR02	9/15/12	155	3.82	166	-0.10	44.6	11	3.72	6.24
RHR02	8/18/12	168	4.05	192	-0.10	50.5	6	3.97	5.75
RHR02	7/16/12	168	4.02	200	-0.10	49.6	-5	3.91	5.17
RHR02	6/29/12	161	3.89	181	-0.10	46.7	8	3.84	6.01

Sample ID	Sample Date	Alkalinity ppm as CaCO$_3^-$	Total Anions meq/L	Alkalinity ppm as HCO$_3^-$	Br$^-$ ppm	Ca^{2+} ppm	Alkalinity ppm as CO$_3^{2-}$	Total Cations meq/L	Cl$^-$ ppm
RHR02	6/2/12		3.61	180	0.042	48	5	3.65	5.6
RHR02	5/13/12		3.30	150	0.030	43		3.33	5.8
RHR02	5/13/12		3.23	155	0.030	43	-5	3.33	6.6
RHR02	3/24/12		2.50	115	0.015	34		2.56	6.5
RHR04	3/14/13	72	2.00	87.0	-0.10	27.1	-5	1.92	7.45
RHR04	11/16/12	79	2.06	97.0	-0.10	28.1	-5	1.95	3.15
RHR04	10/5/12	132	3.13	161	-0.10	44	-5	3.01	4.5
RHR04	10/5/12	132		161	-0.10	44.3	-5		4.51
RHR04	9/15/12	126	3.03	154	-0.10	44.3	-5	3.02	4.91
RHR04	8/18/12	129	3.05	158	-0.10	42.7	-5	2.93	4.43
RHR04	7/16/12	120	2.85	147	-0.10	41.8	-5	2.84	3.95
RHR04	6/29/12	115	2.78	140	-0.10	38.5	-5	2.65	4.81
RHR04	6/29/12	113	2.73	138	-0.10	39.1	-5	2.69	4.85
RHR04	6/2/12		2.40	120	-0.010	35		2.37	4.2
RHR04	5/13/12		2.10	98	0.0	31		2.15	4.5
RHR04	3/24/12		1.78	79	-0.010	26		1.84	5.9
RHR10	3/16/13	64	1.75	78	-0.10	28.3	-5	1.69	1.16
RHR10	11/17/12	57	1.67	70	-0.10	26.9	-5	1.57	0.6
RHR10	10/6/12	54	1.62	66	-0.10	26.2	-5	1.52	0.54
RHR10	9/15/12	52	1.57	64	-0.10	26.1	-5	1.51	0.56
RHR10	8/18/12	51	1.53	62	-0.10	24.4	-5	1.41	0.48
RHR10	7/17/12	50	1.47	61	-0.10	24.7	-5	1.43	0.49
RHR10	6/28/12	48	1.44	59	-0.10	24.6	-5	1.43	0.84
RHR10	5/31/12		1.36	54	-0.10	23		1.31	0.61
RHR10	5/31/12		1.38	55	-0.10	23		1.32	0.61
RHR10	5/31/12		1.31	51	-0.10	23		1.30	0.76
RHR10	5/13/12		1.39	55	-0.010	25		1.43	0.54
RHR10	3/23/12		1.74	78	-0.010	28		1.70	1.4
RHR11	3/14/13	80	1.75	97	-0.10	22.7	-5	1.64	0.66
RHR11	11/17/12	84	1.83	102	-0.10	24.4	-5	1.75	0.6
RHR11	10/6/12	85	1.84	103	-0.10	24.7	-5	1.76	0.56
RHR11	9/15/12	81	1.78	99	-0.10	25	-5	1.76	0.71
RHR11	8/18/12	82	1.79	101	-0.10	24.3	-5	1.69	0.49
RHR11	7/17/12	77	1.68	94	-0.10	24.2	-5	1.67	0.48
RHR11	6/28/12	75	1.66	92	-0.10	23.6	-5	1.63	1
RHR11	5/13/12		1.18	66	-0.10	21		1.39	0.70
RHR11	5/13/12		1.33	75	-0.010	20		1.39	0.52
RHR11	3/23/12		1.57	88	-0.010	23		1.64	0.64
RHR11	3/23/12		1.58	89	-0.010	23		1.64	0.63
RHR14	3/14/13	72	1.94	87.0	-0.10	29.8	-5.0	1.85	0.68
RHR14	3/14/13	72		87.4	-0.10	29.2	-5.0		0.68
RHR14	11/17/12	74	1.96	90.0	-0.10	27.9	-5	1.74	0.6

Sample ID	Sample Date	Alkalinity ppm as $CaCO_3^-$	Total Anions meq/L	Alkalinity ppm as HCO_3^-	Br^- ppm	Ca^{2+} ppm	Alkalinity ppm as CO_3^{2-}	Total Cations meq/L	Cl^- ppm
RHR14	10/6/12	68	1.82	83.0	-0.10	27.7	-5	1.72	0.62
RHR14	9/15/12	67	1.8	82	-0.10	28.1	-5	1.74	0.64
RHR14	8/18/12	66	1.76	80	-0.10	26.6	-5	1.66	0.61
RHR14	7/18/12	64	1.72	78	-0.10	26.7	-5	1.66	0.62
RHR14	6/29/12	65	1.74	79	-0.10	26.9	-5	1.68	1.09
RHR14	5/31/12		1.48	71	-0.10	24		1.48	0.83
RHR14	5/13/12		1.32	64	-0.010	21		1.35	0.61
RHR14	3/24/12		1.76	80	-0.1	29		1.78	-1
RHR14	3/24/12	72	1.76	80	-0.010	29	-5	1.78	0.73
RHR15	3/14/13	69	2.04	87	-0.10	27.1	-5	1.96	11.2
RHR15	11/17/12	68	1.78	84	-0.10	25.8	-5	1.68	2.73
RHR15	10/6/12	68	1.77	83	-0.10	26.9	-5	1.69	1.82
RHR15	9/15/12	65	1.76	83	-0.10	26.8	-5	1.69	1.95
RHR15	8/18/12	65	1.69	79	-0.10	25.1	-5	1.59	1.65
RHR15	7/18/12	61	1.65	79	-0.10	25.2	-5	1.58	1.74
RHR15	6/29/12		1.58	74	-0.10	24.8	-5	1.56	1.84
RHR15	6/1/12		1.42	64	-0.10	23		1.39	1.4
RHR15	5/13/12		1.41	65	0.011	23		1.43	1.7
RHR15	3/24/13		1.67	76	-0.010	25		1.72	6.4
RHR16	3/14/13	36	1.10	44	-0.10	15.1	-5	1.02	0.74
RHR16	11/17/12	36	1.23	45	-0.10	17.2	-5	1.14	0.6
RHR16	10/6/12	38	1.22	46	-0.10	17.3	-5	1.14	0.55
RHR16	9/15/12	36	1.17	45	-0.10	16.7	-5	1.09	0.55
RHR16	8/18/12	38	1.17	46	-0.10	16.2	-5	1.07	0.49
RHR16	7/18/12	33	1.08	41	-0.10	16	-5	1.06	0.45
RHR16	6/29/12	37	1.14	45	-0.10	15.8	-5	1.07	0.81
RHR16	6/1/12		0.82	32	-0.10	12		0.81	0.68
RHR16	6/1/12		0.82	32	-0.10	12		0.78	0.60
RHR16	5/13/12		0.28		-0.10	12		0.78	-1.0
RHR16	5/13/12		0.76	29	-0.010	12		0.79	0.490
RHR16	3/24/12		1.04	41	-0.010	16		1.06	0.58
RHR18	11/16/12	42	1.56	51.0	-0.10	24.8	-5	1.39	0.4
RHR18	10/6/12	40	1.48	48.0	-0.10	24.8	-5	1.38	0.42
RHR18	9/14/12	39	1.43	47	-0.10	24	-5	1.34	0.43
RHR18	8/17/12	40	1.37	48	-0.10	23.9	-5	1.34	0.41
RHR18	7/17/12	37	1.29	45	-0.10	21.9	-5	1.23	0.40
RHR18	6/28/12	39	1.32	47	-0.10	21.7	-5	1.23	0.73
RHR18	5/31/12		1.23	42	-0.10	22		1.23	0.60
RHR18	5/13/12		1.32	43	-0.010	24		1.35	0.37
RHR18	3/23/12		1.49	50	-0.010	27		1.50	0.64
RHR20	7/18/12	23	0.58	28	-0.10	5.46	-5.0	0.58	1.15
RHR20	6/29/12	27	0.78	33	-0.10	6.25	-5.0	0.81	4.25

Sample ID	Sample Date	Alkalinity ppm as CaCO$_3^-$	Total Anions meq/L	Alkalinity ppm as HCO$_3^-$	Br$^-$ ppm	Ca^{2+} ppm	Alkalinity ppm as CO$_3^{2-}$	Total Cations meq/L	Cl$^-$ ppm
RHR20	6/1/12		0.37	17	-0.10	3.9		0.41	0.90
RHR20	5/12/12		0.25	10	-0.010	3		0.30	0.60
RHR20	3/25/12		0.33	10	-0.010	3.6		0.40	1.8
RHR21	3/15/13	62	1.81	75.0	-0.10	24.5	-5.0	1.73	8.25
RHR21	11/17/12	62	1.67	75.0	-0.10	23.9	-5	1.58	2.29
RHR21	10/6/12	67	1.79	82.0	-0.10	25.5	-5	1.68	2.32
RHR21	9/15/12	65	1.74	79	-0.10	24.9	-5	1.64	2.27
RHR21	8/18/12	63	1.67	76	-0.10	24.3	-5	1.59	2.04
RHR21	7/18/12	60	1.58	73	-0.10	23.6	-5	1.55	2.03
RHR21	6/29/12	58	1.58	71	-0.10	23.6	-5	1.54	2.32
RHR21	6/2/12		1.36	61	-0.010	21		1.32	1.6
RHR21	5/13/12		1.24	55	-0.010	20		1.29	1.9
RHR22	10/5/12	36	1.47	45	-0.10	25	-5	1.38	0.42
RHR22	9/14/12	33	1.32	41	-0.10	22.1	-5	1.25	0.65
RHR22	8/17/12	33	1.31	41	-0.10	22.7	-5	1.27	0.36
RHR22	7/18/12	33	1.3	41	-0.10	21.5	-5	1.24	0.83
RHR22	6/28/12	29	1.2	36	-0.10	20.3	-5	1.15	0.69
RHR22	6/1/12		0.83	28	-0.10	14		0.79	0.59
RHR22	6/1/12		0.82	28	-0.10	14		0.79	0.59
RHR22	5/14/12		0.95	32	-0.010	17		0.96	0.33
RHR23	6/1/12		1.23	51	-0.10	22		1.28	0.7
RHR23	5/15/12		1.40	61	-0.010	22		1.34	0.72
RHR24	11/17/12	67	1.81	82	-0.10	27	-5	1.71	1.83
RHR24	10/5/12	63	1.73	76	-0.10	27	-5	1.64	0.86
RHR24	9/14/12	62	1.69	75	-0.10	26	-5	1.61	0.89
RHR24	8/18/12	58	1.62	71	-0.10	25	-5	1.54	0.82
RHR24	7/17/12	60	1.58	73	-0.10	24.5	-5	1.53	0.92
RHR24	6/28/12	56	1.54	69	-0.10	24.4	-5	1.52	1.13
RHR24	6/1/12		1.37	59	-0.10	22		1.31	0.86
RHR24	5/15/12		1.41	62	-0.010	23		1.39	0.75
RHRO01	3/23/12		1.42	74	-0.010	21		1.39	2.5
RHRO02	8/17/12	38	1.33	46	-0.10	23.3	-5	1.3	0.40
RHRO02	7/17/12	38	1.29	46	-0.010	21.9	-5	1.23	0.16
RHRO02	6/28/12	36	1.24	43	-0.010	21	-5	1.18	0.44
RHRO02	6/1/12		1.26	46	-0.10	22		1.24	0.58
RHRO02	5/14/12		1.36	48	-0.010	23		1.30	0.35
RHRO03	6/28/12	37	1.26	45	-0.100	21.3	-5	1.2	0.75
RHRO03	6/1/12		1.40	56	-0.10	24		1.32	0.55
RHRO03	6/1/12		1.27	48	-0.10	22		1.23	0.56
RHRO03	5/14/12		1.40	50	0.010	24		1.35	0.40
RHRO04	9/14/12	39	1.41	47	-0.1	23.5	-5	1.32	0.43
RHRO04	7/17/12	37	1.26	45	-0.10	22	-5	1.23	0.40

134

Sample ID	Sample Date	Alkalinity ppm as $CaCO_3^-$	Total Anions meq/L	Alkalinity ppm as HCO_3^-	Br^- ppm	Ca^{2+} ppm	Alkalinity ppm as CO_3^{2-}	Total Cations meq/L	Cl^- ppm
RHRO04	6/28/12	37	1.26	45	-0.10	20.8	-5	1.18	0.76
RHRO04	6/1/12		1.31	50	-0.10	22		1.23	0.57
RHRO04	5/14/12		1.41	50	-0.010	24		1.37	0.40
RHRO05	10/6/12	64	1.77	78	-0.10	30	-5	1.67	0.45
RHRO05	10/6/12	64		77.7	-0.10	29.8	-5		0.45
RHRO05	9/15/12	63	1.75	76	-0.10	29.4	-5	1.66	0.47
RHRO05	8/17/12	62	1.71	75	-0.10	29.5	-5	1.66	0.41
RHRO05	7/17/12	61	1.66	74	-0.10	28.1	-5	1.58	0.40
RHRO05	7/17/12	60	1.64	73	-0.10	28.3	-5	1.6	0.40
RHRO05	6/28/12	56	1.55	69	-0.10	26.6	-5	1.53	0.79
RHRO05	6/1/12		1.25	57	-0.10	21		1.20	0.58
RHRO05	5/14/12		0.34		-0.10	23		1.32	-1.0
RHRO05	5/14/12		1.39	64	-0.010	23		1.32	0.41
RHRO06	6/1/12		1.44	60	-0.10	24		1.42	0.66
RHRO06	5/15/12		1.40	57	-0.010	23		1.35	0.41
RHRO07	3/15/13	50	1.12	61	-0.100	16	-5	1.04	0.80
RHS01	3/15/13	65	1.92	79	-0.100	27	-5	1.81	6.38
RHS01	11/17/12	72	1.94	88	-0.10	28	-5	1.84	2.78
RHS01	10/6/12	73	1.95	89	-0.10	28	-5	1.84	2.72
RHS01	9/15/12	72	1.92	88	-0.10	28	-5	1.85	2.74
RHS01	8/18/12	72	1.9	88	-0.10	28	-5	1.85	2.76
RHS01	7/18/12	68	1.81	83	-0.010	28	-5	1.86	2.7
RHS01	6/29/12	67	1.79	82	0.011	26.6	-5	1.78	3.06
RHS01	6/2/12		1.75	80	-0.010	25		1.68	4.0
RHS01	6/2/12		1.80	83	-0.010	25		1.69	3.9
RHS01	5/14/12		1.84	82	0.011	26		1.78	5.4
RHS01	3/24/12		1.80	76	0.010	28		1.90	6.0
RHS01	3/24/12		1.79	75	-0.010	28		1.88	6.1
RHS03	7/18/12	31	0.77	38	-0.10	8.23	-5.0	0.8	1.16
RHS03	6/29/12	30	0.78	37	-0.10	8.1	-5.0	0.81	1.33
RHS03	6/1/12		0.55	24	-0.10	5.3		0.57	1.5
RHS03	5/12/12		0.47	20	-0.010	4.9		0.50	0.84
RHS03	3/25/12		0.20	9.0	-0.010	1.7		0.18	1.2
RHS04	3/16/13	44	1.60	53.0	-0.10	26.6	-5.0	1.49	0.48
RHS04	11/16/12	41	1.55	50.0	-0.10	25.7	-5	1.44	0.5
RHS04	10/6/12	38	1.46	46.0	-0.10	24.7	-5	1.38	0.43
RHS04	9/14/12	41	1.5	50	-0.10	24.5	-5	1.4	0.44
RHS04	8/17/12	35	1.32	42.0	-0.10	22.5	-5	1.26	0.41
RHS04	7/17/12	34	1.27	42	-0.10	21.7	-5	1.22	0.39
RHS04	6/28/12	36	1.28	43	-0.10	21.4	-5	1.22	0.77
RHS04	5/31/12		1.26	43	-0.010	22		1.26	0.51
RHS04	5/13/12		1.34	42	-0.010	23		1.32	0.35

Sample ID	Sample Date	Alkalinity ppm as $CaCO_3^-$	Total Anions meq/L	Alkalinity ppm as HCO_3^-	Br^- ppm	Ca^{2+} ppm	Alkalinity ppm as CO_3^{2-}	Total Cations meq/L	Cl^- ppm
RHS04	3/23/12		1.43	50	0.017	27		1.49	0.35
RHS05	3/14/13	72	1.95	87	-0.10	29.4	-5	1.82	0.73
RHS05	10/6/12	71	1.89	87	-0.10	28.5	-5	1.76	0.62
RHS05	9/15/12	67	1.8	82	-0.10	27.6	-5	1.71	0.64
RHS05	8/18/12	66	1.77	80	-0.10	27.3	-5	1.68	0.63
RHS05	7/18/12	65	1.73	79	-0.10	27.3	-5	1.69	0.61
RHS05	6/29/12	66	1.75	80	-0.10	29	-5	1.81	1.07
RHS05	5/31/12		1.63	76	-0.10	26		1.62	0.90
RHS05	5/13/12		1.62	75	-0.010	25		1.58	0.66
RHS05	3/24/12		1.81	82	0.013	29		1.81	0.63
RHS06	11/16/12	53	1.43	65.0	-0.10	21.4	-5	1.33	0.5
RHS06	10/6/12	53	1.42	65	-0.10	22.2	-5	1.36	0.48
RHS06	9/15/12	52	1.4	64	-0.10	21.9	-5	1.34	0.48
RHS06	8/17/12	52	1.40	64.0	-0.10	21.3	-5	1.30	0.48
RHS06	7/17/12	50	1.39	61	-0.10	22.5	-5	1.37	0.48
RHS06	6/28/12	53	1.48	65	-0.10	23.6	-5	1.46	0.92
RHS06	6/1/12		1.35	62	-0.10	22		1.35	0.72
RHS06	5/15/12		1.33	62	-0.010	21		1.32	0.55
RHS07	10/6/12	50	1.58	61	-0.10	25	-5	1.47	0.46
RHS07	9/15/12	50	1.57	61	-0.10	24.9	-5	1.46	0.45
RHS07	8/17/12	48	1.53	59	-0.10	25	-5	1.49	0.52
RHS07	7/17/12	48	1.52	59	-0.10	25.4	-5	1.49	0.53
RHS08	11/16/12	50	1.58	61	-0.10	25.1	-5	1.48	0.5
RHS08	10/6/12	50	1.58	61	-0.10	25.1	-5	1.48	0.46
RHS08	9/15/12	49	1.55	60	-0.10	25.1	-5	1.47	0.45
RHS08	8/17/12	48	1.53	59	-0.10	25.1	-5	1.48	0.49
RHS08	7/17/12	48	1.52	59	-0.10	25.3	-5	1.48	0.44
RHS09	11/16/12	58	1.45	71	-0.10	24.8	-5	1.35	0.5
RHS09	10/5/12	56	1.38	69	-0.10	24.5	-5	1.34	0.53
RHS09	9/14/12	57	1.38	70	-0.10	23.7	-5	1.3	0.51
RHS09	8/17/12	55	1.32	67	-0.10	23.3	-5	1.27	0.49
RHS10	6/28/13	32	0.74	40	-0.10	10.1	-5	0.73	0.53
RHS10	6/28/13	32.4		39.6	-0.10	9.98	-5		0.52
RHSNO01	3/23/12		0.31	13	-0.10	1.9		0.29	3.2
RHSNO01	3/23/12		0.32	14	-0.010	1.8		0.29	3.1
RHSNO02	5/14/12		0.04	2.0	-0.010	0.17		0.01	0.12
RHSNO03	5/14/12		0.05	3.0	-0.010	0.32		0.03	0.15
RHSNO04	5/14/12		0.05	3.0	-0.010	0.33		0.02	0.15
RHSNO05	5/15/12		0.00		-0.10	0.15		0.01	-1.0
RHSNO05	5/15/12		0.04	2.0	-0.010	0.15		0.01	0.12
RHW02	3/14/13	108	2.75	132.0	-0.10	38.2	-5	2.69	2.37
RHW02	10/6/12	111	2.83	135.0	-0.10	39.7	-5	2.78	2.19

Sample ID	Sample Date	Alkalinity ppm as CaCO$_3^-$	Total Anions meq/L	Alkalinity ppm as HCO$_3^-$	Br$^-$ ppm	Ca^{2+} ppm	Alkalinity ppm as CO$_3^{2-}$	Total Cations meq/L	Cl$^-$ ppm
RHW02	9/15/12	107	2.71	130	-0.10	38.2	-5	2.67	2.27
RHW02	8/18/12	105	2.69	129.0	-0.10	37.6	-5	2.62	2.25
RHW02	7/18/12	97	2.47	118	0.013	35.5	-5	2.46	2.27
RHW02	6/28/12	102	2.59	125	0.01	37.3	-5	2.59	3.11
RHW02	6/2/12		2.73	130	0.011	40		2.78	3.2
RHW02	6/2/12		2.73	130	-0.10	40		2.75	3.2
RHW02	5/14/12		2.80	135	-0.10	40		2.76	3.2
RHW02	3/24/12		2.99	140	0.014	43		3.10	3.5
RHW05	3/14/13	94	5.49	114.0	0.11	57.6	-5	5.32	5
RHW05	10/5/12	92	5.44	112	0.11	56.2	-5	5.23	4.93
RHW05	9/14/12	93	5.49	113	0.1	57.1	-5	5.27	4.9
RHW05	8/17/12	88	5.37	107	0.10	57.2	-5	5.27	4.92
RHW05	7/17/12	87	5.44	106	0.1	56	-5	5.18	4.85
RHW05	6/29/12	90	5.32	110	0.13	56.7	-5	5.26	5.58
RHW05	6/1/12		5.48	115	0.092	58		5.28	5.5
RHW05	5/15/12		5.22	105	0.11	53		5.03	5.4
RHW05	3/25/12		5.09	110	0.094	57		5.41	5.4
RHW06	3/14/13	94	2.55	114.0	-0.10	36.4	-5.0	2.49	13.5
RHW06	10/6/12	92	2.42	112	-0.10	34.1	-5	2.35	10.4
RHW06	10/6/12	92		112	-0.10	34.50	-5		10.5
RHW06	9/15/12	93	2.46	113	-0.10	34.4	-5	2.38	11.1
RHW06	8/18/12	90	2.43	110	-0.10	34.2	-5	2.36	12
RHW06	7/17/12	89	2.46	108	-0.01	35.3	-5	2.44	13.9
RHW06	6/28/12	94	2.64	115	0.01	36.8	-5	2.58	15.1
RHW06	5/31/12		2.64	110	0.015	38		2.63	19
RHW06	5/31/12		2.65	110	0.014	38		2.67	19
RHW06	5/13/12		2.65	110	0.013	38		2.64	19
RHW06	3/24/12		2.52	115	-0.010	37		2.55	13
RHW10	3/15/13	166	8.51	203.0	0.32	84.8	-5.0	8.39	12.4
RHW10	10/6/12	140	8.31	171	0.29	79	-5	8.01	11.4
RHW10	9/15/12	136	8.19	166	0.28	78.3	-5	7.92	11.1
RHW10	8/18/12	129	8.22	158	0.28	76.1	-5	7.78	11
RHW10	7/18/12	150	8.24	183	0.3	82.5	-5	8.05	11.9
RHW10	6/29/12	130	8.01	158	0.3	77	-5	7.92	11.9
RHW10	6/2/12		8.03	160	0.29	79		8.03	12
RHW10	5/13/12		8.17	180	0.28	80		8.01	13
RHW10	3/24/12		8.05	200	0.29	86		8.59	12
RHW11	10/5/12	86	1.85	104	-0.10	20.0	-5	1.8	1.6
RHW11	9/14/12	85	1.84	103	-0.10	20.1	-5	1.8	1.65
RHW11	8/17/12	82	1.83	101.0	-0.10	20	-5	1.78	1.9200
RHW11	7/17/12	84	1.81	102	-0.10	20.3	-5	1.8	1.59
RHW11	6/29/12	88	1.93	107	-0.10	20.7	-5	1.86	2.17

Sample ID	Sample Date	Alkalinity ppm as $CaCO_3^{2-}$	Total Anions meq/L	Alkalinity ppm as HCO_3^-	Br^- ppm	Ca^{2+} ppm	Alkalinity ppm as CO_3^{2-}	Total Cations meq/L	Cl^- ppm
RHW11	5/15/12		1.78	100	0.036	20		1.77	2.0
RHW11	5/15/12		1.79	100	0.032	20		1.76	2.0
RHW11	3/25/12		1.78	100	0.03	20		1.86	2.1
RHW12	3/16/13	98	2.20	120.0	-0.10	35.0	-5.0	2.10	0.58
RHW12	9/14/12	98	2.19	120	-0.1	34.9	-5	2.1	0.56
RHW12	8/17/12	98	2.19	120.0	-0.10	34.9	-5.0	2.09	0.54
RHW12	7/17/12	96	2.14	117	-0.10	34.9	-5.0	2.1	0.54
RHW12	6/28/12	98	2.2	120	-0.10	34	-5.0	2.08	1.06
RHW12	6/28/12	99	2.22	121	-0.10	34.2	-5.0	2.08	0.94
RHW12	5/31/12		2.17	120	-0.10	35		2.12	0.80
RHW13	3/14/13	225	7.81	274	-0.1	62	-5		5.33
RHW13	3/14/13	225	7.78	274	-0.1	62	-5	7.62	5.34
RHW13	9/15/12	221	7.84	270	-0.1	60.9	-5	7.49	5.2
RHW13	8/18/12	225	7.94	274	-0.10	62	-5	7.67	5.3
RHW13	7/16/12	223	7.74	272	-0.10	62.8	-5	7.61	5.22
RHW13	6/28/12	222	7.72	271	-0.10	60.7	-5	7.57	6.32
RHW13	6/28/12	221	7.72	270	-0.10	60.8	-5	7.64	6.34
RHW13	6/2/12		7.72	270	0.058	63		7.72	6.3
WL01	10/5/12	46	2.20	56	-0.10	37.1	-5	2.07	0.52
WL01	9/14/12	36	1.62	45	-0.10	27.5	-5	1.56	0.84
WL01	8/17/12	43	1.88	52	-0.10	31.3	-5	1.75	0.46
WL01	7/18/12	41	1.67	50	-0.10	28.9	-5	1.61	0.46
WL01	6/28/12	36	1.5	43	-0.10	25.2	-5	1.42	0.82
WL01	6/1/12		1.00	32	-0.10	17		0.97	0.66
WL01	5/14/12		0.73	23	-0.010	12		0.71	0.30
WL02	10/5/12	19	1.98	23	-0.10	29	-5	1.86	0.42
WL02	9/14/12	19	1.44	23	-0.10	21.2	-5	1.35	0.44
WL02	8/17/12	16	1.55	19	-0.10	23	-5	1.47	0.40
WL02	7/18/12	17	1.58	20	-0.10	23.6	-5	1.5	0.43
WL02	6/28/12	15	1.45	18	-0.10	21.9	-5	1.39	0.71

Sample ID	Sample Date	F⁻ ppm	Hardness ppm as CaCO₃	Fe²⁺ ppm	Mg²⁺ ppm	NO₃⁻ ppm	NO₂⁻ ppm	PO₄³⁻ ppm	Charge Balance %
Ditch	9/14/12	-0.10	64.5	-0.02	1.09	1.59	-0.10	-0.50	-2.85
EFF	3/15/13	-0.10	100	0.063	4.62	0.63	-0.10	-0.50	-3.84
EFF	10/5/12	-0.10	81	-0.02	2.99	54.2	0.16	-0.50	-1.81
EFF	9/14/12	0.1	75.4	-0.02	2.72	5.94	0.11	-0.5	-1.87
EFF	8/17/12	0.1	71.5	0.029	2.72	4.17	-0.1	-0.5	-0.56
EFF	7/17/12	-0.1	74.8	0.041	2.51	3	0.47	-0.5	-2.87
EFF	6/28/12	-0.10	79	-0.02	2.84	7.98	0.2	-0.50	-0.71
EFF	6/1/12	-0.10	84		2.9	30	-0.10	-0.50	-1.03
EFF	5/15/12	-0.10	90		3.3	3.5	-0.10	-0.50	0.91
EFF	5/15/12	-0.10	90		3.3	3.5	-0.10	-0.50	-0.12
ISO1	3/16/13								
ISO1	12/18/12								
ISO1	10/5/12	0.15	10	0.096	0.6	0.5	-0.10	6.45	-52.60
ISO1	7/17/12	0.12	21.1	0.039	0.747	3.49	-0.10	3.9	-34.99
ISO1	5/31/12	-0.10	14		0.46	0.56	-0.10	-0.50	1.82
ISO1	3/23/12	-0.10	21		0.52	0.47	-0.10	-0.50	0.70
ISO1	1/8/12	-0.10	17.7		0.29	-0.10	-0.10	-0.50	-0.05
ISO2	3/16/13								
ISO2	12/18/12								
ISO2	10/5/12	0.13	5.4	0.03	0.353	0.41	-0.10	2.32	-30.27
ISO2	7/17/12	0.1	12.6	0.029	0.633	0.15	-0.10	11.1	-38.58
ISO2	5/31/12	-0.10	10		0.56	0.19	-0.10	-0.50	-1.90
ISO2	1/9/12								
ISO3	3/15/13								
ISO3	12/18/12								
ISO3	10/6/12	0.19	33.9	0.066	0.763	0.78	-0.10	-0.50	-3.98
ISO3	7/17/12	-0.10	52	0.096	0.694	-0.10	-0.10	3.54	3.87
ISO3	6/1/12	-0.10	27		0.73	-0.10	-0.10	-0.50	-1.22
ISO3	3/24/12	-0.10	14		0.21	-0.10	-0.10	-0.50	1.54
ISO4	3/15/13								
ISO4	12/18/12								
ISO4	10/6/12	0.13	39.0	0.028	0.835	0.38	-0.10	-0.50	-2.54
ISO4	7/17/12	-0.10	59	-0.02	0.742	-0.10	-0.10	0.57	-3.19
ISO4	6/1/12	-0.10	37		0.74	-0.10	-0.10	-0.50	-1.36
ISO4	6/1/12	-0.10	36		0.74	-0.10	-0.10	-0.50	-1.97
ISO4	3/24/12	-0.10	9.2		0.24	-0.10	-0.10	-0.50	-9.08
ISO4	1/9/12	-0.10	3.6		0.12	-0.10	-0.10	-0.50	2.50
ISO5	3/15/13								
ISO5	12/19/12								
ISO5	10/6/12	2.78	130	1.32	8.62	0.73	-0.10	48.00	25.30
ISO5	7/17/12	0.1	123	0.276	3.72	0.77	-0.10	9.23	-21.57
ISO5	6/2/12	-0.10	67		1.6	0.20	-0.10	1.4	-38.75

Sample ID	Sample Date	F⁻ ppm	Hardness ppm as $CaCO_3$	Fe^{2+} ppm	Mg^{2+} ppm	NO_3^- ppm	NO_2^- ppm	PO_4^{3-} ppm	Charge Balance %
ISO5	3/24/12	-0.10	30		1.2	-0.10	-0.10	7.7	-30.90
ISO5	3/24/12	-0.10	30		1.2	-0.10	-0.10	7.7	-30.71
ISO5	1/9/12	-0.10	52		1.2	-0.10	-0.10	13	-39.47
ISO6	3/14/13								
ISO6	12/19/12								
ISO6	10/5/12	6.94	55.0	0.431	2.06	0.62	-0.10	10.1	-23.76
ISO6	7/16/12	-0.10	68.2	-0.02	0.765	-0.10	-0.10	-0.50	-1.88
ISO6	6/2/12	-0.10	85		1.7	-0.10	-0.10	-0.50	1.40
ISO6	3/24/12	-0.10	66		1.4	-0.10	-0.10	2.3	-27.26
ISO6	1/9/12	-0.10	7.0		0.23	-0.10	-0.10	-0.5	-29.65
PCAPS-1 (15cm)	6/29/13	0.11	9.23	0.069	0.721	-0.1	-0.10	-0.50	2.21
PCAPS-1 (18cm)	6/29/13	-0.1	8.45	0.096	0.622	-0.1	-0.10	-0.50	8.06
PCAPS-1 Upper	10/20/12								
PCAPS-1 Lower	10/20/12								
PCAPS-2 (25-42cm)	6/29/13	-0.1	6.98	-0.02	0.301	2.83	-0.10	-0.50	-7.2
PCAPS-2 Upper	10/20/12								
PCAPS-2 Lower	10/20/12								
RHA01	7/18/12	0.18	66.4	-0.02	2.25	0.53	-0.10	-0.50	-1.34
RHA01	6/29/12	0.17	62.9	-0.02	2.26	0.69	-0.10	-0.50	-3.59
RHA01	6/2/12	0.14	56		1.8	0.91	-0.10	-0.50	-2.03
RHA01	6/2/12	0.14	56		1.7	0.91	-0.10	-0.50	-1.77
RHA01	5/13/12	0.16	54		1.8	0.78	-0.10	-0.50	-1.75
RHR01	3/14/13	0.18	73.2	0.0	2.67	0.99	-0.1	-0.50	-1.94
RHR01	11/17/12	0.19	70.5	-0.02	2.6	0.94	-0.10	-0.50	-2.67
RHR01	11/17/12	0.19	70.8	-0.02	2.62	0.95	-0.10	-0.50	-2.52
RHR01	10/6/12	0.18	72.1	-0.02	2.46	0.68	-0.10	-0.50	-2.24
RHR01	9/15/12	0.19	71.1	-0.02	2.45	0.66	-0.10	-0.50	-1.08
RHR01	8/18/12	0.18	67	-0.02	2.33	0.63	-0.10	-0.50	-2.86
RHR01	7/18/12	0.16	64.8	-0.02	2.26	0.51	-0.10	-0.50	-2.37
RHR01	6/29/12	0.18	65.8	-0.02	2.44	0.74	-0.10	-0.50	-2.26
RHR01	6/29/12	0.18	66.3	-0.02	2.46	0.74	-0.10	-0.50	-1.83
RHR01	6/1/12	0.14	56		1.7	0.72	-0.10	-0.50	-2.59
RHR01	5/13/12	0.16	56		1.9	0.84	-0.10	-0.50	1.24
RHR01	3/24/12	0.17	70		2.6	0.72	-0.10	-0.50	1.17
RHR02	3/14/13	0.23	108.0	-0.02	5.37	1.24	-0.10	-0.5	-1.75
RHR02	11/16/12	0.29	125.0	-0.02	6.59	1.60	-0.10	-0.50	-3.14
RHR02	10/5/12	0.36	160.0	-0.02	9.12	1.96	-0.10	-0.50	-1.98
RHR02	9/15/12	0.37	149	-0.02	8.97	0.98	-0.10	-0.50	-1.72
RHR02	9/15/12	0.37	148	-0.02	8.92	0.98	-0.10	-0.50	-1.32
RHR02	8/18/12	0.38	163	-0.02	8.82	1.8	-0.10	-0.50	-0.97
RHR02	7/16/12	0.38	160	-0.02	8.83	1.9	-0.10	-0.50	-1.3
RHR02	6/29/12	0.36	157	-0.02	9.85	1.52	-0.10	-0.50	-0.64

Sample ID	Sample Date	F⁻ ppm	Hardness ppm as CaCO$_3$	Fe^{2+} ppm	Mg^{2+} ppm	NO$_3^-$ ppm	NO$_2^-$ ppm	PO$_4^{3-}$ ppm	Charge Balance %
RHR02	6/2/12	0.29	153		7.8	0.94	-0.10	-0.50	0.53
RHR02	5/13/12	0.27	137		7.1	0.89	-0.10	-0.50	0.44
RHR02	5/13/12	0.28	136		7.0	0.90	-0.10	-0.50	1.57
RHR02	3/24/12	0.23	106		5.1	2.2	-0.10	-0.50	1.30
RHR04	3/14/13	0.18	81.8	-0.02	3.4	0.68	-0.10	-0.50	-2.03
RHR04	11/16/12	0.22	85.9	-0.02	3.84	0.21	-0.10	-0.50	-2.85
RHR04	10/5/12	0.24	134.0	0.043	5.78	0.9	-0.10	-0.50	-1.96
RHR04	10/5/12	0.24		0.043	5.79	0.9	-0.10	-0.50	
RHR04	9/15/12	0.25	134	0.043	5.69	0.81	-0.10	-0.50	-0.09
RHR04	8/18/12	0.26	130	0.044	5.56	0.54	-0.10	-0.50	-1.89
RHR04	7/16/12	0.24	126	0.046	5.31	0.8	-0.10	-0.50	-0.23
RHR04	6/29/12	0.25	117	0.037	5.18	0.46	-0.10	-0.50	-2.38
RHR04	6/29/12	0.25	119	0.038	5.19	0.45	-0.10	-0.50	-0.87
RHR04	6/2/12	0.21	106		4.3	0.12	-0.10	-0.50	-0.57
RHR04	5/13/12	0.20	95		4.0	0.19	-0.10	-0.50	1.29
RHR04	3/24/12	0.17	78		3.2	0.19	-0.10	-0.50	1.56
RHR10	3/16/13	-0.1	79.2	0.046	2.06	1.65	-0.10	-0.50	-1.78
RHR10	11/17/12	-0.10	74.7	-0.02	1.82	1.71	-0.10	-0.50	-2.97
RHR10	10/6/12	-0.10	72.3	-0.02	1.66	1.47	-0.10	-0.50	-3.13
RHR10	9/15/12	-0.10	71.8	-0.02	1.62	1.47	-0.10	-0.50	-1.94
RHR10	8/18/12	-0.10	66.9	-0.02	1.46	1.36	-0.10	-0.50	-4.19
RHR10	7/17/12	-0.10	67.8	-0.02	1.48	1.23	-0.10	-0.50	-1.21
RHR10	6/28/12	-0.10	67.8	-0.02	1.57	1.28	-0.10	-0.50	-0.62
RHR10	5/31/12	-0.10	62		1.2	1.5	-0.10	-0.50	-1.82
RHR10	5/31/12	-0.10	63		1.2	1.5	-0.10	-0.50	-2.07
RHR10	5/31/12	-0.10	61		1.2	1.5	-0.10	-0.50	-0.57
RHR10	5/13/12	-0.1	68		1.4	1.7	-0.1	-0.50	1.19
RHR10	3/23/12	-0.10	79		2.1	1.6	-0.10	-0.50	-1.27
RHR11	3/14/13	-0.1	78.3	-0.02	5.22	0.46	-0.10	-0.50	-3.04
RHR11	11/17/12	-0.10	83.7	-0.02	5.56	0.46	-0.10	-0.50	-2.30
RHR11	10/6/12	0.1	84.1	-0.02	5.45	0.31	-0.10	-0.50	-2.22
RHR11	9/15/12	0.1	84	-0.02	5.26	0.49	-0.10	-0.50	-0.77
RHR11	8/18/12	0.11	81	-0.02	4.93	0.43	-0.10	-0.50	-2.86
RHR11	7/17/12	-0.10	79.5	-0.02	4.65	0.24	-0.10	-0.50	-0.37
RHR11	6/28/12	0.11	77.9	-0.02	4.59	0.3	-0.10	-0.50	-0.96
RHR11	5/13/12	-0.10	66		3.5	0.34	-0.10	-0.50	7.98
RHR11	5/13/12	-0.10	66		3.6	0.49	-0.10	-0.50	2.12
RHR11	3/23/12	-0.10	78		5.1	0.57	-0.10	-0.50	2.02
RHR11	3/23/12	-0.10	78		5.1	0.32	-0.10	-0.50	1.76
RHR14	3/14/13	0.14	85.9	0.0	2.8	0.44	-0.10	-0.50	-2.39
RHR14	3/14/13	0.14		0.0	2.74	0.44	-0.10	-0.50	
RHR14	11/17/12	0.15	80.8	-0.02	2.67	0.31	-0.10	-0.50	-5.93

Sample ID	Sample Date	F⁻ ppm	Hardness ppm as CaCO₃	Fe²⁺ ppm	Mg²⁺ ppm	NO₃⁻ ppm	NO₂⁻ ppm	PO₄³⁻ ppm	Charge Balance %
RHR14	10/6/12	0.15	79.8	-0.02	2.57	0.26	-0.10	-0.50	-2.79
RHR14	9/15/12	0.16	80.9	-0.02	2.59	0.26	-0.10	-0.50	-1.51
RHR14	8/18/12	0.17	76.8	-0.02	2.5	0.28	-0.10	-0.50	-2.96
RHR14	7/18/12	0.14	76.8	-0.02	2.48	0.27	-0.10	-0.50	-1.87
RHR14	6/29/12	0.16	78	-0.02	2.62	0.3	-0.10	-0.50	-1.74
RHR14	5/31/12	0.12	69		2.2	0.24	-0.10	-0.50	-0.17
RHR14	5/13/12	-0.10	62		2.1	0.29	-0.10	-0.50	1.06
RHR14	3/24/12	0.14	82		2.7	0.10	-0.10	-0.50	0.41
RHR14	3/24/12	0.14	83		2.7	0.10	-0.10	-0.50	0.59
RHR15	3/14/13	0.1	79.1	-0.02	2.75	1.20	-0.10	-0.50	-2.00
RHR15	11/17/12	0.11	74.9	-0.02	2.57	0.93	-0.10	-0.50	-3.09
RHR15	10/6/12	0.1	77.2	-0.02	2.45	0.84	-0.10	-0.50	-2.19
RHR15	9/15/12	0.11	77.1	-0.02	2.48	0.82	-0.10	-0.50	-2.09
RHR15	8/18/12	0.11	72.3	-0.02	2.34	0.82	-0.10	-0.50	-3.01
RHR15	7/18/12	-0.10	72.3	-0.02	2.3	0.71	-0.10	-0.50	-1.99
RHR15	6/29/12	0.1	71.8	-0.02	2.38	0.91	-0.10	-0.50	-0.9
RHR15	6/1/12	-0.10	65		1.8	0.90	-0.10	-0.50	-1.14
RHR15	5/13/12	-0.10	66		2.0	0.92	-0.10	-0.50	0.62
RHR15	3/24/12	0.11	72		2.5	0.66	-0.10	-0.50	1.43
RHR16	3/14/13	0.34	45.0	0.087	1.78	0.89	-0.10	-0.50	-3.72
RHR16	11/17/12	0.35	51.0	-0.02	1.98	1.37	-0.10	-0.50	-3.88
RHR16	10/6/12	0.35	51.1	-0.02	1.9	0.79	-0.10	-0.50	-3.25
RHR16	9/15/12	0.34	49.1	-0.02	1.82	0.84	-0.10	-0.50	-3.41
RHR16	8/18/12	0.35	48	-0.02	1.83	0.64	-0.10	-0.50	-4.38
RHR16	7/18/12	0.35	47.1	-0.02	1.74	0.47	-0.10	-0.50	-1.02
RHR16	6/29/12	0.39	48.2	-0.02	2.09	0.55	-0.10	-0.50	-2.99
RHR16	6/1/12	0.34	36		1.3	0.70	-0.10	-0.50	-0.89
RHR16	6/1/12	0.34	35		1.2	0.66	-0.10	-0.50	-2.27
RHR16	5/13/12	0.36	34		1.3	0.84	-0.10	-0.50	47.34
RHR16	5/13/12	0.36	35		1.3	0.86	-0.10	-0.50	2.09
RHR16	3/24/12	0.37	47		1.8	0.64	-0.10	-0.50	0.97
RHR18	11/16/12	-0.10	66.8	-0.02	1.16	1.72	-0.10	-0.50	-5.51
RHR18	10/6/12	-0.10	66.4	-0.02	1.1	1.56	-0.10	-0.50	-3.38
RHR18	9/14/12	-0.10	64.3	-0.02	1.06	1.45	-0.10	-0.50	-3.18
RHR18	8/17/12	-0.10	64	-0.02	1.04	1.16	-0.10	-0.50	-1.4
RHR18	7/17/12	-0.10	58.6	-0.02	0.966	1.21	-0.10	-0.50	-2.37
RHR18	6/28/12	-0.10	59	-0.02	1.19	1.24	-0.10	-0.50	-3.6
RHR18	5/31/12	-0.10	59		0.95	1.6	-0.10	-0.50	0.02
RHR18	5/13/12	-0.10	65		1.1	1.9	-0.10	-0.50	1.29
RHR18	3/23/12	-0.10	71		1.2	2.2	-0.10	-0.50	0.35
RHR20	7/18/12	0.52	20.5	1.03	1.68	-0.10	-0.10	-0.50	-0.14
RHR20	6/29/12	0.93	23.6	0.629	1.95	0.22	-0.10	-0.50	1.84

Sample ID	Sample Date	F⁻ ppm	Hardness ppm as CaCO₃	Fe²⁺ ppm	Mg²⁺ ppm	NO₃⁻ ppm	NO₂⁻ ppm	PO₄³⁻ ppm	Charge Balance %
RHR20	6/1/12	0.54	15		1.2	-0.10	-0.10	-0.50	5.20
RHR20	5/12/12	0.51	10		0.8	0	-0.10	-0.50	10.13
RHR20	3/25/12	0.53	13		1.0	0.77	0.26	-0.50	9.83
RHR21	3/15/13	0.17	71.9	0.0	2.61	0.9	-0.10	-0.50	-2.32
RHR21	11/17/12	0.19	70.2	-0.02	2.56	0.89	-0.10	-0.50	-3.01
RHR21	10/6/12	0.2	75.1	-0.02	2.81	0.4	-0.10	-0.50	-2.91
RHR21	9/15/12	0.2	73.1	-0.02	2.64	0.51	-0.10	-0.50	-2.92
RHR21	8/18/12	0.2	71.3	-0.02	2.54	0.55	-0.10	-0.50	-2.43
RHR21	7/18/12	0.17	69.2	-0.02	2.48	0.45	-0.10	-0.50	-1.01
RHR21	6/29/12	0.19	69.6	-0.02	2.61	0.57	-0.10	-0.50	-1.14
RHR21	6/2/12	0.16	60		2.0	0.82	-0.10	-0.50	-1.57
RHR21	5/13/12	0.17	58		2.0	0.74	-0.10	-0.50	2.03
RHR22	10/5/12	-0.10	66	-0.02	1.2	1.33	-0.10	-0.50	-3.00
RHR22	9/14/12	-0.10	59.4	-0.02	1.03	1.38	-0.10	-0.50	-2.45
RHR22	8/17/12	-0.10	61	-0.02	1.05	0.71	-0.10	-0.50	-1.26
RHR22	7/18/12	-0.10	58	-0.02	1.02	0.53	-0.10	-0.50	-2.49
RHR22	6/28/12	-0.10	54.6	-0.02	0.971	0.49	-0.10	-0.50	-2.11
RHR22	6/1/12	-0.10	37		0.66	0.83	-0.10	-0.50	-2.49
RHR22	6/1/12	-0.10	37		0.67	0.83	-0.10	-0.50	-1.91
RHR22	5/14/12	-0.10	45		0.82	1.2	-0.10	-0.50	0.28
RHR23	6/1/12	-0.10	61		1.6	1.2	-0.10	-0.50	1.85
RHR23	5/15/12	-0.10	63		1.9	1.4	-0.10	-0.50	-2.08
RHR24	11/17/12	-0.10	77	-0.02	2.7	1.5	-0.10	-0.50	-2.85
RHR24	10/5/12	-0.10	76	-0.02	2.4	1.5	-0.10	-0.50	-2.59
RHR24	9/14/12	0.1	74.7	-0.02	2.34	1.11	-0.10	-0.50	-2.19
RHR24	8/18/12	-0.10	71.4	-0.02	2.17	1.16	-0.10	-0.50	-2.34
RHR24	7/17/12	-0.10	70.6	-0.02	2.26	0.96	-0.10	-0.50	-1.71
RHR24	6/28/12	-0.10	71.1	-0.02	2.44	1.1	-0.10	-0.50	-0.73
RHR24	6/1/12	-0.10	62		1.7	1.4	-0.10	-0.50	-2.05
RHR24	5/15/12	-0.10	65		1.9	1.4	-0.10	-0.50	-0.90
RHRO01	3/23/12	0.15	61		1.9	1.1	-0.10	-0.50	-1.08
RHRO02	8/17/12	-0.10	62.3	-0.02	1.02	1.35	-0.10	-0.50	-0.91
RHRO02	7/17/12	-0.10	58.5	-0.02	0.948	1.41	-0.10	-0.50	-2.44
RHRO02	6/28/12	-0.10	56.2	-0.02	0.925	1.4	-0.10	-0.50	-2.26
RHRO02	6/1/12	-0.10	59		0.96	1.6	-0.10	-0.50	-0.58
RHRO02	5/14/12	-0.10	62		1.0	1.6	-0.10	-0.50	-2.15
RHRO03	6/28/12	-0.10	57.2	-0.02	1	1.45	-0.10	-0.50	-2.52
RHRO03	6/1/12	-0.10	63		0.98	1.7	-0.10	-0.50	-2.91
RHRO03	6/1/12	-0.10	59		0.97	1.7	-0.10	-0.50	-1.51
RHRO03	5/14/12	-0.10	64		1.1	1.9	-0.10	-0.50	-1.97
RHRO04	9/14/12	-0.1	63	-0.02	1.05	1.58	-0.10	-0.50	-3.38
RHRO04	7/17/12	-0.10	58.8	-0.02	0.943	1.34	-0.10	-0.50	-1.25

143

Sample ID	Sample Date	F^- ppm	Hardness ppm as $CaCO_3$	Fe^{2+} ppm	Mg^{2+} ppm	NO_3^- ppm	NO_2^- ppm	PO_4^{3-} ppm	Charge Balance %
RHRO04	6/28/12	-0.10	56.1	-0.02	0.972	1.4	-0.10	-0.50	-3.29
RHRO04	6/1/12	-0.10	59		0.97	1.7	-0.10	-0.50	-3.18
RHRO04	5/14/12	-0.10	65		1.1	1.8	-0.10	-0.50	-1.56
RHRO05	10/6/12	-0.10	80		1.6	1.2	-0.10	-0.50	-2.99
RHRO05	10/6/12	-0.10		-0.02	1.56	1	-0.10	-0.50	
RHRO05	9/15/12	-0.10	79.8	-0.02	1.55	1.12	-0.10	-0.50	-2.49
RHRO05	8/17/12	-0.10	79.8	-0.02	1.48	0.92	-0.10	-0.50	-1.35
RHRO05	7/17/12	-0.10	75.9	-0.02	1.41	0.82	-0.10	-0.50	-2.31
RHRO05	7/17/12	-0.10	76.6	-0.02	1.42	0.83	-0.10	-0.50	-1.2
RHRO05	6/28/12	-0.10	73.2	-0.02	1.65	0.88	-0.10	-0.50	-0.78
RHRO05	6/1/12	-0.10	57		1.1	1.0	-0.10	-0.50	-2.29
RHRO05	5/14/12	-0.10	63		1.2	1.3	-0.10	-0.50	58.73
RHRO05	5/14/12	-0.10	63		1.2	1.3	-0.10	-0.50	-2.88
RHRO06	6/1/12	-0.10	67		1.7	2.4	-0.10	-0.50	-0.79
RHRO06	5/15/12	-0.10	64		1.6	2.4	-0.10	-0.50	-1.79
RHRO07	3/15/13	0.17	47	0.03	1.7	-0.1	-0.10	-0.50	-3.97
RHS01	3/15/13	0.19	80	-0.02	2.9	1.0	-0.10	-0.50	-2.87
RHS01	11/17/12	0.21	82	-0.02	3.1	0.5	-0.10	-0.50	-2.64
RHS01	10/6/12	0.21	82	-0.02	3.0	0.5	-0.10	-0.50	-2.81
RHS01	9/15/12	0.22	82.1	-0.02	2.97	0.51	-0.10	-0.50	-1.81
RHS01	8/18/12	0.24	82.1	-0.02	2.97	0.71	-0.10	-0.50	-1.56
RHS01	7/18/12	0.2	82.3	-0.02	3.01	0.67	-0.10	-0.50	1.19
RHS01	6/29/12	0.22	78.5	-0.02	2.91	0.71	-0.10	-0.50	-0.27
RHS01	6/2/12	0.19	74		2.7	0.60	-0.10	-0.50	-2.06
RHS01	6/2/12	0.20	74		2.7	0.62	-0.10	-0.50	-3.33
RHS01	5/13/12	0.18	78		2.9	0.62	-0.10	-0.50	-1.69
RHS01	3/24/12	0.18	83		3.2	0.81	-0.10	-0.50	2.48
RHS01	3/24/12	0.18	82		3.2	0.99	-0.10	-0.50	2.45
RHS03	7/18/12	0.72	30.8	1.6	2.5	0.25	-0.10	-0.50	2.15
RHS03	6/29/12	0.93	31.3	1.27	2.69	0.38	-0.10	-0.50	1.97
RHS03	6/1/12	0.84	20		1.7	-0.10	-0.10	-0.50	2.18
RHS03	5/12/12	0.84	19		1.6	-0.10	-0.10	-0.50	3.75
RHS03	3/25/12	0.20	5.5	0.0	0.33	0.28	-0.10	-0.50	-5.34
RHS04	3/16/13	-0.1	71.4	-0.02	1.21	1.97	-0.10	-0.50	-3.40
RHS04	11/16/12	-0.10	68.9	-0.02	1.17	1.84	-0.10	-0.50	-3.74
RHS04	10/6/12	-0.10	66.3	-0.02	1.11	1.7	-0.10	-0.50	-2.78
RHS04	9/14/12	-0.10	67.1	-0.02	1.45	1.59	-0.10	-0.50	-3.43
RHS04	8/17/12	-0.10	60.2	-0.02	0.993	1.41	-0.10	-0.50	-2.32
RHS04	7/17/12	-0.10	58.3	-0.02	0.973	1.39	-0.10	-0.50	-2.02
RHS04	6/28/12	-0.10	58.4	-0.02	1.2	1.46	-0.10	-0.50	-2.35
RHS04	5/31/12	-0.10	60		0.97	1.7	-0.10	-0.50	-0.09
RHS04	5/13/12	-0.10	63		1.1	2.0	-0.10	-0.50	-0.96

Sample ID	Sample Date	F⁻ ppm	Hardness ppm as CaCO₃	Fe²⁺ ppm	Mg²⁺ ppm	NO₃⁻ ppm	NO₂⁻ ppm	PO₄³⁻ ppm	Charge Balance %
RHS04	3/23/12	-0.10	71		1.2	1.1	-0.10	-0.50	2.19
RHS05	3/14/13	0.15	84.5	-0.02	2.73	0.3	-0.1	-0.50	-3.30
RHS05	10/6/12	0.16	81.7	-0.02	2.58	0.11	-0.10	-0.50	-3.53
RHS05	9/15/12	0.16	79.3	-0.02	2.52	0.19	-0.10	-0.50	-2.56
RHS05	8/18/12	0.18	78.3	-0.02	2.45	0.2	-0.10	-0.50	-2.42
RHS05	7/18/12	0.15	78.3	-0.02	2.5	0.15	-0.10	-0.50	-1.37
RHS05	6/29/12	0.16	84.2	-0.02	2.89	0.16	-0.10	-0.50	1.69
RHS05	5/31/12	0.14	75		2.4	0.18	-0.10	-0.50	-0.47
RHS05	5/13/12	0.14	73		2.4	0.22	-0.10	-0.50	-1.03
RHS05	3/24/12	0.14	84		2.7	-0.10	-0.10	-0.50	0.10
RHS06	11/16/12	-0.10	61.7	-0.02	2	2.5	-0.10	-0.50	-3.93
RHS06	10/6/12	-0.10	63.4	-0.02	1.95	2.48	-0.10	-0.50	-2.22
RHS06	9/15/12	-0.10	62.5	-0.02	1.91	2.44	-0.10	-0.50	-1.96
RHS06	8/17/12	-0.10	60.8	-0.02	1.84	2.57	-0.10	-0.50	-3.74
RHS06	7/17/12	-0.10	64.2	-0.02	1.94	2.57	-0.10	-0.50	-0.68
RHS06	6/28/12	-0.10	68.1	-0.02	2.24	2.57	-0.10	-0.50	-0.71
RHS06	6/1/12	-0.10	63		2.0	2.4	-0.10	-0.50	-0.19
RHS06	5/15/12	-0.10	61		1.9	2.4	-0.10	-0.50	-0.51
RHS07	10/6/12	-0.10	70	-0.02	1.8	2.7	-0.10	-0.50	-3.39
RHS07	9/15/12	-0.10	69.1	-0.02	1.72	2.64	-0.10	-0.50	-3.58
RHS07	8/17/12	0.13	71	-0.02	1.8	2.7	-0.10	-0.50	-1.31
RHS07	7/17/12	-0.10	70.5	-0.02	1.76	2.73	-0.10	-0.50	-0.85
RHS08	11/16/12	-0.10	70.1	-0.02	1.78	2.84	-0.10	-0.50	-3.35
RHS08	10/6/12	-0.10	70	-0.02	1.77	2.79	-0.10	-0.50	-3.28
RHS08	9/15/12	-0.10	69.7	-0.02	1.73	2.73	-0.10	-0.50	-2.54
RHS08	8/17/12	0.11	69.9	-0.02	1.73	2.75	-0.10	-0.50	-1.96
RHS08	7/17/12	-0.10	70.4	-0.02	1.76	2.79	-0.10	-0.50	-1.15
RHS09	11/16/12	0.10	64.9	-0.02	0.69	3.15	-0.10	-0.50	-3.44
RHS09	10/5/12	0.15	63.8	-0.02	0.663	2.82	-0.10	-0.50	-1.47
RHS09	9/14/12	0.14	61.8	-0.02	0.636	2.51	-0.10	-0.50	-3.21
RHS09	8/17/12	0.14	60.7	-0.02	0.625	2.48	-0.10	-0.50	-2.11
RHS10	6/28/13	-0.10	33.5	-0.02	1.98	0.33	-0.10	-0.50	-0.52
RHS10	6/28/13	-0.10		-0.02	1.97	0.33	-0.10	-0.50	
RHSNO01	3/23/12	-0.10	5.6		0.21	0.34	-0.10	-0.50	-2.86
RHSNO01	3/23/12	-0.10	5.4		0.21	0.35	-0.10	-0.50	-6.01
RHSNO02	5/14/12	-0.10	0.43		-0.05	0.28	-0.10	-0.50	-62.81
RHSNO03	5/14/12	-0.10	1.0		0.058	0.22	-0.10	-0.50	-29.97
RHSNO04	5/14/12	-0.10	1.0		0.051	0.32	-0.10	-0.50	-41.93
RHSNO05	5/15/12	-0.10	0.38		-0.05	0.21	-0.10	-0.50	38.84
RHSNO05	5/15/12	-0.10	0.38		-0.05	0.21	-0.10	-0.50	-60.68
RHW02	3/14/13	0.17	121.0	-0.02	6.26	0.61	-0.10	-0.50	-1.25
RHW02	10/6/12	0.2	125	-0.02	6.16	0.65	-0.10	-0.50	-1.01

Sample ID	Sample Date	F⁻ ppm	Hardness ppm as CaCO₃	Fe²⁺ ppm	Mg²⁺ ppm	NO₃⁻ ppm	NO₂⁻ ppm	PO₄³⁻ ppm	Charge Balance %
RHW02	9/15/12	0.21	120	-0.02	5.98	0.77	-0.10	-0.50	-0.79
RHW02	8/18/12	0.23	118	-0.02	5.88	0.72	-0.10	-0.50	-1.28
RHW02	7/18/12	0.18	111	-0.02	5.43	0.88	-0.10	-0.50	-0.23
RHW02	6/28/12	0.18	117	-0.02	5.86	1.08	-0.10	-0.50	0.05
RHW02	6/2/12	0.15	126		6.1	1.9	-0.10	-0.50	0.78
RHW02	6/2/12	0.15	124		5.9	1.9	-0.10	-0.50	0.23
RHW02	5/14/12	0.16	125		6.3	3.6	-0.10	-0.50	-0.86
RHW02	3/24/12	0.16	135		6.8	1.7	0.38	-0.50	1.71
RHW05	3/14/13	0.17	219.0	0.0	18.4	-0.10	-0.10	-0.50	-1.60
RHW05	10/5/12	0.2	214	-0.02	18	-0.10	-0.10	-0.50	-1.99
RHW05	9/14/12	0.19	218	-0.02	18.2	-0.10	-0.10	-0.50	-2.05
RHW05	8/17/12	0.23	216	-0.02	17.8	-0.10	-0.10	-0.50	-0.93
RHW05	7/17/12	0.23	211	-0.02	17.4	-0.10	-0.10	-0.50	-2.41
RHW05	6/29/12	0.21	216	-0.02	18.2	-0.10	-0.10	-0.50	-0.53
RHW05	6/1/12	0.18	219		18	-0.10	-0.10	-0.50	-1.86
RHW05	5/15/12	0.22	204		17	-0.10	-0.10	-0.50	-1.88
RHW05	3/25/12	0.18	220		19	-0.10	-0.10	-0.50	3.11
RHW06	3/14/13	0.15	107.0	-0.02	4.03	2.22	-0.10	-0.50	-1.17
RHW06	10/6/12	0.16	101	-0.02	3.76	1.11	-0.10	-0.50	-1.50
RHW06	10/6/12	0.16		-0.02	3.8	1.1	-0.10	-0.50	
RHW06	9/15/12	0.17	102	-0.02	3.83	1.16	-0.10	-0.50	-1.56
RHW06	8/18/12	0.18	101	-0.02	3.78	1.24	-0.10	-0.50	-1.40
RHW06	7/17/12	0.14	104	-0.02	3.87	1.42	-0.10	-0.50	-0.32
RHW06	6/28/12	0.16	110	-0.02	4.33	1.37	-0.10	-0.50	-1.15
RHW06	5/31/12	0.14	111		4.2	1.9	-0.10	-0.50	-0.17
RHW06	5/31/12	0.14	113		4.2	1.9	-0.10	-0.50	0.37
RHW06	5/13/12	0.14	112		4.3	2.1	-0.10	-0.50	-0.28
RHW06	3/24/12	0.14	109		4.1	1.6	-0.10	-0.50	0.60
RHW10	3/15/13	1.3	364.0	-0.02	37	-0.10	-0.10	-0.50	-0.72
RHW10	10/6/12	1.58	342.0	-0.02	35.2	-0.10	-0.10	-0.50	-1.80
RHW10	9/15/12	1.58	338	-0.02	34.5	-0.10	-0.10	-0.50	-1.63
RHW10	8/18/12	1.65	331.0	-0.02	34.2	-0.10	-0.10	-0.50	-2.77
RHW10	7/18/12	1.58	346	0.081	34.1	-0.10	-0.10	-0.50	-1.12
RHW10	6/29/12	1.48	337	-0.02	35.2	-0.10	-0.10	-0.50	-0.57
RHW10	6/2/12	1.5	342		35	-0.10	-0.10	-0.50	0.02
RHW10	5/13/12	1.3	344		35	-0.10	-0.10	-0.50	-0.98
RHW10	3/24/12	1.1	371		38	-0.10	-0.10	-0.50	3.23
RHW11	10/5/12	0.59	69.3	-0.02	4.690	0.61	-0.10	-0.50	-1.46
RHW11	9/14/12	0.59	69.2	-0.02	4.64	0.67	-0.10	-0.50	-1.22
RHW11	8/17/12	0.65	68.7	-0.02	4.570	0.76	-0.10	-0.50	-1.21
RHW11	7/17/12	0.57	69.7	-0.02	4.61	0.8	-0.10	-0.50	-0.42
RHW11	6/29/12	0.59	72.6	-0.02	5.06	0.62	-0.10	-0.50	-1.88

Sample ID	Sample Date	F⁻ ppm	Hardness ppm as CaCO₃	Fe²⁺ ppm	Mg²⁺ ppm	NO₃⁻ ppm	NO₂⁻ ppm	PO₄³⁻ ppm	Charge Balance %
RHW11	5/15/12	0.56	68		4.6	0.57	-0.10	-0.50	-0.45
RHW11	5/15/12	0.56	68		4.5	0.60	-0.10	-0.50	-0.83
RHW11	3/25/12	0.51	71		4.7	0.56	0.14	-0.50	2.22
RHW12	3/16/13	-0.1	97.7	-0.02	2.490	1.8	-0.10	-0.50	-2.16
RHW12	9/14/12	-0.1	97.4	-0.02	2.52	2.11	-0.10	-0.50	-2.06
RHW12	8/17/12	-0.10	97.5	-0.02	2.520	2.09	-0.10	-0.50	-2.17
RHW12	7/17/12	-0.10	97.6	-0.02	2.51	2.14	-0.10	-0.50	-1.04
RHW12	6/28/12	-0.10	96.7	-0.02	2.84	1.9	-0.10	-0.50	-2.88
RHW12	6/28/12	-0.10	96.9	-0.02	2.79	1.9	-0.10	-0.50	-3.18
RHW12	5/31/12	-0.10	99		2.5	1.4	0.17	-0.50	-1.23
RHW13	3/14/13	0.33		-0.02	12.2	5.8	-0.10	-0.50	
RHW13	3/14/13	0.33	204	-0.02	12.2	5.8	-0.10	-0.50	-1.22
RHW13	9/15/12	0.37	201	-0.02	11.9	5.75	-0.10	-0.50	-1.85
RHW13	8/18/12	0.37	205	-0.02	12.2	5.7	-0.10	-0.50	-1.12
RHW13	7/16/12	0.36	207	-0.02	12.1	5.64	-0.10	-0.50	-2.14
RHW13	6/28/12	0.29	202	-0.02	12.2	5.21	-0.10	-0.50	-1.13
RHW13	6/28/12	0.29	203	-0.02	12.4	5.2	-0.10	-0.50	-0.52
RHW13	6/2/12	0.28	208		12	5.2	-0.10	-0.50	0.02
WL01	10/5/12	-0.10	99.8	0.022	1.760	1.290	-0.10	-0.50	-2.95
WL01	9/14/12	-0.10	74.3	-0.02	1.35	1.5	-0.10	-0.50	-1.95
WL01	8/17/12	-0.10	84.4	-0.02	1.52	0.88	-0.10	-0.50	-3.46
WL01	7/18/12	-0.10	77.6	0.031	1.34	0.85	-0.10	-0.50	-1.74
WL01	6/28/12	-0.10	68	-0.02	1.21	0.52	-0.10	-0.50	-2.58
WL01	6/1/12	-0.10	46		0.83	1.0	-0.10	-0.50	-1.26
WL01	5/14/12	-0.10	34		0.63	0.93	-0.10	-0.50	-1.62
WL02	10/5/12	0.15	89	-0.02	3.71	2.28	-0.10	-0.50	-3.21
WL02	9/14/12	0.17	63.6	0.054	2.59	2.45	-0.10	-0.50	-3.51
WL02	8/17/12	0.16	70	-0.02	2.95	2.12	-0.10	-0.50	-2.57
WL02	7/18/12	0.14	71.4	-0.02	3.02	2	-0.10	-0.50	-2.76
WL02	6/28/12	0.15	66	-0.02	2.77	1.69	-0.10	-0.50	-2.04

Sample ID	Sample Date	pH SU	K$^+$ ppm	SiO$_2$ ppm	Na$^+$ ppm	Conductivity (μS/cm)	Sr^{2+} ppm	SO$_4^{2-}$ ppm	Total Dissolved Solids ppm
Ditch	9/14/12	7.7	0.481	5.07	1.12	144	0.099	28.5	87
EFF	3/15/13	7.5	18.3	5.39	190	1090	0.104	49.9	634
EFF	10/5/12	7.5	8.27	3.58	112	685	0.092	29.1	411
EFF	9/14/12	7.6	7.6	3.46	117	661	0.088	33.7	392
EFF	8/17/12	7.7	8.56	3.6	116	656		28.6	382
EFF	7/17/12	7.4	8.34	4.25	74.3	502		26.1	291
EFF	6/28/12	7.6	7.42	3.43	76.7	506		25.5	293
EFF	6/1/12	7.3	4.4	4.5	66	445		23	279
EFF	5/15/12	7.6	2.5	4.0	62	430		16	251
EFF	5/15/12	7.6	2.5	4.0	62	435		16	253
ISO1	3/16/13								
ISO1	12/18/12								
ISO1	10/5/12	7.3	3.7	0.5	2	134	0.013	2	51
ISO1	7/17/12	6.6	3.06	0.56	0.892	108		3.93	52
ISO1	5/31/12	7.7	0.15	0.42	0.33	29		1.1	15
ISO1	3/23/12	6.6	0.11	0.12	0.19	44		-1	22
ISO1	1/8/12	7.2	0.064	0.19	0.13	37		-1.0	18.3
ISO2	3/16/13								
ISO2	12/18/12								
ISO2	10/5/12	7.2	3.89	0.38	1.91	59	0.006	2.05	26.0
ISO2	7/17/12	6.9	16.5	0.57	0.68	151		4.49	75
ISO2	5/31/12	7.5	0.53	0.30	0.45	24		1.0	13
ISO2	1/9/12								
ISO3	3/15/13								
ISO3	12/18/12								
ISO3	10/6/12	7	4.74	0.88	2.97	113	0.016	1	55.0
ISO3	7/17/12	6.4	3.11	3.89	0.399	133		-1	64
ISO3	6/1/12	7.0	0.78	0.13	0.27	62		1.0	31
ISO3	3/24/12	6.1	-0.050	0.18	0.15	32		-1	15
ISO4	3/15/13								
ISO4	12/18/12								
ISO4	10/6/12	7	2.42	0.45	1.88	108	0.014	1.25	52.0
ISO4	7/17/12	6.6	2.97	2.96	0.267	154		1.4	75
ISO4	6/1/12	6.9	1.6	0.71	0.66	84		1.6	44
ISO4	6/1/12	6.9	1.6	0.73	0.65	84		1.6	44
ISO4	3/24/12	5.9	0.42	0.10	0.22	27		-1	12
ISO4	1/9/12	6.5	0.17	0.43	1.0	13		-1	6.5
ISO5	3/15/13								
ISO5	12/19/12								
ISO5	10/6/12	4.5	66.2	23.2	9.85	579	0.494	1.52	242.0
ISO5	7/17/12	6.9	9.38	2.47	11	502		1.23	231
ISO5	6/2/12	7.7	6.4	2.6	1.5	370		-1.0	150

Sample ID	Sample Date	pH SU	K+ ppm	SiO2 ppm	Na+ ppm	Conductivity (μS/cm)	Sr2+ ppm	SO4^2- ppm	Total Dissolved Solids ppm
ISO5	3/24/12	6.4	13	0.22	2.1	205		4.8	89
ISO5	3/24/12	6.4	13	0.22	2.1	210		4.8	88
ISO5	1/9/12	6.5	4.3	0.96	1.0	275		-1	112
ISO6	3/14/13								
ISO6	12/19/12								
ISO6	10/5/12	6.4	15.6	1.62	2.59	341	0.034	-1	121.0
ISO6	7/16/12	7.2	1.53	1.81	0.614	169		-1	82
ISO6	6/2/12	7.4	0.60	1.4	0.90	185		1.2	94
ISO6	3/24/12	6.5	6.7	1.7	2.0	305		-1	122
ISO6	1/9/12	6.0	1.2	0.37	0.99	47		-1	18
PCAPS-1 (15cm)	6/29/13	6.7	0.324	3.4	3.87	33	0.005	1	22
PCAPS-1 (18cm)	6/29/13	6.6	1.11	3.44	2.8	29	0.007	1.06	19
PCAPS-1 Upper	10/20/12								
PCAPS-1 Lower	10/20/12								
PCAPS-2 (25-42cm)	6/29/13	5.8	0.595	1.51	0.667	23	0.01	2.28	14
PCAPS-2 Upper	10/20/12								
PCAPS-2 Lower	10/20/12								
RHA01	7/18/12	7.8	0.805	7.16	3.1	149		15.4	89
RHA01	6/29/12	8.2	0.694	6.97	2.64	148		14.9	86
RHA01	6/2/12	7.7	0.63	6.4	2.2	120		14	76
RHA01	6/2/12	7.7	0.62	6.5	2.1	120		14	75
RHA01	5/13/12	8.0	0.71	7.0	2.4	125		13	74
RHR01	3/14/13	8	0.914	11.7	6.28	179	0.147	15.6	109.0
RHR01	11/17/12	8	0.807	8.1	3.57	160	0.144	16.9	97.0
RHR01	11/17/12	8	0.814	8.13	3.57	160	0.144	16.9	97.0
RHR01	10/6/12	7.9	0.848	7.38	3.26	162	0.142	16.9	97.0
RHR01	9/15/12	7.9	0.825	6.72	3.3	158	0.138	16.6	94
RHR01	8/18/12	8.1	0.818	6.79	3.23	154		15.9	91
RHR01	7/18/12	7.9	0.796	7.17	3.03	151		14.5	88
RHR01	6/29/12	8.3	0.723	7.07	2.72	147		14.9	88
RHR01	6/29/12	8.3	0.718	7.25	2.72	148		14.9	88
RHR01	6/1/12	7.9	0.66	6.3	2.1	120		14	76
RHR01	5/13/12	7.9	0.70	7.1	2.4	120		13	74
RHR01	3/24/12	7.5	0.87	8.0	5.1	165		14	96
RHR02	3/14/13	8.4	1.09	11.90	9.74	255	0.208	19.8	154.0
RHR02	11/16/12	8.2	1.32	16	10.5	293	0.241	22.9	180.0
RHR02	10/5/12	8.5	1.51	21.90	16.5	371	0.319	26	235.0
RHR02	9/15/12	8.7	1.73	19.6	16.4	339	0.308	24.8	220
RHR02	9/15/12	8.8	1.7	19.5	16.5	338	0.31	24.8	218
RHR02	8/18/12	8.5	1.59	22.1	15.7	369		22.8	232
RHR02	7/16/12	8.5	1.22	21.8	15.6	362		21.8	229
RHR02	6/29/12	8.6	1.19	21.4	15.4	351		22	223

Sample ID	Sample Date	pH SU	K$^+$ ppm	SiO$_2$ ppm	Na$^+$ ppm	Conductivity (μS/cm)	Sr^{2+} ppm	SO$_4^{2-}$ ppm	Total Dissolved Solids ppm
RHR02	6/2/12	8.4	1.4	17	13	315		23	208
RHR02	5/13/12	8.6	2.0	16	12	300		23	191
RHR02	5/13/12	8.6	2.5	16	13	305		23	189
RHR02	3/24/12	7.5	1.2	12	9.4	245		18	147
RHR04	3/14/13	8	0.954	8.09	6.12	193	0.158	16.3	114.0
RHR04	11/16/12	8	0.972	10.5	4.7	197	0.165	17.8	118.0
RHR04	10/5/12	8	1.71	17.5	6.74	293	0.261	16.4	178.0
RHR04	10/5/12	8	1.72		6.79	293	0.263	16.4	
RHR04	9/15/12	8	1.98	17.1	6.81	286	0.261	16.1	175
RHR04	8/18/12	8	1.72	16.9	6.9	285		14.9	173
RHR04	7/16/12	7.9	1.24	16.3	6.46	269		15	164
RHR04	6/29/12	8.2	1.06	15.5	6.3	261		15.4	158
RHR04	6/29/12	8	1.06	15.4	6.43	260		15.4	157
RHR04	6/2/12	7.8	1.1	12	5.5	215		15	137
RHR04	5/13/12	8.0	1.9	11	4.9	205		17	124
RHR04	3/24/12	7.1	0.90	8.3	5.7	180		15	105
RHR10	3/16/13	8	0.747	6.23	1.98	167	0.136	19.8	101.0
RHR10	11/17/12	8	0.646	6.00	1.43	162	0.127	22.6	97.0
RHR10	10/6/12	8.2	0.625	5.74	1.4	158	0.123	23.6	94.0
RHR10	9/15/12	8.2	0.596	5.59	1.38	155	0.121	23.1	92
RHR10	8/18/12	8.1	0.541	5.45	1.28	150		22.4	89
RHR10	7/17/12	8.2	0.602	5.33	1.35	145		20.4	86
RHR10	6/28/12	8.4	0.569	5.32	1.29	141		20.8	86
RHR10	5/31/12	7.9	0.54	5.1	1.2	130		22	81
RHR10	5/31/12	7.9	0.53	5.0	1.2	130		22	82
RHR10	5/13/12	7.7	0.59	5.1	1.3	130		22	79
RHR10	5/13/12	8.0	0.58	5.3	1.3	145		22	85
RHR10	3/23/12	7.4	0.80	6.1	2.0	170		19	100
RHR11	3/14/13	8	0.692	6.26	1.42	158	0.078	5.96	92.0
RHR11	11/17/12	7.7	0.667	6.59	1.33	168	0.084	6.38	97.0
RHR11	10/6/12	8.2	0.74	6.94	1.39	170	0.087	5.92	98.0
RHR11	9/15/12	8.1	0.73	6.87	1.39	167	0.088	5.85	96
RHR11	8/18/12	8.1	0.682	6.93	1.32	167		5.63	95
RHR11	7/17/12	8.3	0.718	6.65	1.38	159		5.44	91
RHR11	6/28/12	8.4	0.674	6.51	1.31	157		5.7	85
RHR11	5/31/12	7.9	0.65	6.2	1.2	125		4.6	70
RHR11	5/13/12	8.1	0.66	6.1	1.2	130		4.4	74
RHR11	3/23/12	7.8	0.72	6.5	1.5	155		5.7	87
RHR11	3/23/12	7.6	0.72	6.4	1.5	155		5.7	87
RHR14	3/14/13	7.8	0.817	9.25	2.6	181	0.333	22.8	113.0
RHR14	3/14/13	7.8	0.8		2.57	183	0.328	22.9	
RHR14	11/17/12	8	0.767	9.74	2.4	176	0.319	21.3	111.0

Sample ID	Sample Date	pH SU	K+ ppm	SiO2 ppm	Na+ ppm	Conductivity (µS/cm)	Sr2+ ppm	SO4 2- ppm	Total Dissolved Solids ppm
RHR14	10/6/12	8	0.757	9.69	2.41	176	0.315	20.6	106
RHR14	9/15/12	7.9	0.771	9.66	2.45	173	0.321	20.6	106
RHR14	8/18/12	7.9	0.747	9.38	2.43	172		19.9	103
RHR14	7/18/12	7.9	0.728	9.35	2.36	168		19.4	101
RHR14	6/29/12	8.1	0.744	9.46	2.35	169		19.2	102
RHR14	5/31/12	7.9	0.71	8.6	2.1	140		15	88
RHR14	5/13/12	8.0	0.70	8.0	1.9	135		13	79
RHR14	3/24/12	7.6	0.80	9.4	2.6	175		21	106
RHR14	3/24/12	7.6	0.81	9.5	2.6	175		21	106
RHR15	3/14/13	8.2	0.989	6.40	8.14	199		12.8	114.0
RHR15	11/17/12	8	0.734	6.89	3.67	172	0.155	14.7	100.0
RHR15	10/6/12	8.1	0.751	6.29	2.97	171	0.152	16.3	100
RHR15	9/15/12	7.9	0.73	6.01	3.05	167	0.145	16	99
RHR15	8/18/12	8.1	0.725	6.05	2.95	163	0.144	15.8	95
RHR15	7/18/12	8.2	0.712	6.22	2.78	156		13.9	93
RHR15	6/29/12	8.3	0.657	6.15	2.4	155		14.4	91
RHR15	6/1/12	8.0	0.62	5.5	1.9	135		15	83
RHR15	5/13/12	8.1	0.67	6.1	2.3	140		14	83
RHR15	3/24/12	7.4	0.87	7.1	5.9	170		11	97
RHR16	3/14/13	7.9	0.795	10.50	2.39	107	0.078	16	70.0
RHR16	11/17/12	8.1	0.834	9.63	2.23	120	0.088	21.2	78.0
RHR16	10/6/12	8.1	0.938	9.68	2.2	122	0.089	20.1	77
RHR16	9/15/12	7.8	0.889	9.26	2.05	116	0.086	18.8	74
RHR16	8/18/12	8	0.873	12.1	2.06	115		18	75
RHR16	7/18/12	8	0.894	9.5	2.12	111		17.8	70
RHR16	6/29/12	8.5	0.867	9.27	2.06	109		17.2	71
RHR16	6/1/12	7.9	0.80	7.9	1.6	81		13	54
RHR16	6/1/12	7.7	0.76	7.9	1.5	79		13	53
RHR16	5/13/12	7.8	0.77	8.7	1.8	80		12	NA
RHR16	5/13/12	7.9	0.77	8.6	1.8	80		12	52
RHR16	3/24/12	7.2	0.80	10	2.4	110		16	68
RHR18	11/16/12	8	0.472	4.92	1.08	152	0.109	32.5	93.0
RHR18	10/6/12	7.9	0.437	4.93	1.05	146	0.109	31	90
RHR18	9/14/12	7.9	0.463	4.88	1.05	144	0.108	29.7	87
RHR18	8/17/12	7.8	0.445	4.96	1.05	140		26.2	84
RHR18	7/17/12	7.6	0.444	4.76	1.03	132		25.1	78
RHR18	6/28/12	8.2	0.416	4.73	0.99	131		24.2	79
RHR18	5/31/12	6.7	0.43	4.6	1.0	125		25	76
RHR18	5/13/12	7.8	0.49	4.8	1.1	140		28	83
RHR18	3/23/12	7.3	0.67	5.4	1.4	160		31	93
RHR20	7/18/12	7.6	0.915	25.4	3.35	56		2.95	56
RHR20	6/29/12	7.9	3.41	21.9	5.66	81		2.71	65

Sample ID	Sample Date	pH SU	K$^+$ ppm	SiO$_2$ ppm	Na$^+$ ppm	Conductivity (μS/cm)	Sr^{2+} ppm	SO$_4^{2-}$ ppm	Total Dissolved Solids ppm
RHR20	6/1/12	7.1	0.51	19	2.3	37		2.8	40
RHR20	5/12/12	7.4	0.41	17	2.0	28		2.7	32
RHR20	3/25/13	6.4	0.88	15	2.6	39		3.4	35
RHR21	3/15/13	8	0.912	7.29	6.18	177	0.145	15.4	104.0
RHR21	11/17/12	8	0.797	8.14	3.5	161	0.14	16.9	97.0
RHR21	10/6/12	7.8	0.847	8.98	3.71	173	0.145	17.6	103
RHR21	9/15/12	7.8	0.809	7.96	3.59	167	0.142	17.1	100
RHR21	8/18/12	7.7	0.775	7.81	3.35	162		16.3	96
RHR21	7/18/12	7.7	0.813	7.97	3.29	157		15.1	92
RHR21	6/29/12	7.6	0.725	8.28	3.06	155		15.4	92
RHR21	6/2/12	7.2	0.68	6.8	2.5	125		14	80
RHR21	5/13/12	7.8	0.69	7.3	2.6	125		13	76
RHR22	10/5/12	8.0	0.43	4.7	1.1	149	0.091	34	90
RHR22	9/14/12	8	0.389	4.44	1.28	135	0.084	28.9	81
RHR22	8/17/12	7.9	0.386	4.4	1.01	137		29.4	80
RHR22	7/18/12	7.6	0.664	4.14	1.41	136		28.7	79
RHR22	6/28/12	7.8	0.399	3.89	1.02	124		27.9	74
RHR22	6/1/12	7.2	0.37	3.8	0.82	81		17	51
RHR22	6/1/12	7.3	0.37	3.7	0.82	81		17	51
RHR22	5/14/12	7.8	0.43	4.3	0.89	100		20	60
RHR23	6/1/12	7.5	0.52	5.2	1.2	135		18	75
RHR23	5/15/12	7.9	0.57	5.4	1.3	145		18	81
RHR24	11/17/12	8.0	0.73	6.1	3.3	173	0.117	19	102
RHR24	10/5/12	8.0	0.74	5.9	2.3	168	0.117	20	99
RHR24	9/14/12	8	0.709	5.78	2.38	163	0.116	19.4	96
RHR24	8/18/12	7.9	0.647	5.73	2.27	159		19.3	93
RHR24	7/17/12	8	0.731	5.75	2.33	156		16.7	91
RHR24	6/28/12	8.4	0.654	5.54	1.94	149		17.4	89
RHR24	6/1/12	7.7	0.56	5.2	1.6	130		18	80
RHR24	5/15/12	7.9	0.58	5.4	1.6	145		18	83
RHRO01	3/23/12	7.0	1.6	3.6	3.1	135		5.5	78
RHRO02	8/17/12	7.5	0.443	5.06	1.07	138		25.8	81
RHRO02	7/17/12	7.4	0.439	4.93	1.04	130		24	78
RHRO02	6/28/12	7.6	0.495	4.83	1.08	126		22.9	75
RHRO02	6/1/12	7.4	0.49	5.1	1.2	125		23	77
RHRO02	5/14/12	7.4	0.46	5.0	1.1	140		26	83
RHRO03	6/28/12	7.7	0.445	4.8	1.09	130		23.1	76
RHRO03	6/1/12	7.7	0.45	5.2	1.1	130		22	83
RHRO03	6/1/12	7.6	0.45	5.1	1.1	130		22	77
RHRO03	5/14/12	7.6	0.49	5.0	1.2	145	0.098	26	85
RHRO04	9/14/12	7.8	0.439	5	1.08	143		28.5	85
RHRO04	7/17/12	7.7	0.434	5.26	1.04	131		23.8	78

Sample ID	Sample Date	pH SU	K$^+$ ppm	SiO$_2$ ppm	Na$^+$ ppm	Conductivity (μS/cm)	Sr^{2+} ppm	SO$_4^{2-}$ ppm	Total Dissolved Solids ppm
RHRO04	6/28/12	7.7	0.428	4.82	1.07	127		22.9	76
RHRO04	6/1/12	7.6	0.43	5.1	1.1	125		22	79
RHRO04	5/14/12	7.7	0.5	4.9	1.2	145		26.9	86
RHRO05	10/6/12	8.0	0.5	6.0	1.2	172	0.123	22.2	102
RHRO05	10/6/12	8.0	0.50		1.22	173	0.1	22.2	
RHRO05	9/15/12	7.9	0.507	5.99	1.24	169	0.122	22.1	101
RHRO05	8/17/12	8	0.521	5.88	1.23	167		21.3	99
RHRO05	7/17/12	8.1	0.527	5.67	1.2	162		20.2	95
RHRO05	7/17/12	8.1	0.54	5.65	1.21	161		20.1	95
RHRO05	6/28/12	8.3	0.5	5.26	1.2	153		18.4	90
RHRO05	6/1/12	7.8	0.50	5.1	1.0	115		14	73
RHRO05	5/14/12	8.0	0.49	5.4	1.1	140		16	NA
RHRO05	5/14/12	8.0	0.50	5.4	1.1	140		16	80
RHRO06	6/1/12	7.6	0.63	5.8	1.5	140		20	86
RHRO06	5/15/12	7.7	0.62	5.6	1.4	145		21	84
RHRO07	3/15/13	7.6	0.46	6.9	2.1	103	0.065	4	63
RHS01	3/15/13	7.2	0.80	8.0	4.6	186	0.148	20	110
RHS01	11/17/12	7.4	0.90	9.2	4.2	187	0.157	20	112
RHS01	10/6/12	7.6	0.88	9.5	4.3	190	0.158	19	112
RHS01	9/15/12	7.4	0.886	9.26	4.37	186	0.159	18.5	111
RHS01	8/18/12	7.2	0.842	9.2	4.25	185		17.3	110
RHS01	7/18/12	7.1	0.832	9.07	4.4	180		17.3	108
RHS01	6/29/12	7.4	0.83	8.88	4.5	178		16.7	105
RHS01	6/2/12	7.2	0.83	8.5	4.4	165		15	101
RHS01	6/2/12	7.0	0.76	8.5	4.3	165		15	103
RHS01	5/13/12	7.2	0.80	8.1	4.6	185		15	105
RHS01	3/24/12	7.2	0.85	8.1	5.1	190		18	108
RHS01	3/24/12	7.2	0.85	8.3	5.0	190		18	107
RHS03	7/18/12	7.7	1.19	30.9	3.63	74		3.33	73
RHS03	6/29/12	8	1.15	28	3.57	72		3.7	68
RHS03	6/1/12	7.3	1.0	24	3.2	51		3.1	54
RHS03	5/12/12	7.5	0.71	23	2.6	47		3.2	49
RHS03	3/25/12	6.5	0.60	8.5	1.2	20		-1	18
RHS04	3/16/13	7.4	0.509	4.89	1.2	157	0.109	32.3	96.0
RHS04	11/16/12	7.7	0.479	4.91	1.12	153	0.104	33.1	94.0
RHS04	10/6/12	7.8	0.454	4.85	1.08	149	0.102	32	89
RHS04	9/14/12	7.8	0.456	4.91	1.07	149	0.102	30.7	90
RHS04	8/17/12	7.5	0.42	4.71	1.01	135		27.9	81.0
RHS04	7/17/12	7.5	0.431	4.66	0.981	130		26.1	78
RHS04	6/28/12	7.7	0.44	4.53	1.01	132		24.8	78
RHS04	5/31/12	7.3	0.43	4.8	1.1	120		25	78
RHS04	5/13/12	7.4	0.45	4.6	1.1	145		30	84

Sample ID	Sample Date	pH SU	K$^+$ ppm	SiO$_2$ ppm	Na$^+$ ppm	Conductivity (μS/cm)	Sr^{2+} ppm	SO$_4^{2-}$ ppm	Total Dissolved Solids ppm
RHS04	3/23/12	7.2	0.48	5.1	1.3	155	0.327	28	89
RHS05	3/14/13	7.5	0.786	9.27	2.64	183	0.321	23.1	113.0
RHS05	10/6/12	7.6	0.662	9.97	2.47	178	0.313	21	109
RHS05	9/15/12	7.7	0.663	9.66	2.43	171		20.6	105
RHS05	8/18/12	7.5	0.624	9.64	2.33	172		20.1	104.0
RHS05	7/18/12	7.3	0.65	9.7	2.37	168		19.7	103
RHS05	6/29/12	7.6	0.679	9.11	2.6	170		19	105
RHS05	5/31/12	7.2	0.66	9.1	2.4	155		18	97
RHS05	5/13/12	7.5	0.70	8.9	2.3	160		18	96
RHS05	3/24/12	7.4	0.80	9.6	2.6	180		22	108
RHS06	11/16/12	7.9	0.768	7.21	1.66	138	0.118	14.9	84.0
RHS06	10/6/12	8	0.763	7.26	1.68	139	0.122	14.3	84
RHS06	9/15/12	8	0.766	7.23	1.68	138	0.12	14.1	82
RHS06	8/17/12	7.9	0.711	7.17	1.58	137		14.4	82.0
RHS06	7/17/12	7.9	0.779	7.1	1.63	140		15.9	84
RHS06	6/28/12	8.2	0.836	6.76	1.73	144		16.3	88
RHS06	6/1/12	7.8	0.81	6.9	1.8	130		14	81
RHS06	5/15/12	8.0	0.94	6.7	1.9	135		13	79
RHS07	10/6/12	7.9	0.60	6.0	1.4	156	0.117	25	93
RHS07	9/15/12	7.9	0.602	5.83	1.46	155	0.116	24.3	93
RHS07	8/17/12	7.8	0.65	6.1	1.5	156		25	92
RHS07	7/17/12	7.6	0.681	5.94	1.53	155		23.9	92
RHS08	11/16/12	8	0.627	5.93	1.45	155	0.117	24.8	94
RHS08	10/6/12	7.9	0.615	6.07	1.47	156	0.116	24.6	94
RHS08	9/15/12	8	0.608	5.96	1.46	156	0.116	24.3	92
RHS08	8/17/12	7.9	0.6	10.3	1.47	155		24.4	96
RHS08	7/17/12	7.9	0.626	6.06	1.43	152		23.9	92
RHS09	11/16/12	7.9	0.462	5.04	1.04	137	0.07	10.1	82
RHS09	10/5/12	7.8	0.555	5.15	1.12	136	0.069	8.73	79
RHS09	9/14/12	7.8	0.515	4.99	1.09	132	0.068	8.18	77
RHS09	8/17/12	7.7	0.443	5.07	1.04	131		7.93	75
RHS10	6/28/13	7.3	0.798	5.95	0.936	72	0.027	3.04	44
RHS10	6/28/13	7.3	0.78		0.921	72	0.027	3.03	
RHSNO01	3/23/12	6.7	1.5	0.46	3.3	34		-1	17
RHSNO01	3/23/12	6.7	1.5	0.47	3.2	35		-1	18
RHSNO02	5/14/12	6.8	-0.05	0.53	-0.05	4.0		-1.0	2.0
RHSNO03	5/14/12	6.4	0.21	0.26	0.06	5.0		-1.0	2.6
RHSNO04	5/14/12	6.5	0.053	0.64	-0.05	4.0		-1.0	3.0
RHSNO05	5/15/12	6.3	-0.05	0.31	-0.05	4.0		-1.0	NA
RHSNO05	5/15/12	6.4	0.052	0.31	-0.05	3.0		-1.0	1.8
RHW02	3/14/13	7.5	1.31	16.7	5.25	257	0.226	23.8	161.0
RHW02	10/6/12	7.7	1.34	17.3	5.81	272	0.233	25.7	167

Sample ID	Sample Date	pH SU	K$^+$ ppm	SiO$_2$ ppm	Na$^+$ ppm	Conductivity (μS/cm)	Sr^{2+} ppm	SO$_4^{2-}$ ppm	Total Dissolved Solids ppm
RHW02	9/15/12	7.9	1.28	17.1	5.44	259	0.226	23.6	160
RHW02	8/18/12	7.8	1.26	17	5.37	258		23.7	158
RHW02	7/18/12	7.7	1.18	16.7	4.88	240		21.2	148
RHW02	6/28/12	7.6	1.19	17	4.97	247		20.4	154
RHW02	6/2/12	7.4	1.3	18	5.4	240		23	163
RHW02	6/2/12	7.4	1.3	17	5.3	240		23	163
RHW02	5/14/12	7.6	1.3	17	5.1	270		21	165
RHW02	3/24/12	7.3	2.2	18	7.9	295		27	180
RHW05	3/14/13	7.8	1.44	23.4	20.7	509	2.16	167	351.0
RHW05	10/5/12	7.8	1.44	24.5	20.9	516	2.2	166	348.0
RHW05	9/14/12	7.9	1.48	24	20.4	515	2.2	167	350
RHW05	8/17/12	7.9	1.42	24.9	21.1	509		166	347.0
RHW05	7/17/12	7.8	1.39	24.5	21.2	501		156	349
RHW05	6/29/12	8	1.44	24.1	20.8	508		161	343
RHW05	6/1/12	7.8	1.5	24	20	490		165	350
RHW05	5/15/12	8.0	1.5	24	21	505		160	336
RHW05	3/25/12	7.5	1.8	25	23	515		150	336
RHW06	3/14/13	7.7	0.844	7.76	7.41	249	0.25	12.2	142.0
RHW06	10/6/12	7.8	0.802	7.87	7.24	240	0.24	12.4	134
RHW06	10/6/12	7.8	0.81		7.31	240	0.242	12.4	
RHW06	9/15/12	7.8	0.842	8.23	7.5	240	0.244	12.3	136
RHW06	8/18/12	7.9	0.807	7.95	7.52	242		12.4	135.0
RHW06	7/17/12	7.7	0.82	7.88	7.8	247		12.4	138
RHW06	6/28/12	7.9	0.861	7.74	8.32	255		12.4	146
RHW06	5/31/12	7.6	0.97	7.8	8.9	250		13	148
RHW06	5/15/12	7.6	0.96	8.0	8.9	255		13	149
RHW06	5/13/12	7.7	0.90	7.7	8.5	265		13	148
RHW06	3/24/12	7.5	1.1	7.9	8.1	255		11	142
RHW10	3/15/13	7.8	0.995	20.6	25	247	2.07	229	513.0
RHW10	10/6/12	7.7	0.898	22.8	26.5	747	2.7	245	508
RHW10	9/15/12	7.9	0.897	22.5	26.5	725	2.72	244	502
RHW10	8/18/12	7.8	0.831	23.9	26.4	725		251	505.0
RHW10	7/18/12	7.6	0.956	21.6	25.5	736		232	501
RHW10	6/29/12	7.8	0.849	22.9	26.8	726		241	496
RHW10	6/2/12	7.7	0.85	23	27	700		240	498
RHW10	5/13/12	7.9	1.0	21	26	745		230	497
RHW10	3/24/12	7.8	1.1	21	26	760		210	496
RHW11	10/5/12	7.9	0.691	21.7	9.140	176	0.13	2.46	114
RHW11	9/14/12	7.8	0.697	21.4	9.18	172	0.131	2.91	114
RHW11	8/17/12	7.8	0.738	21.6	9.030	174		3.5100	113.0
RHW11	7/17/12	7.6	0.684	21.7	8.94	171		2.52	113
RHW11	6/29/12	7.9	0.707	21	8.91	179		3.08	117

Sample ID	Sample Date	pH SU	K$^+$ ppm	SiO$_2$ ppm	Na$^+$ ppm	Conductivity (μS/cm)	Sr^{2+} ppm	SO$_4^{2-}$ ppm	Total Dissolved Solids ppm
RHW11	5/15/12	7.8	0.74	21	9.1	170		2.4	111
RHW11	5/15/12	7.8	0.74	21	8.9	170		2.5	111
RHW11	3/25/12	7.5	1.0	22	9.9	175		2.2	114
RHW12	3/16/13	7.9	0.663	8.04	3.110	204	0.50	8.58	120.0
RHW12	9/14/12	7.9	0.676	8.06	3.06	206	0.506	8.12	120
RHW12	8/17/12	7.9	0.661	8.07	2.98	205		8.19	120
RHW12	7/17/12	7.9	0.656	8.06	3.01	204		8.1	119
RHW12	6/28/12	8	0.667	7.78	3.02	209		8.46	120
RHW12	6/28/12	8.1	0.652	7.88	3	208		8.48	120
RHW12	5/31/12	7.9	0.65	6.9	3.0	195		8.6	119
RHW13	3/14/13	7.9	2.68		80.2	710	0.322	147.0	477
RHW13	3/14/13	7.8	2.66	25.4	80.0	704	0.321	146.0	475
RHW13	9/15/12	7.8	2.63	26	78.4	711	0.325	148	480
RHW13	8/18/12	7.7	2.71	25.8	80.3	714		148	485
RHW13	7/16/12	7.7	2.64	26.3	78.5	708		141	473
RHW13	6/28/12	7.8	2.69	25.6	79.7	711		145	474
RHW13	6/28/12	7.8	2.74	25.9	80.8	712		144	476
RHW13	6/2/12	7.8	2.7	26	80	680		145	
WL01	10/5/12	8	0.429	3.74	1.470	220	0.203	59.4	134
WL01	9/14/12	8.1	0.503	3.65	1.43	169	0.149	40.3	99
WL01	8/17/12	8.3	0.351	3.38	1.32	188		47.6	113
WL01	7/18/12	7.9	0.383	3.37	1.24	171		39.8	101
WL01	6/28/12	8.1	0.384	2.96	1.25	155		36.2	90
WL01	6/1/12	7.6	0.40	3.4	0.9	98		22	61
WL01	5/14/12	7.6	0.25	2.9	0.63	79		16	45
WL02	10/5/12	8.0	0.76	6.4	1.43	208	0.1	74	130
WL02	9/14/12	7.8	0.736	5.96	1.3	152	0.078	48.3	95
WL02	8/17/12	7.6	0.71	5.8	1.28	166		57	103
WL02	7/18/12	7.5	0.717	5.85	1.25	167		57.5	105
WL02	6/28/12	7.7	0.747	5.46	1.26	158		53	97

APPENDIX C

SUMMARY OF GEOCHEMICAL ANALYTES AND ANALYTICAL METHODS

Parameter	Units	Method	Test	Upper Limit	Lower Limit
Alkalinity as $CaCO_3$	mg/L	EPA 310.1	Alkalinity		5
Anions total	meq/L	SM 1030E	Checking correctness w OES Si		
Bicarbonate (HCO_3)	mg/L	EPA 310.1	Alkalinity		5
Bromide	mg/L	EPA 300.0	Anions by IC	10	0.1
Calcium	mg/L	EPA 200.7	Cations by ICPOES	100	0.05
Carbonate (CO_3)	mg/L	EPA 310.1	Alkalinity		5
Cations total	meq/L	SM 1030E	Checking correctness w OES Si		
Chloride	mg/L	EPA 300.0	Anions by IC	100	1
Fluoride	mg/L	EPA 300.0	Anions by IC	10	0.1
Hardness	mg $CaCO_3$/ L	SM 2340B	Hardness by calculation		
Iron	mg/L	EPA 200.7	Cations by ICPOES	100	0.02
Magnesium	mg/L	EPA 200.7	Cations by ICPOES	100	0.05
Nitrate	mg/L	EPA 300.0	Anions by IC	10	0.1
Nitrite	mg/L	EPA 300.0	Anions by IC	10	0.1
Ortho Phosphate	mg/L	EPA 300.0	Anions by IC	50	0.5
Percent difference	%	SM 1030E	Checking correctness w OES Si		
pH	ph Units	EPA 150.1	pH		
Potassium	mg/L	EPA 200.7	Cations by ICPOES	100	0.05
SiO2	mg/L	SM 1030E	Checking correctness w OES Si		0.05
Sodium	mg/L	EPA 200.7	Cations by ICPOES	200	0.05
Specific Conductance	µS/cm	EPA 120.1	Specific Conductance		
Strontium	mg/L	EPA 200.7	Cations by ICPOES	5	0.0005
Sulfate	mg/L	EPA 300.0	Anions by IC	100	1
TDS calc	mg/L	SM 1030E	Checking correctness w OES Si		

APPENDIX D

STABLE ISOTOPIC RESULTS

Sample ID	Sample Date	$\delta^{18}O$ (‰)	δ^2H (‰)
Ditch	9/14/12	-13.11	-91.09
EFF	3/15/13	-15.41	-86.24
EFF	10/5/12	-14.07	-90.91
EFF	9/14/12	-13.02	-91.41
EFF	8/17/12	-14.88	-91.07
EFF	7/17/12	-14.56	-93.64
EFF	6/28/12	-14.87	-92.79
EFF	6/1/12	-13.85	-95.16
EFF	5/15/12	-13.79	-92.16
EFF	5/15/12	-13.79	-92.16
ISO1	3/16/13	-19.13	-112.63
ISO1	12/18/12	-15.48	-95.05
ISO1	10/5/12	-9.26	-47.01
ISO1	7/17/12	-9.81	-47.51
ISO1	5/31/12	-12.45	-84.40
ISO1	3/23/12	-13.73	-87.20
ISO1	1/8/12	-16.31	-106.20
ISO2	3/16/13	-19.29	-114.51
ISO2	12/18/12	-13.91	-81.82
ISO2	10/5/12	-9.60	-51.46
ISO2	7/17/12	-8.99	-43.34
ISO2	5/31/12	-12.86	-86.52
ISO2	1/9/12	-15.76	-102.66
ISO3	3/15/13	-19.05	-113.68
ISO3	12/18/12	-15.86	-96.62
ISO3	10/6/12	-8.35	-42.81
ISO3	7/17/12	-7.50	-37.32
ISO3	6/1/12	-12.97	-89.07
ISO3	3/24/12	-14.13	-91.58
ISO4	3/15/13	-19.44	-114.14
ISO4	12/18/12	-16.41	-100.42
ISO4	10/6/12	-7.88	-40.31
ISO4	7/17/12	-7.52	-36.53
ISO4	6/1/12	-11.07	-74.39
ISO4	6/1/12	-11.07	-74.39
ISO4	3/24/12	-13.19	-81.29
ISO4	1/9/12	-16.24	-105.41
ISO5	3/15/13	-19.35	-114.49
ISO5	12/19/12	-15.08	-93.68
ISO5	10/6/12	-7.06	-37.32
ISO5	7/17/12	-6.23	-31.04

Sample ID	Sample Date	$\delta^{18}O$ (‰)	δ^2H (‰)
ISO5	6/2/12	-11.83	-81.42
ISO5	3/24/12	-13.97	-92.19
ISO5	3/24/12	-13.97	-92.19
ISO5	1/9/12	-13.52	-83.88
ISO6	3/14/13	-18.23	-107.59
ISO6	12/19/12	-16.72	-104.82
ISO6	10/5/12	-6.92	-34.41
ISO6	7/16/12	-7.15	-32.08
ISO6	6/2/12	-10.60	-72.97
ISO6	3/24/12	-14.13	-90.34
ISO6	1/9/12	-13.10	-83.75
PCAPS-1 (15cm)	6/29/13	-19.15	-123.24
PCAPS-1 (18cm)	6/29/13	-18.81	-122.46
PCAPS-1 Upper	10/20/12	-15.40	-125.68
PCAPS-1 Lower	10/20/12	-12.42	-85.19
PCAPS-2 (25-42cm)	6/29/13	-18.93	-124.58
PCAPS-2 Upper	10/20/12	-9.34	-76.78
PCAPS-2 Lower	10/20/12	-10.41	-77.83
RHA01	7/18/12	-14.50	-93.98
RHA01	6/29/12	-15.05	-92.44
RHA01	6/2/12	-14.01	-95.59
RHA01	6/2/12	-14.01	-95.59
RHA01	5/13/12	-13.89	-93.86
RHR01	3/14/13	-15.58	-93.43
RHR01	11/17/12	-14.58	-92.10
RHR01	11/17/12	-14.15	-92.50
RHR01	10/6/12	-14.35	-92.62
RHR01	9/15/12	-13.28	-91.88
RHR01	8/18/12	-14.52	-91.84
RHR01	7/18/12	-14.27	-94.36
RHR01	6/29/12	-14.69	-92.30
RHR01	6/29/12	-14.55	-93.33
RHR01	6/1/12	-13.82	-95.72
RHR01	5/13/12	-13.94	-93.69
RHR01	3/24/12	-13.86	-93.48
RHR02	3/14/13	-14.98	-93.32
RHR02	11/16/12	-14.76	-91.59
RHR02	10/5/12	-14.05	-93.40
RHR02	9/15/12	-13.05	-92.78
RHR02	9/15/12	-12.93	-92.95
RHR02	8/18/12	-14.29	-91.04

Sample ID	Sample Date	$\delta^{18}O$ (‰)	δ^2H (‰)
RHR02	7/16/12	-13.80	-93.25
RHR02	6/29/12	-14.42	-92.25
RHR02	6/2/12	-13.42	-94.77
RHR02	5/13/12	-13.70	-93.17
RHR02	5/13/12	-13.62	-93.17
RHR02	3/24/12	-13.87	-94.06
RHR04	3/14/13	-15.69	-92.70
RHR04	11/16/12	-14.24	-92.20
RHR04	10/5/12	-14.08	-92.13
RHR04	10/5/12	-14.08	-92.13
RHR04	9/15/12	-12.83	-91.99
RHR04	8/18/12	-14.36	-89.89
RHR04	7/16/12	-14.20	-92.10
RHR04	6/29/12	-14.28	-91.51
RHR04	6/29/12	-13.99	-92.53
RHR04	6/2/12	-13.55	-94.16
RHR04	5/13/12	-13.66	-92.87
RHR04	3/24/12	-13.82	-93.55
RHR10	3/16/13	-16.03	-90.24
RHR10	11/17/12	-14.69	-90.52
RHR10	10/6/12	-14.23	-91.62
RHR10	9/15/12	-13.39	-91.60
RHR10	8/18/12	-14.33	-93.17
RHR10	7/17/12	-14.62	-94.08
RHR10	6/28/12	-14.76	-92.40
RHR10	5/31/12	-13.76	-95.00
RHR10	5/31/12	-13.76	-95.00
RHR10	5/31/12	-13.76	-95.00
RHR10	5/13/12	-14.00	-93.85
RHR10	3/23/12	-14.10	-93.68
RHR11	3/14/13	-16.59	-97.01
RHR11	11/17/12	-15.51	-97.22
RHR11	10/6/12	-15.01	-98.09
RHR11	9/15/12	-14.01	-96.91
RHR11	8/18/12	-14.46	-97.04
RHR11	7/17/12	-15.21	-98.61
RHR11	6/28/12	-15.28	-97.69
RHR11	5/31/12	-14.28	-99.37
RHR11	5/13/12	-14.38	-98.78
RHR11	3/23/12	-14.54	-97.93
RHR11	3/23/12	-14.44	-97.53

Sample ID	Sample Date	$\delta^{18}O$ (‰)	δ^2H (‰)
RHR14	3/14/13	-16.03	-91.98
RHR14	3/14/13	-16.03	-91.98
RHR14	11/17/12	-14.70	-92.99
RHR14	10/6/12	-14.55	-94.52
RHR14	9/15/12	-13.54	-94.24
RHR14	8/18/12	-14.42	-94.51
RHR14	7/18/12	-14.54	-95.24
RHR14	6/29/12	-15.25	-92.96
RHR14	5/31/12	-13.76	-95.75
RHR14	5/13/12	-13.87	-93.82
RHR14	3/24/12	-13.99	-93.29
RHR15	3/14/13	-16.20	-93.42
RHR15	11/17/12	-14.73	-93.81
RHR15	10/6/12	-14.22	-94.18
RHR15	9/15/12	-13.37	-93.60
RHR15	8/18/12	-14.41	-94.12
RHR15	7/18/12	-14.49	-95.15
RHR15	6/29/12	-14.85	-94.52
RHR15	6/1/12	-13.89	-96.38
RHR15	5/13/12	-14.11	-94.96
RHR15	3/24/12	-13.98	-93.84
RHR16	3/14/13	-15.79	-90.48
RHR16	11/17/12	-14.47	-90.34
RHR16	10/6/12	-13.68	-90.51
RHR16	9/15/12	-12.97	-88.47
RHR16	8/18/12	-14.28	-86.74
RHR16	7/18/12	-14.35	-91.81
RHR16	6/29/12	-14.78	-90.45
RHR16	6/1/12	-13.86	-94.26
RHR16	6/1/12	-13.82	-94.21
RHR16	5/13/12	-13.65	-92.00
RHR16	5/13/12	-13.65	-92.00
RHR16	3/24/12	-13.69	-90.40
RHR18	11/16/12	-13.61	-87.84
RHR18	10/6/12	-14.13	-89.38
RHR18	9/14/12	-13.21	-89.77
RHR18	8/17/12	-15.01	-91.54
RHR18	7/17/12	-14.65	-94.36
RHR18	6/28/12	-14.36	-94.06
RHR18	5/31/12	-14.11	-95.89
RHR18	5/13/12	-14.12	-93.89

Sample ID	Sample Date	$\delta^{18}O$ (‰)	δ^2H (‰)
RHR18	3/23/12	-13.84	-92.00
RHR20	7/18/12	-10.73	-71.67
RHR20	6/29/12	-8.53	-63.23
RHR20	6/1/12	-11.78	-84.74
RHR20	3/25/12	-11.77	-79.87
RHR21	3/15/13	-15.95	-92.80
RHR21	11/17/12	-14.49	-92.41
RHR21	10/6/12	-14.26	-92.44
RHR21	9/15/12	-13.35	-91.80
RHR21	8/18/12	-14.35	-92.48
RHR21	7/18/12	-14.60	-93.71
RHR21	6/29/12	-14.87	-91.60
RHR21	6/2/12	-13.91	-95.69
RHR21	5/13/12	-13.88	-93.36
RHR22	10/5/12	-13.75	-85.87
RHR22	9/14/12	-12.05	-81.77
RHR22	8/17/12	-13.49	-86.10
RHR22	7/18/12	-14.41	-89.89
RHR22	6/28/12	-14.78	-91.00
RHR22	6/1/12	-14.08	-95.76
RHR22	6/1/12	-14.08	-95.76
RHR22	5/14/12	-14.46	-95.65
RHR23	6/1/12	-13.93	-96.49
RHR23	5/15/12	-13.77	-93.24
RHR24	11/17/12	-14.83	-91.52
RHR24	10/5/12	-14.21	-93.12
RHR24	9/14/12	-13.20	-92.95
RHR24	8/18/12	-15.00	-92.54
RHR24	7/17/12	-14.83	-94.71
RHR24	6/28/12	-15.15	-92.93
RHR24	6/1/12	-13.97	-96.41
RHR24	5/15/12	-13.99	-95.37
RHRO01	3/23/12	-13.94	-95.39
RHRO02	8/17/12	-15.01	-92.01
RHRO02	7/17/12	-14.80	-94.45
RHRO02	6/28/12	-14.82	-93.76
RHRO02	6/1/12	-13.93	-96.16
RHRO02	5/14/12	-14.27	-93.86
RHRO03	6/28/12	-14.39	-94.51
RHRO03	6/1/12	-13.97	-96.16
RHRO03	6/1/12	-13.97	-96.16

Sample ID	Sample Date	$\delta^{18}O$ (‰)	δ^2H (‰)
RHRO03	5/14/12	-13.67	-92.76
RHRO04	9/14/12	-13.30	-90.55
RHRO04	7/17/12	-14.76	-94.51
RHRO04	6/28/12	-14.42	-94.40
RHRO04	6/1/12	-13.97	-96.39
RHRO04	5/14/12	-14.16	-94.29
RHRO05	10/6/12	-14.40	-93.50
RHRO05	10/6/12	-14.40	-93.50
RHRO05	9/15/12	-13.32	-92.11
RHRO05	8/17/12	-14.98	-90.98
RHRO05	7/17/12	-14.65	-94.08
RHRO05	7/17/12	-14.57	-92.82
RHRO05	6/28/12	-14.55	-93.63
RHRO05	6/1/12	-13.97	-95.42
RHRO05	5/14/12	-14.07	-95.10
RHRO05	5/14/12	-14.07	-95.10
RHRO06	6/1/12	-13.34	-91.12
RHRO06	5/15/12	-13.70	-89.97
RHRO07	3/15/13	-17.04	-100.02
RHS01	3/15/13	-15.72	-91.95
RHS01	11/17/12	-14.83	-91.05
RHS01	10/6/12	-14.34	-92.91
RHS01	9/15/12	-13.38	-92.33
RHS01	8/18/12	-14.35	-93.27
RHS01	7/18/12	-14.74	-94.15
RHS01	6/29/12	-15.02	-92.69
RHS01	6/2/12	-13.72	-94.94
RHS01	6/2/12	-13.72	-94.94
RHS01	5/13/12	-13.95	-93.60
RHS01	3/24/12	-14.12	-94.26
RHS01	3/24/12	-13.91	-94.19
RHS03	7/18/12	-10.48	-72.35
RHS03	6/29/12	-10.15	-73.01
RHS03	6/1/12	-11.42	-82.71
RHS03	5/12/12	-12.31	-83.90
RHS03	3/25/12	-10.52	-72.62
RHS04	3/16/13	-15.40	-85.36
RHS04	11/16/12	-14.36	-86.81
RHS04	10/6/12	-13.47	-88.77
RHS04	9/14/12	-13.13	-90.37
RHS04	8/17/12	-15.15	-91.58

Sample ID	Sample Date	$\delta^{18}O$ (‰)	δ^2H (‰)
RHS04	7/17/12	-14.65	-94.15
RHS04	6/28/12	-14.19	-94.82
RHS04	5/31/12	-14.08	-96.13
RHS04	5/13/12	-13.64	-93.08
RHS04	3/23/12	-13.78	-91.52
RHS05	3/14/13	-15.97	-91.75
RHS05	10/6/12	-14.54	-94.52
RHS05	9/15/12	-13.29	-94.86
RHS05	8/18/12	-14.85	-94.02
RHS05	7/18/12	-14.12	-94.89
RHS05	6/29/12	-14.74	-94.40
RHS05	5/31/12	-13.88	-95.78
RHS05	5/13/12	-14.09	-94.82
RHS05	3/24/12	-14.16	-95.00
RHS06	11/16/12	-14.57	-92.99
RHS06	10/6/12	-14.73	-93.49
RHS06	9/15/12	-13.37	-92.53
RHS06	8/17/12	-15.02	-92.34
RHS06	7/17/12	-14.43	-93.34
RHS06	6/1/12	-13.73	-95.11
RHS06	5/15/12	-14.14	-94.67
RHS07	10/6/12	-14.09	-88.40
RHS07	9/15/12	-12.69	-87.84
RHS07	8/17/12	-14.59	-87.18
RHS07	7/17/12	-14.08	-88.85
RHS08	11/16/12	-14.19	-87.56
RHS08	10/6/12	-14.08	-88.58
RHS08	9/15/12	-13.00	-87.78
RHS08	8/17/12	-14.53	-87.29
RHS08	7/17/12	-14.14	-89.15
RHS09	11/16/12	-14.74	-88.74
RHS09	10/5/12	-14.41	-92.70
RHS09	9/14/12	-13.53	-92.70
RHS09	8/17/12	-14.30	-93.33
RHS10	6/28/13	-15.52	-97.92
RHS10	6/28/13	-15.52	-97.92
RHSNO01	3/23/12	-15.75	-106.47
RHSNO02	5/14/12	-14.71	-100.14
RHSNO03	5/14/12	-13.26	-88.88
RHSNO04	5/14/12	-13.19	-87.93
RHSNO05	5/15/12	-13.15	-88.23

Sample ID	Sample Date	$\delta^{18}O$ (‰)	δ^2H (‰)
RHSNO05	5/15/12	-13.15	-88.23
RHW02	3/14/13	-15.45	-94.06
RHW02	10/6/12	-14.51	-96.72
RHW02	9/15/12	-13.68	-95.56
RHW02	8/18/12	-14.80	-95.32
RHW02	7/18/12	-14.78	-96.20
RHW02	6/28/12	-14.18	-95.84
RHW02	6/2/12	-13.92	-97.08
RHW02	6/2/12	-13.92	-97.08
RHW02	5/14/12	-14.11	-96.02
RHW02	3/24/12	-14.19	-97.00
RHW05	3/14/13	-15.48	-91.63
RHW05	10/5/12	-14.00	-94.78
RHW05	9/14/12	-12.95	-94.51
RHW05	8/17/12	-14.45	-93.74
RHW05	7/17/12	-14.16	-95.52
RHW05	6/29/12	-14.46	-93.67
RHW05	6/1/12	-13.38	-96.35
RHW05	5/15/12	-13.61	-95.03
RHW05	3/25/12	-13.54	-94.59
RHW06	3/14/13	-14.91	-94.51
RHW06	10/6/12	-14.68	-96.16
RHW06	10/6/12	-14.68	-96.16
RHW06	9/15/12	-13.42	-95.52
RHW06	8/18/12	-15.12	-95.06
RHW06	7/17/12	-14.65	-97.25
RHW06	6/28/12	-14.89	-96.06
RHW06	5/31/12	-13.94	-98.28
RHW06	5/31/12	-13.94	-98.28
RHW06	5/13/12	-13.86	-96.87
RHW06	3/24/12	-14.34	-96.22
RHW10	3/15/13	-14.45	-85.61
RHW10	10/6/12	-13.10	-88.96
RHW10	9/15/12	-12.05	-88.58
RHW10	8/18/12	-13.39	-88.28
RHW10	7/18/12	-13.25	-89.53
RHW10	6/29/12	-13.41	-86.67
RHW10	6/2/12	-12.40	-90.48
RHW10	5/13/12	-12.34	-89.47
RHW10	3/24/12	-12.55	-88.65
RHW11	10/5/12	-13.62	-91.63

Sample ID	Sample Date	$\delta^{18}O$ (‰)	δ^2H (‰)
RHW11	9/14/12	-12.60	-90.58
RHW11	8/17/12	-14.11	-90.18
RHW11	7/17/12	-13.96	-91.72
RHW11	6/29/12	-14.08	-90.00
RHW11	5/15/12	-13.16	-91.77
RHW11	5/15/12	-13.16	-91.77
RHW11	3/25/12	-13.34	-90.95
RHW12	3/16/13	-16.26	-92.09
RHW12	9/14/12	-13.65	-95.24
RHW12	8/17/12	-15.38	-94.26
RHW12	7/17/12	-14.59	-96.87
RHW12	6/28/12	-15.07	-94.31
RHW12	6/28/12	-14.17	-95.74
RHW12	5/31/12	-14.05	-97.26
RHW13	3/14/13	-15.78	-94.65
RHW13	3/14/13	-15.78	-94.65
RHW13	9/15/12	-13.59	-96.85
RHW13	8/18/12	-15.04	-96.24
RHW13	7/16/12	-14.90	-97.70
RHW13	6/28/12	-14.79	-96.79
RHW13	6/28/12	-14.58	-96.83
RHW13	6/2/12	-14.10	-98.57
WL01	10/5/12	-12.67	-80.13
WL01	9/14/12	-11.55	-78.86
WL01	8/17/12	-12.87	-80.17
WL01	7/18/12	-13.56	-84.55
WL01	6/28/12	-14.29	-88.99
WL01	6/1/12	-13.96	-95.51
WL01	5/14/12	-13.74	-91.83
WL02	10/5/12	-13.73	-85.95
WL02	9/14/12	-12.21	-82.39
WL02	8/17/12	-14.26	-84.93
WL02	7/18/12	-14.61	-91.55
WL02	6/28/12	-15.03	-93.06

APPENDIX E

GEOCHEMICAL PLOTS

APPENDIX F

RESULTS FROM END-MEMBER MIXING ANALYSIS
STREAMFLOW SEPARATIONS
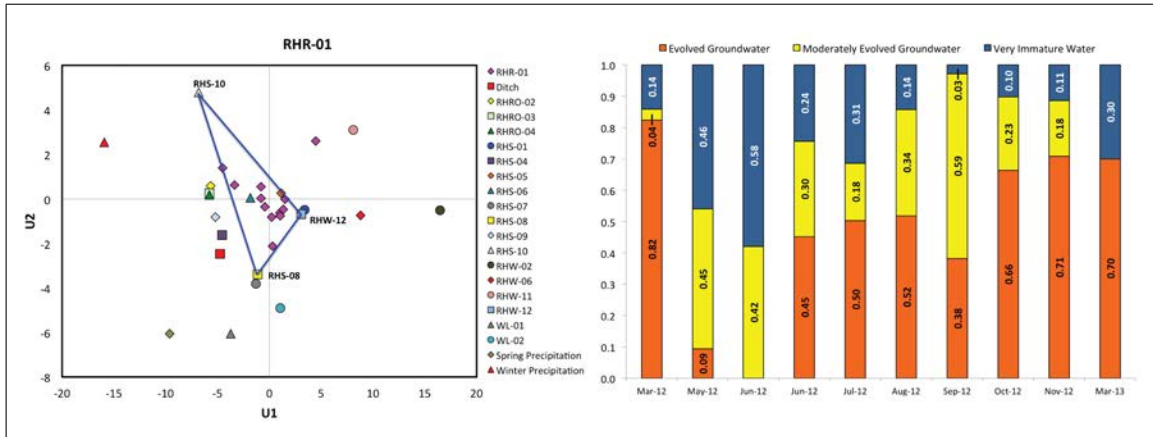
Figure F.1: U-space projection showing mixing sub-space and time series of relative contributions from selected end-members for RHR-01.
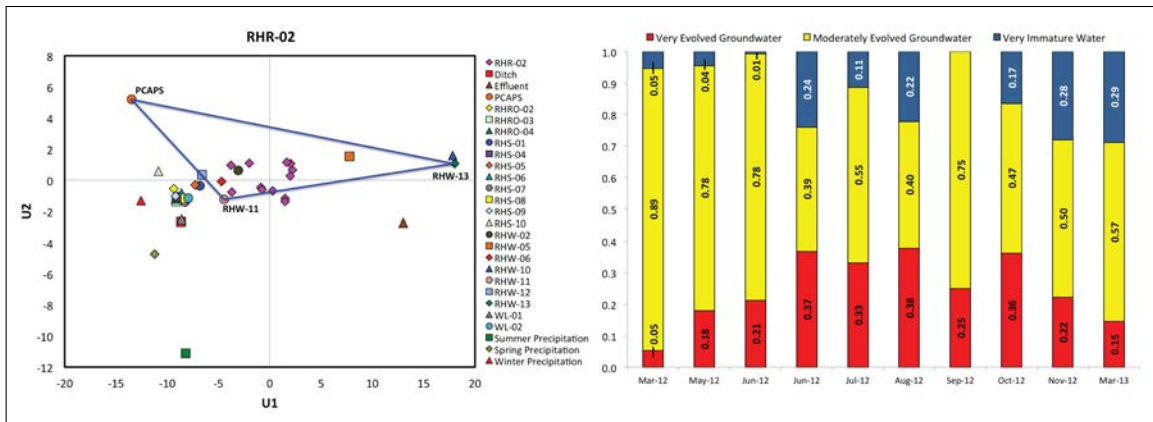
Figure F.2: U-space projection showing mixing sub-space and time series of relative contributions from selected end-members for RHR-02.
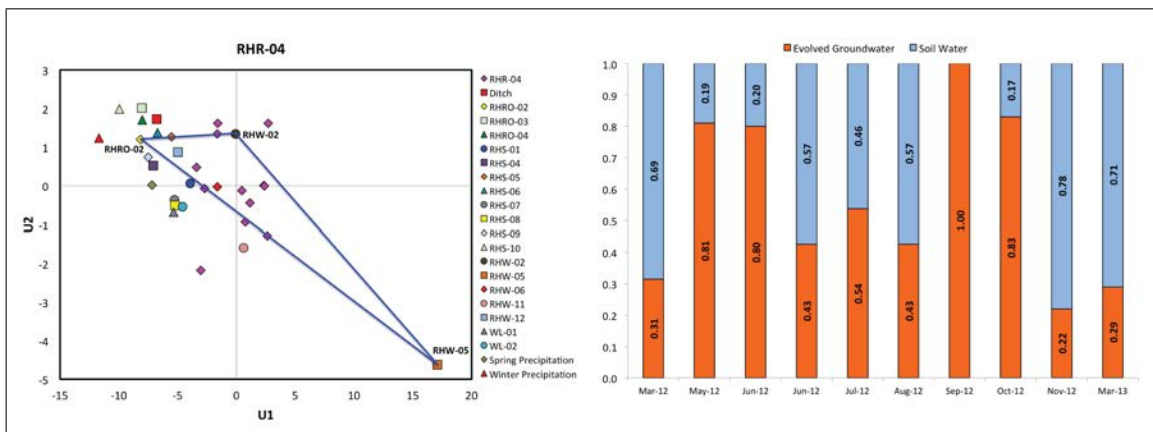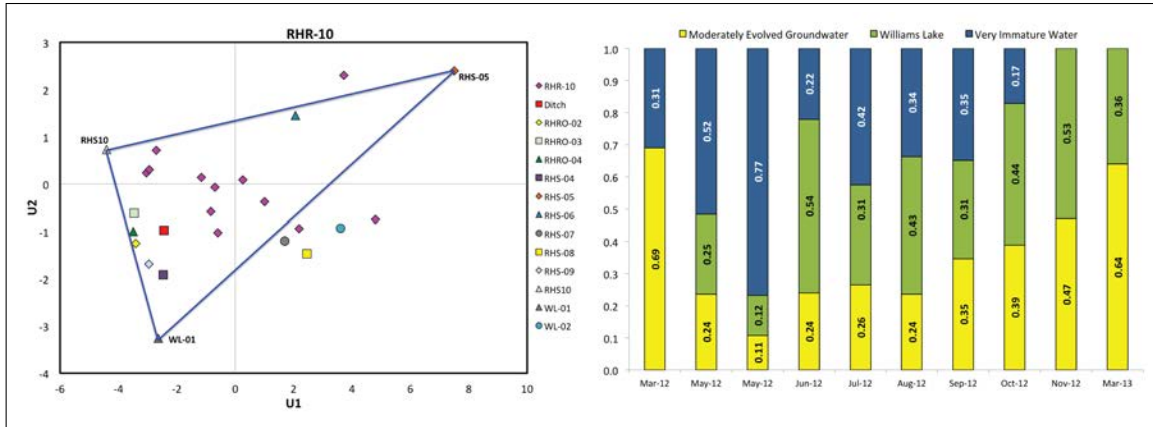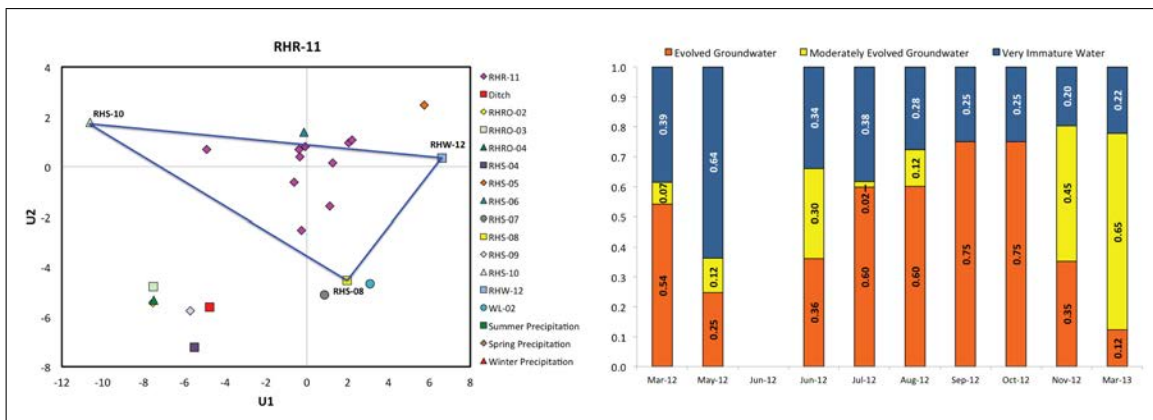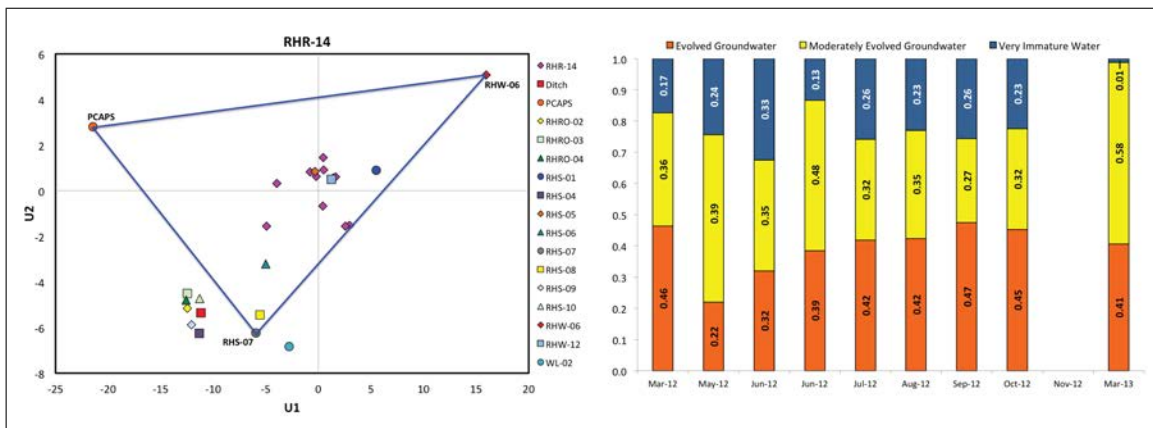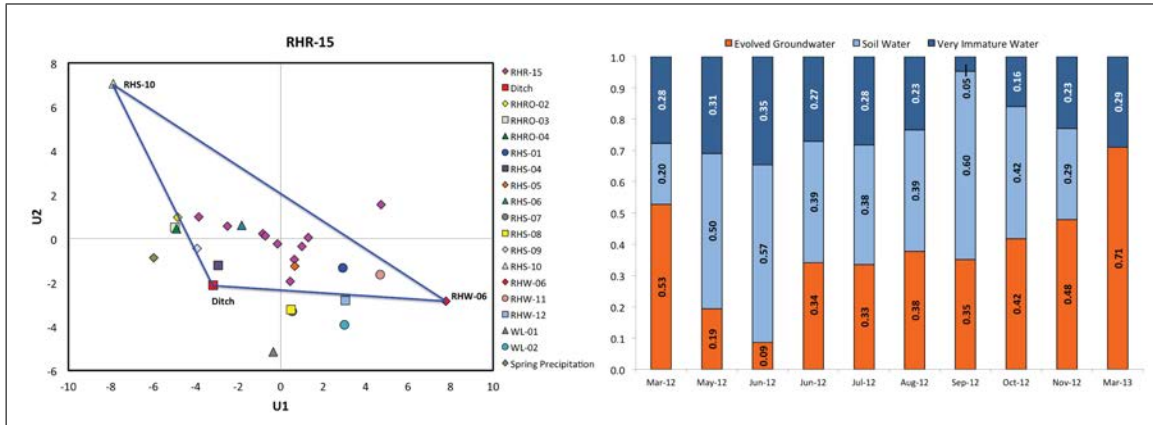

Figure F.3: U-space projection showing mixing sub-space and time series of relative contributions from selected end-members for RHR-04.

Figure F.4: U-space projection showing mixing sub-space and time series of relative contributions from selected end-members for RHR-010.
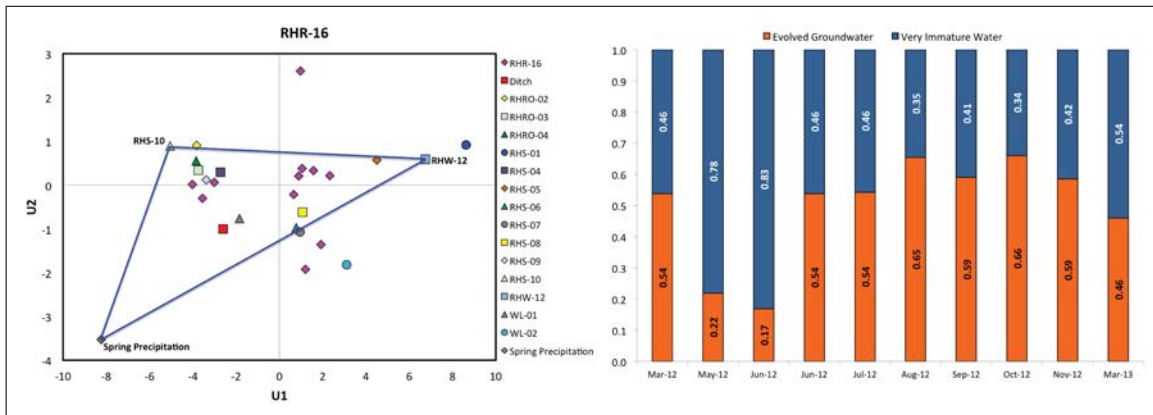

Figure F.5: U-space projection showing mixing sub-space and time series of relative contributions from selected end-members for RHR-11.

Figure F.6: U-space projection showing mixing sub-space and time series of relative contributions from selected end-members for RHR-14.
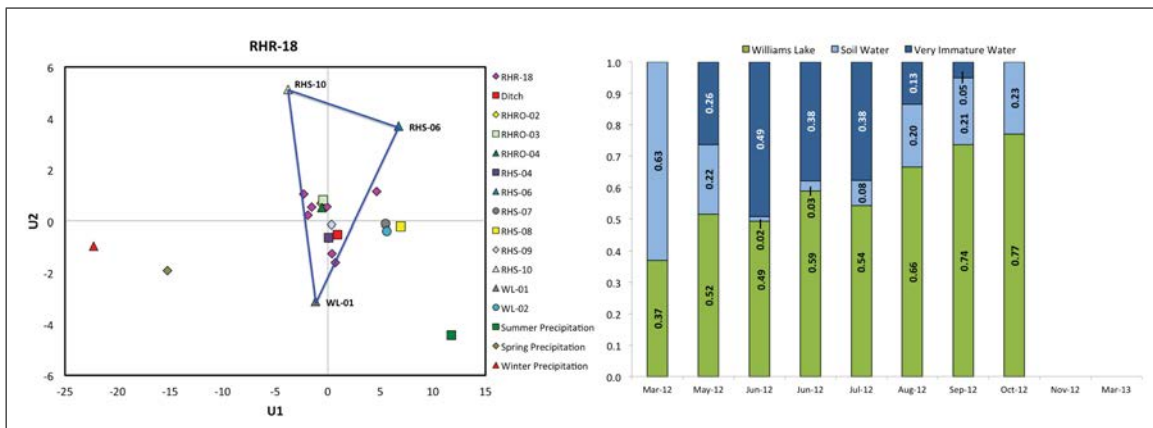
Figure F.7: U-space projection showing mixing sub-space and time series of relative contributions from selected end-members for RHR-15.

Figure F.8: U-space projection showing mixing sub-space and time series of relative contributions from selected end-members for RHR-16.

Figure F.9: U-space projection showing mixing sub-space and time series of relative contributions from selected end-members for RHR-18.
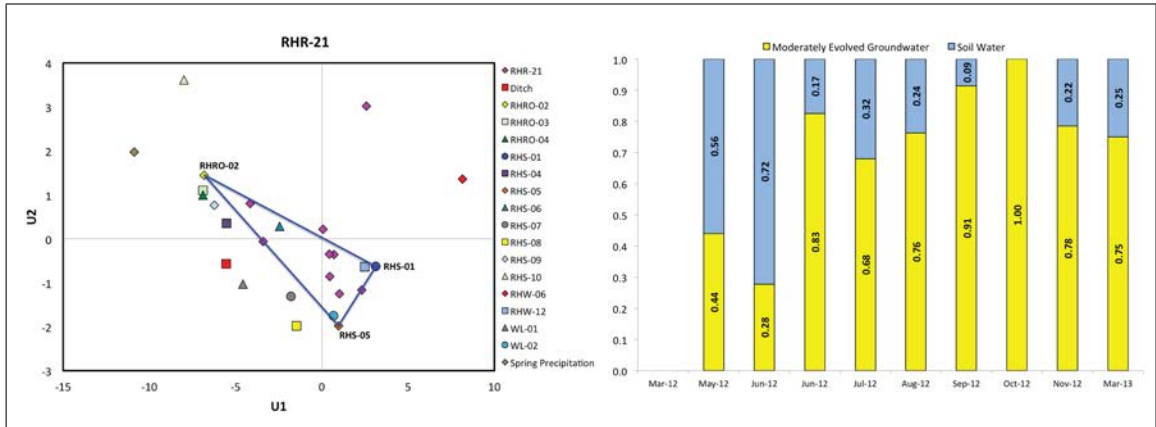
Figure F.10: U-space projection showing mixing sub-space and time series of relative contributions from selected end-members for RHR-21.
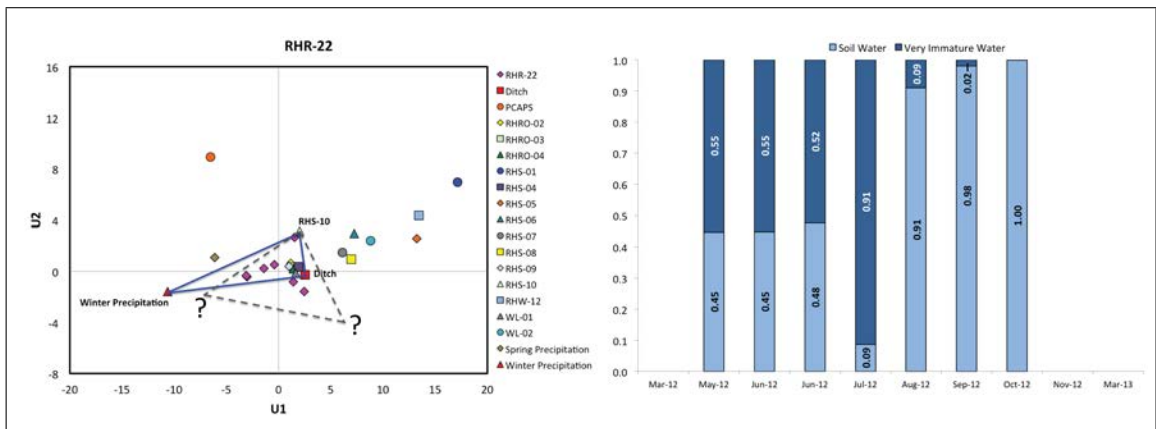

Figure F.11: U-space projection showing mixing sub-space and time series of relative contributions from selected end-members for RHR-22.
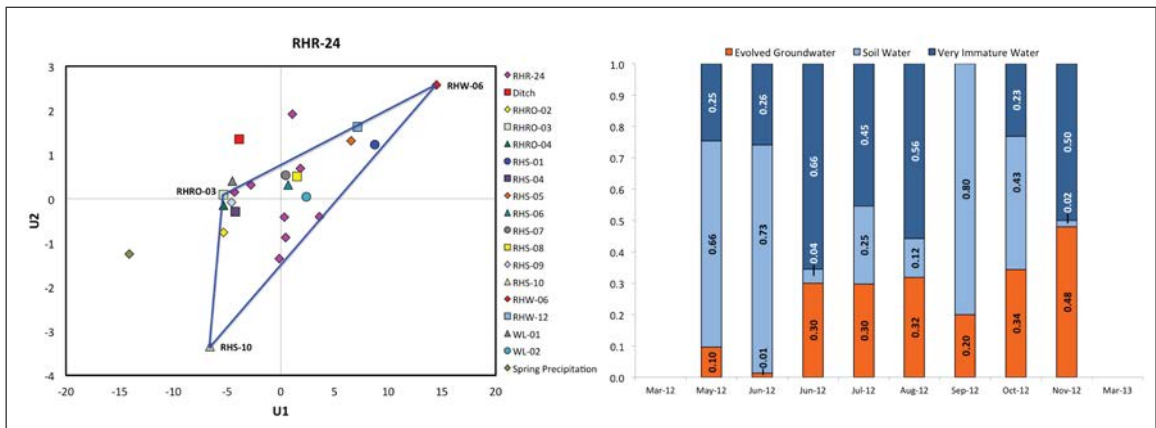

Figure F.12: U-space projection showing mixing sub-space and time series of relative contributions from selected end-members for RHR-24.

APPENDIX G

AGE DATING RESULTS SUMMARY

Sample ID	CFC's				Tritium		Radiocarbon		
	CFC Age (All)	+/-	CFC Age (CFC-12)	+/-	Tritium (TU)	+/-	Activity (pmC)	+/-	$\delta^{13}C$
Ditch									
RHS-01	30.0	3.7	29.0	0.7	7.9	0.8	0.9177	0.0034	-17.7
RHS-04					6.2	0.8			
RHS-08	25.6	1.8	23.8	0.3	7.2	0.8	0.6468	0.0024	-16.8
RHS-09					7	0.8			
RHW-02					8.5	0.8	0.9502	0.0035	-18.9
RHW-05	55.5	4.9	60.7	0.3					
RHW-06	28.4	2.0	27.3	0.4			0.8962	0.0033	-18.3
RHW-10	44.0	4.7	43.5	0.0	1.5	0.8	0.7128	0.0026	-22.4
RHW-12	28.5	3.5			4.8	0.8	0.6901	0.0025	-18.2
RHW-13					13.2	0.8	0.9876	0.0036	-16.2
RHR-01					6.59	0.22			
RHR-14					6.67	0.22			
RHR-18					7.41	0.24			

New Mexico Institute of Mining and Technology
Center For Graduate Studies

Student's Full Name: **Douglas G. Tolley III**

Title: High-Elevation Mountain Streamflow Generation: The Role of Deep Groundwater in the Rio Hondo Watershed, Northern New Mexico

Degree: ☒ MS ☐ PhD   Department: Earth & Environmental Science   Graduation Date   May 2014

NMT Copyright Agreement

I hereby certify that this is my original work and I have the authority to grant the non-exclusive right and license specified herein. I further certify that, if appropriate, I have obtained and attached hereto a written permission statement from the owner(s) of each third party copyrighted matter to be included in my thesis, dissertation, or record of study, allowing distribution as specified below.

I certify that the version I submitted is the same as the approved by my advisory committee.

I hereby grant in perpetuity, without restriction, royalty free to New Mexico Tech or its agents the non-exclusive right and license to archive and make accessible, under the conditions specified below, my thesis, dissertation, or record of study in while or in part in all forms of media, now or hereafter known. This agreement shall survive assignment of any and all exclusive rights provided to copyright holders in Section 106 or the United States copyright law.

FERPA. To the extent this thesis, dissertation, or record of study is an educational record as defined in the Family Educational Rights and Privacy Act (FERPA) (20 USC 1232g), I consent to disclosure of it to anyone who requests a copy.

I retain all other ownership rights to the copyright of the thesis, dissertation, or record of study. I also retain the right to use in future works (such as articles or books) all or part of this thesis, dissertation, or record of study.

Availability Option (check one)

☒ Release the work immediately for worldwide access on the Internet.

☐ *(Patent Hold)* Secure the work temporarily for patent and/or proprietary purposes, then release the work for worldwide access on the Internet.

☐ *(Journal Hold)* Hold the work for one year, then release the work for worldwide access on the Internet. *(One-year extension on request, if needed)*

Chair/Co-Chair Certification

I have discussed the availability choices with my student and I am aware of the choice my student has made.

Chair/Co-Chair's Signature: *John L Wilson ᎪᎪᎪ*
(Only one Chair or Co-Chair signature is required).

Student Copyright Agreement

I have read and fully agree to the NMT copyright agreement regarding my thesis/dissertation. I agree to the thesis/dissertation availability option I selected above. I understand that the availability option is my choice and that there may be publishing consequences to my selection.

Student's Signature: _____

Approval _____ Effective Date _____